Alkaline earth mediated carbon monoxide activation

Anker, Mathew

Award date:
2017

Awarding institution:
University of Bath

Alkaline Earth Mediated Carbon Monoxide Activation

Mathew David Anker

A thesis submitted for the degree of Doctor of Philosophy

University of Bath

Department of Chemistry

April 2017

Table of Contents

I. Publications as a Result of this Thesis

I.I Publications as a Result of Work Contained Herein:

1. M. D. Anker, M. S. Hill, J. P. Lowe and M. F. Mahon, *Angewandte Chemie International Edition*, 2015, **54**, 10009–10011.

2. M. D. Anker, Y. Yang, J. Fang, M. F. Mahon, L. Maron, C. Weetman and M. S. Hill. *Chemical Science*, 2017, **8**, 3529–3537.

3. M. S. Hill and M. D. Anker. Alkaline Earth Catalysis, *Encyclopaedia of Inorganic and Bioinorganic Chemistry*. In press.

I.II Publications as a Result of Other Work Throughout this Thesis:

1. M. D. Anker, M. Arrowsmith, P. Bellham, M. S. Hill, G. Kociok–Kohn, D. J. Liptrot, M. F. Mahon and C. Weetman, *Chemical Science*, 2014, **5**, 2826–2830.

2. C. Weetman, M. D. Anker, M. Arrowsmith, M. S. Hill, G. Kociok–Kohn, D. J. Liptrot and M. F. Mahon, *Chemical Science*, 2016, **7**, 628–641.

3. P. Bellham, M. D. Anker, M. S. Hill, G. Kociok–Kohn and M. F. Mahon, *Dalton Transactions*, 2016, **45**, 13969–13978

4. M. D. Anker, A. L Colebatch, K. J Iversen, D. J. D. Wilson, L. Garcia, M. S. Hill, D. J. Liptrot and M. F. Mahon. *Organometallics*, **2017**, 36, 1173–1178.

5. M. D. Anker, C. Balasanthiran, V. Balasanthiran, M. H. Chisholm, S. Jayaraj, K. Mathieu, P. Piromjitpong, S. Praban, B. Raya, W. J. Simonsick. *Dalton Transactions*, 10.1039/C6DT03198F.

6. M. D. Anker, M. Arrowsmith, R. Arrowsmith, M. S. Hill and M. F. Mahon. *Inorganic Chemistry*. In press.

II. Acknowledgements

First and foremost, my biggest thanks must go to Prof. M. Hill. The help and support that not only I, but every member of the Hill group have received is at a level that every academic should aspire to. Whether in the confines of our cosy office over a coffee, to Moose McGillycuddy's, I have never stopped learning on this epic journey and for that, Mike, I thank you.

My next thanks goes to those that have helped and supported me throughout this era of my life. To Peter Barnet, thank you for your unwavering friendship, faith and loyal support. Without you a great deal would not have been possible. Hollie, Andy and Niall; working, living, supporting each other as well as the infrequent trips to the pub together has been a truly exciting time of my life, the friendships made over this PhD I know will never waver in the years to come.

To all the Hill Group, both past members and new: Cath, Merle, Annie, Anne, Amanda, Louis and Pete you have helped shape me into the chemist that I am, for better or for worse I thank you. A special thanks must go to David Liptrot, the hairiest member of the Hill Group, who through my good fortune saw fit to drag me up by my shoe laces and polish me up enough that Mike took me on. Andrew Wilson has his own section of thanks, for only he and I know just where the bottom level can be drawn, and who without which life would have been infinitely less interesting.

To Prof. M. Whittlesey, thank you for not only putting up with me thought out my undergraduate but for your patience with me as a postgraduate. Dr A. Johnson, thank you for all of your colourful words of advice, between the Hill, Johnson and Whittlesey groups there has never been a dull moment. Dr M. Mahon thank you for all your patience and help with X-ray crystallography.

Finally, to my parents, David and Ann Anker, without which I would never have been made, loved, supported and encouraged to follow my passions. My thanks goes to you, for you have endured me the longest.

III. Abstract

The aim of this thesis is to investigate the synthetic utility of insertion reactions with Group two complexes, specifically towards the activation of the small molecular gas; carbon monoxide. Extension of this Group two mediated reactivity into catalytic regimes exploits both σ–bond metathesis and insertion chemistries with hydride sources such as $PhSiH_3$ or HBpin to generate value added chemicals.

Chapter Two demonstrates organoisocyanates are readily converted to methyl amines through hydrodeoxygenation with HBpin in the presence of the *β*–diketiminato magnesium catalyst, **Ib**. A series of catalytically relevant species have been identified and fully characterized through stoichiometric reactivity studies. These data suggest that overall reduction and C–O activation occur through the intermediacy of well–defined magnesium formamidato and magnesium boryloxide species. This reaction is further explored through a DFT study which complements the experimental findings.

Chapter Three explores the reaction between both *β*–diketiminato magnesium, **Ih**, and calcium, **Ii**, hydride complexes with carbon monoxide, resulting in the isolation of dimeric *cis*–enediolate species by the reductive coupling of two CO molecules. Under catalytic conditions with $PhSiH_3$, an observable magnesium formyl species may be intercepted for the mild reductive cleavage of the CO triple bond to a methane analogue in the case of **Ih**. The related calcium formyl species could not be identified but under identical catalytic conditions reduced CO to a methoxysilane species, demonstrating the variability in the chemistries of the group two elements.

Chapter Four investigates the carbonylation of a range of *in situ* generated *β*–diketiminato Ae–NRR′ (Ae = Mg or Ca, R = H or Me and R′ = H, Alkyl or aryl) complexes, resulting in the isolation of a number of formamidate complexes and including a carbenic formamide dimagnesium species. The hydrodeoxygenation chemistry that was explored in Chapter Two is then extended to the range of isolated compounds providing a novel route to methyl amines.

IV. Abbreviations

9–BBN	9–Borabicyclo[3.3.1]nonane
Ae	Alkaline Earth
Bn	Benzyl
CO	Carbon Monoxide
Cy	Cyclohexyl
CyNC	Cyclohexyl isocyanate
DFT	Density Functional Theory
Di	1,4–Dioxane
Dipp	2,6–Diisopropylphenyl
DMAB	Dimethyl amine borane
DMAT	2–dimethylaminobenzyl
Dmpe	1,2–Bis(dimethylphosphino)ethane
Et	Ethyl
F–T	Fisher–Tropsch
HBpin	Pinacolborane
HSQC	Heteronuclear Single Quantum Coherence spectroscopy
^{i}Pr	*iso*–propyl
Mes	1,3,5–trimethylbenzene
NCO	Isocyanate
NMR	Nuclear Magnetic Resonance spectroscopy
^{n}Pr	Propyl
Ph	Phenyl
$PhSiH_3$	Phenyl silane
Py	Pyridine
RT	Room temperature
^{t}Bu	*tert*–butyl
To^{M}	Trisoxazolinylborate

Chapter One

Introduction

1.1 Group Two

Since their initial development by Victor Grignard, alkyl–, vinyl– and aryl–magnesium halides have been prominent stoichiometric reagents for more than a century.[1] More recent advances have seen the emergence of heavier alkaline earth (Ae = Ca, Sr and Ba) chemistry and, specifically, the catalytic activity of these elements as a well–defined field of research in its own right. While transition metals are renowned for their extensive catalytic chemistry and a vast range of transformations, many are of low natural abundance and thus great expense, Table 1.1. In contrast, many of the group two metals are notable for their high relative abundance in the lithosphere and resultant low cost. Furthermore the environmentally benign nature of these elements marks their catalytic chemistry as both sustainable and economical.[1]

Table 1.1: Cost comparison between common catalytic transition and alkaline earth metals.[1]

Metal	Palladium	Iridium	Ruthenium	Magnesium	Calcium
$/kg	$27,941	$30,684	$1,938	$2.18	$4.80

The chemistry of the group two metals is defined by their immutable +2 oxidation state, with only a few notable exceptions.[2] Despite all congeners possessing the highly stable M^{2+} ions with d^0 electron configurations, a marked increase in the ionic radii is observed upon descending the group, concurrent with an increase in polarisability and electropositivity, Figure 1.1.

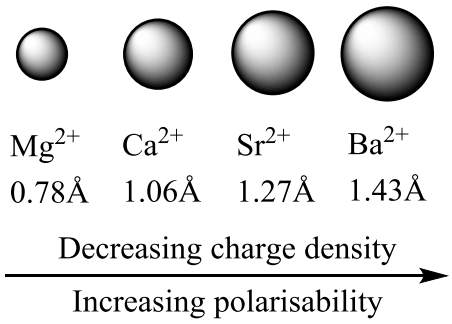

Figure 1.1: The variation in ionic radii of group two M^{2+} ions.

Consequently, metal–ligand bonding for the group two cations, albeit with a degree of covalency accessible for magnesium which is precluded for its heavier congeners, is dominated by increasingly non–directional ionic interactions as the group is descended. These bonding characteristics represent a challenge for the synthesis of well defined, heteroleptic heavier group two complexes owing to their propensity to undergo Schlenk–type equilibria, Scheme 1.1.

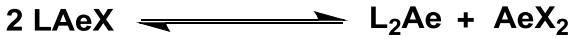

Scheme 1.1: The Schlenk–like redistribution to which group two M^{2+} complexes are prone.

Redistribution of heteroleptic complexes often yields metal centres ligated by two large stabilising ligands. Consequently, approaches to spectator ligands for group two have focused on polydentate monoanionic frameworks encompassing hard donor sites and significant steric bulk to aid in kinetic stability and suppress the Schlenk–like redistribution. Large stabilising ligands include β–diketiminates (**Ia – Ig**),[3] anilido–imines (**IVa – IVc**)[4] and borates (**V**).[5] An alternative approach to circumvent redistribution has utilised homoleptic group two complexes including those incorporating bulky amides (**IIa – IIId**).[6] Both classes of compound that are pertinent to this work are summarised in Figure 1.2.

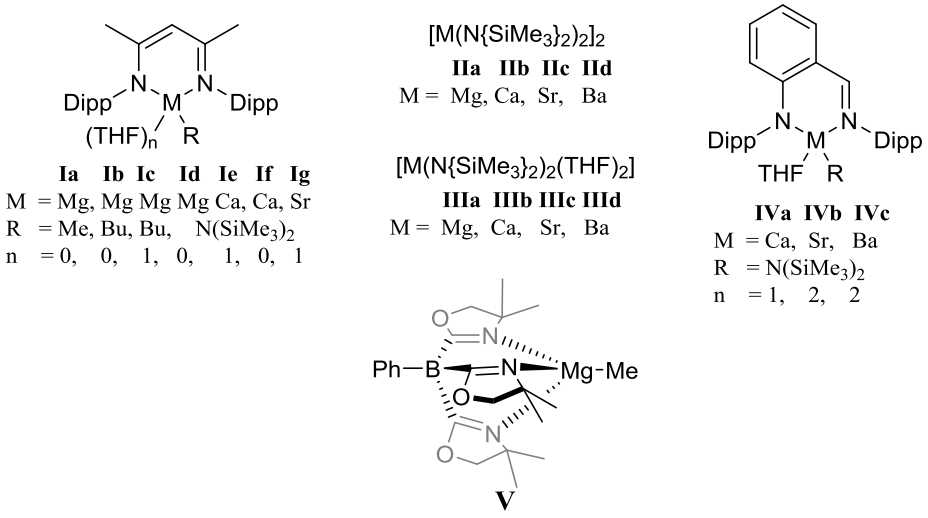

Figure 1.2: Range of pre–catalysts utilised in group two mediated catalysis.

An inability to perform redox chemistry unlike the transition metals, led to an initial comparison to the reactivity observed in lanthanide chemistry.[7] While lanthanides have a strong propensity to form their respective M^{3+} ions with d^0 electronic configurations, the f–block contraction leads to only minor variations in ionic radii. Thus a marked dissimilarity is

observed between the chemistries of the alkaline earth and lanthanide ions and,[4, 6d] as a consequence, only the former will be discussed herein.

1.2 Redox–Inactive Group Two Mediated Catalysis

Group two chemistry is dominated by two principal mechanistic steps, σ–bond metathesis and insertion, which ensue without alteration of metal oxidation state. These steps are summarised in Scheme 1.2.

(a) σ–Bond metathesis

(i) Protic H

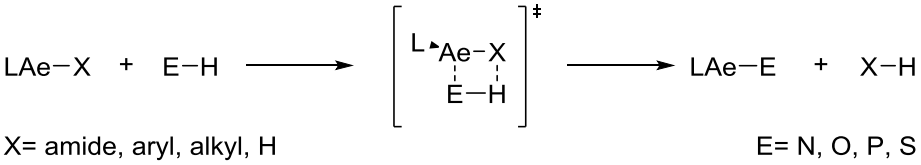

(ii) Hydridic H

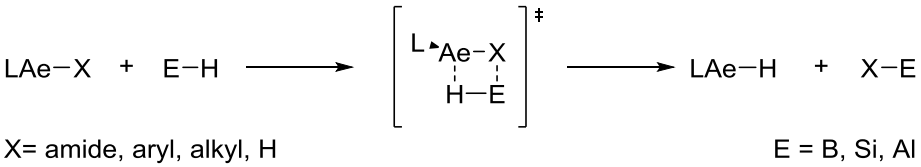

(b) Insertion of E=C unsaturated bond into a Ae–X σ–bond

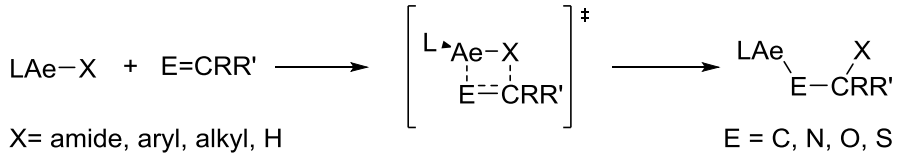

Scheme 1.2: Two principal reaction chemistries of group two complexes.

Protonlysis of the form shown in Scheme 1.2 (a)(i) yields, in the case of an amine N–H bond, a group two amide of the form $LAeNR_2$ (L = monoanionic spectator ligand).[8] Exploitation of these species in insertion reactions as shown in Scheme 1.2 (b) initially yielded a variety of stoichiometric heterofunctionalisations of unsaturated bonds. In contrast, Scheme 1.2 (a)(ii) shows the case wherein the E–H bond is polarised with a greater electron density localised upon the hydrogen, as in silanes and boranes. In this case σ–bond metathesis yields a metal hydride, LAeH and an E–X bond (L = monoanionic spectator ligand, E = Si or B).

Initial reactions with group two metal complexes focused on the protonolysis step (Scheme 1.2, (a)(i)), in order to yield a potentially catalytically relevant species. The activity of group two amides and alkyls with alcohols, pyrroles, terminal alkynes, phosphines and C–

H acidic heterocycles has been shown to yield alkoxide,[9] pyrrolide,[10] acetylide,[11] phosphide[6b, 12] and carbanion[13] fragments bound to a group two centre along with, in every case, the respective protonated fragment. This is exemplified for the metal hexamethyldisilazides (**IIa–d**) in Scheme 1.3.

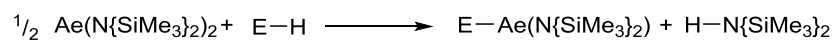

Scheme 1.3: Protonolysis of a protic E–H bond by group two hexamethyldisilazides, forming a new Ae–E bond.

Further work by Westerhausen and co–workers disclosed the metallophosphination of 1,4–diphenylbutadiyne with group two phosphides, $[M\{P(SiMe_3)_2\}_2(THF)_2]$ (M = Ca, Sr, Ba). Similarly, their amide analogues **IIa–d** were shown to readily add across the C≡N bond of benzonitrile,[11c, 14] evidencing the inclination of group two complexes to mediate insertion chemistry. This was further demonstrated by Harder and co–workers who reported the polymerisation of styrene by the group two benzyl complexes, $[M(DMAT)_2(THF)_2]$ (M = Ca, Sr. DMAT = 2–dimethylaminobenzyl).[15] The combination of these σ–bond metathesis and insertion chemistries, allows two catalytic manifolds to be envisaged mediated by group two metal centres, Scheme 1.4.

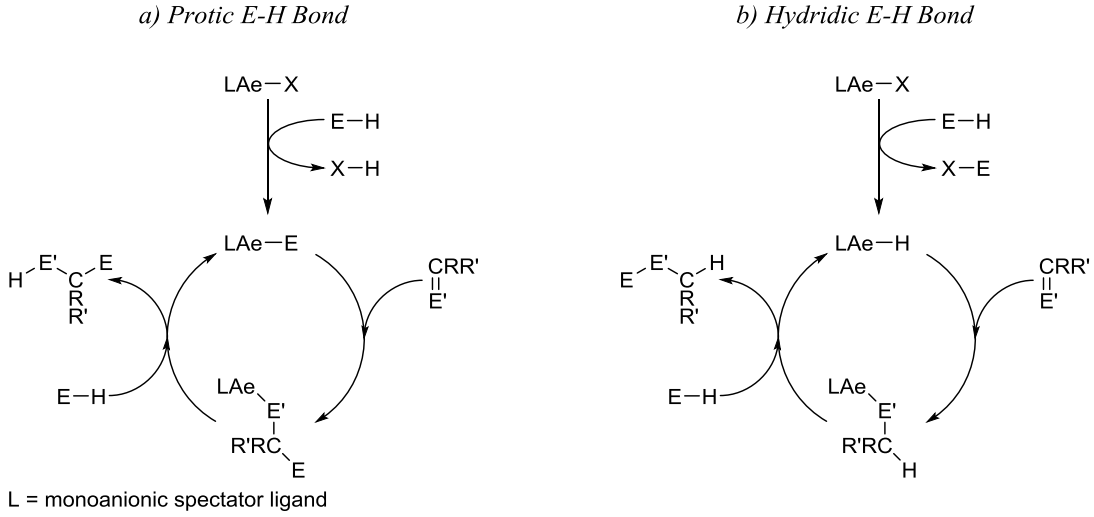

Scheme 1.4: Protic (*a*) and hydridic (*b*) catalytic cycles, assembled from a series of σ–bond metathesis and insertion steps mediated by a group two centre.

1.2.1 Group Two Mediated Hydroamination

In 2004 Hill and co-workers reported that Chisholm's *β*–diketiminate–stabilised calcium amide **Ie**, was a highly effective catalyst for the intramolecular hydroamination of aminoalkenes and aminoalkynes.[16] The reaction was postulated to occur through a

combination of both σ–bond metathesis and insertion steps, to give the generalised catalytic cycle outlined in Scheme 1.5.

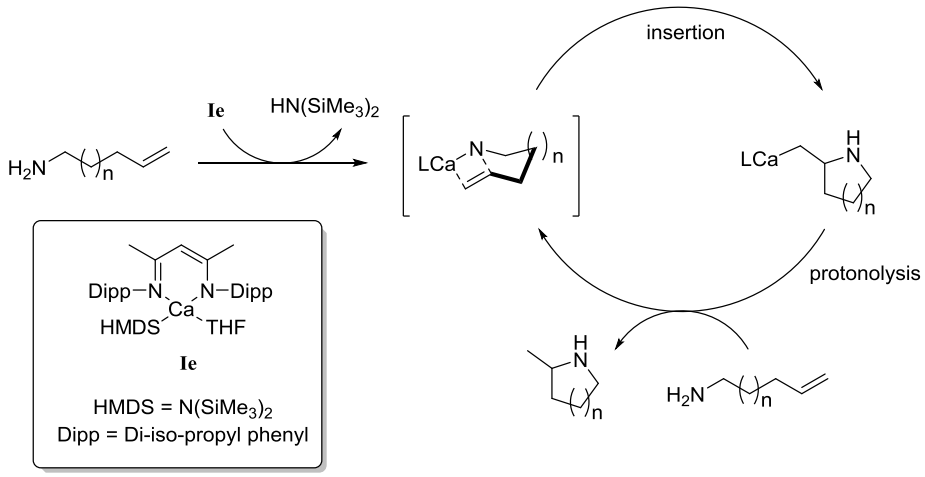

Scheme 1.5: Generalised postulated catalytic cycle for calcium–mediated intramolecular hydroamination.

This study was initially extended to include the *n*–butyl magnesium *β*–diketiminato complex **Ib**. Both **Ib** and **Ie** were reported as efficient pre-catalysts for hydroamination/cyclisation of a range of aminoalkenes. These reactions proceed under mild conditions (25–80°C) with moderate to low catalyst loadings (2–20 mol%), allowing the synthesis of five–, six–, and seven–membered heterocyclic compounds. Qualitative assessment of these reactions revealed that the ease of catalytic turnover increases (i) for smaller ring sizes (5 > 6 > 7); (ii) For substrates that do not possess additional substitution on the alkene entity. A series of stoichiometric reactions between the pre-catalysts and primary amines provided an important model for catalyst initiation and suggested that these reactions are facile at room temperature.

Both external and coordinated amine/amide exchange were observed in model complexes, suggesting that these processes occur via low activation energy pathways. As a result of the formation of potentially reactive by–products such as $HN(SiMe_3)_2$ for calcium–catalyst **Ie**, initiation is reversible, whereas for the alkyl magnesium pre-catalyst **Ib** this process is non–reversible. This gives rise to a complex mechanistic landscape moving from the magnesium complex **Ib**, to the heavier calcium congener **Ie**, (Scheme 1.6).

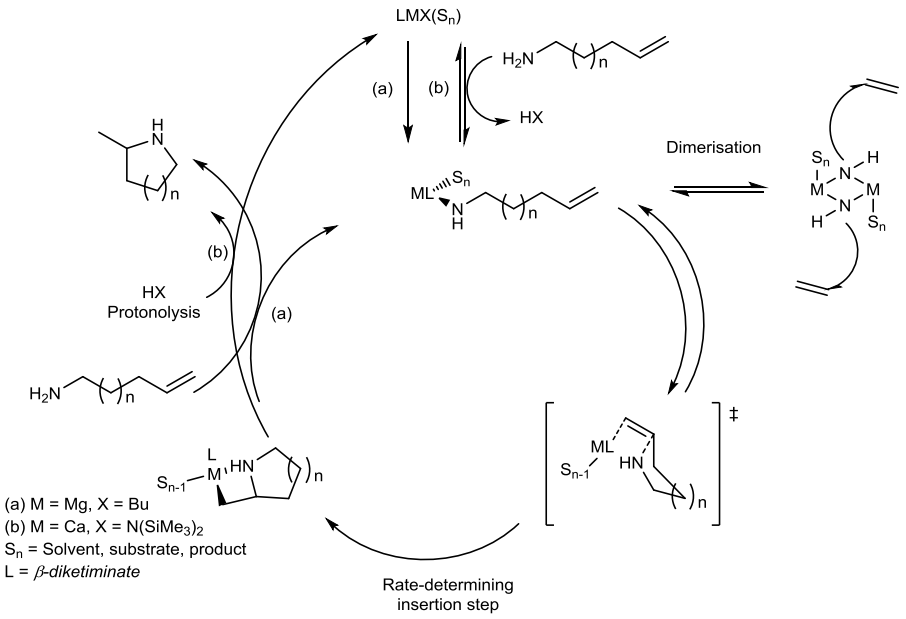

Scheme 1.6: Proposed mechanism of group two mediated intramolecular hydroamination catalysis for (a) non–reversible catalyst initiation, and (b) reversible catalyst initiation.

1.2.2 Further Group Two-mediated Heterofunctionalisations

A wide range of combinations of further protic E–H and multiple C=E' bonds have also been reported as suitable substrates for group two catalysed heterofunctionalisation reactions. Hill and co–workers described the catalytic intermolecular hydrophosphination of alkenes utilising, **If**.[17] Westerhausen and co–workers subsequently extended the scope of this reaction to alkynes using a homoleptic calcium phosphanide pre–catalyst[18] and the Sarazin group have described the hydrophosphination of alkenes catalysed by the same collection of heteroleptic calcium, strontium and barium amides employed in their studies of hydroamination.[19] In this latter case, the order of reactivity was also found to be Ca < Sr < Ba and both anilidoimine– and phenoxide–supported catalysts were shown to provide higher activity than their analogous β–diketiminato counterparts.[4, 20] Moving beyond the activation of P(III)–H bonds, the Sarazin group have also reported the hydrophosphonylation of ketones and aldehydes mediated by **IIIb** – **IIId**.[19]

The scope of these reactions has been further expanded to unsaturated substrates beyond alkenes, alkynes and ketones. Extensive reports of carbodiimide heterofunctionalisation have been made, which include hydroamination[21] and hydrophosphination[11b] to provide the guanidine and phosphaguanidine species respectively.

Terminal alkynes, readily deprotonated by group two amides (**IIIa** – **IIId)**, allow for the facile hydroacetylenation of carbodiimides and the catalytic synthesis of

propargylamidines.[22] Although a number of catalytic group two-mediated transformations of isocyanates to isocyanurates[23] and ureas[24] have been described, attempted extension of these chemistries to the catalytic synthesis of propargylamides was unsuccessful. Rather, addition of a combination of an organoisocyanate and a terminal alkyne to alkyl magnesium species resulted in a cascade of inter– and intramolecular insertion events to yield a unique series of bis(imidazolin–2,4–dione) molecules.[25] While this stoichiometric reactivity could not be extended into a catalytic regime, the *in situ* formation of propargyl amidines by pre–catalysts **IIIa** – **IIId** and interception with RNCO, RNCS (R = aryl or alkyl) and CS_2 substrates has recently enabled the catalytic and atom–efficient one pot assembly of a wide variety of functionalised imidazolidine–2–ones and –thiones, 2–imino–imidazolidines and thiazolidine–2–thiones.[26]

1.3 Synthesis and Reactivity of Group Two Hydrides

Extension of this group two-catalysed heterofunctionalisation chemistry to systems appropriate for the hydrogenation, hydrosilylation or hydroboration of multiply bonded substrates implicates the generation of alkaline earth hydride intermediates. This requirement has resulted in a focus on the isolation of well–defined and isolable molecular hydrides.

1.3.1 Synthesis of Group two Hydrides

These studies were initiated by Harder's seminal report of the *β*–diketiminato calcium hydride, **Ii**, the synthesis of which relied upon the σ–bond metathesis pathway illustrated in Scheme 1.7. A subsequent report by Jones and Stasch described the synthesis of a variety of *β*–diketiminato magnesium hydrides,[27] utilising Harder's reaction conditions, Scheme 1.7. This σ–bond metathesis route utilising phenylsilane as a hydride source has also now yielded a variety of higher magnesium hydrides reported by Hill,[28] Harder[29] and Okuda.[30]

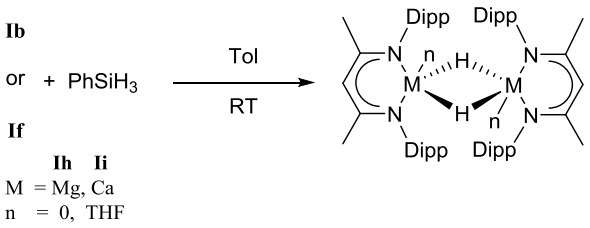

Scheme 1.7: Synthesis of group two Hydrides.

An exploration of the stoichiometric reactivity of both **Ih** and **Ii** with a variety of unsaturated substrates provided well–defined and predictable insertive behaviour, Scheme 1.8.[27b, 31]

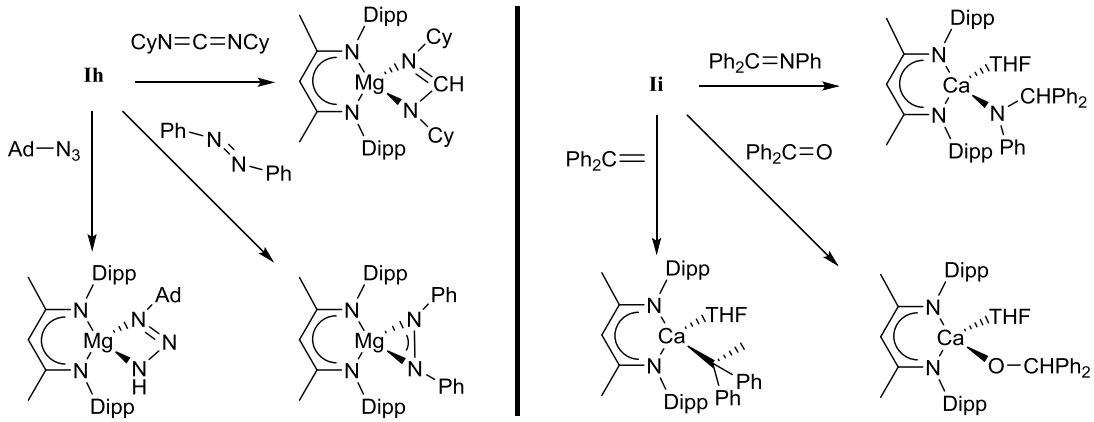

Scheme 1.8: Reactivity of **Ih** and **Ii** with a range of unsaturated moieties.

These data establish a foundation for the catalytic implementation of heavier group two element hydrides.

1.4 Synthesis and Reactivity of Magnesium (I) Species

The basis for all the aforementioned group two chemistry is predicated upon the redox inactivity and thus stability of the +2 oxidation state. In contrast, in 2007 Jones and co–workers reported the first synthesis of molecular magnesium(I) compounds, containing a magnesium–magnesium bond.[2a] Reduction of magnesium iodide compounds **VIa** and **VIb** with an excess of potassium metal in toluene over 24 hours led to the crystalline magnesium(I) compounds, **VIIa** and **VIIb** respectively, Scheme 1.9.

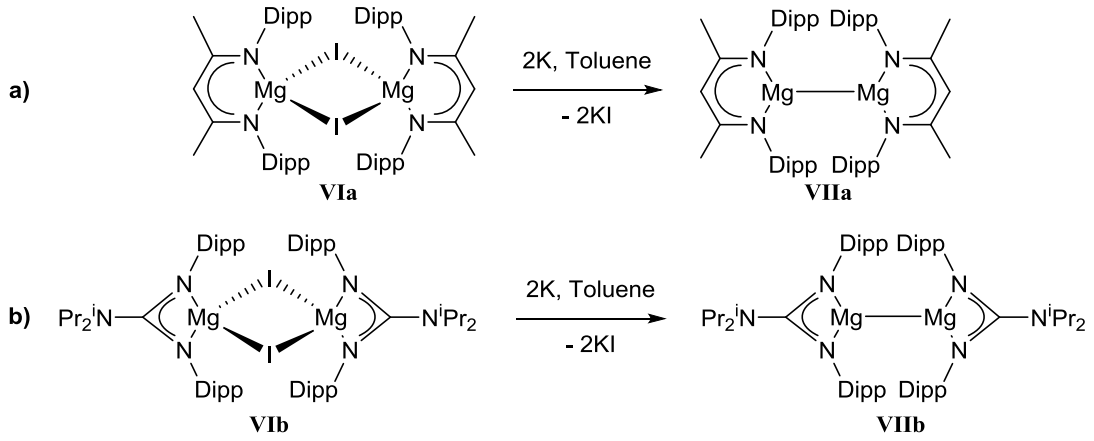

Scheme 1.9: Reduction of the iodide bridged dimers **VIa** and **VIb** by potassium to yield magnesium(I) dimers, **VIIa** and **VIIb**.

Compounds **VIIa** and **VIIb** were reported to react as facile two centre/two–electron reductants, yielding novel doubly reduced, C–C or N–N coupled products. The reaction with dicyclohexylcarbodiimide for example, gives the doubly reduced product, **VIIIa**. Similarly, treatment of **VIIa** with azobenzene gave the reduced product **VIIIb**. In contrast, the reaction with adamantyl azide led to reductive N–N coupling to give the unusual hexazenediide complex **VIIIc**, Scheme 1.10. For comparison, reactions of the aforementioned magnesium hydride **Ih** with the same substrates only yields hydromagnesiation products.[32]

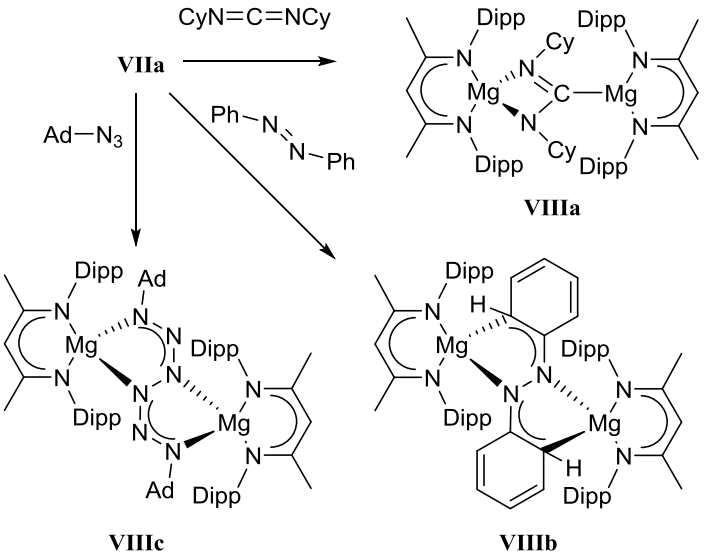

Scheme 1.10: Two centre/two–electron reductions of dicyclohexylcarbodiimide, azobenzene and adamantyl azide by compound **VIIa**.[32]

However striking, the reactivity of these magnesium(I) species is confined to stoichiometric reduction. Regeneration of the magnesium(I) dimer in a catalytic regime is disfavoured due to the high negative reduction potential of magnesium(II). While these and related compounds demonstrate unusual chemistry as bespoke reducing agents, they are beyond the scope of this thesis and thus will not be discussed further.

1.5 Group Two Mediated Dehydrocoupling

The selective catalytic formation of homo– and heteronuclear element–element bonds is of vital importance to the synthesis of both molecular and macromolecular entities. While a majority of attention will remain fixated on the construction of C–C and C–E (E = *p*–block element) bonds, there is a growing interest in the development of catalytic routes to homonuclear E–E (E = B, Si, Sn, P, As, etc.) and heteronuclear E–E' (E' = B, Si, Sn, etc.) linkages.[33] Without exception, all of these can be achieved through the catalytic

dehydrocoupling of E–H and E–H or E–H and E'–H substrates with concomitant elimination of dihydrogen.

An initial advance toward dehydrocoupling utilising alkaline earth complexes, was observed in a stoichiometric study reported by Hill and co–workers in 2007. The heteroleptic calcium amide, **Ie**, underwent σ–bond metathesis with one equivalent of the dimeric 9–borabicyclo[3.3.1]nonane (9–BBN) at 60°C to afford a new calcium hydridoborate species, **IXa**, and the amidoborane, **Xa**, Scheme 1.11.[34]

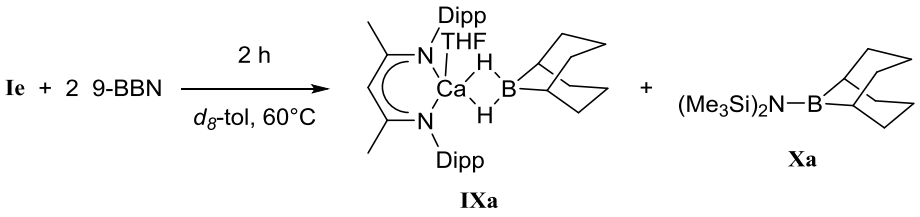

Scheme 1.11: Reaction of **Ie** with 9–BBN to give the calcium hydridoborate, **IXa**, and the borylated amine, **Xa**.

An analogous reaction performed between a related calcium diphenylamide, **XI**, and two equivalents 9–BBN again gave the calcium hydridoborate, **IXa**, and generated the amidoborane, **Xb**, Scheme 1.12.

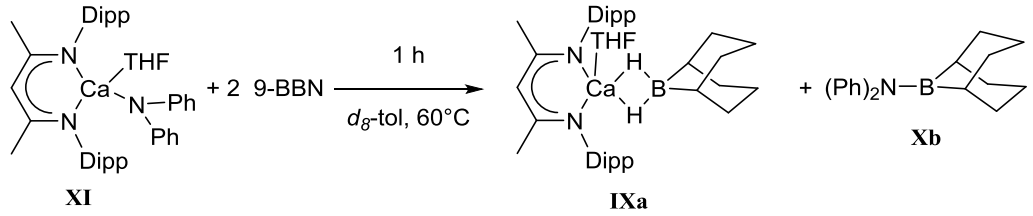

Scheme 1.12: Hydroboration of calcium complex **XI** with 9–BBN to give the calcium borate, **Xa**, and the borylated amine, **Xb**.

The calcium hydridoborate, **IXa**, generated in both of the reactions (Scheme 1.11 and Scheme 1.12) can be viewed as an adduct between **Ii** and half an equivalent of 9–BBN. While this product has the potential to exhibit interesting onward reactivity, the side products of these reactions were judged to be of greater significance, as both compounds **Xa** and **Xb** represent the construction of a new N–B bond via σ–bond metathesis between Ca–N/B–H.[34]

Although these chemistries were not extended into a catalytic regime, it can be envisaged that the generation of the calcium hydridoborate, **IXa**, could react with further equivalents of either Ph_2NH or $(Me_3Si)_2NH$ and 9–BBN to catalytically generate new B–N

containing compounds through a dehydrocoupling reaction. This reactivity could be further exploited, incorporating the conventional insertion chemistry of the alkaline earth metals in conjunction with the Ae–N/B–H σ–bond metathesis explored in this report.[34]

1.5.1 Amine–Borane Dehydrocoupling

The chemistry of metallated amidoborane derivatives and their role in the catalytic heterodehydrocoupling of B–H and N– H moieties has been significantly extended during the last decade. The attractive properties of ammonia borane, $H_3N{\cdot}BH_3$, as a potential hydrogen storage material,[33, 35] initially drove the metal centred dehydrocoupling reactivity of primary and secondary organoamine derivatives ($RH_2N{\cdot}BH_3$ and $R_2HN{\cdot}BH_3$). This has provided a plethora of mechanistic information as model systems for ammonia borane dehydrocoupling.[36] The furthest advances have been based around the study of mid or late transition metals and only recently with alkaline earth mediated systems. An initial report by Harder based on **Ii** and a stoichiometric equivalent of ammonia borane led to the facile formation of a calcium amidoborane complex that upon exposure to elevated temperatures led to a dehydrocoupling reaction (Scheme 1.13).[37] It was also found that using a stoichiometric equivalent of the more sterically demanding, $DippNH_2{\cdot}BH_3$, led to facile dehydrocoupling but only yielded a monomeric β–diketiminato calcium $DippNHBH_3$ complex. Repeated attempts at elevated temperatures failed to couple the amine borates together, most likely as a result of the increased steric bulk of the Dipp groups (Scheme 1.13).[38] While these reports are restricted to stoichiometric reactions, based on these observations catalytic reactions could be envisaged.

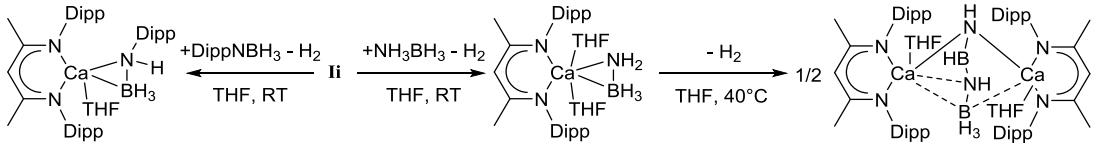

Scheme 1.13: Dehydrocoupling reactions between **Ii** and amine boranes.

A report by Hill and co–workers disclosed that both homo– and heteroleptic alkyl and amide complexes of the alkaline earth elements Mg and Ca are active catalysts for the dehydrocoupling of dimethylamine borane (DMAB), Scheme 1.14.[39]

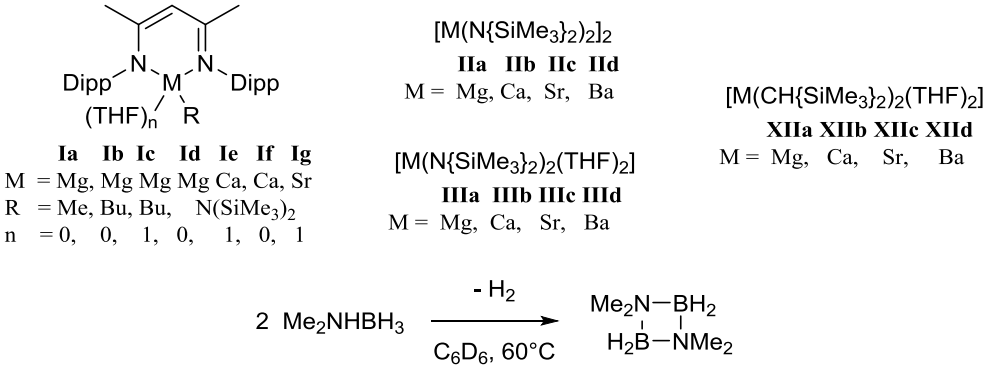

Scheme 1.14: Catalytic dehydrocoupling of DMAB at 60ºC in benzene by alkaline earth pre–catalysts **Ia** – **IIId** and **XIIa** – **XIId**.[39–40]

An initial stoichiometric reaction between either of the magnesium complexes, **Ia** or **XIIa** and two or four equivalents of DMAB, respectively afforded compounds, **XIIIa** and **XIIIb**, containing the $[H_3BNMe_2BH_2Me_2N]^-$ ion. The ligand coordinates to the metal centres through a combination of Mg–N and Mg···HB interactions in both solution and solid states as identified by crystallographic and heteronuclear NMR experiments, Scheme 1.15.[39]

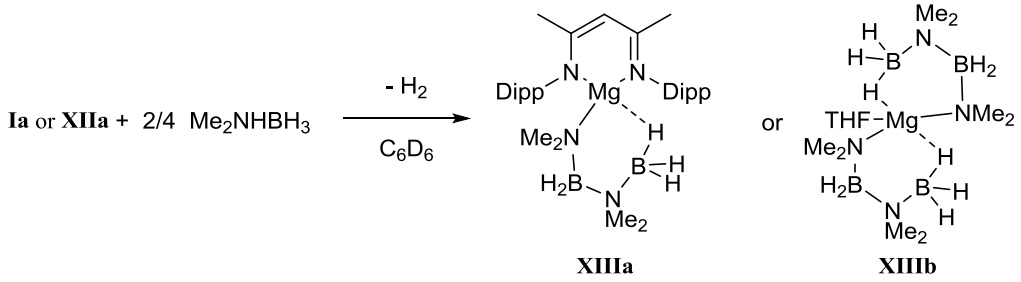

Scheme 1.15: Addition of either two or four equivalents of DMAB to **Ia** or **XIIa** respectively.

Thermolysis of both **XIIIa** and **XIIIb** at 60ºC liberated the cyclic borazane, $[(H_2BNMe_2)_2]$ and, it was proposed, a magnesium hydrido species by an unprecedented δ–hydride elimination process.[39] Extension to the heavier calcium and strontium homo– and heteroleptic alkyl and amide complexes, however, afforded the simple amidoborane derivative containing the $[H_3BNMe_2]^-$ ion. Increasing the stoichiometry of the reaction only led to catalytic dehydrocoupling of DMAB.[39–40] A proposed catalytic cycle was disclosed accounting for these experimental observations, based on a series of N–H/M–H metathesis and B–H/M–N β– or δ– elimination steps, Scheme 1.16.

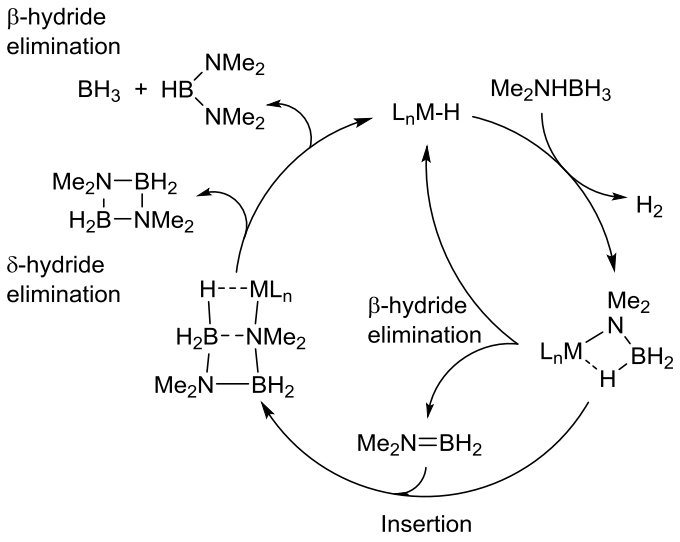

Scheme 1.16: Proposed catalytic scheme for amine borane dehydrocoupling.

Most notable in this chemistry was the rate–dependence of the amine borane dehydrocoupling upon metal identity, with an increase in cation charge density (Ba < Sr < Ca < Mg) yielding increasingly efficient dehydrocoupling. Further validation of this postulate was evidenced by the observation that the even greater charge density of the Sc^{3+} ion provided a rate of catalytic DMAB dehydrocoupling well in excess of that of magnesium.[41]

Moving beyond the dehydrocoupling of amine boranes, the sole precedent for the coupling of an amine and monohydrido borane arises from the initial report by Hill and co–workers, between **XI** and 9–BBN (Section 1.5, Scheme 1.12) that undergoes a dehydrocoupling reaction yielding a calcium borohydride **IX**, and the formation of a new B–N bond, **Xb**.[34] These chemistries were further explored by the Hill group, in an initial assessment of the catalytic activity of 10 mol% **Ib** and **Ie** with diethylamine and the commercially available pinacolborane (HBpin) Scheme 1.17.

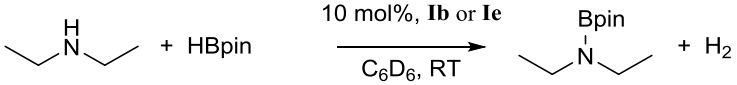

Scheme 1.17: Dehydrocoupling of diethylamine and HBpin catalysed by **Ib** and **Ie**.

Both **Ib** and **Ie** are competent catalysts for this dehydrocoupling reaction, however, the magnesium based system provided superior reactivity and subsequently all further reactivity reported was based on the pre–catalyst **Ib**. A plethora of primary amines and either HBpin or 9–BBN were exposed to 10 mol% **Ib** at room temperature, which led to a facile dehydrocoupling reaction Scheme 1.18.

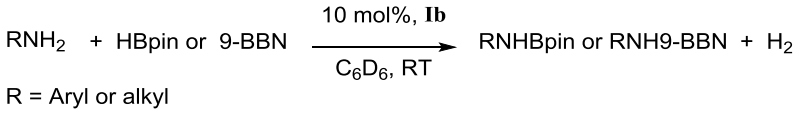

Scheme 1.18: Boron–nitrogen dehydrocoupling catalysed by **Ib**.

In situ monitoring by ^{1}H NMR spectroscopy of the reaction between *N*–methyl aniline and either HBpin or 9–BBN catalysed by 10 mol% **Ib** delineated a considerable mechanistic variance across the two reactions. These observations were attributed to the significant differences in Lewis acidity of the boron centres between 9–BBN and the deactivated HBpin. In the case of 9–BBN, the increased Lewis acidity of the boron atom allowed for the isolation of a magnesium hydridoborate **IXb**, analogous to the aforementioned calcium hydridoborate **IXa**. Experimental observations suggested that **Ih** and **IXb** (Scheme 1.19, (a)) are in equilibrium, favoured towards **IXb**. In contrast, **Ih** and **IXc** (Scheme 1.19, (b)) are in equilibrium favouring **Ih** and this rationale explains the increased activity of the HBpin system.[42]

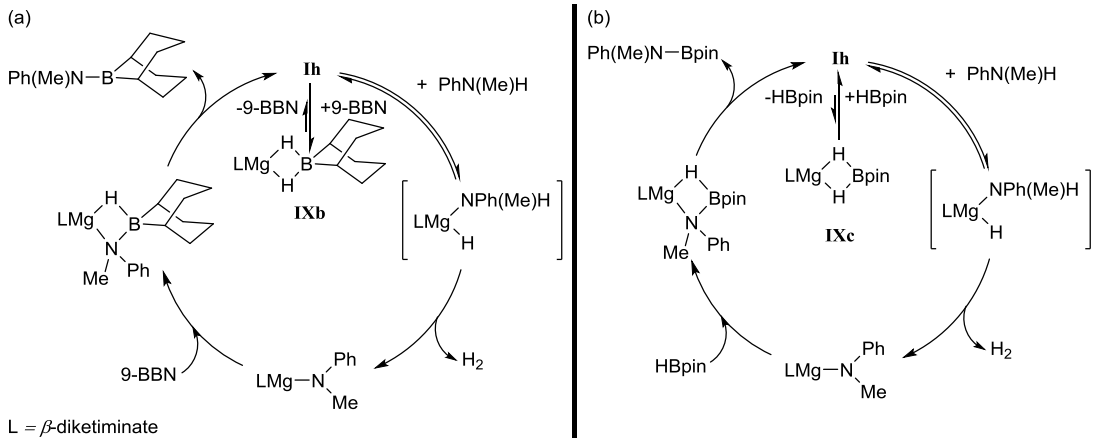

Scheme 1.19: Proposed mechanism for **Ib** catalysed dehydrocoupling of *N*–methyl aniline and 9–BBN (Left) or HBpin (Right).

1.5.2 Silicon–Nitrogen Dehydrocoupling

An initial report by Harder and co–workers demonstrated the ability of a calcium metalla azacyclopropane pre–catalyst for the Si–N dehydrocoupling between a variety of silanes and amines.[43] More recently, Sadow and co–workers have performed an in–depth study into the dehydrocoupling of amines and silanes mediated by the trisoxazolinylborate magnesium pre–catalyst, **V**.[5b] This reaction was postulated to occur *via* a manifold similar to that shown in Scheme 1.20, and allows access to a range of silazanes in excellent yields.

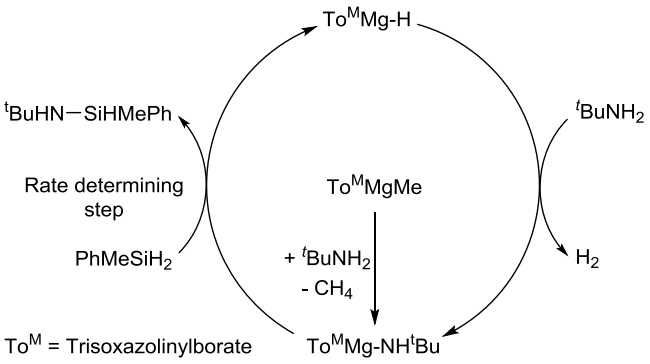

Scheme 1.20: Proposed catalytic cycle for silicon nitrogen dehydrocoupling.

Kinetic studies employing deuterated methyl phenyl silane provided a negligible kinetic isotope effect (k_H / k_D = 1.0(2)) indicating limited involvement of Si–H cleavage in the rate determining step. A Hammett plot with a moderate positive slope was interpreted to suggest a rate determining transition state involving a five–coordinate silicon centre, due to the stabilising effects of electron withdrawing moieties on this species. This observation was suggested to favour a limited degree of Si–H cleavage in the transition state, whereby increasingly electron–withdrawing aryl substituents would disfavour hydride transfer to the magnesium centre. On this basis, Sadow postulated nucleophilic attack of the magnesium amide on silane as the rate determining process of the catalysis. This was followed by rapid hydride transfer, reminiscent of β–hydride elimination, to provide the neutral silazane product.[5b]

In a similar manner, the homoleptic alkaline earth amides, **IIIa** – **IIIc**, have been established as active pre–catalysts for the dehydrocoupling of Si–H and N–H bonds. Although reactions performed with all three pre–catalysts presented a number of common features, variations in overall reaction order, mode of pre–catalyst activation and nature of the rate determining step were postulated to arise as a consequence of the marked variations in the ionic radii of the Ae^{2+} ions observed upon descending the group, concurrent with an increase in polarisability and electropositivity.[44]

A recent report has also employed the anildo–imine alkaline earth amide species, **IVa–IVc**, as very active and productive pre–catalysts (Ca < Sr < Ba) for N–H/H–Si dehydrocoupling, Scheme 1.21. Density Functional Theory (DFT) investigations again suggested that the experimentally observed process is best described as a nucleophilic attack of a metal amide on the incoming silane and subsequent turnover limiting hydrogen transfer to the metal centre.[45]

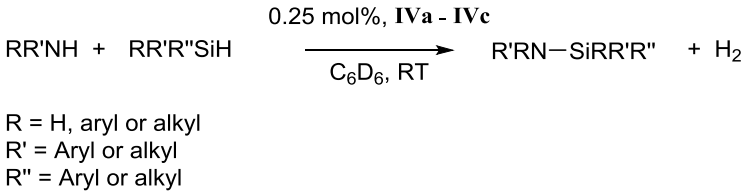

Scheme 1.21: Dehydrocoupling of amines and silane by **Iva** – **IVc**.

1.5.3 Boron–Nitrogen Desilacoupling

All of the above advances providing new element–element bonds, without exception have been achieved through the catalytic dehydrocoupling of E–H and E–H or E–H and E'–H substrates and concomitant elimination of dihydrogen. This constraint was overcome in a recent report by Hill and co–workers of the catalytic 'desilacoupling' of a range of amines, RR'NH (R = alkyl or aryl, R' = H, alkyl or aryl) and pinBSiMe$_2$Ph, employing alkaline earth pre–catalysts, **IIIa** – **IIIc** (Scheme 1.22).[46]

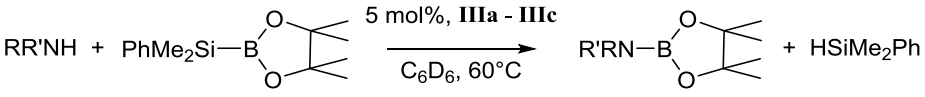

Scheme 1.22: Catalytic desilacoupling of a range of amines by **IIIa** – **IIIc**.

A stoichiometric reaction involving the *β*–diketiminato magnesium complex, **Ib**, and an equimolar quantity of pinBSiMe$_2$Ph produced the first reported three coordinate magnesium silyl complex as identified by both X–ray and multinuclear NMR spectroscopy. However, no further reactivity between the magnesium silyl and diethyl amine was observed, rationalised as a result of the sterically encumbered *β*–diketiminate ligand. A catalytic cycle was rationalised to be a result of the both the basic character of the Si–Mg moiety and the ability of boron to attain a hypervalent 4–coordinate geometry during the assembly of the B–N bond forming reaction step, Scheme 1.23.

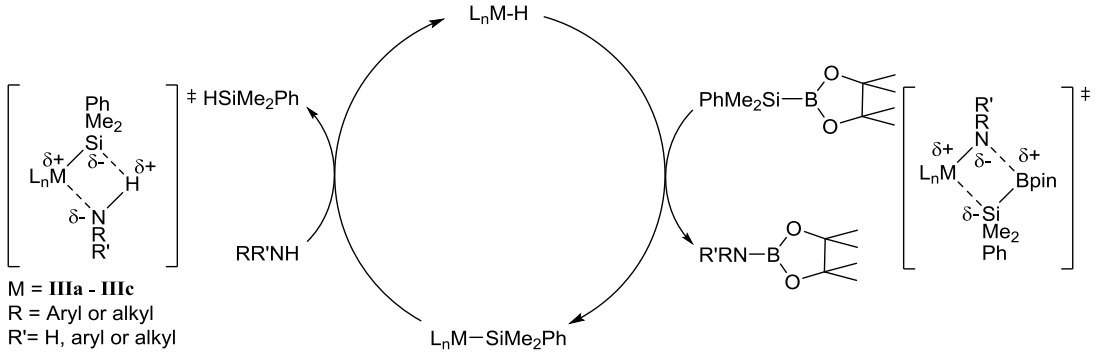

Scheme 1.23: Proposed alkaline earth mediated boron–nitrogen desilacoupling reaction.

While this reactivity produces a stoichiometric quantity of Me_2PhSiH, that did not display any onward reactivity, it does provide the first example of a catalytic main–group element–element coupling that is not dependent of the concurrent elimination of dihydrogen. This work potentially lays the foundation for the development of a more generalised set of substrate design principals, which could greatly expand the scope of main–group catalysed reactivity.[46]

1.6 Magnesium Mediated Hydroboration Reactions

1.6.1 Hydroboration of Pyridines

Dearomatisation of pyridine and its derivatives can provide access to a plethora of functionalised molecules primed for further transformations.[47] Although it is well known that stoichiometric addition reactions of alkali metal hydrides and alkyls give rise to reducing dihydropyridide derivatives,[48] the harsh conditions employed and the relative instability of the dearomatized products does not necessarily lend itself to extension into a more attractive catalytic regime. Reports of homogeneous catalytic transformations of this nature are scarce, limited to an initial report of titanocene–based pyridine hydrosilylation by Harrod and a more recent description of ruthenium centred process by Nikonov and co–workers.[49]

An initial stoichiometric reaction by Hill and co–workers, of **Ib** and phenylsilane in the presence of pyridine derivatives was reported to yield simple dearomatised dihydropyridide species, **XIV**,[27a] Scheme 1.24. However, all attempts to incorporate this reactivity into a catalytic scenario were unsuccessful.[50]

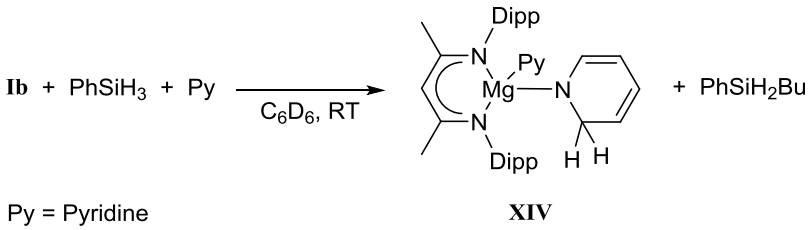

Scheme 1.24: Stoichiometric dearomatisation of pyridine with **Ib** and phenylsilane.

In the absence of catalytic reactivity for the silane based systems, attention turned to the hydroboration of pyridine with HBpin, in the hope that the Lewis acidic boron centre would more effectively compete for access to the Mg–N bond. Addition of one equivalent of HBpin and **Ib** to a solution of pyridine resulted in the formation of an orange solution, which provided a ^{1}H NMR spectrum effectively identical with that observed for the previously reported magnesium dihydropyridide spices, **XIV**.[50] Addition of a further equivalent of HBpin

resulted in the observation of a new singlet resonance at *ca.* δ 1 ppm with a relative 12H integration in the ^{1}H NMR spectrum, which was attributed to the formation of dearomatised and hydroborated pyridine, Scheme 1.25.

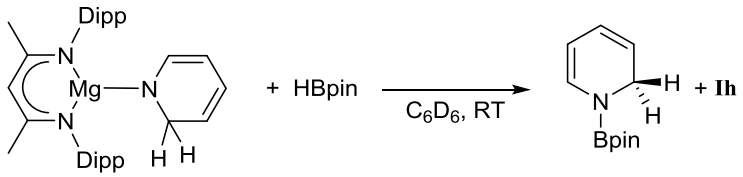

XIV

Scheme 1.25: Stoichiometric reduction of **XIV** with HBpin to yield hydroborated dehydropyridine and regenerate **Ih**.

This reactivity was subsequently incorporated into a catalytic regime that was applied to a plethora of subsisted pyridines and broadly provided the facile dearomatisation hydroboration. This protocol, however, displayed poor functional group tolerance, preferentially resulting in the hydroboration of polar functionalites over dearomatisation, thus, only these reactions will be discussed herein.

In the case of aldehyde or ester functionalities, instead of forming the dearomatised species, HBpin was observed to add across the carbonyl double bond (Scheme 1.26, (a)) and, in the case of methyl nicotinate, complete rupture of the C–O bond was observed to occur yielding a methylboronester, Scheme 1.26, (b).

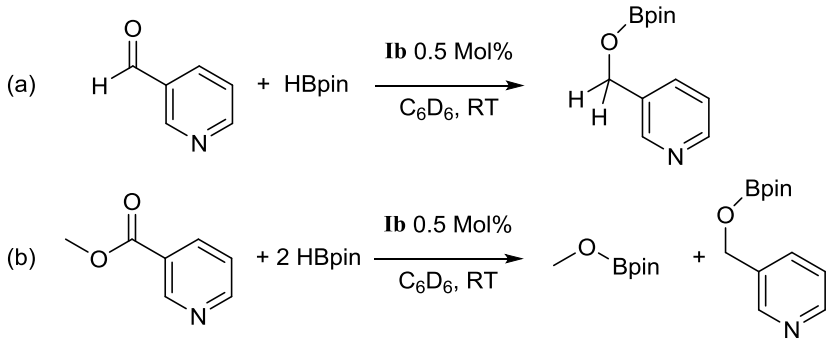

Scheme 1.26: (a) Catalytic hydroboration of the aldehyde function of nicotinaldehyde. (b) Catalytic hydroboration of the aldehyde function of methyl nicotinate.

Similar reactivity was also observed with nicotinonitrile whereby the C≡N unit was completely reduced by two equivalents of HBpin at room temperature (Scheme 1.27), to provide the bis(borylated)amino pyridine.

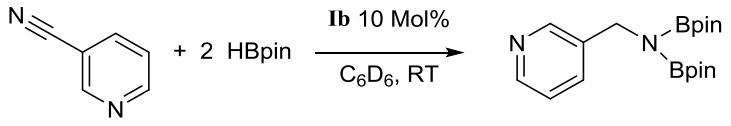

Scheme 1.27: Catalytic hydroboration of the aldehyde function of nicotinonitrile.

While this study by Hill and co–workers does provide a novel route to dihydropyridide species utilising the magnesium catalyst **Ib**, the poor functional group tolerance of the regime also evidenced the potential for new catalytic transformations.

1.6.2 Hydroboration of Imines

Imines are readily available from condensation of carbonyl compounds and primary amines and are, thus, precursors of choice for the synthesis of unsymmetrically substituted secondary amines.[51] Although the catalytic hydrogenation of imines provides an effective means for the reduction of the C=N double bond, the synthetic utility of these reactions can be restricted by issues of selectivity and low product yields. Similarly, the heterogeneous nature and consequent poor selectivity of borohydride reducing agents such as $NaBH_4$, has led to the development of a profusion of homogeneous late transition metal catalysts.[51e–g] Reduction with homogeneous hydride sources, such as boranes[52] to afford the corresponding hydroboration products is also gaining prominence over the traditional use of molecular hydrogen[53] owing to the necessary milder reaction conditions and higher selectivity, especially in the asymmetric reduction of prochiral imines.

Pyridines may be viewed as aromatised cyclic imines, thus, research by Hill and co–workers focused on extending the catalytic hydroboration protocol of **Ib** to the imine function. An initial trial reaction between HBpin and PhCH=NPh in the presence of 5 mol%, provided quantitative conversion to the hydroborated amine product within 10 minutes at room temperature (Scheme 1.28), identified by the characteristic methylene singlet resonance at δ 4.76 ppm with a relative 2H integral in the ^{1}H NMR spectrum.

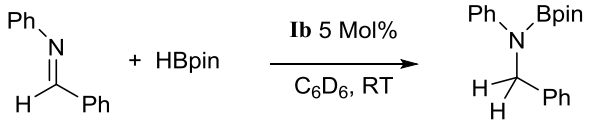

Scheme 1.28: Ib catalysed hydroboration of *N*–diphenylmethanimine.

Encouraged by this result, a broad range of imine substrates were synthesised and their activity towards hydroboration catalysed by **Ib**, was assessed. A representative sample of the imines investigated are displayed in Table 1.2.

Table 1.2: Sample of **Ib**–catalysed hydroboration of substituted imines, reported by Hill and co–workers.[54]

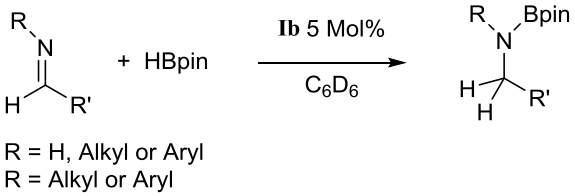

Entry	R	R′	Time (h)	T (°C)	NMR Conv. (%)
1	Ph	Ph	0.2	25	>99
2	^{n}Bu	Ph	1	25	92
3	Bn	Ph	0.5	25	90
4	3–Py	Ph	8	50	93

Compound, **Ib**, was observed to be an efficient pre–catalyst for the hydroboration of a broad range of imine substrates under mild conditions. Kinetic and stoichiometric studies found the reaction to occur through magnesium hydride and amide intermediates, which are formed by consecutive Mg–N/B–N metathesis and C=N/Mg–H insertion steps and the facility of which is strongly influenced on the basicity and steric demands of the imine substrate.[54]

1.6.3 Hydroboration of Nitriles

The reduction of nitriles can be achieved thought the use of stoichiometric quantities of main group reducing agents such as $LiAlH_4$.[55] The flammable nature of these reagents, however, coupled with large amounts of inorganic waste by–products, renders them unattractive. Whilst nitrile hydrogenation provides a direct route to the desired amine product, reductive hydroboration can be advantageous in the provision of further functionality to the resultant amine.[56] With these considerations in mind Hill and co–workers described a magnesium–centred protocol for the hydroboration of organic nitriles with HBpin.[57]

An initial reaction using 10 mol% of **Ib** with respect to one equivalent of propionitrile and two equivalents of HBpin at room temperature proceeded slowly. Warming the reaction to 60°C provided quantitative conversion to the 1,1–bis(boryl)amine product within 30 minutes. Clean formation of the catalytic product was evidenced through the emergence of a triplet methylene resonance in the ^{1}H NMR spectrum at δ 3.42 ppm, with an integral of 2H,

concomitant with a new singlet signal in the ^{11}B NMR spectrum at δ 29.5 ppm. Encouraged by this result, the substrate scope was extended to a range of commercially available organic nitriles, Table 1.3.

Table 1.3: Catalytic dihydroboration of organonitriles with HBpin and 10 mol% of **Ib**.

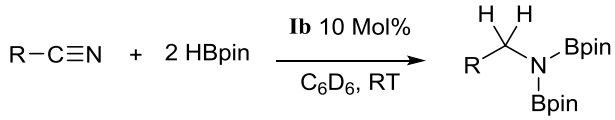

Entry	R	Time (h)	NMR yield (%)	Isolated Conv. (%)
1	Et	0.5	99	70
2	^{i}Pr	1	93	96
3	^{t}Bu	5.5	97	54
4	Cy	1	94	75
5	C_6H_5	12	92	56
6	*o*–(Me)C_6H_4	15	86	73
7	*m*–(Me)C_6H_4	15	87	81
8	*m*–(F)C_6H_4	14	88	57
9	*m*–(MeO)C_6H_4	15	90	60
10	*p*–(Me)C_6H_4	13	91	72
11	*p*–(F)C_6H_4	12	94	61
12	*p*–(Cl)C_6H_4	12	93	59
13	*p*–(CF_3)C_6H_4	12.5	89	76
14	*p*–(MeO)C_6H_4	13.5	88	58
15	Ph_2CH	30	75	43

Catalysis was hypothesised to require the consumption of two molecules of HBpin and the intermediacy of an initial magnesium bound imide, a borylated imine as the product of initial B–H/Mg–N metathesis and amide species formed by formal Mg–H insertion of the borylimine. While this initial proposal provided a common mechanism for all nitriles, a series of kinetic experiments utilising both electron donating and withdrawing aryl nitrile substitutions and alkyl nitriles evidenced significant variability across the range of substrates. The differing kinetic profiles for the three substrate classes was rationalised as the result of a series of substrate dependant pre–equilibria established during the multi–step catalytic reaction. Scheme 1.29, depicts a catalytic mechanism that allows discrimination of divergent turnover limiting behaviour for (a) aryl nitriles with electron withdrawing groups, (b) aryl nitriles with electron donating substitutions and (c) alkyl nitriles.

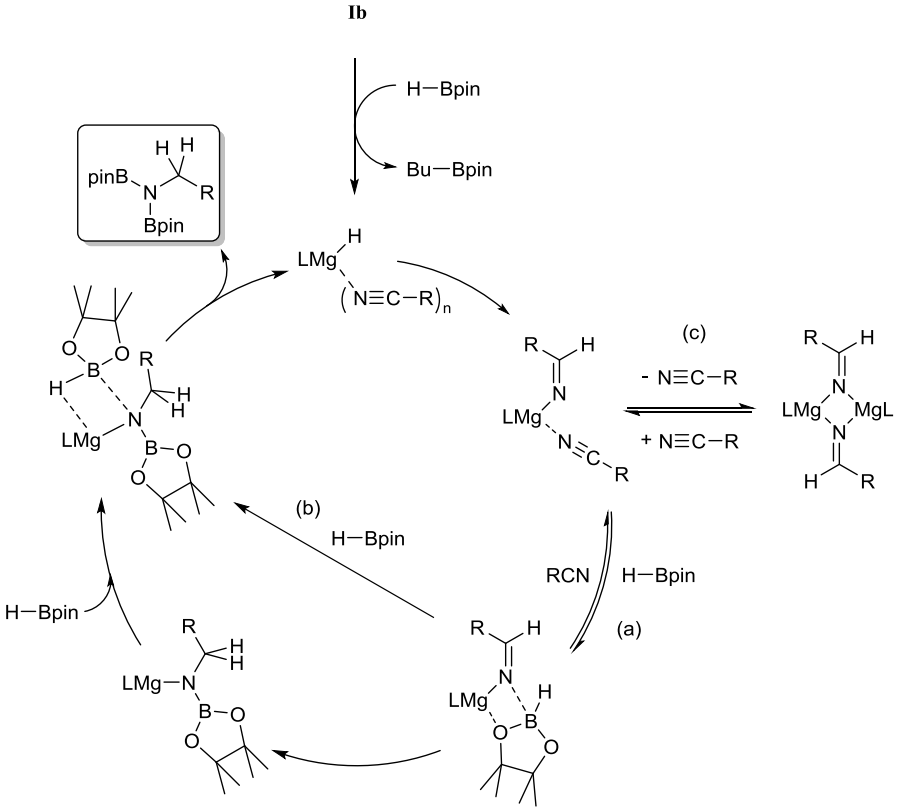

Scheme 1.29: Compound **Ib** is a selective pre-catalyst for the reductive hydroboration of organic nitriles with pinacolborane. Kinetic studies highlighted mechanistic variation for electron donating and withdrawing substituents.[57]

The more basic character of electron withdrawing alkyl nitriles ensure that the monomer/dimer equilibrium ((c), Scheme 1.29), favours the monomeric species. The catalytic hydroboration of alkyl nitriles is instead reported to be determined by the pre–equilibrium, (a), between the monomeric magnesium imide and the aldimidohydridoborate anions and

subsequent consumption through B–H transfer to the coordinated aldimide moiety, Scheme 1.29. The observed rate of catalysis for alkyl nitrile hydroboration is dictated by both the ability of HBpin to replace a nitrile in the magnesium coordination sphere and also the subsequent ease of intramolecular C=N hydride reduction.

Whilst both electron donating and withdrawing aryl nitriles are prone to the aforementioned monomer–dimer pre–equilibria, magnesium aldimide derivatives bearing electron donating *N*–aryl substitution will benefit from enhanced conjugative stability, and consequent, increased resistance to the intramolecular hydride transfer of the aldimidoborate. The conjugative stability of the resultant aldimidoborate toward intramolecular C=N reduction suggests that sequential reactions are inoperable for these intermediates. Instead an alternative pathway involving a further molecule of HBpin induces hydride transfer and allows for catalytic turnover, ((b), Scheme 1.29).

Aryl nitrile insertion into the Mg–H bond provides a dimeric aldimide that is maintained in solution, ((c), Scheme 1.29). Absence of a kinetic isotope effect in the reactions of electron withdrawing aryl nitriles utilising DBpin/HBpin demonstrated that the rated determing process was entirely dependent on the ability of the weakly basic nitrile to coordinate to the magnesium centre and rupture the dimer allowing for catalytic turnover.[57]

The catalytic hydroboration of nitriles utilising **Ib** is, thus, critically dependant on a variety of pre–equilibria dictated by minor variations in substrate basicity and stability of monomer/dimer intermediates. These observations highlight that there is likely to be considerable variation across even superficially identical reactions when catalysed by alkaline earth reagents.

1.6.4 Hydroboration of Isonitriles

The reactivity of organic isonitriles is dictated by their ability to behave as both nucleophile and electrophile. A plethora of metal–catalysed multicomponent condensations have been shown to yield complex and medicinally relevant nitrogenous structures. In contrast, the reductive heterofunctionalisation of isonitriles appears to be solely represented by Figueroa and Hill,[58] despite the relevance to Fischer–Tropsch (F–T) reactivity arising from the isoelectronic relationship of the isonitrile moiety and carbon monoxide (CO).

Figueroa and co-workers recently reported that the uncatalysed stoichiometric hydroboration of *m*–terphenylisocyanide with 9–BBN afforded the fully reduced 1,2–diborylated amine, whilst use of a substoichiometric half equivalent of 9–BBN provided the boryl(imino)methane 1,1–hydroboration product, Scheme 1.30.[59] A similar reaction was

carried out using the less Lewis acidic HBpin, from which the sole product was the singly reduced boryl(imino)methane even under the more forcing conditions with a tenfold excess of HBpin at 100°C.[59]

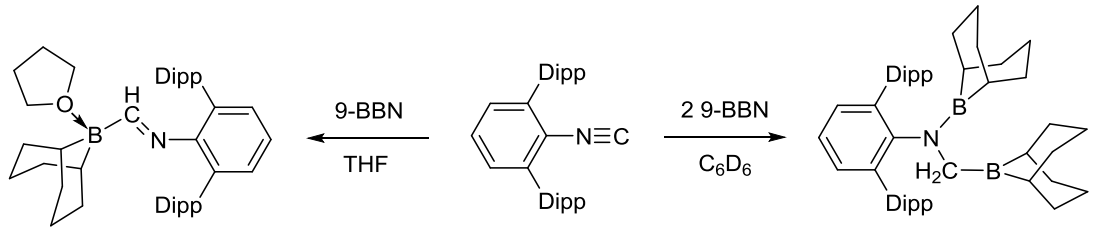

Scheme 1.30: Uncatalysed hydroboration of *m*–terphenylisocyanide with 9–BBN.

Following the report of the hydroboration of nitriles,[57] Hill and co-workers described the catalytic hydroboration of isonitriles[58] as a natural extension. An initial trial reaction using 5 mol% of **Ib** with cyclohexylisonitrile (CyNC) and two molar equivalents of HBpin proceeded to full consumption of the starting materials within 30 minutes at 60°C, Scheme 1.31.

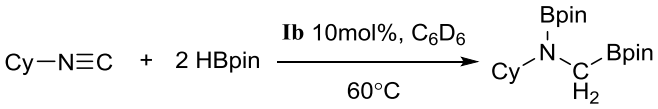

Scheme 1.31: Hydroboration of CyNC with HBpin catalysed by 5 mol% of **Ib**.

Full conversion to the sole *N*–alkylated 1,2–bis(boryl)amine product, CyN(Bpin)CH_2Bpin, was demonstrated by the complete consumption of HBpin in the resultant ^{11}B NMR spectrum and emergence of a single new species characterised by two new signals in a 1:1 ratio at δ 37.5 ppm and δ 27.8 ppm attributed to the formation of two new B–N and B–C bonds. The corresponding ^{1}H NMR spectrum further evidenced complete consumption of CyNC and the appearance of a new methylene singlet resonance at δ 2.81 ppm with an integral of 2H. Notably repetition of the reaction with one equivalent of HBpin only afforded the fully reduced product with half of the isonitrile reagent remaining unreacted. These positive results allowed the reaction scope to expand and include a range of commercially available isonitriles, Table 1.4.

Table 1.4: Magnesium–catalysed, **Ib**, hydroboration of commercially available isonitriles.

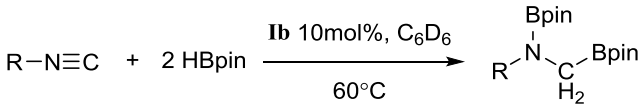

Entry	Isonitrile, RNC (R)	Time (h)	Temperature (°C)	NMR Conv. (%)
1	Cy	1	60	>90
2	1–pentyl	1	60	>90
3	^{t}Bu	1	60	>90
4	Bn	0.5	60	>90
5	2–Napthyl	48	100	55
6	2,6–Dimethylphenyl	48	100	53

A catalytic cycle for the magnesium–catalysed hydroboration of isonitriles was envisaged, Scheme 1.32. While pre–catalyst initiation requires conversion of **Ib** to the magnesium hydride, **Ih**, this species is likely to be very short lived and to undergo rapid insertion by the polarised isonitrile N≡C moiety. A series of kinetic experiments revealed the reaction to be zero order, with the rate of reaction governed solely by the starting concentration of **Ib**. The first order dependences with respect to both isonitrile and borane reagents under pseudo first order conditions are consistent with the resulting perturbation of the respective pre–equilibria depicted as (a) and (b) in Scheme 1.32.

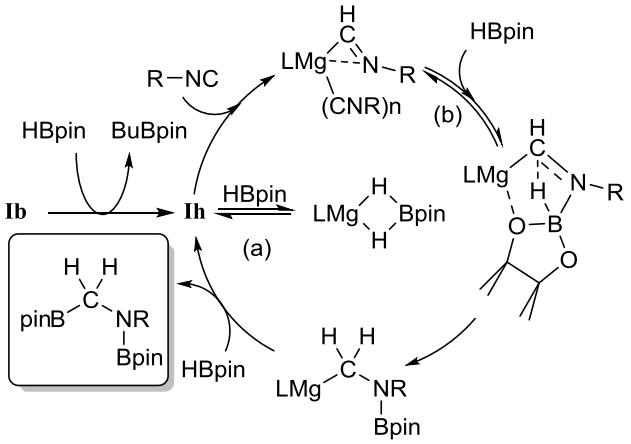

Scheme 1.32: Proposed catalytic cycle for the magnesium–catalysed hydroboration of isonitriles.

1.6.5 Hydroboration of Aldehydes and Ketones

The reduction of aldehydes and ketones to primary and secondary alcohols is one of the most important transformations in organic chemistry. Brown and co–worker's discovery of uncatalysed diborane reduction of aldehydes and ketones in 1939, thus, served to direct research from harsh metal hydride reagents with poor selectivity towards catalytic processes using milder silane and borane hydride sources.[60] In contrast, metal–catalysed hydroboration reactions are relatively uncommon and limited to a handful of heavier group 13,[61] titanium[62] or ruthenium[52h] pre–catalyst.

In 2012 Hill and co–workers reported that the stoichiometric reduction of benzophenone with *in situ* generated **Ih**, by the addition of **Ib** and one equivalent of HBpin in d_6–benzene, resulted in an orange solution, Scheme 1.33. The resultant ^{1}H NMR spectrum suggested the formation of a heteroleptic diphenylmethoxymagnesium species, **XV**, characterised by a singlet resonance at δ 5.98 ppm with a 1H relative integration, resulting from the insertion of the carbonyl functionality into the Mg–H bond.

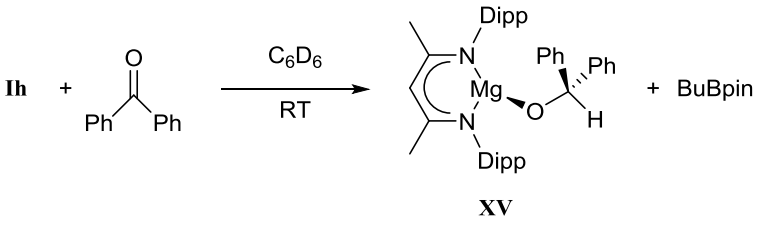

Scheme 1.33: Stoichiometric reduction of benzophenone by *in situ* generated **Ih**.

A preliminary reaction demonstrated that this chemistry could be extended to a catalytic protocol. One equivalent of benzophenone and HBpin with 0.1 mol% of **Ib** in d_6–

benzene, led to the facile production of the diphenylmethoxyborate, in two hours (Scheme 1.34).

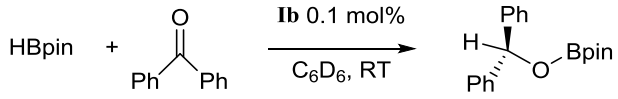

Scheme 1.34: Catalytic reduction of benzophenone with one equivalent of HBpin by **Ib**.

Encouraged by this result, this activity was extended to a range of aromatic and aliphatic aldehydes (1 – 4, Table 1.5) and ketones (5 – 10, Table 1.5) summarised in Table 1.5.

Table 1.5: Hydroboration of commercially available aldehydes and ketones, catalysed by **Ib**.

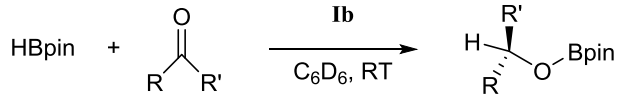

R = aryl or alkyl
R' = H, aryl or alkyl

Entry	R	R′	Cat. (mol%)	Time (h)	NMR Conv. (%)
1a	Ph	H	–	2	2
1b	Ph	H	0.05	0.25	95
2	*p*–(CH=O)C_6H_4	H	0.05	<1	>99
3	2,4,6,–$Me_3C_6H_2$	H	0.5	1.5	96
4	9–anthracenyl	H	0.5	1	97
5	Ph	Ph	0.1	2	98
6	9–fluroenyl		0.1	3	95
7	4–FC_6H_4	4–FC_6H_4	0.1	<1.2	>99

8	Ph	PhC=O	0.1	<2	>99
9	Ph	Me	1	4	94
10	2,4,6,–$Me_3C_6H_2$	Me	1	1.25	91

The catalytic hydroboration of aldehydes with **Ib**, proceeded more rapidly with lower catalyst loadings (Entry 1 – 4, Table 1.5) compared to the more sterically hindered ketones (Entry 5 – 10, Table 1.5), which generally required slightly higher catalyst loadings to achieve similar results.

Based on both the initial stoichiometric results and the facile catalytic activity, a catalytic cycle was envisaged, Scheme 1.35. Catalytic turnover most likely proceeds *via* formation of a catalytically active magnesium hydride species, **Ih**. Insertion of the carbonyl moiety into the Mg–H bond and subsequent σ–bond metathesis with HBpin, regenerates **Ih** and yields the borylated product.

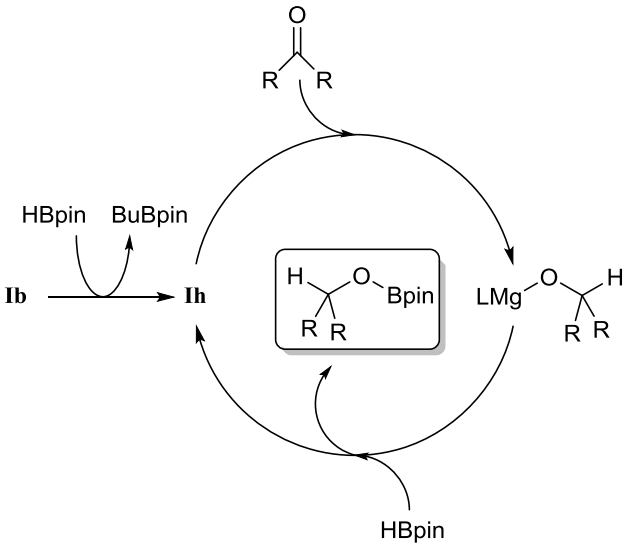

Scheme 1.35: Catalytic aldehyde or ketone hydroboration with **Ib**.

This study demonstrated the propensity of alkaline earth catalysts for the reduction of C=O bond and provided initial insight into the reduction pathways of the related heterocumulenes, (E=C=E′, E = N and E′ = N or O).

1.6.6 Hydroboration of Esters

In contrast to the more extensive ester hydrosilylation literature, few examples of ester hydroboration have been reported.[63] In the aforementioned hydroboration of pyridines (Section 1.6.1), an example of ester cleavage was evidenced but not explored,[63b] attracting the attention of Sadow and co–workers. Ester reduction is thermodynamically more challenging than aldehyde or ketone hydroboration because of the fundamental challenge associated with conversion of oxygenates, utilising highly oxophilic early metal catalysts involves breaking the M–OR bond to complete the catalytic cycle.

A detailed report of the hydroboration of esters catalysed by an alkyl magnesium borate complex, **V**, was provided by the Sadow group. While stoichiometric studies were limited by the instability of the **V** in both hydrocarbon and chlorinated solvents, a plethora of esters were successfully catalytically reduced using two equivalents of HBpin, Scheme 1.36.[64]

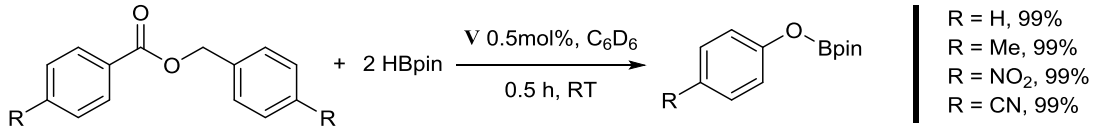

Scheme 1.36: Magnesium complex **V**, catalysed ester hydroboration.

1.6.7 Hydroboration of Carbodiimides

As previously discussed, magnesium–centred multiple bond heterofunctionalisation reactivity may be applied to the addition of HBpin to a variety of multiply bonded and heteroatomic C=E (E = O, NR) and C≡N substrates through the use of the magnesium complex, **Ib**. In contrast to these advances, reports of heteroallene (E=C=E', e.g. E, E' = RN, RN; RN, O) hydroboration are extremely limited. Hill and co–workers addressed this lacuna in 2016, reporting the selective catalytic hydroboration of carbodiimides to the mono reduced formamidine product.[65] It was envisaged that use of **Ib** would enable the construction of the catalytic cycle such as that shown in Scheme 1.37. Catalyst initiation was proposed to occur through B–H/Mg–C metathesis, with a series of subsequent Mg–H/C=N insertion and B–H/Mg–N metathesis steps[27b, 64] to effect the catalytic hydroboration of carbodiimides and the atom–efficient production of *N*–boryl formamidines.

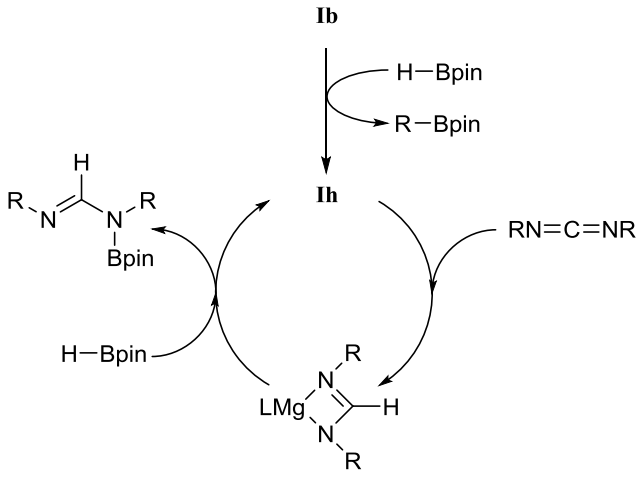

Scheme 1.37: Magnesium–catalysed reactivity of carbodiimides.

Initial investigations focused on catalytic reactions using 10 mol% of **Ib**, with *N*,*N*–diisopropyl carbodiimide and an equimolar equivalent of HBpin at 60°C, Scheme 1.38. This reaction exhibited proficient turnover to give the desired singly reduced *N*–boryl formamidine product within 15 h.

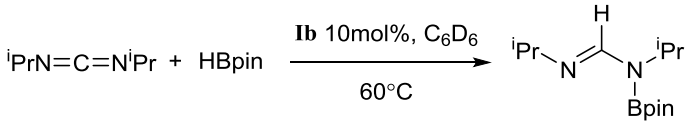

Scheme 1.38: Catalytic reduction of *N*,*N*–diisopropyl carbodiimide with HBpin by **Ib**.

These data were evidenced through the emergence of a singlet resonance at δ 8.23 ppm, integrating to 1H in the resultant ^{1}H NMR spectrum and assigned to the formamidine methane proton (NC*H*N). Concurrently a new singlet resonance in the ^{11}B NMR at 28.5 ppm was assigned to the formation of a new N–Bpin bond. In contrast to these observations, repetition of the reaction with either no **Ib** or two equivalents HBpin at elevated temperatures led to no product formation or solely the singly reduced *N*–boryl formamidine product, respectively.

This observation and the specificity of the reaction led to an expansion of substrate scope to other commercially available carbodiimides. Table 1.6 summarises the results of these catalytic carbodiimide hydroboration reactions utilising 10 mol% of **Ib**.

Table 1.6: Hydroboration of commercially available carbodiimides catalysed by **Ib**.

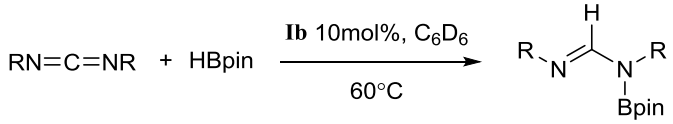

Entry	R, R'	t [h]	T [°C]	NMR Conv. [%]	Isolated Yield (%)
1	^{i}Pr	15	60	90	89
2	Cy	45.5	60	90	69
3	^{t}Bu	60	80	88	87
4	2,6–^{i}Pr$_2$C$_6$H$_4$	24	80	80	77
5	*p*–CH$_3$C$_6$H$_4$	15	80	81	63
6	^{t}Bu, Et	20	60	75	87
7	(CH$_2$)$_3$NMe$_2$, Et	5.5	60	90	87

N,*N*–dialkyl carbodiimides with lower overall steric demands provided efficient turnover to the desired borylated formamidine products, in a manner reminiscent of the previously described magnesium catalysed hydroboration reactivity in this Chapter. Increasing the steric bulk of the R group induced prolonged reaction times and, in some instances, required increased reaction temperatures. Notably, in all cases, a maximum of 90% conversion could not be surpassed for any of the attempted catalytic reactions, even with extended heating.

A series of stoichiometric reactions, provided insight into the mechanism of this catalytic reaction. Magnesium complex **Ih**, was utilised in the stoichiometric reactions owing to its assignment as the catalytically active species. Reaction of **Ih** and ^{i}PrN=C=N^{i}Pr, thus, gave the expected formamidinate insertion product, **XVI**, (Scheme 1.39) which was readily identified in the resultant ^{1}H NMR spectrum through the appearance of a characteristic methine singlet resonance at δ 7.77 ppm and comparison to the previously described complex reported by Jones and co–workers for the CyN=C=NCy insertion reaction with **Ih** (δ = 7.85ppm).[32] Addition of a stoichiometric equivalent of HBpin to compound **XVI** was expected to provide evidence for the final σ–bond metathesis reaction, completing the catalytic cycle,

Scheme 1.37. Surprisingly this was not observed, rather both multinuclear NMR spectroscopy and a single crystal X–ray diffraction experiment divulged the formation of a five–coordinate magnesium species, **XVII**, in which three of the coordination sites are occupied by the bidentate *β*–diketiminate ligand and the imino nitrogen of the singly hydroborated carbodiimide. The magnesium coordination number is further augmented by the coordination to the oxygen of the pinacolate fragment and through an additional interaction with the hydride of the HBpin moiety.

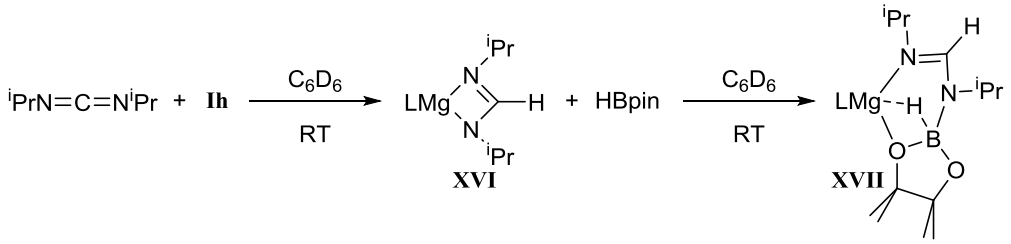

Scheme 1.39: Synthesis of formamidinate insertion product **XVI** and hydroborate complex **XVII**.

Attempted hydride elimination and re–formation of **Ih** and the borylated product, through prolonged heating of **XVII** in C_6D_6 at 80°C was unsuccessful. Onward reactivity reminiscent of catalytic turnover could only be achieved though addition of further stoichiometric equivalents of both HBpin and ^{i}PrN=C=N^{i}Pr. The stability of compound **XVII** and the requirement for both additional HBpin and ^{i}PrN=C=N^{i}Pr to achieve turnover, allowed the renationalisation of the maximum conversion of 90 % observed during the catalytic studies performed with 10 mol% of pre-catalyst, **Ib**. In mitigation of this hypothesis, a further catalytic reaction between HBpin and ^{i}PrN=C=N^{i}Pr using 10 mol% of **XVII** provided an identical level of reactivity to that exhibited by **Ib** indicating that this species represents a likely intermediate during the course of the catalysis.

1.7 Carbon Monoxide Reduction

The deoxygenative conversion of CO to hydrocarbon fuels and lower oxygenates is typically achieved through heterogeneous catalytic methods.[66] Although Fischer-Tropsch (F–T) chemistry and related processes have been successfully implemented for some eighty years to produce a Schultz–Flory distribution of hydrocarbons, only limited success has been achieved with well–defined homogeneous systems at CO pressures typically in excess of 1000 atm.[67]

The desirability of a homogeneous analogue of the eighty year old F–T synthesis has been questioned. There is a general consensus concerning the need for the catalysis of CO and H_2

to oxygenates such as alcohols, esters and carboxylic acids. The conversion of CO and H_2 to water and saturated hydrocarbons is thermodynamically favoured over oxygenates. Hence a key factor needed in new catalysis is selectivity, and it is here that homogeneous systems could play an important role. In this vein extensive studies have been carried out on the hydrogenation of CO by transition metal and lanthanide hydride complexes

1.7.1 Reductive Coupling of Carbon Monoxide

In 1976 Bercaw reported that the facile reaction between the zirconium hydride complex, **XVIII**, and one atmosphere of CO in toluene at room temperature led to the formation of a *trans*–endiolate complex, **XIX** (Scheme 1.40).[68] Repetition of this reaction with ^{13}CO afforded the isotopomer with ^{1}H NMR spectral data displaying a AA′ XX′ pattern centred at δ 6.55 ppm, attributed to the hydrogen nuclei of the *trans*–enediolate moiety. No further compounds were isolated or identified by NMR spectroscopy during the study of this reaction, however, the synthesis of **XIX** was thought to occur through a transition state involving a zirconium formyl species, **XX**, Scheme 1.40.

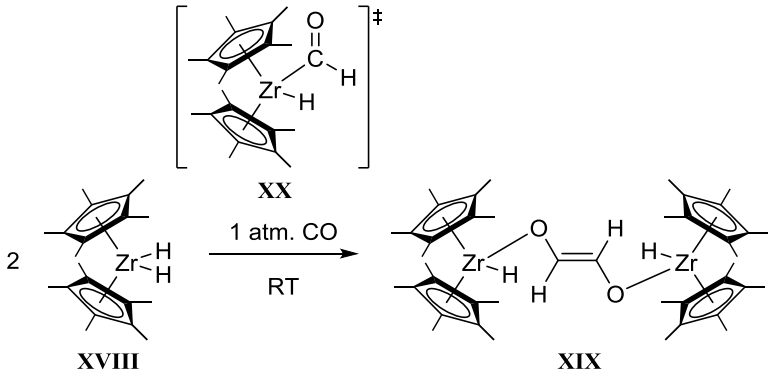

Scheme 1.40: Reduction of CO by zirconium hydride complex **XVIII**.[68]

A related study by Marks and co–workers,[69] with a thorium hydride, **XXI**, also displayed similar CO homologation reactivity to the aforementioned zirconium hydride, **XXIII**, affording the thorium *cis*–enediolate **XXII**, Scheme 1.41. However, these manipulations were performed at –80°C in d_8–toluene and followed by both ^{1}H and $^{13}C\{^{1}H\}$ NMR spectroscopy, which allowed for the identification of a reaction intermediate, **XXIII**, Scheme 1.41. This intermediate was identified as a thorium formyl species, **XXIII**, characterised by the doublet formyl resonance at δ 15.2 ($^{1}J_{CH}$ = 114 Hz) ppm in the ^{1}H NMR spectrum with an accompanying highly deshielded carbenic resonance at δ 372 ppm in the $^{13}C\{^{1}H\}$ NMR spectrum that displayed a doublet resonance (δ 372 ppm, $^{1}J_{HC}$ = 114 Hz) in the ^{1}H–^{13}C gated spectrum.

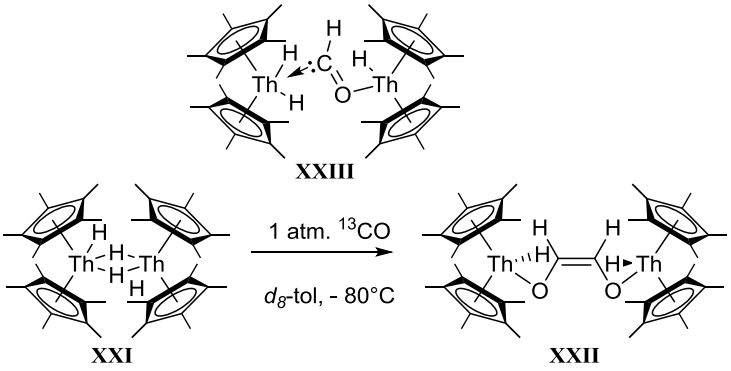

Scheme 1.41: Reduction of ^{13}CO by a thorium hydride complex **XXI**.[69]

A more recent study by Andersen and co–workers,[70] with a cerium hydride, **XXIV**, and one equivalent of CO at room temperature in toluene, afforded a cerium oxomethylene complex, **XXV**, (Scheme 1.42) in which the formaldehyde dianion bridges the two cerium centres.

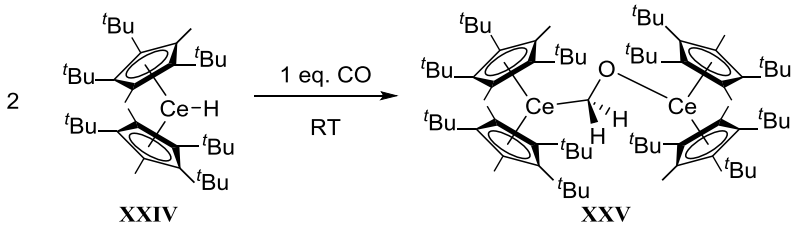

Scheme 1.42: Addition of one equivalent of CO to the cerium hydride, **XXIV**, to give the cerium oxomethylene complex, **XXV**.

Addition of excess CO to **XXIV**, at room temperature in toluene yielded a *cis*–enediolate, **XXVI**, Scheme 1.43. Compound **XXVI** was suggested to form by CO insertion into the Ce–C bond of **XXV**, generating a OCH_2CO unit that undergoes a 1,2–hydrogen shift to form the final *cis*–enediolate complex, **XXVI**. The stereochemistry of the *cis*–enediolate is determined by anti–periplanar bond relative to the carbene lone pair within the OCH_2CO function.[70]

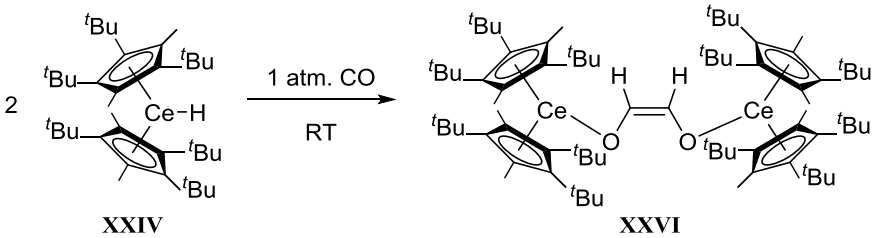

Scheme 1.43: Reduction of CO by cerium hydride, **XXIV**.

This CO homologation chemistry displayed by both transition metals[68] and actinides[69] is encouraging and indicates that these chemistries could be extended to the similarly electropositive d^0 alkaline earth metal hydrides.

1.8 Project Aims

The aim of the research described in this thesis is to investigate the synthetic utility of insertion reactions with group two complexes, specifically towards the activation of the small molecular gas; carbon monoxide. Extension of this group two mediated reactivity into catalytic regimes exploiting both σ–bond metathesis and insertion chemistries with hydride sources such as $PhSiH_3$ or HBpin to generate value added chemicals will also be explored. These investigations will rely upon a combination of synthetic and mechanistic investigations utilising crystallographic determination of solid state structures, NMR spectroscopic analysis of solution structure and kinetic investigations to yield mechanistic insight.

Chapter Two demonstrates that organoisocyanates are readily converted to methyl amines through hydrodeoxygenation with HBpin in the presence of the *β*–diketiminato magnesium catalyst, **Ib**. The reactivity is proposed to occur through the intermediacy of well–defined magnesium formamidato and magnesium boryloxide species.

Chapter Three explores the reaction between both *β*–diketiminato magnesium, **Ih**, and calcium, **Ii**, hydride complexes with carbon monoxide, resulting in the isolation of a dimeric *cis*–enediolate species by the reductive coupling of two CO molecules. Under catalytic conditions with $PhSiH_3$, an observable magnesium formyl species may be intercepted for the mild reductive cleavage of the CO triple bond.

Chapter Four investigates the carbonylation of a range of *in situ* generated *β*–diketiminato Ae–NRR′ (Ae = Mg or Ca, R = H or Me and R′ = H, Alkyl or aryl) complexes, resulting in the isolation of a number of formamidate derivatives including a carbenic formamide dimagnesium species. The hydrodeoxygenation chemistry that was explored in Chapter Two is then extended to the range of isolated compounds providing a novel route to methyl amines, in which carbon monoxide acts as the primary C_1 source during the methylation reaction.

1.9 References

1. a) A. A. Yaroshevsky, *Geochem. Int.*, 2006, **44**, 48–55; b) http://www.infomine.com/investment/metal–prices.
2. a) S. P. Green, C. Jones and A. Stasch, *Science*, 2007, **318**, 1754–1757; b) S. Krieck, H. Görls, L. Yu, M. Reiher and M. Westerhausen, *Journal of the American Chemical Society*, 2009, **131**, 2977–2985.

3. a) M. H. Chisholm, J. Gallucci and K. Phomphrai, *Chemical Communications*, 2003, 48–49; b) M. H. Chisholm, J. C. Gallucci and K. Phomphrai, *Inorganic Chemistry*, 2004, **43**, 6717–6725.
4. B. Liu, T. Roisnel, J.–F. Carpentier and Y. Sarazin, *Angewandte Chemie International Edition*, 2012, **51**, 4943–4946.
5. a) J. F. Dunne, J. Su, A. Ellern and A. D. Sadow, *Organometallics*, 2008, **27**, 2399–2401; b) J. F. Dunne, S. R. Neal, J. Engelkemier, A. Ellern and A. D. Sadow, *Journal of the American Chemical Society*, 2011, **133**, 16782–16785.
6. a) B. A. Vaartstra, J. C. Huffman, W. E. Streib and K. G. Caulton, *Inorganic Chemistry*, 1991, **30**, 121–125; b) M. Westerhausen, M. H. Digeser, B. Wieneke, H. Nöth and J. Knizek, *European Journal of Inorganic Chemistry*, 1998, **1998**, 517–521; c) M. R. Crimmin, A. G. M. Barrett, M. S. Hill, D. J. MacDougall, M. F. Mahon and P. A. Procopiou, *Chemistry – A European Journal*, 2008, **14**, 11292–11295; d) M. Arrowsmith, M. S. Hill and G. Kociok–Köhn, *Organometallics*, 2010, **29**, 4203–4206.
7. a) G. A. Molander and J. A. C. Romero, *Chemical Reviews*, 2002, **102**, 2161–2186; b) P. J. Walsh, A. M. Baranger and R. G. Bergman, *Journal of the American Chemical Society*, 1992, **114**, 1708–1719; c) A. L. Casalnuovo, J. C. Calabrese and D. Milstein, *Journal of the American Chemical Society*, 1988, **110**, 6738–6744; d) J.–J. Brunet, D. Neibecker and K. Philippot, *Tetrahedron Letters*, 1993, **34**, 3877–3880; e) Y. Li and T. J. Marks, *Organometallics*, 1996, **15**, 3770–3772; f) M. R. Gagne and T. J. Marks, *Journal of the American Chemical Society*, 1989, **111**, 4108–4109; g) S. Hong, S. Tian, M. V. Metz and T. J. Marks, *Journal of the American Chemical Society*, 2003, **125**, 14768–14783; h) S. D. Wobser, C. J. Stephenson, M. Delferro and T. J. Marks, *Organometallics*, 2013, **32**, 1317–1327; i) B. D. Stubbert and T. J. Marks, *Journal of the American Chemical Society*, 2007, **129**, 4253–4271; j) X. Yu, S. Seo and T. J. Marks, *Journal of the American Chemical Society*, 2007, **129**, 7244–7245; k) A. Dzudza and T. J. Marks, *Organic Letters*, 2009, **11**, 1523–1526; l) P. W. Roesky, U. Denninger, C. L. Stern and T. J. Marks, *Organometallics*, 1997, **16**, 4486–4492; m) A. Motta, I. L. Fragalà and T. J. Marks, *Organometallics*, 2005, **24**, 4995–5003; n) A. M. Kawaoka, M. R. Douglass and T. J. Marks, *Organometallics*, 2003, **22**, 4630–4632; o) S. Seo, X. Yu and T. J. Marks, *Journal of the American Chemical Society*, 2009, **131**, 263–276; p) S. Hong, A. M. Kawaoka and T. J. Marks, *Journal of the American Chemical Society*, 2003, **125**, 15878–15892; q) M. R. Douglass, C. L. Stern and T. J. Marks, *Journal of the American Chemical Society*, 2001, **123**, 10221–10238; r) C. J. Weiss, S. D. Wobser and T. J. Marks, *Organometallics*, 2010, **29**, 6308–6320; s) A. Dzudza and T. J. Marks, *The Journal of Organic Chemistry*, 2008, **73**, 4004–4016; t) C. J. Weiss and T. J. Marks, *Dalton Transactions*, 2010, **39**, 6576–6588; u) J.–S. Ryu, G. Y. Li and T. J. Marks, *Journal of the American Chemical Society*, 2003, **125**, 12584–12605; v) A. S. Dudnik, V. L. Weidner, A. Motta, M. Delferro and T. J. Marks, *Nat Chem*, 2014, **6**, 1100–1107.
8. A. G. M. Barrett, I. J. Casely, M. R. Crimmin, M. S. Hill, J. R. Lachs, M. F. Mahon and P. A. Procopiou, *Inorganic Chemistry*, 2009, **48**, 4445–4453.
9. a) M. Westerhausen, S. Schneiderbauer, Alexander N. Kneifel, Y. Söltl, P. Mayer, H. Nöth, Z. Zhong, Pieter J. Dijkstra and J. Feijen, *European Journal of Inorganic Chemistry*, 2003, **2003**, 3432–3439; b) Y. Sarazin, R. H. Howard, D. L. Hughes, S. M. Humphrey and M. Bochmann, *Dalton Transactions*, 2006, 340–350; c) M. G. Davidson, C. T. O'Hara, M. D. Jones, C. G. Keir, M. F. Mahon and G. Kociok–Köhn, *Inorganic Chemistry*, 2007, **46**, 7686–7688.
10. W. Vargas and K. Ruhlandt–Senge, *European Journal of Inorganic Chemistry*, 2003, **2003**, 3472–3479.
11. a) D. J. Burkey and T. P. Hanusa, *Organometallics*, 1996, **15**, 4971–4976; b) A. G. M. Barrett, M. R. Crimmin, M. S. Hill, P. B. Hitchcock, S. L. Lomas, M. F. Mahon, P. A. Procopiou and K. Suntharalingam, *Organometallics*, 2008, **27**, 6300–6306; c) M. Westerhausen, M. H. Digeser, M. Krofta, N. Wiberg, H. Nöth, J. Knizek, W. Ponikwar and T. Seifert, *European Journal of Inorganic Chemistry*, 1999, **1999**, 743–750.
12. A. G. Avent, M. R. Crimmin, M. S. Hill and P. B. Hitchcock, *Organometallics*, 2005, **24**, 1184–1188.
13. S. E. Baillie, V. L. Blair, T. D. Bradley, W. Clegg, J. Cowan, R. W. Harrington, A. Hernan–Gomez, A. R. Kennedy, Z. Livingstone and E. Hevia, *Chemical Science*, 2013, **4**, 1895–1905.

14. a) M. Westerhausen, M. H. Digeser and W. Schwarz, *Inorganic Chemistry*, 1997, **36**, 521–527; b) M. Westerhausen, M. H. Digeser, H. Nöth, W. Ponikwar, T. Seifert and K. Polborn, *Inorganic Chemistry*, 1999, **38**, 3207–3214; c) M. Westerhausen, M. H. Digeser, C. Gückel, H. Nöth, J. Knizek and W. Ponikwar, *Organometallics*, 1999, **18**, 2491–2496.
15. a) A. Weeber, S. Harder, H. H. Brintzinger and K. Knoll, *Organometallics*, 2000, **19**, 1325–1332; b) F. Feil and S. Harder, *Organometallics*, 2000, **19**, 5010–5015; c) F. Feil and S. Harder, *Organometallics*, 2001, **20**, 4616–4622; d) S. Harder, F. Feil and A. Weeber, *Organometallics*, 2001, **20**, 1044–1046.
16. M. R. Crimmin, I. J. Casely and M. S. Hill, *Journal of the American Chemical Society*, 2005, **127**, 2042–2043.
17. M. R. Crimmin, A. G. M. Barrett, M. S. Hill, P. B. Hitchcock and P. A. Procopiou, *Organometallics*, 2007, **26**, 2953–2956.
18. T. M. A. Al–Shboul, H. Görls and M. Westerhausen, *Inorganic Chemistry Communications*, 2008, **11**, 1419–1421.
19. B. Liu, J.–F. Carpentier and Y. Sarazin, *Chemistry – A European Journal*, 2012, **18**, 13259–13264.
20. B. Liu, T. Roisnel, J.–F. Carpentier and Y. Sarazin, *Chemistry – A European Journal*, 2013, **19**, 13445–13462.
21. a) J. R. Lachs, A. G. M. Barrett, M. R. Crimmin, G. Kociok–Köhn, M. S. Hill, M. F. Mahon and P. A. Procopiou, *European Journal of Inorganic Chemistry*, 2008, **2008**, 4173–4179; b) A. Baishya, M. K. Barman, T. Peddarao and S. Nembenna, *Journal of Organometallic Chemistry*, 2014, **769**, 112–118.
22. a) M. Arrowsmith, M. R. Crimmin, M. S. Hill, S. L. Lomas, M. S. Heng, P. B. Hitchcock and G. Kociok–Kohn, *Dalton Transactions*, 2014, **43**, 14249–14256; b) A. G. M. Barrett, M. R. Crimmin, M. S. Hill, P. B. Hitchcock, S. L. Lomas, M. F. Mahon and P. A. Procopiou, *Dalton Transactions*, 2010, **39**, 7393–7400.
23. L. Orzechowski and S. Harder, *Organometallics*, 2007, **26**, 2144–2148.
24. A. G. M. Barrett, T. C. Boorman, M. R. Crimmin, M. S. Hill, G. Kociok–Kohn and P. A. Procopiou, *Chemical Communications*, 2008, 5206–5208.
25. M. S. Hill, D. J. Liptrot and M. F. Mahon, *Angewandte Chemie International Edition*, 2013, **52**, 5364–5367.
26. a) M. Arrowsmith, W. M. S. Shepherd, M. S. Hill and G. Kociok–Kohn, *Chemical Communications*, 2014, **50**, 12676–12679; b) M. Arrowsmith, M. S. Hill and G. Kociok–Köhn, *Chemistry – A European Journal*, 2015, **21**, 10548–10557.
27. a) S. P. Green, C. Jones and A. Stasch, *Angewandte Chemie International Edition*, 2008, **47**, 9079–9083; b) S. J. Bonyhady, C. Jones, S. Nembenna, A. Stasch, A. J. Edwards and G. J. McIntyre, *Chemistry – A European Journal*, 2010, **16**, 938–955.
28. M. Arrowsmith, M. S. Hill, D. J. MacDougall and M. F. Mahon, *Angewandte Chemie International Edition*, 2009, **48**, 4013–4016.
29. a) S. Harder, J. Spielmann, J. Intemann and H. Bandmann, *Angewandte Chemie*, 2011, **123**, 4242–4246; b) J. Intemann, J. Spielmann, P. Sirsch and S. Harder, *Chemistry – A European Journal*, 2013, **19**, 8478–8489.
30. D. Martin, K. Beckerle, S. Schnitzler, T. P. Spaniol, L. Maron and J. Okuda, *Angewandte Chemie International Edition*, 2015, **54**, 4115–4118.
31. J. Spielmann and S. Harder, *Chemistry – A European Journal*, 2007, **13**, 8928–8938.
32. S. J. Bonyhady, S. P. Green, C. Jones, S. Nembenna and A. Stasch, *Angewandte Chemie International Edition*, 2009, **48**, 2973–2977.
33. E. M. Leitao, T. Jurca and I. Manners, *Nat Chem*, 2013, **5**, 817–829.
34. A. G. M. Barrett, M. R. Crimmin, M. S. Hill, P. B. Hitchcock and P. A. Procopiou, *Organometallics*, 2007, **26**, 4076–4079.
35. A. Staubitz, A. P. M. Robertson, M. E. Sloan and I. Manners, *Chemical Reviews*, 2010, **110**, 4023–4078.
36. a) A. Kumar, N. A. Beattie, S. D. Pike, S. A. Macgregor and A. S. Weller, *Angewandte Chemie International Edition*, 2016, **55**, 6651–6656; b) H. C. Johnson, E. M. Leitao, G. R. Whittell, I. Manners, G. C. Lloyd–Jones and A. S. Weller, *Journal of the American Chemical Society*, 2014, **136**, 9078–9093.
37. J. Spielmann, G. Jansen, H. Bandmann and S. Harder, *Angewandte Chemie International Edition*, 2008, **47**, 6290–6295.

38. J. Spielmann and S. Harder, *Journal of the American Chemical Society*, 2009, **131**, 5064–5065.
39. D. J. Liptrot, M. S. Hill, M. F. Mahon and D. J. MacDougall, *Chemistry – A European Journal*, 2010, **16**, 8508–8515.
40. P. Bellham, M. S. Hill, D. J. Liptrot, D. J. MacDougall and M. F. Mahon, *Chemical Communications*, 2011, **47**, 9060–9062.
41. M. S. Hill, G. Kociok–Kohn and T. P. Robinson, *Chemical Communications*, 2010, **46**, 7587–7589.
42. D. J. Liptrot, M. S. Hill, M. F. Mahon and A. S. S. Wilson, *Angewandte Chemie International Edition*, 2015, **54**, 13362–13365.
43. F. Buch and S. Harder, *Organometallics*, 2007, **26**, 5132–5135.
44. M. S. Hill, D. J. Liptrot, D. J. MacDougall, M. F. Mahon and T. P. Robinson, *Chemical Science*, 2013, **4**, 4212–4222.
45. C. Bellini, J.–F. Carpentier, S. Tobisch and Y. Sarazin, *Angewandte Chemie International Edition*, 2015, **54**, 7679–7683.
46. D. J. Liptrot, M. Arrowsmith, A. L. Colebatch, T. J. Hadlington, M. S. Hill, G. Kociok–Köhn and M. F. Mahon, *Angewandte Chemie International Edition*, 2015, n/a–n/a.
47. a) S. P. Roche and J. A. Porco, *Angewandte Chemie International Edition*, 2011, **50**, 4068–4093; b) N. Edraki, A. R. Mehdipour, M. Khoshneviszadeh and R. Miri, *Drug Discovery Today*, 2009, **14**, 1058–1066.
48. a) D. R. Armstrong, R. E. Mulvey, D. Barr, R. Snaith and D. Reed, *Journal of Organometallic Chemistry*, 1988, **350**, 191–205; b) J. G. Keay, in *Advances in Heterocyclic Chemistry*, ed. R. K. Alan, Academic Press, Editon edn., 1986, vol. Volume 39, pp. 1–77; c) R. E. Mulvey, L. Dunbar, W. Clegg and L. Horsburgh, *Angewandte Chemie International Edition in English*, 1996, **35**, 753–755; d) R. A. Sulzbach, *Journal of Organometallic Chemistry*, 1970, **24**, 307–314; e) K. Ziegler and H. Zeiser, *Berichte der deutschen chemischen Gesellschaft (A and B Series)*, 1930, **63**, 1847–1851.
49. a) L. Hao, J. F. Harrod, A.–M. Lebuis, Y. Mu, R. Shu, E. Samuel and H.–G. Woo, *Angewandte Chemie International Edition*, 1998, **37**, 3126–3129; b) I. Piras, R. Jennerjahn, R. Jackstell, A. Spannenberg, R. Franke and M. Beller, *Angewandte Chemie International Edition*, 2011, **50**, 2–2; c) D. V. Gutsulyak, A. van der Est and G. I. Nikonov, *Angewandte Chemie International Edition*, 2011, **50**, 1384–1387.
50. M. S. Hill, G. Kociok–Kohn, D. J. MacDougall, M. F. Mahon and C. Weetman, *Dalton Transactions*, 2011, **40**, 12500–12509.
51. a) J. G. de Vries and N. Mrsic, *Catalysis Science & Technology*, 2011, **1**, 727–735; b) S. Guizzetti and M. Benaglia, *European Journal of Organic Chemistry*, 2010, **2010**, 5529–5541; c) T. C. Nugent and M. El–Shazly, *Advanced Synthesis & Catalysis*, 2010, **352**, 753–819; d) O. Riant, N. Mostefaï and J. Courmarcel, *Synthesis*, 2004, **2004**, 2943–2958; e) J.–H. Xie, S.–F. Zhu and Q.–L. Zhou, *Chemical Reviews*, 2011, **111**, 1713–1760; f) Z. Yu, W. Jin and Q. Jiang, *Angewandte Chemie International Edition*, 2012, **51**, 6060–6072; g) S. Díez–González and S. P. Nolan, *Organic Preparations and Procedures International*, 2007, **39**, 523–559.
52. a) R. T. Baker, J. C. Calabrese and S. A. Westcott, *Journal of Organometallic Chemistry*, 1995, **498**, 109–117; b) P. A. Chase, G. C. Welch, T. Jurca and D. W. Stephan, *Angewandte Chemie*, 2007, **119**, 8196–8199; c) P. A. Chase, G. C. Welch, T. Jurca and D. W. Stephan, *Angewandte Chemie International Edition*, 2007, **46**, 8050–8053; d) P. A. Chase, T. Jurca and D. W. Stephan, *Chemical Communications*, 2008, 1701–1703; e) P. Eisenberger, A. M. Bailey and C. M. Crudden, *Journal of the American Chemical Society*, 2012, **134**, 17384–17387; f) Z. M. Heiden and D. W. Stephan, *Chemical Communications*, 2011, **47**, 5729–5731; g) E. H. M. Kirton, G. Tughan, R. E. Morris and R. A. Field, *Tetrahedron Letters*, 2004, **45**, 853–855; h) L. Koren–Selfridge, H. N. Londino, J. K. Vellucci, B. J. Simmons, C. P. Casey and T. B. Clark, *Organometallics*, 2009, **28**, 2085–2090; i) Z.–H. Lu, N. Bhongle, X. Su, S. Ribe and C. H. Senanayake, *Tetrahedron Letters*, 2002, **43**, 8617–8620; j) P. Spies, G. Erker, G. Kehr, K. Bergander, R. Frohlich, S. Grimme and D. W. Stephan, *Chemical Communications*, 2007, 5072–5074.
53. a) C. Wang, B. Villa–Marcos and J. Xiao, *Chemical Communications*, 2011, **47**, 9773–9785; b) A. Fabrello, A. Bachelier, M. Urrutigoïty and P. Kalck, *Coordination Chemistry Reviews*, 2010, **254**, 273–287; c) N. Fleury–Brégeot, V. de la Fuente, S. Castillón and C. Claver, *ChemCatChem*, 2010, **2**, 1346–1371.

54. M. Arrowsmith, M. S. Hill and G. Kociok–Köhn, *Chemistry – A European Journal*, 2013, **19**, 2776–2783.
55. J. J. Eisch, *Journal of the American Chemical Society*, 1998, **120**, 6631–6632.
56. a) D. Addis, S. Das, K. Junge and M. Beller, *Angewandte Chemie International Edition*, 2011, **50**, 6004–6011; b) R. J. P. Corriu, J. J. E. Moreau and M. Pataud–Sat, *Journal of Organometallic Chemistry*, 1982, **228**, 301–308; c) S. Das, B. Wendt, K. Möller, K. Junge and M. Beller, *Angewandte Chemie International Edition*, 2012, **51**, 1662–1666; d) D. V. Gutsulyak and G. I. Nikonov, *Angewandte Chemie International Edition*, 2010, **49**, 7553–7556.
57. C. Weetman, M. D. Anker, M. Arrowsmith, M. S. Hill, G. Kociok–Kohn, D. J. Liptrot and M. F. Mahon, *Chemical Science*, 2016, **7**, 628–641.
58. C. Weetman, M. S. Hill and M. F. Mahon, *Chemical Communications*, 2015, **51**, 14477–14480.
59. B. R. Barnett, C. E. Moore, A. L. Rheingold and J. S. Figueroa, *Chemical Communications*, 2015, **51**, 541–544.
60. H. C. Brown, H. I. Schlesinger and A. B. Burg, *Journal of the American Chemical Society*, 1939, **61**, 673–680.
61. A. J. Blake, A. Cunningham, A. Ford, S. J. Teat and S. Woodward, *Chemistry – A European Journal*, 2000, **6**, 3586–3594.
62. C. W. Lindsley and M. DiMare, *Tetrahedron Letters*, 1994, **35**, 5141–5144.
63. a) A. Y. Khalimon, P. Farha, L. G. Kuzmina and G. I. Nikonov, *Chemical Communications*, 2012, **48**, 455–457; b) M. Arrowsmith, M. S. Hill, T. Hadlington, G. Kociok–Köhn and C. Weetman, *Organometallics*, 2011, **30**, 5556–5559.
64. D. Mukherjee, A. Ellern and A. D. Sadow, *Chemical Science*, 2014, **5**, 959–964.
65. C. Weetman, M. S. Hill and M. F. Mahon, *Chemistry – A European Journal*, 2016, **22**, 7158–7162.
66. a) A. A. Adesina, *Applied Catalysis A: General*, 1996, **138**, 345–367; b) P. M. Maitlis, *Journal of Organometallic Chemistry*, 2004, **689**, 4366–4374; c) P. M. Maitlis and V. Zanotti, *Chemical Communications*, 2009, 1619–1634; d) H. Schulz, *Applied Catalysis A: General*, 1999, **186**, 3–12; e) B. H. Davis and M. L. Occelli, *Advances in Fischer–Tropsch synthesis, catalysts, and catalysis*, CRC Press, 2009.
67. N. M. West, A. J. M. Miller, J. A. Labinger and J. E. Bercaw, *Coordination Chemistry Reviews*, 2011, **255**, 881–898.
68. a) J. M. Manriquez, D. R. McAlister, R. D. Sanner and J. E. Bercaw, *Journal of the American Chemical Society*, 1976, **98**, 6733–6735; b) J. M. Manriquez, D. R. McAlister, R. D. Sanner and J. E. Bercaw, *Journal of the American Chemical Society*, 1978, **100**, 2716–2724.
69. P. J. Fagan, K. G. Moloy and T. J. Marks, *Journal of the American Chemical Society*, 1981, **103**, 6959–6962.
70. E. L. Werkema, L. Maron, O. Eisenstein and R. A. Andersen, *Journal of the American Chemical Society*, 2007, **129**, 2529–2541.

Chapter Two

Hydrodeoxygenation of Isocyanates

2.1 Introduction

The utility of reagents derived from magnesium in homogeneous catalysis has advanced rapidly during the last decade.[1] As outlined in Chapter 1, investigations in the Hill group have centred on the readily available and easily synthesised *β*–diketiminato magnesium *n*–butyl derivative, **Ib**, as a convenient prototype reagent for the development of a number of molecular catalytic transformations. It has been shown (*vide supra*) that the use of compound **Ib**, enables the hydroboration of an assortment of multiply bonded and heteroatomic C=E (E = O,[2] N[3,4]), and C≡N[5] substrates.

Hydrodeoxygenation of carbonyl–containing compounds has attracted increasing attention given its potential applications in biofuels and fine chemical syntheses.[6] Although a number of stoichiometric protocols for deoxygenation are known,[7] these methods typically require harsh reaction conditions. While Stephan has recently reported that ketones are efficiently deoxygenated in the presence of silane using catalytic quantities of highly electrophilic phosphonium cations, (Scheme 2.1, (a)) [8] of greater relevance to the current work are a number of magnesium–based processes that have also been described. As previously discussed in Chapter One (Section 1.6.1), Hill and co–workers observed that compound **Ib**, was able to effect ester cleavage during the hydroboration of 3–methylnicotinate with pinacolborane (Scheme 2.1, (b)).[3a] This reactivity was subsequently extended by Sadow and co–workers to a variety of ester hydroboration and amide reduction reactions mediated by a magnesium tris(oxazolinyl)phenylborate catalyst, **V** (Scheme 2.1, (c)).[9]

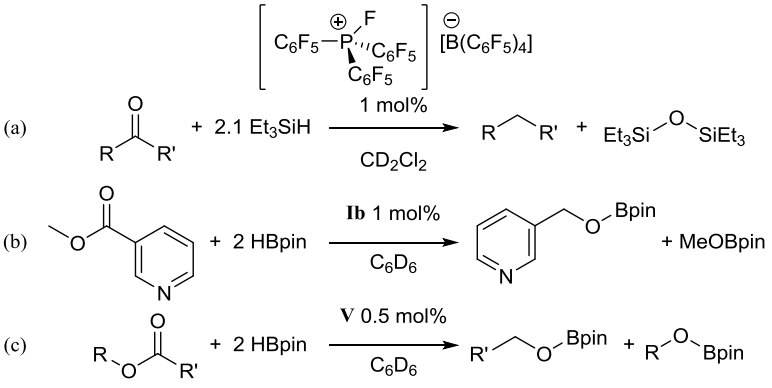

Scheme 2.1: (a) Stephan's recently reported deoxygenation of ketones with phosphonium cations and Et_3SiH.[8] (b) hydroboration of 3–methylnicotinate with HBpin, catalysed by **Ib**, that led to ester cleavage. (c) Sadow's hydroboration of esters with HBpin catalysed by **V**.

Importantly, mechanistic analysis of these latter reactions implicated the intermediacy of zwitterionic alkoxyborate species rather than a conventional σ–bond metathesis pathway. In related work, the Hill group have shown that carbon dioxide may be subjected to the complete and selective rupture of a C=O bond and the formation of the methanol–equivalent $H_3COBpin$ through the use of a modified catalyst system derived from **Ib** and a $B(C_6F_5)_3$ co–catalyst, Scheme 2.2.[10]

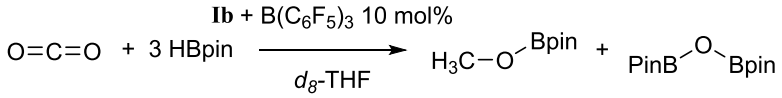

Scheme 2.2: Selective hydroboration of CO_2 to a methanol and water equivalent catalysed by **Ib** and $B(C_6F_5)_3$.[10]

In this Chapter, it is demonstrated that analogous hydrodeoxygenation can be applied to the isoelectronic isocyanate (NCO) moiety to provide a viable and unprecedented route to methyl amines.

2.2 Catalytic Hydrodeoxygenation of Isocyanates

An initial reaction between isopropyl isocyanate (^{i}PrNCO) and three molar equivalents of HBpin performed at 60°C in C_6D_6 evidenced no observable reaction after 12 hours by ^{1}H and ^{11}B NMR spectroscopy. In contrast, monitoring of an otherwise identical reaction in the presence of 10 mol% of **Ib** for one and a half hours indicated the consumption of *ca.*76% of the isocyanate and borane starting materials, Scheme 2.3.

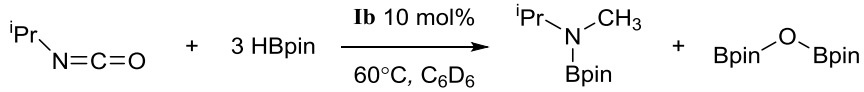

Scheme 2.3: Initial hydrodeoxygenation reaction with isopropyl isocyanate.

More notably, the formation of a predominant new organic product was apparent from the emergence of a singlet resonance at δ 2.56 ppm, Figure 2.1 (a), in the ^{1}H NMR spectrum. Analysis of the corresponding ^{11}B NMR spectrum revealed the presence of unreacted HBpin along with two further singlet resonances in a 1:2 ratio by integration at δ 27.4 and δ 24.9 ppm respectively and a further broad but low intensity signal at δ 7.8 ppm, which was observed to persist throughout the course of the reaction, Figure 2.1 (b). The resonance centred at δ 24.9 ppm was identified as the bis(boryl)oxide, $O(Bpin)_2$, through comparison with literature data[11] indicating that HBpin reduction of ^{i}PrNCO had resulted in cleavage of the C=O bond within

the substrate with consequent formation of the *N*–borylated *N*–methyl isopropyl amine, Scheme 2.3.

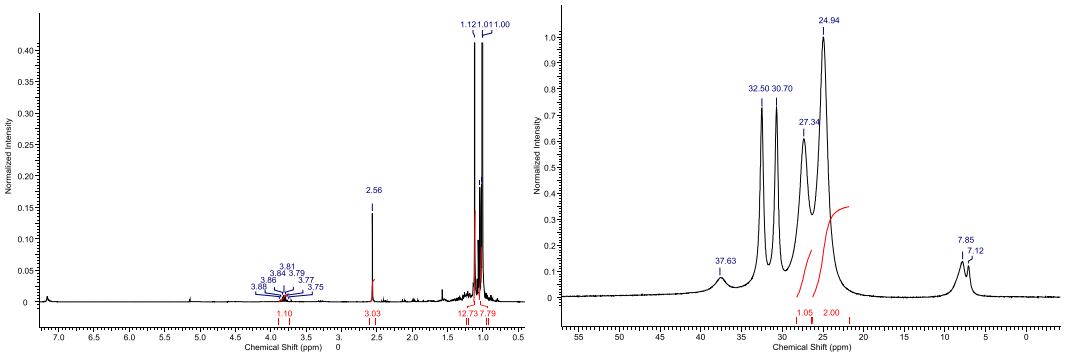

Figure 2.1: (a) Left: ^{1}H NMR spectrum (300 MHz), indicating the formation of O(Bpin)$_2$ and ^{i}PrN(Me)Bpin. (b) Right: ^{11}B NMR spectrum (96.3 MHz) displaying 1:2 ratio of product signals at *ca.* 76% conversion.

Encouraged by this result, this reactivity was extended to a range of commercially available organic isocyanates, (Table 2.1). Entries 1 to 6 present the outcome of these reactions performed with a range of alkyl isocyanates of varying steric bulk. All the reactions provided analogous transformations to that observed for ^{i}PrNCO and were characterised by a new singlet methyl ^{1}H NMR resonance in the range δ 2.5 – δ 3.0 ppm and a single new *N*–B resonance at *ca.* δ 27 ppm, which appeared along with the signal associated with the O(Bpin)$_2$ by–product in the ^{11}B NMR spectra.

Table 2.1: Hydroboration and reductive C=O cleavage of organic isocyanates catalysed by **Ib**.

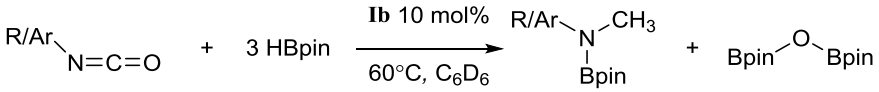

Entry	Ar/R	Cat. (mol%)	Time (h)	Temp. (°C)	NMR Conv. (%)[a]
1	Ad	10	4.5	60	75
2	Et	10	21	60	70
3	^{n}Pr	10	21	60	75
4	^{i}Pr	10	1.5	60	76
5	^{t}Bu	10	3.5	60	81

6	Cy	10	4.5	60	90
7	Ph	10	24	25	86
8	Mes	10	24	60	90
9	Dipp	10	24	60	50

[a] To *N*–methyl amine product

Contrary to expectation, increased RNCO substituent steric demands provided generally faster reaction times; R = ^{i}Pr (entry 4) and ^{t}Bu (entry 5) evidenced complete consumption of the isocyanate in less than 4 hours compared to Et (entry 2) and ^{n}Pr (entry 3), both of which required 21 hours.

The increased reactivity associated with enhanced alkyl substituent steric demands, however, also coincided with the onset of secondary side reactions. Although attempts to identify the products of these side reactions were unsuccessful it is likely that oligomerization of the isocyanates is competitive with the reductive C=O cleavage.[12] Notably, further reactions performed with *N*–phenyl (Ph) and *N*–mesityl (Mes) isocyanate substitution provided *ca*. 90% conversion in 24 hours (entries 7 and 8), while an increase of the *N*–aryl substituent's steric demands to 2,6–di–isopropylphenyl (Dipp) resulted in a significantly reduced conversion during the same time period, (entry 9).

2.3 Mechanistic Investigations

Having established the viability of this magnesium–centred hydrodeoxygenation, a series of stoichiometric reactions were performed to investigate the elementary processes taking place during catalysis. The Hill group have previously reported that addition of HBpin to a solution of compound **Ib** at room temperature leads to stoichiometric formation of *n*–BuBpin and a heteroleptic magnesium hydride species, **Ih·BuBpin**, which exists in equilibrium with a labile magnesium borohydride of the anion [*n*–BuHBpin]$^{-}$.[2] Addition of a single equivalent of the sterically encumbered DippNCO to a solution prepared in this manner provided stoichiometric conversion to the magnesium formamidate species, compound **2.1**. The formation of **2.1** was clearly apparent from the presence of a new downfield singlet resonance at δ 7.92 ppm with a 1H integral in the resultant ^{1}H NMR spectrum, Scheme 2.4.

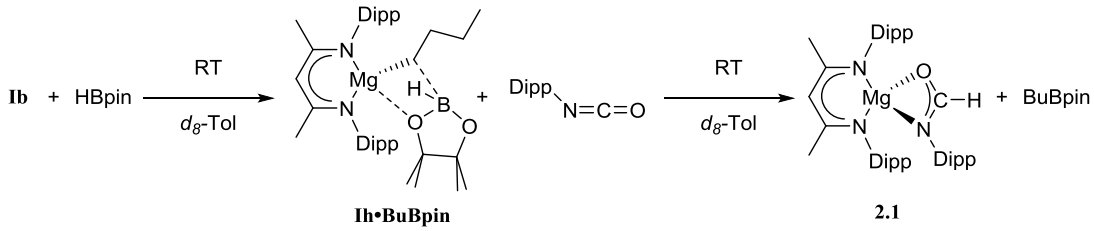

Scheme 2.4: DippNCO reduction to the *β*–diketiminato magnesium formamidate, **2.1**, from *in situ* generated **Ih**.

Crystallisation of compound **2.1** directly from the reaction solution provided a sample suitable for a single crystal X–ray diffraction analysis. The results of this analysis, Figure 2.2, confirmed that compound **2.1** was a magnesium formamidate, the mononuclear constitution of which is most likely imposed by the steric demands of the three *N*–Dipp substituents. The *β*–diketiminate ligand makes up two contacts to the magnesium centre, with the remaining two from O1 and N3, completing a distorted tetrahedral arrangement.

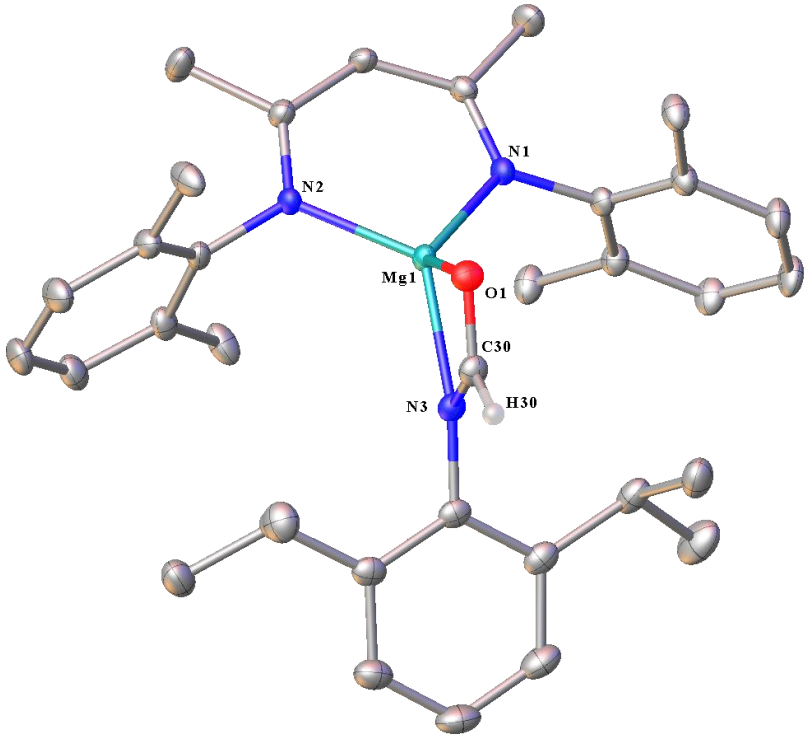

Figure 2.2: ORTEP representation of compound **2.1** with thermal ellipsoids at 30%. Isopropyl groups and hydrogen atoms except H30 have been removed for clarity. Selected bond lengths (Å) and bond angles (°): Mg1–O1 2.0118(10), Mg1–N1 2.0179(11), Mg1–N2 2.0156(11), Mg1–N3 2.0983(11), O1–Mg1–N1 121.64, O1–Mg1–N2 122.69, O1–Mg1–N3 65.86(4), N1–Mg1–N3 128.04(4), N1–Mg1–N2 95.09(4), N2–Mg1–N3 125.20(5).

Addition of one equivalent of HBpin to a solution of isolated compound **2.1** in d_8–toluene at room temperature resulted in the immediate formation of a single species, compound **2.2**, Scheme 2.5. The formation of compound **2.2** was characterised by the appearance of a single new resonance at δ 4.3 ppm in the ^{11}B NMR spectrum and a subtle shift of the formamidate singlet resonance in the ^{1}H NMR spectrum from δ 7.92 ppm to δ 7.69 ppm. X–ray quality crystals of **2.2** were obtained by removal of the reaction solvent *in vacuo*, redissolving in hexane and storage at –35°C overnight.

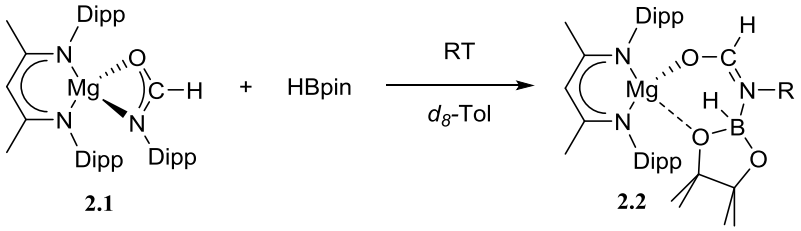

Scheme 2.5: Addition of HBpin at room temperature to **2.1** yields the magnesium hydridoborate species, **2.2**, in stoichiometric yield.

A subsequent single crystal X–ray diffraction analysis confirmed compound **2.2** **(**Figure 2.3) to be a borate species formed by the formal insertion of HBpin into the Mg–N bond of the magnesium formamidate, **2.1**.

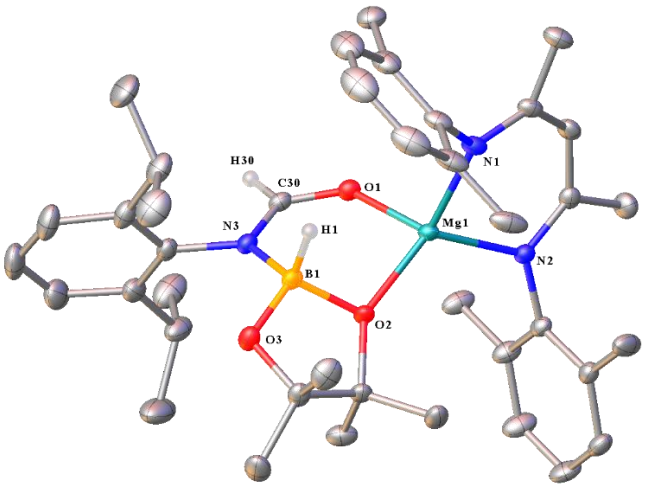

Figure 2.3: ORTEP representation of compound **2.2** with thermal ellipsoids at 30%. Isopropyl groups and hydrogen atoms except H1 and H30 have been removed for clarity. Selected bond lengths (Å) and bond angles (°): Mg1–O1 1.9631(12), Mg1–O2 1.9734(12), Mg1–N1 2.0547(14), Mg1–N2 2.0320(14), Mg1–B1 2.797(2), O1–C30 1.262(2), N3–C30 1.309(2), N3–B1 1.590(2). O1–Mg1–O2 91.39(5), O1–Mg1–N1 106.55(6), O1–Mg1–N2 115.27(5), O1–Mg1–O2 91.39(5), O1–Mg1–N1 106.55(6), O1–Mg1–N2 115.27(7), O2–Mg1–N2 120.02(5), N2–Mg1–N1 92.86(6), O1–C30–N3 124.66(15), C30–N3–B1 120.55(14), O2–B1–N3 112.68(13), O3–B1–N3 107.72(14).

Consistent with the structure of **2.1**, the magnesium centre retains a distorted tetrahedral geometry, however, N3 is displaced by the pinacolate fragment and O2 makes up the fourth contact. The solid state structure of **2.2** is reminiscent of the recently reported *β*–diketiminato magnesium formamidinatoborate, **XVII**,[3c] however in this case the boron–bound hydride (H1) was readily located and freely refined clearly demonstrating that there was no significant Mg–H interaction in the solid state, Figure 2.4.

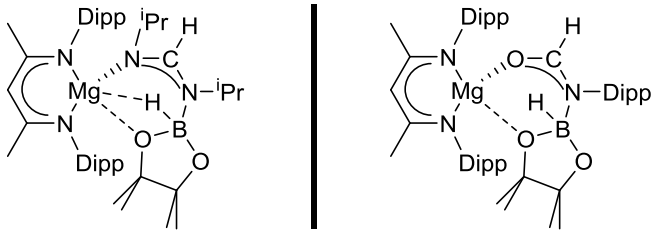

Figure 2.4: Comparison between the magnesium formamidinatoborate, **XVII**, and **2.2**.

Attempts to induce the extrusion of an *N*–borylated formamidine by prolonged (>24 hours) heating of samples of compound **2.2** in d_8–toluene either at 60°C or 80°C failed to provide any evidence of onward reactivity. Similar treatment of **2.2** at the higher temperature of 100°C for 16 hours, however, resulted in the production of a single new *β*–diketiminato species, **2.3**, along with the methylene imine, DippN=CH_2 (Scheme 2.6), which was tentatively assigned through the appearance of an AB spin system in the ^{1}H NMR spectrum with signals at δ 6.90 and δ 7.25 ppm.

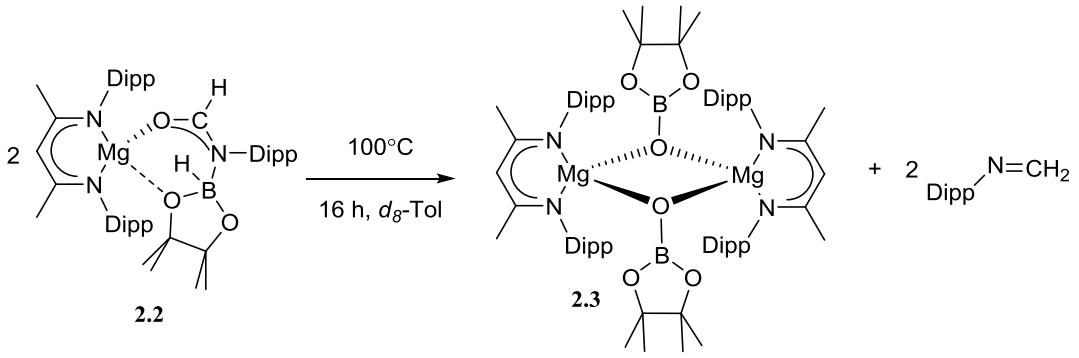

Scheme 2.6: Heating the magnesium *N*– alkyl formamidinatoborate complex, **2.2**, to 100°C causes imine extrusion.

The identity of compound **2.3** was confirmed through the isolation of single crystals suitable for an X–ray diffraction experiment. The results of this analysis revealed that **2.3** was a dimeric magnesium boryloxide species (Figure 2.5) arising from the cleavage of the C–O bond of the amidato moiety of compound **2.2**. Analogous to both **2.1** – **2.2**, the magnesium

centre retains a distorted tetrahedral geometry with two of the contacts made up from the bidentate *β*–diketiminate ligand, and the remaining two made up by O1 and O1^{i}. The Mg1–O1/O1^{i} bond lengths of 2.0400(16) and 1.9874(16) Å respectively, are in the upper range when compared to related *β*–diketiminato magnesium alkoxides (Mg–OR, R = ^{i}Pr, Et, Cy and Bn) that have a Mg–O bond lengths between 1.970 – 2.026 Å.[13] These augmented bond lengths can be attributed to the electrophilic boron withdrawing electron density from the oxygen, thus, decreasing the ionic interaction with the magnesium centre. Although the increased Mg–O/O^{i} bond lengths force a more obtuse Mg1–O1–Mg1^{i} angle (98.17(7)°), this is still within the upper range of the Mg–O–Mg angles of the aforementioned magnesium alkoxides (94.23 – 99.05°).[13] A number of metalla–boryloxide complexes are known, however, these are all restricted to the transition metals[11, 14] but all possess similar bonding distances and angles to **2.3**.

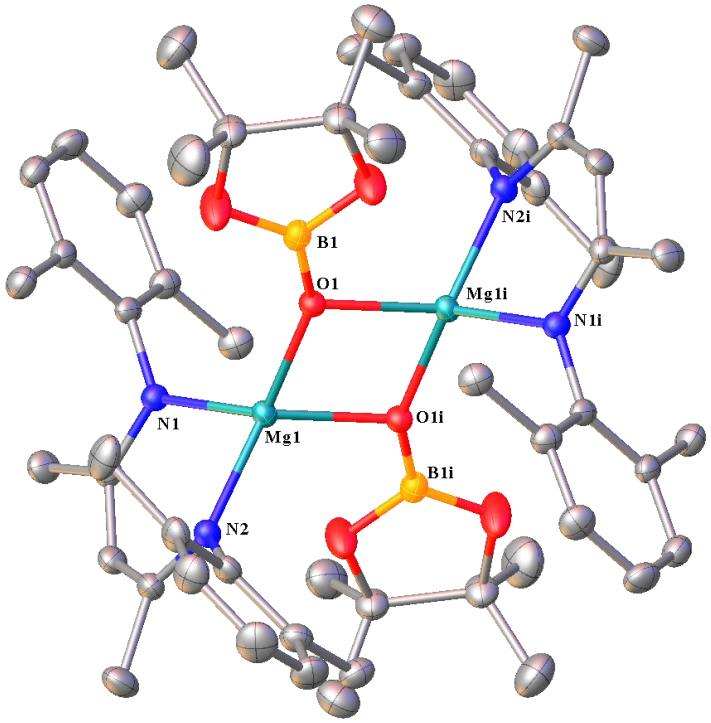

Figure 2.5: ORTEP representation of compound **2.3** with thermal ellipsoids at 30%. Isopropyl groups and hydrogen atoms have been removed for clarity. Selected bond lengths (Å) and bond angles (°): Mg1–O1 2.0400(16), Mg1–O1^{i} 1.9874(16), Mg1–N1 2.0692(19), Mg1–N2 2.085(2), B1–O1 1.343(3). N1–Mg1–N2 93.11(8), O1–Mg1–N1 121.63(7), O1–Mg1–N2 118.09(8), B1–O1–Mg1 112.82(14), Mg1–O1–Mg1^{i} 98.17(7).

While the formation of compound **2.3** implicates the direct extrusion of DippN=CH$_2$ as the mode of C–O activation, the elevated temperature required for this reaction militates against its operation during the aforementioned catalytic reactions. A further reaction between

compound **2.3** and a single equivalent of HBpin was, thus, undertaken. Although no consumption of **2.3** took place at room temperature, heating of this d_8–toluene solution at 60°C for 8 hours resulted in the predominant formation of DippN(Me)Bpin along with a variety of *β*–diketiminato magnesium species which could not be identified with any meaningful level of confidence.

In an attempt to shed further light on this reactivity, compound **Ib** was reacted with three equivalents of HBpin and two equivalents of DippNCO, (Scheme 2.7). This reaction at room temperature surprisingly resulted in the generation of the formamidate derivative **2.2**, along with the concomitant production of a single new compound, **2.4**. This latter species was identified as the bis–borylated hemiaminal, Dipp(pinB)NCH_2OBpin, through the appearance of a distinctive methylene singlet resonance at δ 5.35 ppm in the ^{1}H NMR spectrum and two broad signals of equal intensity at δ 28.3 and δ 24.8 ppm in the corresponding ^{11}B NMR experiment, Scheme 2.7.

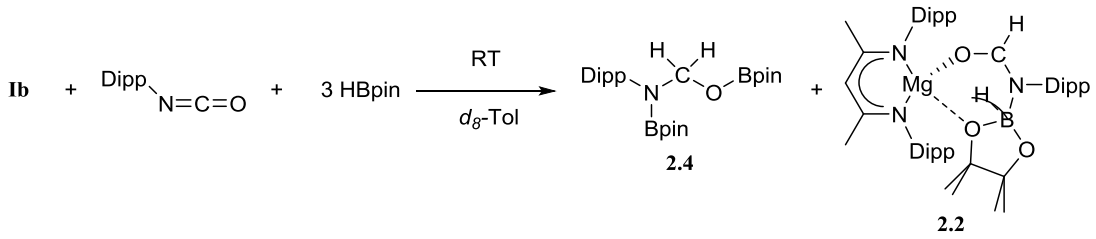

Scheme 2.7: Stoichiometric di–hydroboration of DippNCO mediated by **Ib**.

Continued treatment of this reaction mixture with additional equivalents of HBpin and DippNCO in a 2:1 ratio provided for the catalytic production of compound **2.4**. Subsequent investigation revealed that this catalytic reactivity could be directly replicated through the reactions of either DippNCO or MesNCO with two molar equivalents of HBpin performed in the presence of 10 mol% **Ib** to provide compound **2.4** and an analogous *N*–mesityl species, **2.5**, within 15 minutes at room temperature, Scheme 2.8.

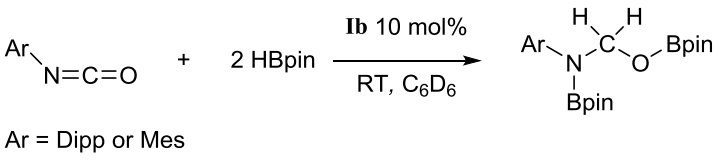

Scheme 2.8: Magnesium catalysed di–hydroboration of aryl isocyanates

A ^{1}H NMR spectrum recorded five minutes after the initiation of the catalytic reduction of DippNCO with two equivalents of HBpin by **Ib**, demonstrated the facile

production of the bis–borylated hemiaminal, Dipp(pinB)NCH$_2$OBpin, **2.4**, Figure 2.6. The aforementioned borate species, **2.2**, was also observed in catalytic quantities identified by the high frequency resonance at δ 7.65 ppm and a methine signal at δ 4.89 ppm in the ^{1}H NMR spectrum, accompanied by the observation of a new compound (**2.6**). **2.6** was characterised by the appearance of a high frequency singlet resonance at δ 9.04 ppm in the ^{1}H NMR spectrum (Figure 2.6) and was assigned as the *N*–borylated formamidine, DippN(Bpin)HC(O), which was completely consumed upon completion of the reaction.

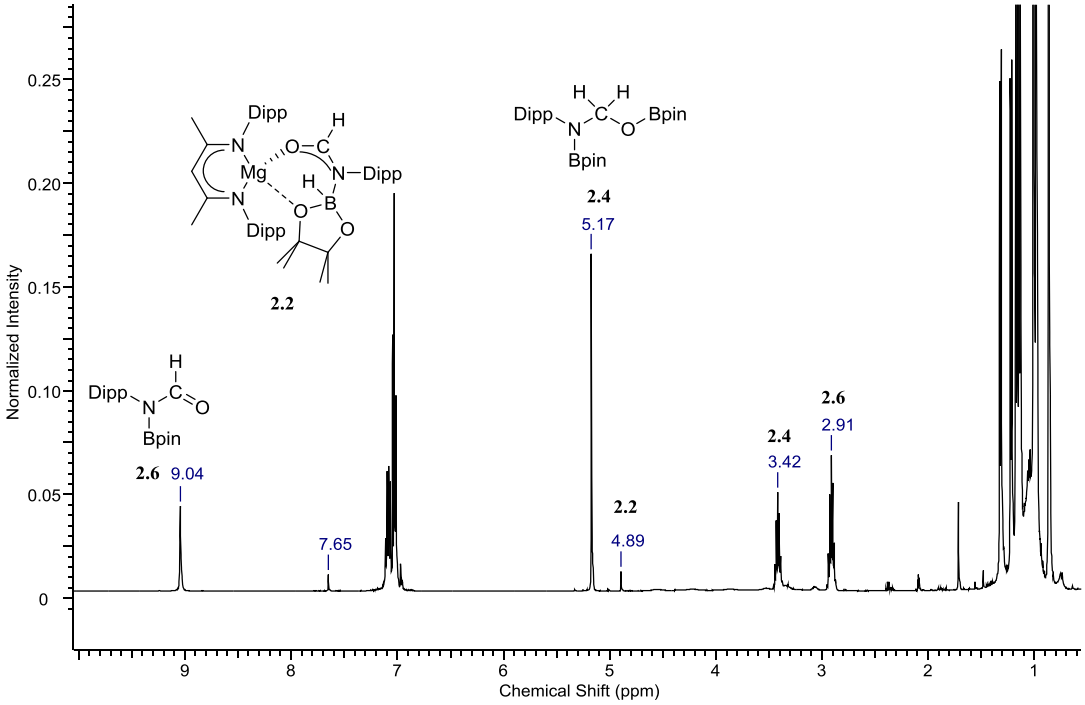

Figure 2.6: ^{1}H NMR spectrum (300 MHz) recorded during the catalytic generation of **2.4** from 2 HBpin and DippNCO catalysed by 10 mol% of **Ib**.

Several attempts to generate **2.6** by the equimolar addition of HBpin and DippNCO to **Ib**, initially failed and resulted in the catalytic production of **2.4**. A similar reaction performed at lower catalyst loading (0.1 mol%) and in the minimum amount of toluene solvent, however, resulted in the formation of a significant quantity of crystalline material. Mechanical separation of single crystals formed within this material enabled a series of single crystal X–ray diffraction analyses, which showed it to be primarily a mixture of compound **2.4** and compound **2.6**. The solid state structure of **2.6,** Figure 2.7, demonstrates the O1–C1 bond distance (1.206(4) Å) and O1–C1–N1 angle (O1–C1–N1 124.9(2)°) to be consistent with the formation of the formamide function, confirming the formation of the *N*–borylated formamide.

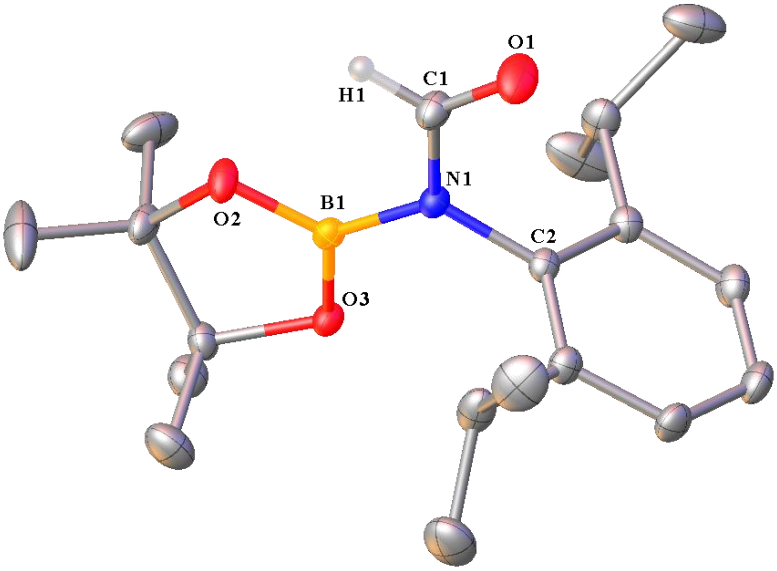

Figure 2.7: ORTEP representation of compound **2.6** with thermal ellipsoids at 30%. Hydrogen atoms have been removed for clarity except the hydrogen attached to C1. Selected bond lengths (Å) and bond angles (°): O1–C1 1.206(4), N1–C1 1.376(3), N1–B1 1.443(3), N1–C2 1.4444(3). O1–C1–N1 124.9(2), C1–N1–B1 120.7(2), C1–N1–C2 117.4(2).

Subsequent preparative scale reactions with both DippNCO and MesNCO and two equivalents of HBpin catalysed by 10 mol% **Ib**, provided single crystals of both compounds **2.4** and **2.5** suitable for X–ray diffraction analysis, which confirmed the formation of the bis–borylated hemiaminal species, Figure 2.8.

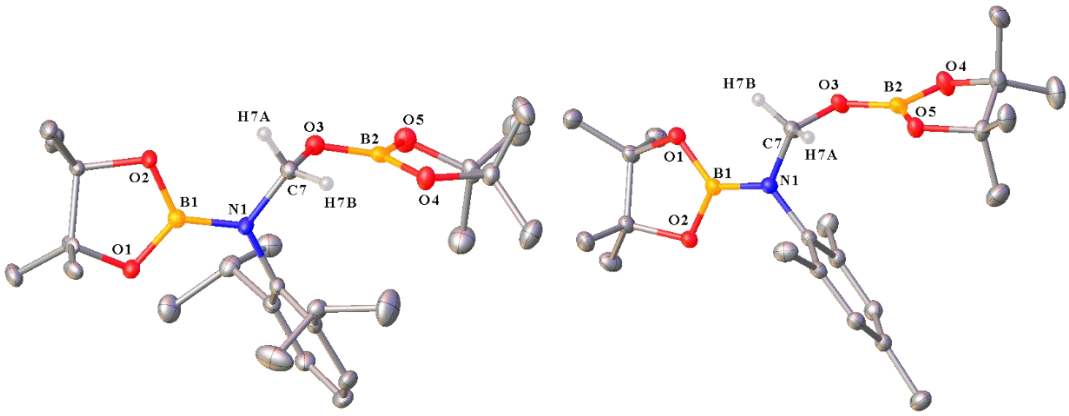

Figure 2.8: ORTEP representation of compound **2.4** (left) and **2.5** (right) with thermal ellipsoids at 30%. Hydrogen atoms have been removed for clarity except the hydrogen attached to C7. Selected bond lengths (Å) and bond angles (°): **2.4**: B1–N1 1.411(4), B2–O3 1.353(4), C7–O3 1.427(3), N1–C7 1.440(3), B2–O3–C7 119.0(2), O3–C7–N1 111.0(2), B1–N1–C7 119.5(2). **2.5**: B1–N1 1.414(2), B2–O3 1.3571(19), C7–O3 1.4404(18), N1–C7 1.4329(18), B2–O3–C7 119.12(12), O3–C7–N1 111.70(12), B1–N1–C7 120.81(12).

Attempted extension of this bis–borylation protocol to PhNCO and the range of *N*–aliphatic isocyanates shown in Table 2.1 was unsuccessful, with no evidence of any reactivity observed at room temperature beyond the initial activation of the pre–catalyst. Although subsequent heating of these reactions at 60°C induced consumption of the borane reagent, this procedure also resulted in C–O cleavage and *ca.* 50% conversion of the isocyanate to the *N*–methylated amine product and the bis(boryl)oxide, $O(Bpin)_2$, by–product.

To provide further insight into the role of these hemiaminal species as potential intermediates during the course of the C–O activation catalysis, a further reaction was carried out between compound **2.5** and Jones's *β*–diketiminato magnesium hydride complex, **Ih**.[15] Monitoring of this reaction by ^{1}H NMR spectroscopy demonstrated that heating to 60°C resulted in the generation of the *N*–borylated methyl amine, pinBN(Me)Mes, along with the magnesium boryloxide, **2.3**, (Scheme 2.9). A further reaction performed by addition of compound **2.5** to a d_8–toluene solution of the pre–catalyst **Ib** and HBpin provided an analogous result.

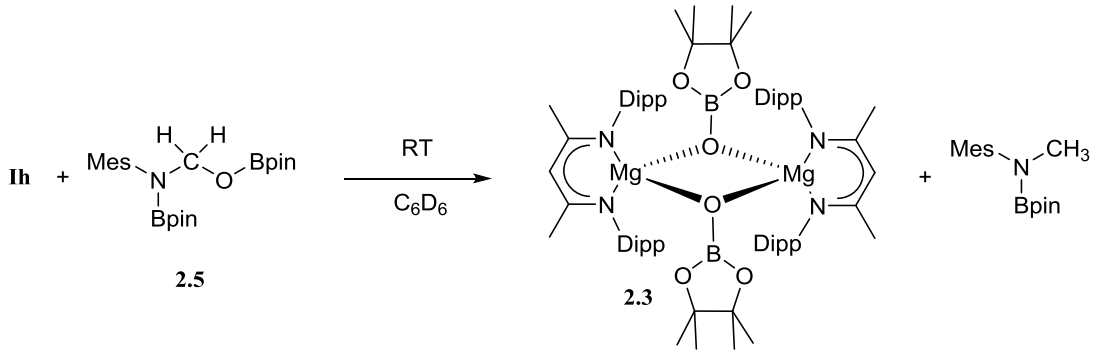

Scheme 2.9: Stoichometric reaction of **Ih** and bis–borylated mesityl hemiaminal, **2.5**, yielding the magnesium boryloxide, **2.3**, and *N*–borylated *N*–methyl mesityl amine.

Subsequent addition of HBpin to either of these reaction mixtures or to a solution of an isolated sample of compound **2.3** in d_8–THF resulted in the consumption of the magnesium boryloxide with concomitant production of $(pinB)_2O$ and the regeneration of **Ih**, Scheme 2.10.

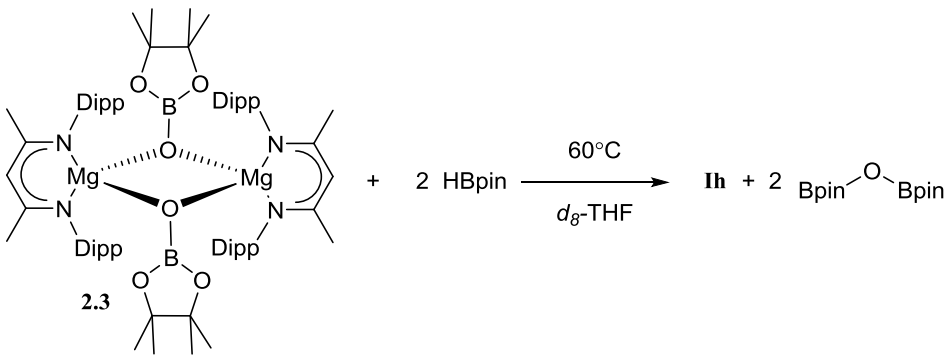

Scheme 2.10: Reaction of **2.3** and HBpin at 60°C regenerates **Ih**.

Although these routes to compound **2.3** and its reactivity with HBpin suggest that the C–O cleavage reaction is primarily magnesium mediated, it is notable that heating of a solution of compound **2.5** at 60°C for 12 hours in the absence of any other reagents also resulted in the consumption of *ca.* 50% of the hemiaminal and production of $(pinB)_2O$ and the methylene imine, $MesN{=}CH_2$, Scheme 2.11.

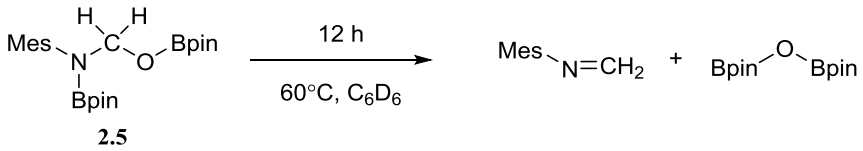

Scheme 2.11: Thermal decomposition of **2.5** to *N*–mesityl methylene imine and the bis(boryl)oxide.

2.4 *In Situ* NMR Monitoring

The significance of these observations with respect to the catalytic reactivity was assessed by *in situ* monitoring of a reaction of HBpin and ^{i}PrNCO catalysed by 10 mol% **Ib** at 60°C by ^{1}H NMR spectroscopy, Scheme 2.12.

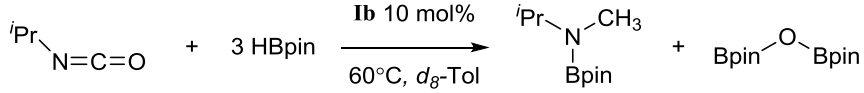

Scheme 2.12: Hydrodeoxygenation of ^{i}PrNCO with three equivalents of HBpin catalysed by **Ib**, monitored by ^{1}H NMR spectroscopy.

Figure 2.9 illustrates the evolution of this reaction over 140 minutes and highlights a complex profile *en route* to the ultimate methyl amine product, through the identification of a number of catalytic intermediates.

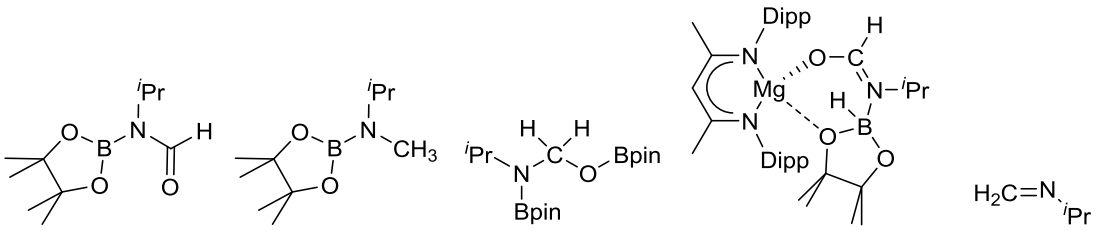

2.7 **2.8** **2.9** **2.10** **2.11**

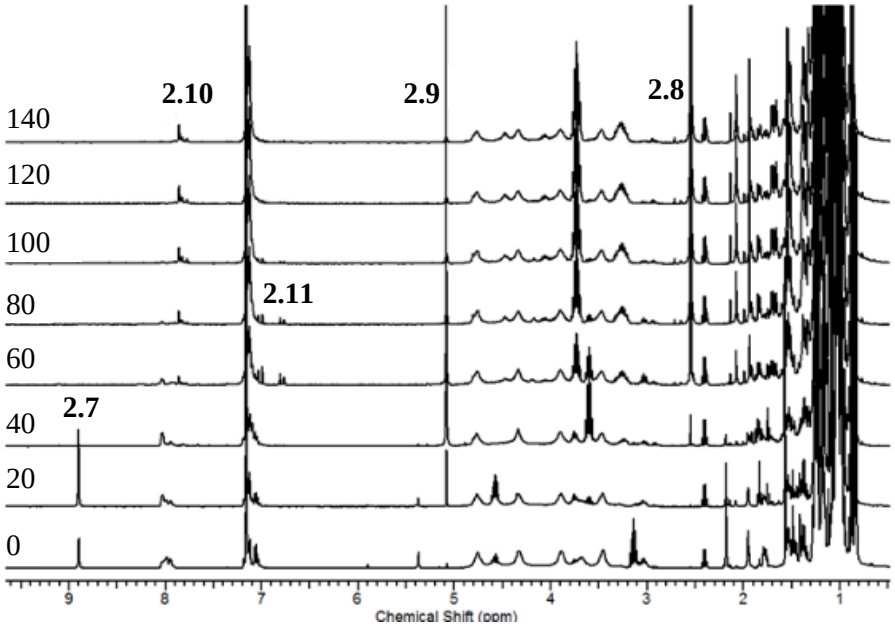

Figure 2.9: ^{1}H NMR spectrum (400 MHz) recorded every 20 minutes for the reaction of HBpin and ^{i}PrNCO catalysed by 10 mol% **Ib** at 60°C.

In the earliest stages of the reaction a new compound was identified, characterised by the appearance of a high frequency singlet resonance at δ 8.90 ppm, **2.7** (Figure 2.9). Although an appreciable quantity of this species was produced after 15 minutes, it was rapidly consumed to a low but observable steady state concentration throughout the reaction. This species, which is tentatively assigned as the *N*–borylated formamidine, ^{i}PrN(Bpin)HC(O), **2.7**, accumulates prior to any observable methyl amine formation, **2.8**, (Figure 2.9) and is consumed simultaneously with the appearance of significant quantities of a bis–borylated hemiaminal derivative, ^{i}Pr(pinB)NCH$_2$OBpin, **2.9**, analogous to compounds **2.4** and **2.5**, which is apparent as a persistent singlet resonance at δ 5.08 ppm. A further low field singlet at δ 7.80 ppm corresponds to **2.10** (Figure 2.9). Once evolved, this latter resonance was observed to persist at an effectively constant intensity throughout the course of the catalysis. This chemical shift is reminiscent of the signal associated with the amidato methine proton observed for compound **2.2** (δ 7.65 ppm) and is suggested to arise from a borate intermediate with a comparable constitution that is formed in a steady state concentration as a key intermediate

during the reduction of ^{i}PrNCO. The initial appearance of this species was accompanied by the emergence of a clear AB spin system (**2.11**, Figure 2.9), which may be assigned to the methylene imine, ^{i}PrN=CH$_2$. This small molecule is evidently consumed, however, at more mature phases of the catalysis.

Evidence for a sequential mechanism was provided by examination of the temporal evolution of the signals assigned to **2.7 – 2.9** during the reduction of ^{i}PrNCO. Figure 2.10 illustrates that the observed intermediate products accumulate during the course of the reactions in quantities greater than that of the catalyst loading, suggesting that the formamidine and hemiaminal species are released but can re–insert into the catalytic cycle to undergo further reduction.

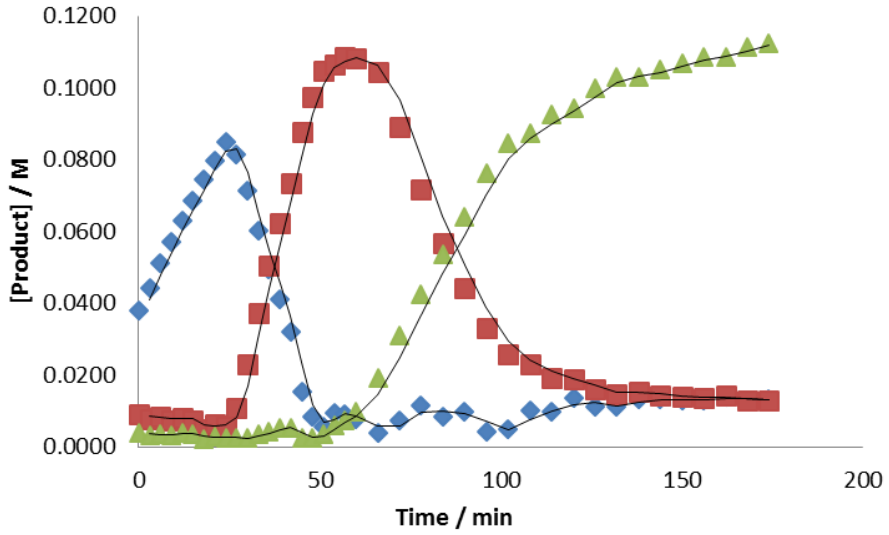

Figure 2.10: Plot of [Product] *versus* time for the hydroboration of ^{i}PrNCO catalysed by **Ib** at 60°C. (♦ = ^{i}PrN(Bpin)HC(O), **2.7**), (■ = ^{i}PrN(Bpin)CH$_2$OBpin, **2.9**), (▲ = ^{i}PrN(Bpin)CH$_3$, **2.8**).

Although these observations attest to a complex mechanism, it is postulated that the gross features of this reactivity may be rationalised by the general mechanism illustrated in Scheme 2.14. Two pathways are delineated, both of which result in the ultimate catalytic production of the *N*–borylated methyl amine product. No attempt is made to discriminate between potentially dimeric or monomeric intermediates. In common with previous mechanistic studies of a variety of reactions catalysed by *β*–diketiminato magnesium centres, however, it is likely that a necessity for dimer to monomer pre–equilibration exerts a crucial influence on the kinetics of the individual reactions[5] (Chapter One, Section 1.6.3) possibly elucidating why increased RNCO substituent steric demands provided generally faster reaction times, Scheme 2.13.

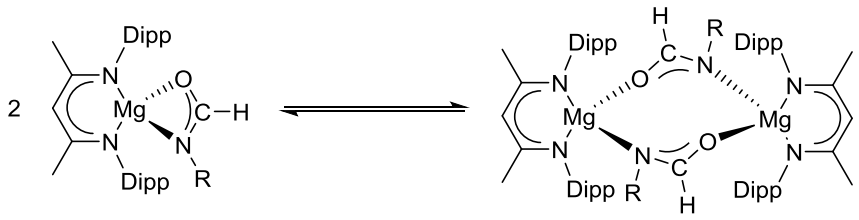

Scheme 2.13: Likely monomer – dimer pre–equilibrium.

Although it is doubtful that any magnesium hydride persists under catalytic conditions, both pathways are rationalised to be initiated through borane activation of the pre–catalyst (**Ib**, not shown) to provide the transient magnesium hydride, **Ih**, necessary to generate formamidate and borate intermediates analogous to compounds **2.1** and **2.2** (Scheme 2.14). The apparent stability of this latter compound mitigated against its direct thermal conversion to boron–containing small molecules at temperatures relevant to the catalysis. It is, thus, suggested that the most kinetically accessible cycle, Scheme 2.14, (***Cycle 1***), necessitates breakdown of a similar borate species to produce **2.7**. This process occurs by the necessary activation of the borate intermediate through its interaction with a further equivalent of Lewis acidic HBpin prior to intramolecular boron to magnesium hydride transfer and is, thus, reminiscent of recent reports by the Hill group on related magnesium borate species identified during the hydroboration of organic carbodiimides[3c] and nitriles[5b]. Although viable concentrations of the *N*–borylated formamidine accumulate during the early stages of catalysis, this species is apparently consumed through its onward reaction with a magnesium hydride. No resultant magnesium hemiaminalate species have been identified but it is suggested that compounds of this type will be rapidly consumed through further B–H/Mg–O metathesis to yield **2.9**. The ultimate production of **2.8** and closure of the catalytic cycle are then predicated upon a sequence of C–O/Mg–H and Mg–O/B–H metathesis steps reminiscent of the stoichiometric reactivity summarised for the isolable species **2.3** and **2.5** in Scheme 2.8 – Scheme 2.10.

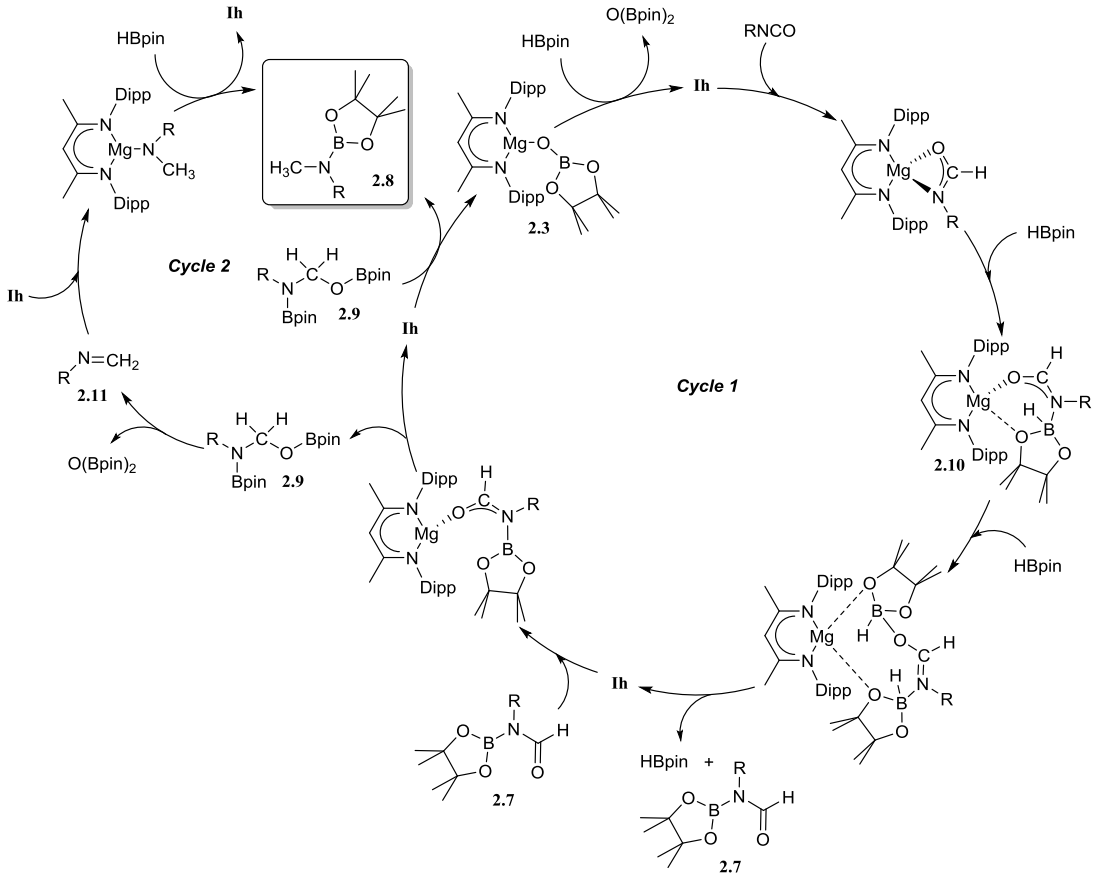

Scheme 2.14: Proposed mechanism for the **Ih** catalysed hydrodeoxygenation of organic isocyanates.

Although these observations suggest that this reaction sequence predominates under the mild conditions applied during catalysis, the mechanism must also reconcile the production and consumption of the imine **2.11**. It is notable that appreciable quantities of this methylene imine are only observed after the generation of significant amounts of **2.9**. It is inferred, therefore, that this small molecule is generated by the direct decomposition of **2.9** rather than any higher energy magnesium–centred process and implicates a second plausible pathway for the production of **2.8**, Scheme 2.12, ***Cycle 2***, analogous to the reaction pathway reported in Chapter One, Section 1.6.2.

2.5 Computational Studies of Catalytic Hydrodeoxygenation of Isocyanates

The mechanism proposed in Scheme 2.14 was investigated by density functional theory (DFT) for the hydroboration of PhNCO. Calculations were performed by Professor L. Maron of the University of Toulouse and his collaborator, Dr Yan Yang of Lanzhou University. Calculations (B3PW91) validated all the individual reaction steps for the complete structures shown in Figure 2.11. Species akin to compounds **2.1** and **2.2** were found to be formed by an overall exothermic (ΔH = –38.8 kcal mol^{-1}) sequence of isocyanate Mg–H

insertion and subsequent reactions of the *in situ* generated magnesium amidate with HBpin. As deduced from the stability of compound **2.2**, the production of a borylated formamide analogous to compound **2.6** entails the interaction of the magnesium amidatoborate with a second equivalent of HBpin to enable the necessary boron to magnesium hydride transfer. While the production of compounds such as **2.6** requires a transversal of several higher energy transition states and intermediates, these processes occur prior to an exothermic re–insertion of the carbonyl function (ΔH = *ca.* –30 kcal mol^{-1}) into the magnesium hydride bond. The subsequent generation of the bis(borylated)hemiaminals such as **2.4** and **2.5** occurs *via* B–H/Mg–O sigma bond metathesis, which incurs an enthalpic penalty of some 25 kcal mol^{-1}. The ultimate cleavage of the C–O bond and production of the final methyl amine product requires the further interaction of these reduced intermediates with a magnesium hydride, whereupon the formation of a boryloxide derivative similar to compound **2.3** is significantly exothermic (ΔH = –46.2 kcal mol^{-1}). Dimerisation and a subsequent Mg–O/H–B metathesis with HBpin yield $(pinB)_2O$ with the regeneration of the magnesium hydride **Ih**.

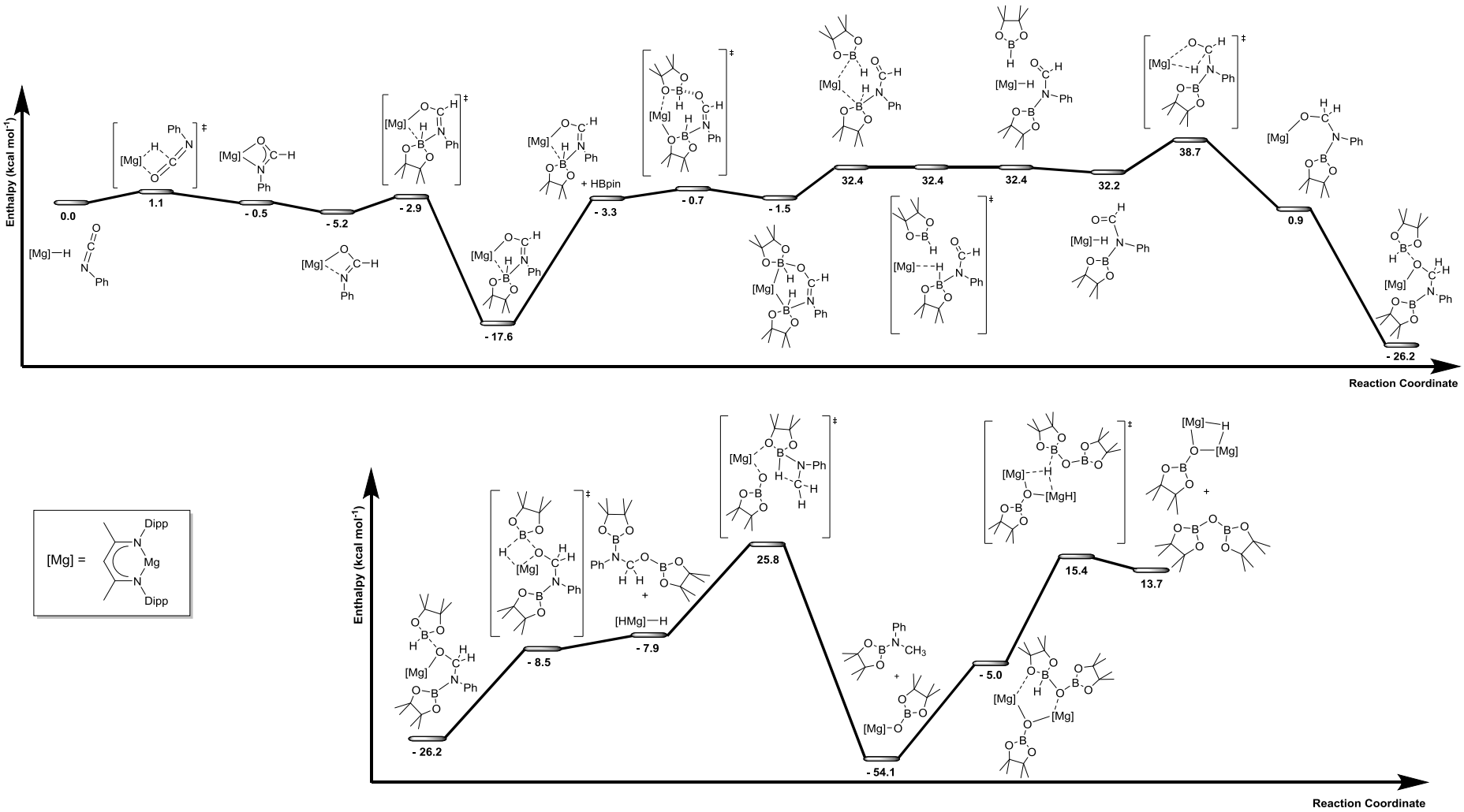

Figure 2.11: DFT calculations (B3PW91) of the mechanism for the **Ib** catalysed hydrodeoxygenation of PhNCO with HBpin.

In conclusion, this Chapter has described a mild protocol for the catalytic transformation of the isocyanate function to a methyl amine. The activation of the heterocumulene occurs through a magnesium–centred hydroboration process and, ultimately, the complete cleavage of the C=O bond. The next two Chapters will explore whether this activity can be extended to the formylation products produced through reactions of magnesium hydrides and primary amides with C≡O and be applied more generally to the heavier alkaline earth congeners.

2.6 References

1. a) R. Rochat, M. J. Lopez, H. Tsurugi and K. Mashima, *ChemCatChem*, 2016, **8**, 10–20; b) M. Arrowsmith and M. S. Hill, in *Comprehensive Inorganic Chemistry II (Second Edition)*, ed. K. Poeppelmeier, Elsevier, Amsterdam, Editon edn., 2013, pp. 1189–1216; c) A. G. M. Barrett, M. R. Crimmin, M. S. Hill and P. A. Procopiou, *Proceedings of the Royal Society of London A: Mathematical, Physical and Engineering Sciences*, 2010, **466**, 927–963; d) M. S. Hill, D. J. Liptrot and C. Weetman, *Chemical Society Reviews*, 2016, **45**, 972–988.
2. M. Arrowsmith, T. J. Hadlington, M. S. Hill and G. Kociok–Kohn, *Chemical Communications*, 2012, **48**, 4567–4569.
3. a) M. Arrowsmith, M. S. Hill, T. Hadlington, G. Kociok–Köhn and C. Weetman, *Organometallics*, 2011, **30**, 5556–5559; b) J. Intemann, M. Lutz and S. Harder, *Organometallics*, 2014, **33**, 5722–5729; c) C. Weetman, M. S. Hill and M. F. Mahon, *Chemistry – A European Journal*, 2016, **22**, 7158–7162.
4. M. Arrowsmith, M. S. Hill and G. Kociok–Köhn, *Chemistry – A European Journal*, 2013, **19**, 2776–2783.
5. a) C. Weetman, M. S. Hill and M. F. Mahon, *Chemical Communications*, 2015, **51**, 14477–14480; b) C. Weetman, M. D. Anker, M. Arrowsmith, M. S. Hill, G. Kociok–Kohn, D. J. Liptrot and M. F. Mahon, *Chemical Science*, 2016, **7**, 628–641.
6. a) W. Y. Lee, C. H. Park, H.–J. Kim and S. Kim, *The Journal of Organic Chemistry*, 1994, **59**, 878–884; b) K. Baumann, H. Knapp, G. Strnadt, G. Schulz and M. A. Grassberger, *Tetrahedron Letters*, 1999, **40**, 7761–7764; c) A. M. Ruppert, K. Weinberg and R. Palkovits, *Angewandte Chemie International Edition*, 2012, **51**, 2564–2601; d) J. J. Bozell and G. R. Petersen, *Green Chemistry*, 2010, **12**, 539–554; e) P. N. R. Vennestrøm, C. M. Osmundsen, C. H. Christensen and E. Taarning, *Angewandte Chemie International Edition*, 2011, **50**, 10502–10509.
7. a) D. L. J. Clive and J. Wang, *The Journal of Organic Chemistry*, 2002, **67**, 1192–1198; b) M. Huang, *Journal of the American Chemical Society*, 1949, **71**, 3301–3303.
8. M. Mehta, M. H. Holthausen, I. Mallov, M. Pérez, Z.–W. Qu, S. Grimme and D. W. Stephan, *Angewandte Chemie International Edition*, 2015, **54**, 8250–8254.
9. a) D. Mukherjee, A. Ellern and A. D. Sadow, *Chemical Science*, 2014, **5**, 959–964; b) N. L. Lampland, M. Hovey, D. Mukherjee and A. D. Sadow, *ACS Catalysis*, 2015, **5**, 4219–4226.
10. M. D. Anker, M. Arrowsmith, P. Bellham, M. S. Hill, G. Kociok–Kohn, D. J. Liptrot, M. F. Mahon and C. Weetman, *Chemical Science*, 2014, **5**, 2826–2830.
11. S. Hawkeswood and D. W. Stephan, *Dalton Transactions*, 2005, 2182–2187.
12. J. Shi, Z. Guo, X. Wei, D. Liu and M. F. Lappert, *Synlett*, 2011, **2011**, 1937–1939.
13. a) P. J. Bailey, R. A. Coxall, C. M. Dick, S. Fabre, L. C. Henderson, C. Herber, S. T. Liddle, D. Loroño–González, A. Parkin and S. Parsons, *Chemistry – A European Journal*, 2003, **9**, 4820–4828; b) B. M. Chamberlain, M. Cheng, D. R. Moore, T. M. Ovitt, E. B. Lobkovsky and G. W. Coates, *Journal of the American Chemical Society*, 2001, **123**, 3229–3238; c) M. H. Chisholm, J. Gallucci and K. Phomphrai, *Inorganic Chemistry*, 2002, **41**, 2785–2794; d) M. H. Chisholm, K. Choojun, J. C. Gallucci and P. M. Wambua, *Chemical Science*, 2012, **3**, 3445–3457.
14. a) M. Ahijado Salomon, T. Braun and A. Penner, *Angewandte Chemie International Edition*, 2008, **47**, 8867–8871; b) C. Borner and C. Kleeberg, *European Journal of Inorganic Chemistry*, 2014, **2014**, 2486–2489; c) A. C. Fernandes, J. A. Fernandes, F. A. Almeida Paz

and C. C. Romao, *Dalton Transactions*, 2008, 6686–6688; d) S. I. Kallane, T. Braun, M. Teltewskoi, B. Braun, R. Herrmann and R. Laubenstein, *Chemical Communications*, 2015, **51**, 14613–14616; e) D. S. Laitar, P. Müller and J. P. Sadighi, *Journal of the American Chemical Society*, 2005, **127**, 17196–17197; f) J. Plotzitzka and C. Kleeberg, *Organometallics*, 2014, **33**, 6915–6926.

15. S. P. Green, C. Jones and A. Stasch, *Science*, 2007, **318**, 1754–1757.

Chapter Three

Alkaline Earth Mediated CO Homologation and Reduction

3.1 Introduction

As previously discused in Chapter One (Section 1.7) the deoxygenative conversion of carbon monoxide to hydrocarbon fuels is typically achieved through heterogeneous catalytic methods.[1] In contrast, only limited progress has been achieved with well–defined homogeneous systems and at CO pressures typically in excess of 1000 atm.[2]

More recent activity has targeted the synthesis of putative Fischer–Tropsch (F–T) intermediates including, and most pertinent to this Chapter, enediolates such as the aforementioned zirconium, **XIX**, thorium, **XXII**, and cerium species, **XXVI**, **(**Figure 3.1) which were prepared through treatment of the relevant metal hydride with CO.[3]

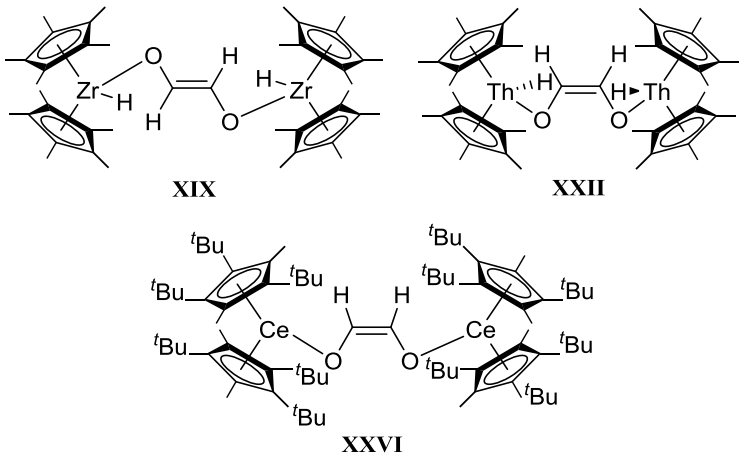

XIX **XXII** **XXVI**

Figure 3.1: Zirconium, thorium and cerium enediolates prepared though treatment of the relevant metal hydride with CO.

In this Chapter it is demonstrated that similar CO homologation reactivity may be achieved through exposure of the *β*–diketiminato magnesium **Ih**,[4] and calcium **Ii**,[5] hydride complexes to one atmosphere of CO. Furthermore, the intermediate species produced during the formation of these alkaline earth enediolates may be intercepted and incorporated into a catalytic regime to afford the highly selective catalytic reduction of the carbon monoxide molecule to a methane analogue, in the case of magnesium, or a methoxysilane species in the case of calcium.

3.2 Alkaline Earth Mediated CO Homologation

It was envisaged that exposure of compounds **Ih** and **Ii,** to one atmosphere of CO would lead to the reductive coupling of two CO molecules, and form enediolate species (Scheme 3.1) analogous to those resulting from the reaction of the rare earth and electropositive transition metal hydrides, **XXII** and **XXVI**.

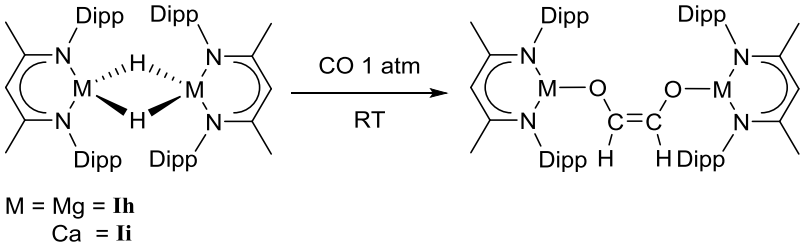

Scheme 3.1: Postulated products from the reaction of **Ih** and **Ii** with CO.

Compound **Ih** was exposed to one atmosphere of CO at room temperature for two hours, providing a single new species, **3.1**, characterised by the appearance of a singlet resonance at δ 5.53 ppm in the resultant ^{1}H NMR spectrum. An accompanying vinylic carbon resonance at δ 131.7 ppm was also observed in the corresponding ^{13}C{^{1}H} NMR spectrum (Scheme 3.2).

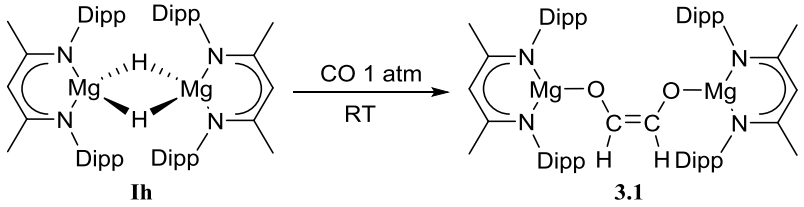

Scheme 3.2: Postulated product from the reaction of **Ih** with CO.

Repetition of this reaction with ^{13}CO provided ready access to the isotopomer (**3.1**–^{13}C), which comprised diagnostic 10 line AA′ XX′ patterns ($^{1}J_{CH}$ = 174.4, $^{2}J_{CH}$ = 20.4, $^{1}J_{CC}$ = 79.5, $^{3}J_{HH}$ = 1.3 Hz) in both the ^{1}H and ^{1}H–^{13}C gated NMR spectra, and matched simulated data (Figure 3.2). Replacement of the atmosphere of this sample with ^{12}CO resulted in no simplification of the AA'XX' spin system even at elevated temperatures indicating that the formation of compound **3.1** is irreversible. These data are closely comparable to those reported for compounds **XXII** and **XXVI** and are thus similarly indicative of the reductive coupling of two molecules of CO to form a dinuclear magnesium enediolate species, Scheme 3.2.[3]

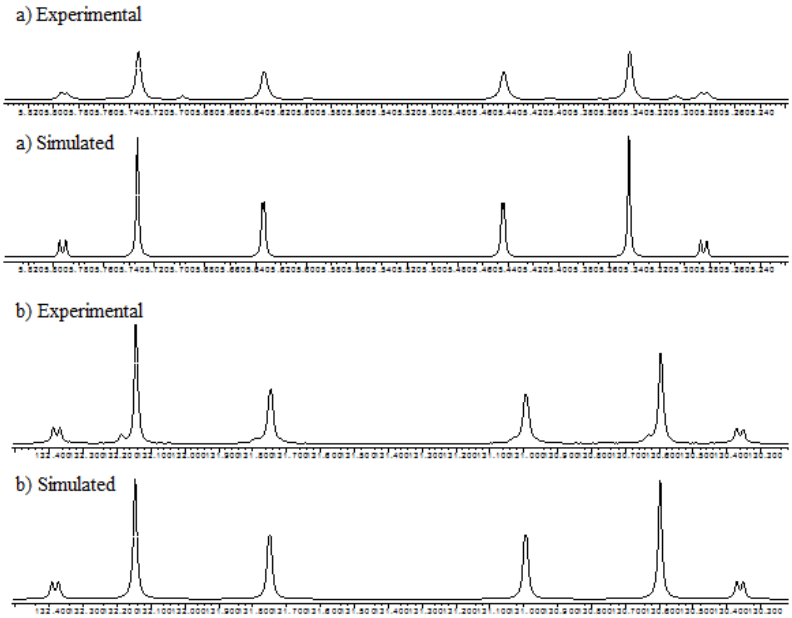

Figure 3.2: 10 line AA′ XX′ patterns resulting from compound **3.1** ($^{1}J_{CH}$ = 174.4, $^{2}J_{CH}$ = 20.4, $^{1}J_{CC}$ = 79.5, $^{3}J_{HH}$ = 1.3 Hz). a) ^{1}H NMR (500 MHz) and simulated spectra. b) ^{1}H–^{13}C NMR (125.75 MHz) and simulated spectra.

These deductions were confirmed through a subsequent X–ray diffraction analysis, the results of which are illustrated in Figure 3.3, performed on single crystals of compound **3.1** grown from a saturated *n*–pentane solution. While the C30–C31 distance (1.327(3) Å) is clearly indicative of the formation of a C=C double bond and a *cis*–enediolate similar to that observed in both compounds **XXII** and **XXVI**, the ligand does not adopt a directly analogous symmetrical bridging disposition. Rather, the planar *cis*–enediolate adopts an asymmetric bridging mode in which one four–coordinate *pseudo*–tetrahedral magnesium (Mg1) centre is bound through chelation by both O1 (Mg1–O1 1.92(1) Å) and O2 (Mg1–O2 2.01(1) Å). This latter bond is slightly elongated as O2 is also bound to the further trigonal Mg2 centre (Mg2–O2 1.88(1) Å).

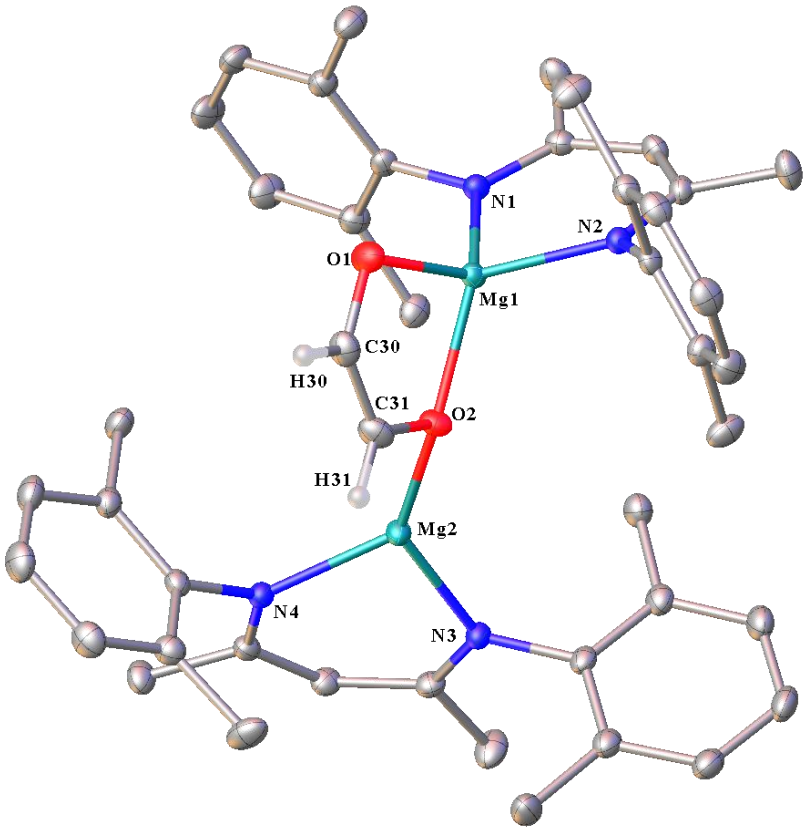

Figure 3.3: ORTEP representation of compound **3.1** (30% probability ellipsoids). Hydrogen atoms except those attached to C30 and C31 and iso–propyl methyl groups are removed for clarity. Selected bond lengths (Å) and angles (°):Mg1–O1 1.9270(14), Mg1–O2 2.0142(14), Mg1–N1 2.0515(15), Mg1–N2 2.0484(15), Mg2–O2 1.8836(14), Mg2–N4 2.0140(15), Mg2–N3 2.0057(16), C30–C31 1.327(3), O1–Mg1–O2 87.55(6), O1–Mg1–N1 120.14(7), O1–Mg1–N2 118.32(7), O2–Mg2–N3 133.09(7), O2–Mg2–N4 128.81(7), N3– Mg2–N4 97.50(6).

A variable temperature ^{1}H NMR study performed on **3.1** in toluene–d_8 did not display any resolution in the methylene singlet resonance at δ 5.53 ppm down to the low temperature limit of –93°C. It is, thus, suggested that the enediolate chelate undergoes facile exchange between both Mg1 and Mg2 centres at a rate that is faster than the NMR time scale. The geometry and resultant asymmetry of compound **3.1** in the solid state is, therefore, advocated to be reflective of the lowest energy conformer and is not retained in solution.

In contrast to **Ih**, a solution of the calcium hydride **Ii** in d_8–toluene, immediately provided a single new species (**3.2**) when exposed to one atmosphere of CO at room temperature. Compound **3.2** was characterised by the appearance of a singlet resonance at δ 5.00 ppm in the resultant ^{1}H NMR spectrum with an accompanying vinylic carbon resonance at δ 134.9 ppm in the corresponding ^{13}C{^{1}H} NMR spectrum. These data were closely

reminiscent of the aforementioned results arising from compound **3.1**, leading to the postulated formation of the calcium enediolate complex **3.2** (Scheme 3.3).

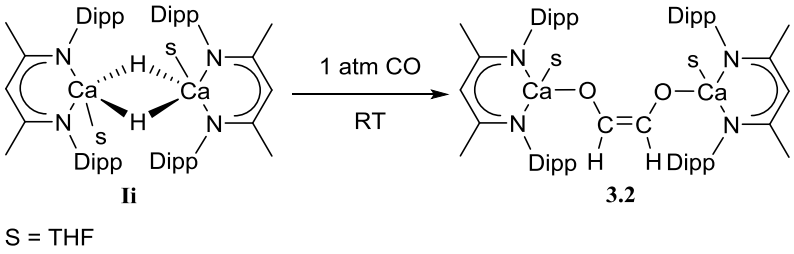

Scheme 3.3: Postulated formation of Compound **3.2** to compound **Ii** under 1 atm. of CO at RT.

Repetition of this reaction with ^{13}CO once more provided ready access to the isotopomer (**3.2**–^{13}C), which comprised diagnostic 10 line AA′ XX′ patterns ($^{1}J_{CH}$ = 180.9, $^{2}J_{CH}$ = 20.4, $^{1}J_{CC}$ = 61.6, $^{3}J_{HH}$ = 1.1 Hz) in both the ^{1}H and ^{1}H gated ^{13}C NMR spectra, consistent with simulated data (Figure 3.4) and with the constitution of compound **3.2** as a *β*–diketiminato calcium *cis*–enediolate.

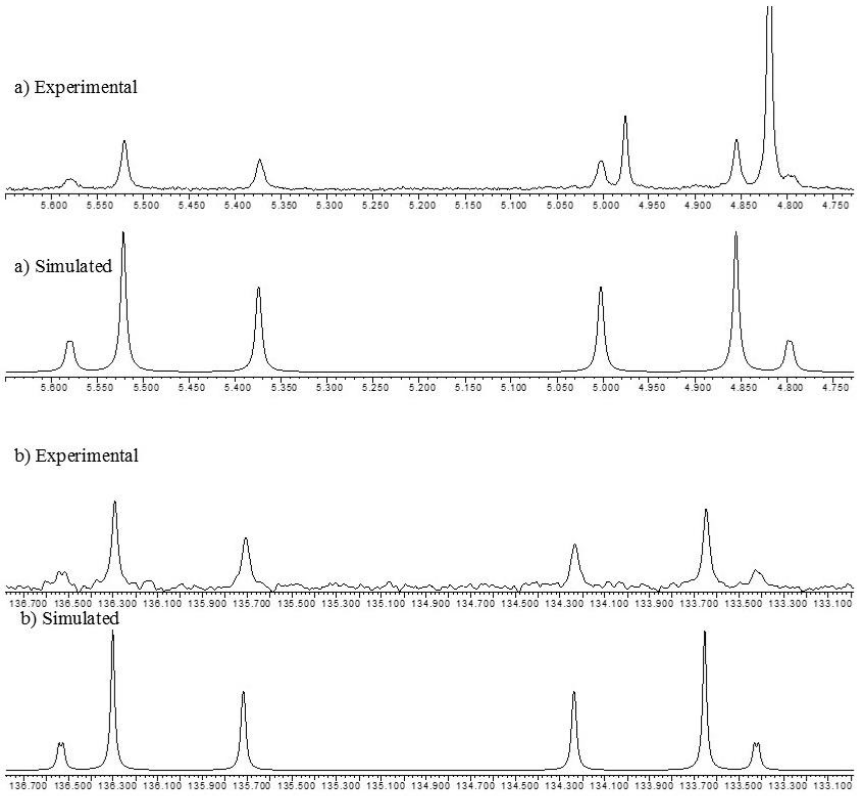

Figure 3.4: 10 line AA′ XX′ patterns resulting from compound **3.2** ($^{1}J_{CH}$ = 180.9, $^{2}J_{CH}$ = 20.4, $^{1}J_{CC}$ = 61.6, $^{3}J_{HH}$ = 1.1 Hz). a) ^{1}H NMR (500 MHz) and simulated spectra. b) ^{1}H gated ^{13}C NMR (125.75 MHz) and simulated spectra.

An X–ray structural analysis, Figure 3.5, was performed on a single crystal of compound **3.2** grown from a saturated toluene solution. The solid state structure of **3.2** confirmed the formation of a dimeric *β*–diketiminato calcium *cis*–endiolate. Calcium centres Ca1 and Ca2 are coordinated by terminal bidentate *β*–diketiminate ligands that are staggered with respect to each other. The bridging *cis*–endiolate (O1–C30–C21–O2) ligand, however, bonds with an η^4–interaction to each calcium centre. Both calcium centres, Ca1 and Ca2, exhibit a distorted pentagonal bipyramidal geometry, with the final coordination sites filled by a THF ligand. This increase in enediolate ligand hapticity between **3.1** and **3.2** is attributed to the increase in ionic radii from magnesium (0.78 Å) to calcium (1.06 Å).

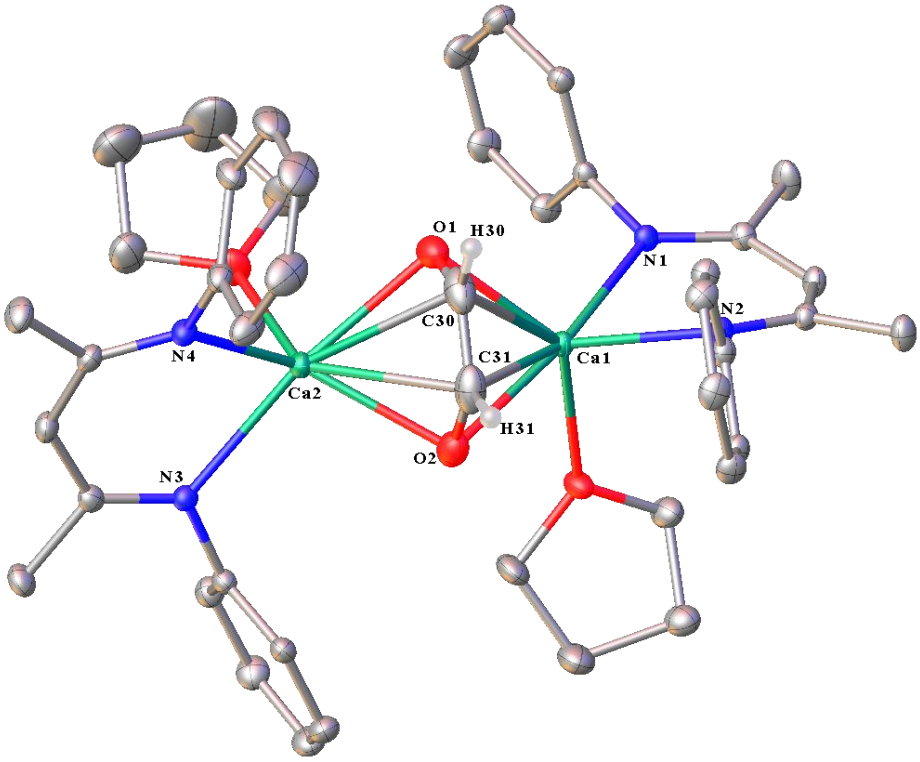

Figure 3.5: ORTEP representation of compound **3.2** (30% probability ellipsoids). Hydrogen atoms except those attached to C30 and C31 and iso–propyl methyl groups are removed for clarity. Selected bond lengths (Å) and angles (°): Ca1–O1 2.329(2), Ca1–O2 2.3558(19), Ca1–O3 2.3803(16), Ca1–N1 2.4126(18), Ca1–N2 2.3758(18), Ca1–C30 2.623(3), Ca1–C31 2.625(3), Ca2–O1 2.349(2), Ca2–O2 2.3505(19), Ca2–O4 2.3663(19), Ca2–N3 2.4028(18), Ca2–N4 2.3859(19), Ca2–C30 2.607(3), Ca2–C31 2.612(3), O1–C30 1.365(4), O2–C31 1.353(4), C30–C31 1.346(5). O2–Ca1–N1 167.26(7), O2–Ca1–N2 113.57(7), O1–Ca1–N1 106.89, O1–Ca1–N2 118.35(7), N1–Ca1–C30 127.62(9), N1–Ca1–C31 156.32(9), N2–Ca1–C30 96.59(8), N2–Ca1–C31 94.73(8), N2–Ca1–N1 78.96(6), O2–Ca2–N3 102.44(7), O2–Ca2–N4 128.38(7), O1–Ca2–N3 165.90(7), O1–Ca2–N4 114.77(7), N3–Ca2–C30 151.82(10), N3–Ca2–C31 122.74(9), N4–Ca2–N3 79.33(6), N4–Ca2–C30 99.77(8), N4–Ca2–C31 105.40(8), C31–C30–O1 119.2(3), C30–C31–O2 119.8(3).

Irrespective of any variation across the solid state binding of the endiolate moiety, the synthesis of compounds **3.1** and **3.2** demonstrates that the reactivity of **Ih** and **Ii** to CO homologation is analogous to that previously observed for rare earth and transition metal hydrides.

3.3 Mechanistic Studies

In order to probe the mechanistic pathway leading to the formation of both the *β*–diketiminato magnesium, **3.1**, and calcium, **3.2**, *cis*–enediolate complexes, a series of low temperature reactions were undertaken, Scheme 3.4.

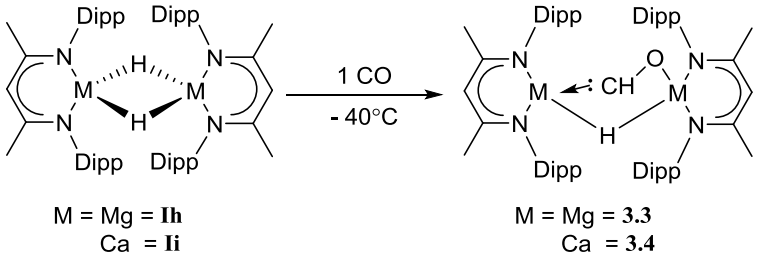

Scheme 3.4: reaction of **Ih** and **Ii** with 1 atm of ^{13}CO at –60°C.

The reaction between compound **Ih** and ^{13}CO in d_8–toluene was performed at –60°C and monitored by ^{1}H and ^{13}C NMR spectroscopy. Even under these reduced temperature conditions, the onset of the formation of the isotopomer, **3.1**–^{13}C was clearly apparent. An increase in temperature to –40°C, however, resulted in the observation of a new species (**3.3**) characterised by a doublet resonance at δ 14.08 ppm ($^{1}J_{CH}$ = 102.5 Hz, Figure 3.6 (a)) in the ^{1}H NMR spectrum and the appearance of a new heavily deshielded singlet signal at δ 358.9 ppm in the $^{13}C\{^{1}H\}$spectrum. In the corresponding ^{1}H gated ^{13}C NMR spectrum, this latter resonance was observed as a doublet of doublets ($^{1}J_{CH}$ = 102.5, $^{2}J_{HH}$ = 12 Hz, Figure 3.6 (b)).

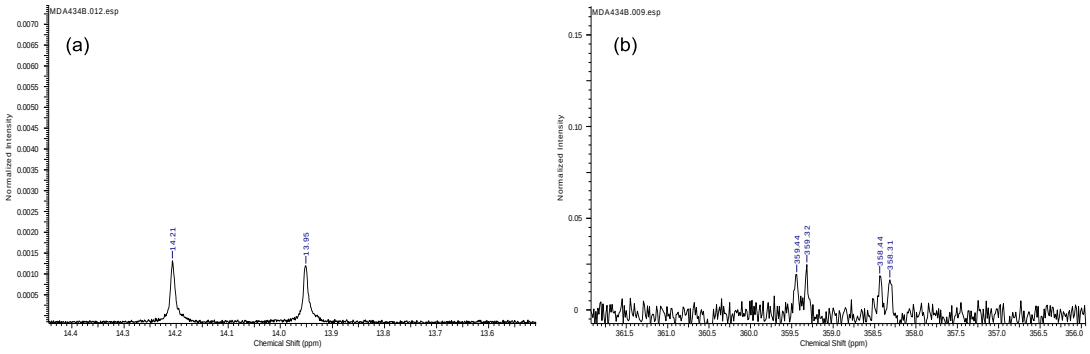

Figure 3.6: (a) ^{1}H NMR (400 MHz) spectrum of doublet resonance at δ 14.08 ppm. (b) ^{1}H – ^{13}C NMR (125.75 MHz) gated spectrum of the deshielded doublet of doublets at δ 358.9 ppm.

A HSQC experiment revealed these two signals to be related and coupled to a further resonance, otherwise obscured by the *β*–diketiminato *iso*–propyl methine signal, at *ca.* δ 3.1 ppm by a ^{13}C–^{1}H correlation experiment, Figure 3.7.

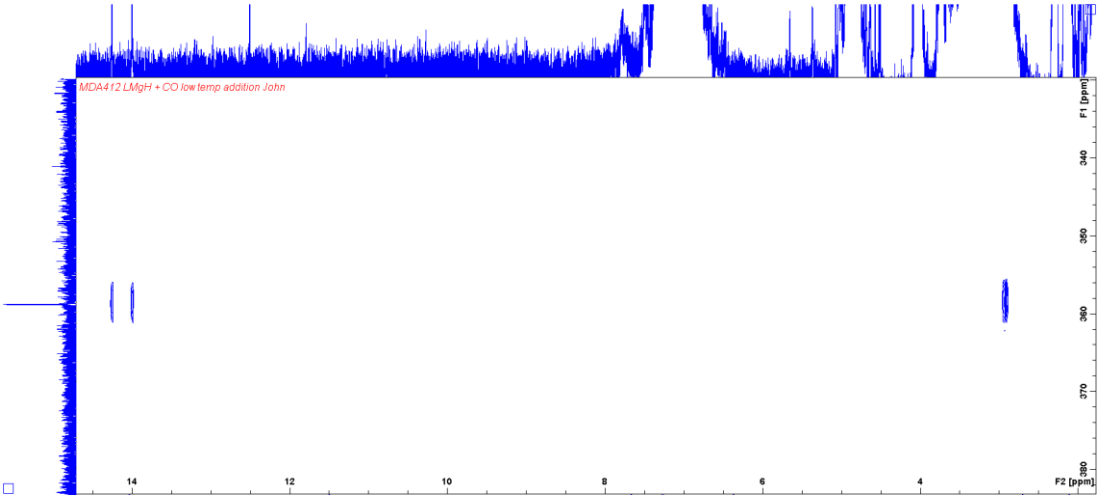

Figure 3.7: HSQC NMR spectra displaying the two related hydrogen atoms of **3.3**.

The heavily deshielded $^{13}C\{^{1}H\}$ NMR signal associated with species **3.2** is strongly reminiscent of the characteristic low field acyl carbon resonances observed for a series of thorium(IV) acyl species, $[Th(\eta^5\text{–}C_5H_5)_3(\eta^2\text{–}COR)]$ (R = H,[3c] alkyl[6]) by Marks and co–workers. In these latter cases the dihapto acyl unit was ascribed a modicum of carbene–like character which was manifest through, in several cases, the observation of a tautomerization process to thorium enolate species. On the basis of these previous observations, compound **3.3** is ascribed as a formyl–hydrido dimagnesium species formed through the reaction of the dimeric compound **Ih** with a single molecule of carbon monoxide, Scheme 3.5. No further species could be discriminated during continued monitoring of the low temperature conversion of **Ih** to **3.1**–^{13}C.

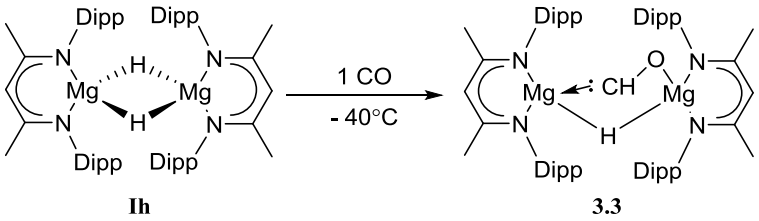

Ih **3.3**

Scheme 3.5: Single CO insertion into the Mg–H bond of **Ih**, gives the formyl–hydrido dimagnesium species, **3.3**.

Analogous monitoring of the reaction between compound **Ii** and ^{13}CO in d_8–toluene at –60°C by ^{1}H and ^{13}C NMR spectroscopy only revealed the formation of **3.2**. Neither a

decrease of the temperature to the lower limit (–93°C) nor an increase of the temperature allowed the identification of any intermediates. This result is most likely due to the increased reactivity of **Ii** to CO homologation, compared to **Ih**.

No other intermediates could be delineated in the reactions of either **Ih** or **Ii** and one atmosphere of CO at reduced temperatures. The identification of **3.3** by NMR spectroscopy, however, led to the postulate that stoichiometric addition of a single equivalent of CO to the alkaline earth hydrides could enable the isolation of an intermediate with a constitution similar to **3.3** and closely related to the cerium oxymethylene compound, **XXV** reported by Andersen and co–workers, Figure 3.8.[3f]

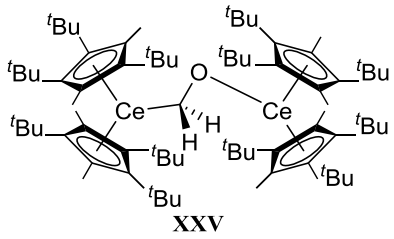

Figure 3.8: Andersen's oxymethylene compound, **XXV**.

In collaboration with Professor F.G.N. Cloke and Dr N Tsoureas of the University of Sussex, one equivalent of CO was added to a solution of **Ih** and **Ii** *via* Toepler pump at room temperature and at –78°C, Scheme 3.6. In all cases, however, these procedures led to the facile formation of half an equivalent of **3.1** and **3.2** respectively and the consumption of only 50% of the hydride starting materials.

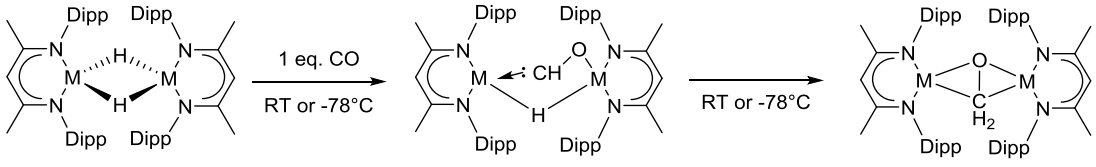

Scheme 3.6: Attempted stoichiometric addition of CO to **Ih** or **Ii** could yield an alkaline earth formyl–hydrido or oxomethylene species.

Although no other intermediates could be identified or isolated, a reaction pathway to the *cis*–enediolate compounds, **3.1** and **3.2** is proposed in Scheme 3.7. The initial carbonylation product, compound **3.3/4**, is proposed to be rapidly consumed through intramolecular hydride transfer to form a dinuclear oxomethylene species, **3.5**, similar to the

cerium complex **XXV**. Species **3.5** is prone to C–C coupling through its reaction with a further molecule of CO while the stereochemistry of the *cis*–enediolate, compounds **3.1** and **3.2**, will ensue through a 1,2–hydrogen shift within species **3.6**, the selectivity of which is dictated by the anti–periplanar orientation of the C–O bond to the carbene lone pair across the OCH_2CO unit.

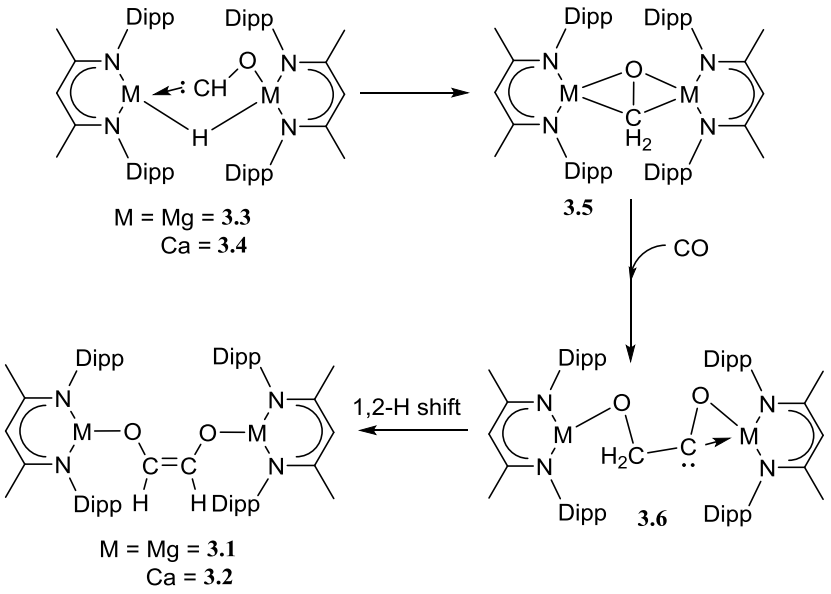

Scheme 3.7: Proposed reaction pathway for the formation of compounds **3.1** and **3.2**.

While alternative pathways may be envisaged, including the dimerisation of two carbene–like formyl units after reaction of **3.3/4** with a further equivalent of CO, there is no compelling justification to suggest that the route to compound **3.1** and **3.2**, contrasts with that formerly deduced for the formation of compounds such as **XXII** and **XXVI**.[3] The identification of **3.3** by NMR spectroscopy and, thus, the inference of **3.4**, purports to interesting onward reactivity if these reactive intermediates can be intercepted.

3.3.1 CO homologation Utilising The Bulkier Magnesium Hydride

The more sterically encumbered ^{t}Bu–substituted *β*–diketiminato magnesium hydride,[4] **XXVII**, was synthesised in anticipation that the increased steric congestion of the metal centre would affect the postulated reduction pathway (Scheme 3.7), to give a solid state structure more closely resembling the literature compounds **XXII** and **XXVI**. Exposure of compound **XXVII** to one atmosphere of ^{13}CO at room temperature provided a single new species, **3.7**, characterised by the diagnostic 10 line AA′ XX′ patterns ($^1J_{CH}$ = 170.2, $^2J_{CH}$ = 24.9, $^1J_{CC}$ = 80.5, $^3J_{HH}$ = 0.7 Hz) in both the ^1H and ^1H–^{13}C gated NMR spectra, indicating the formation of a new *cis*–enediolate complex **3.7**, Scheme 3.8.

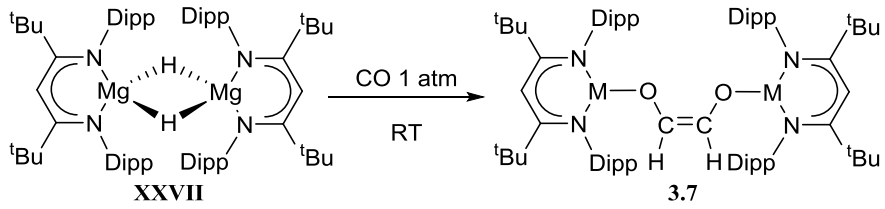

XXVII **3.7**

Scheme 3.8: CO reduction using the bulkier ^{t}Bu β–diketiminato magnesium hydride, **XXVII**.

Crystallisation from the reaction solution at room temperature provided **3.7** as colourless blocks suitable for an X–ray diffraction experiment, Figure 3.9. The solid state structure of **3.7** demonstrates that increased steric congestion of the magnesium centre leads to no conformational change and the adoption of the κ^2– κ^1– magnesium bridging mode by the enediolate ligand which is strongly reminiscent of that observed in **3.1**. Although there are some slight variations across the most relevant bond lengths and angles, the similarity of these species renders any further comment about the structure of **3.7** unnecessary.

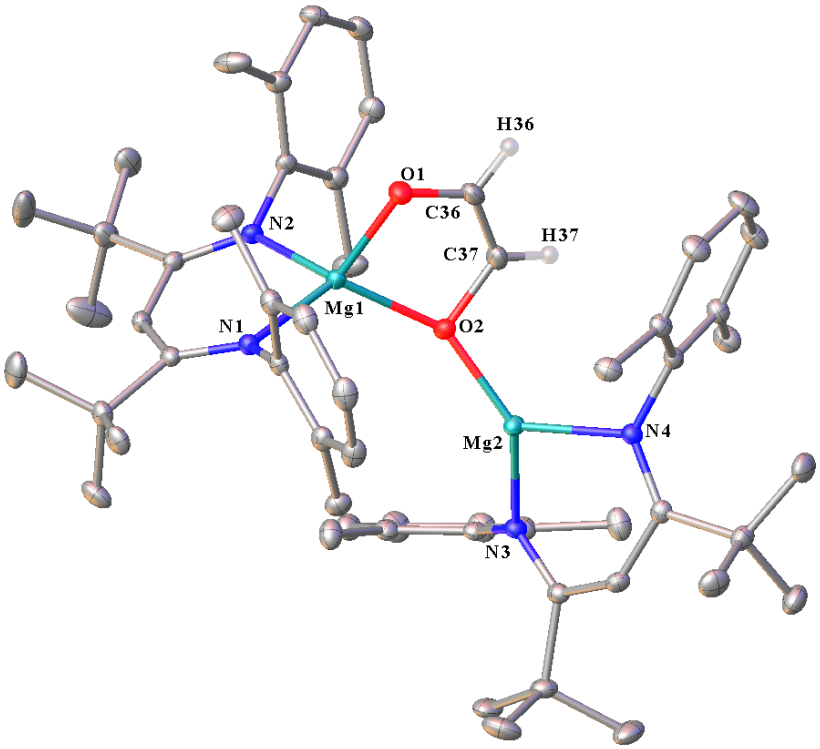

Figure 3.9: ORTEP representation of compound **3.7** (30% probability ellipsoids). Hydrogen atoms except those attached to C36 and C37 and iso–propyl methyl groups are removed for clarity. Selected bond lengths (Å) and angles (°): Mg1–O1 1.9207(10), Mg1–O2 2.0283(10), Mg1–N1 2.0505(11), Mg1–N2 2.0595(11), Mg2–O2 1.9067(10), Mg2–N4 2.0316(11), Mg2–N3 2.0157(11), C36–C37 1.328(2). O1–Mg1–O2 88.80(4), O1–Mg1–N1 119.06(5), O1–Mg1–N2 113.16(5), O2–Mg2–N3 136.76(5), O2–Mg2–N4 123.03(4), N3–Mg2–N4 98.68(5).

3.4 Computational Studies of Alkaline Earth Mediated CO Homologation

In order to gain greater insight into the carbonylation mechanism of alkaline earth hydrides **Ih** and **Ii**, DFT calculations were solicited in collaboration with Professor L. Maron. Simultaneous with the work described in this chapter, Jones and co–workers also reported the synthesis of compound **3.1**, which was characterised as a mono–THF adduct. As DFT calculations on the carbonylation of **Ih** had been included as part of this study,[7] only the carbonylation of **Ii** was computed. These calculations suggested a mechanism congruent with that previously proposed, (*vide supra*, Scheme 3.7) and analogous to those of **Ih**[7] and f–block enediolate complexes.[3] The initial coordination and formal insertion into the Ca–H bond (Figure 3.10) is calculated to proceed via transition state, **T1**, which rearranges to give a formyl–hydrido alkaline earth complex, **3.4**, exothermically (–9.3 kcal mol^{-1}, Figure 3.10). The calculation of the calcium formyl complex **3.4** is consistent with the experimentally predicted pathway. The barrier height for onward reaction of 10.2 kcal mol^{-1} (**T2**, Figure 3.10) is significantly lower than that reported for the magnesium formyl complex of 14.8 kcal mol^{-1},[7] offering an explanation as to why an analogue of **3.3** could not be evidenced in the ^{1}H and $^{13}C\{^{1}H\}$ NMR spectra during the reaction of **Ii**. Hydride transfer to the carbenic carbon of **3.4** is exothermic (–21.4 kcal mol^{-1}) yielding a dinuclear oxomethylene species, **3.5**. The proposed intermediate **3.5** could neither be isolated nor identified by NMR spectroscopy, likely owing to the negligible energy barrier (2.6 kcal mol^{-1}) associated with the second CO insertion into the Ae–C bond, **T3**, (Figure 3.10) to yield **3.6**. The final step from **3.6**, the 1,2–hydrogen shift, was calculated for both the *cis*– and *trans*–enediolate. The sole experimental product at room temperature is the *cis*–enediolate, **3.2**, and is computed as the thermodynamic product (–60.7 kcal mol^{-1}). The formation of the kinetic product (*trans*–enediolate, –35.3 kcal mol^{-1}), has a significantly lower transition state, **T5**, compared to the transition state of the *cis*– product, **T4**. The reaction is, thus, ascribed to be occurring under thermodynamic control. These calculations recapitulate the proposed mechanistic pathway to *cis*–endiolate formation extrapolated from the experimental results (Scheme 3.7) and emphasise the formation of a reactive intermediate (**3.4**) that could be exploited in a catalytic regime.

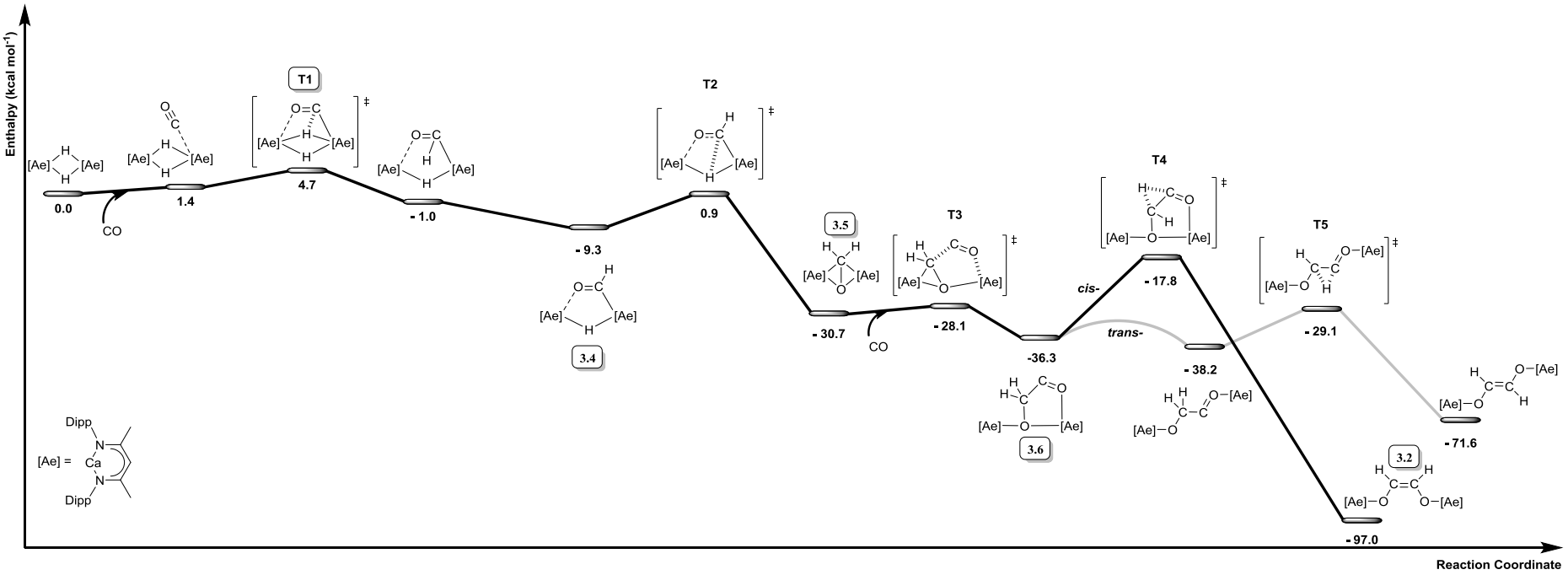

Figure 3.10: DFT calculations of the mechanism for CO homologation by **Ii**, to **3.2**, comparing *cis*– vs. *trans*–enediolate reaction pathways.

3.5 Catalytic Reduction of CO

To further explore the carbonylation chemistry of the alkaline earth hydrides, catalytic quantities of **Ih** and **Ii** were exposed to CO and phenylsilane ($PhSiH_3$) as a further hydride source. In the case of **Ih**, the likely intermediacy of magnesium formyl species, **3.3**, during the synthesis of compound **3.1** was further supported by a study of the reaction of phenylsilane and one atmosphere of ^{13}CO in the presence of 10 mol% **Ih**, Scheme 3.9. This reaction proved to be absolutely selective for the deoxygenative reduction of CO to methylphenylsilane, **3.8**, as the sole ^{13}C–containing product.

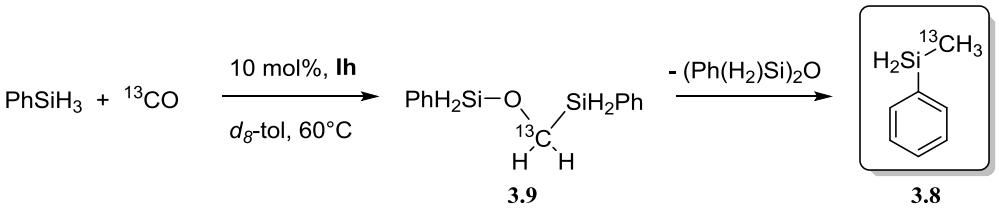

3.9 **3.8**

Scheme 3.9: Reduction of CO with phenylsilane as a hydride source, catalysed by **Ih**.

The formation of **3.8** was evidenced by the development of a resonance at δ –7.32 ppm in the $^{13}C\{^1H\}$ NMR spectrum, which appeared as a quartet of triplets ($^1J_{HC}$ = 122.0, $^3J_{HC}$ = 5.6 Hz, Figure 3.11, (a)) in the corresponding ^1H–^{13}C gated spectrum. Reactions performed at 60°C in toluene required 15 days to achieve 20% consumption of $PhSiH_3$ and, although slow, are the first examples of any homogeneous main group–catalysed reduction of CO to date. Monitoring of these reactions by NMR spectroscopy also revealed the intermediacy of $Ph(H_2)Si–O–CH_2SiPh(H_2)$, **3.9**. The methoxysilane species **3.9** was clearly apparent through the observation of a resonance centred at δ 50.7 ppm in the $^{13}C\{^1H\}$ NMR spectrum, which split as a binomial triplet of triplets signal ($^1J_{HC}$ = 130.7, $^3J_{HC}$ = 4.1 Hz, Figure 3.11, (b)) in the ^1H–^{13}C gated spectrum and was completely consumed at the cessation of the reaction.

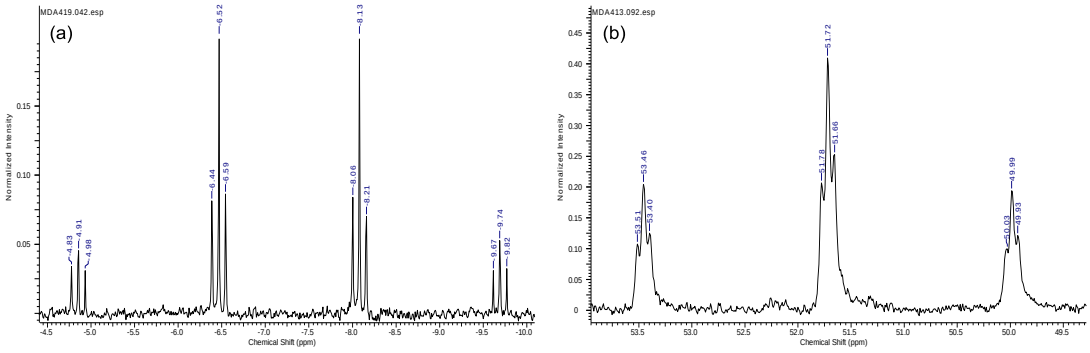

Figure 3.11: ^1H–^{13}C gated NMR spectrum (125.75 MHz) of: Left: (a) Final catalytic product methylphenylsilane. Right: (b) catalytic intermediate $Ph(H_2)Si–O–CH_2SiPh(H_2)$.

Scheme 3.10 depicts a provisional reaction mechanism which accounts for these observations. It is suggested that the initial step of the catalysis again involves the insertion of CO into the Mg–H bond of **Ih** to form a magnesium formyl similar to species **3.3**. The absence of any evidence of C_2 products formed by the reduction of the enediolate component of compound **3.1**, however, suggests that the metathetical reaction between this formyl species and a Si–H bond of phenylsilane occurs more rapidly than any homologation reactivity under one atmosphere of CO. The onward trajectory of the catalysis is then predicated on a sequence of rapid and unobservable C=O/Mg–H insertion and Mg–O/Si–H metathesis events to provide **3.9**. The rate determining process of the catalysis is provided by the activation of the C–O bond of compound **3.9** through O–C/Mg–H and Mg–O/Si–H metathesis steps to yield PhH_2SiCH_3 and $(Ph(H_2)Si)_2O$ respectively. The driving force for the reaction is, thus, provided by the production of this latter siloxane by–product.

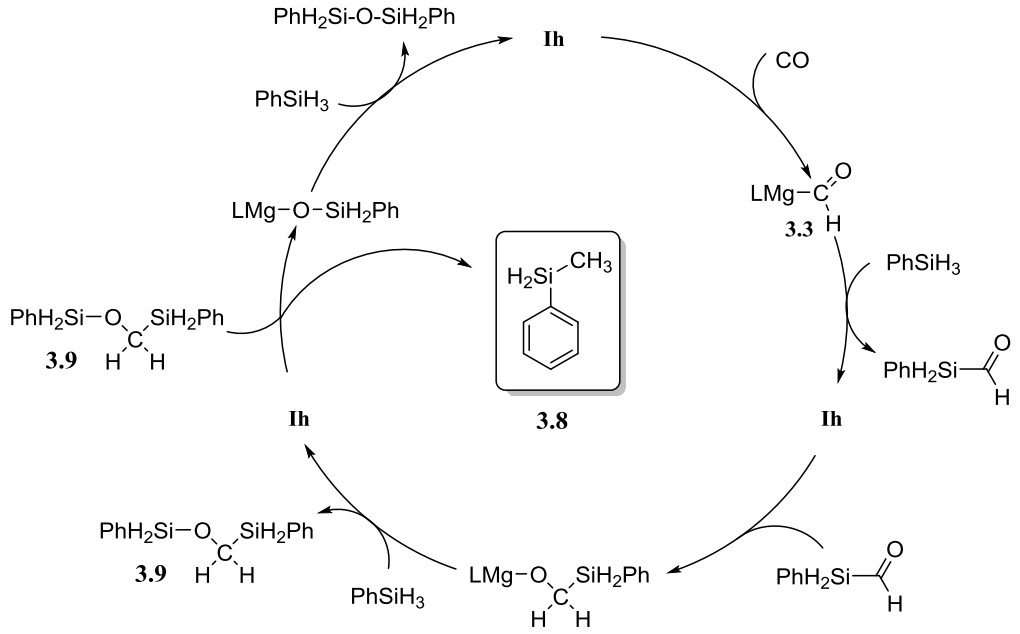

Scheme 3.10: Provisional reaction mechanism of the reduction of CO, catalysed by **Ih**.

In contrast to these observations, the corresponding reaction utilising **Ii** proceeded at room temperature, within an hour to provide the silyl ether **3.9** as the solitary product, Scheme 3.11 (Figure 3.12, (a) and (b)). Prolonged heating of the reaction solution with excess $PhSiH_3$ evidenced no onward reduction of **3.9**.

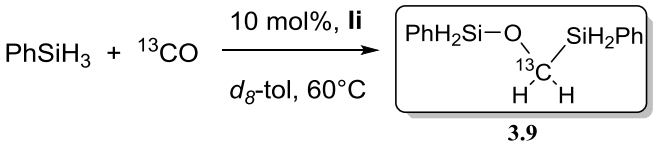

Scheme 3.11: Reduction of CO with phenylsilane as a hydride source, catalysed by **Ii**.

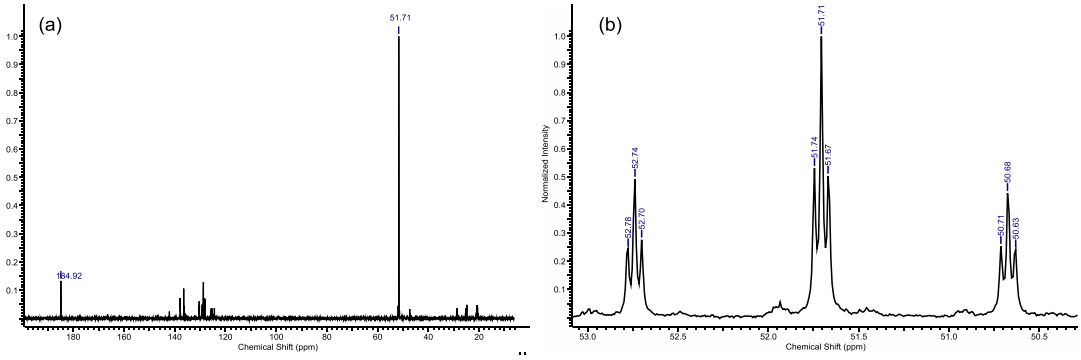

Figure 3.12: Left: (a) $^{13}C\{^{1}H\}$ NMR spectrum (125.75 MHz) immediately after the addition of ^{13}CO to **Ii**. Right: (b) $^{1}H-^{13}C$ gated NMR (125.75 MHz) spectrum of **3.9**.

Analogous to the reaction of **Ih**, it is suggested that the initial step of the catalysis again involves the insertion of CO into the Ca–H bond of **Ii** to form a calcium formyl similar to the predicted species **3.4**, Scheme 3.12. The metathetical reaction between this formyl species and a Si–H bond of phenylsilane occurs more rapidly than any homologation reactivity. Catalysis is then predicated on a sequence of rapid and unobservable C=O/Ca–H insertion and Ca–O/Si–H metathesis events to provide **3.9** as the sole product of the reaction.

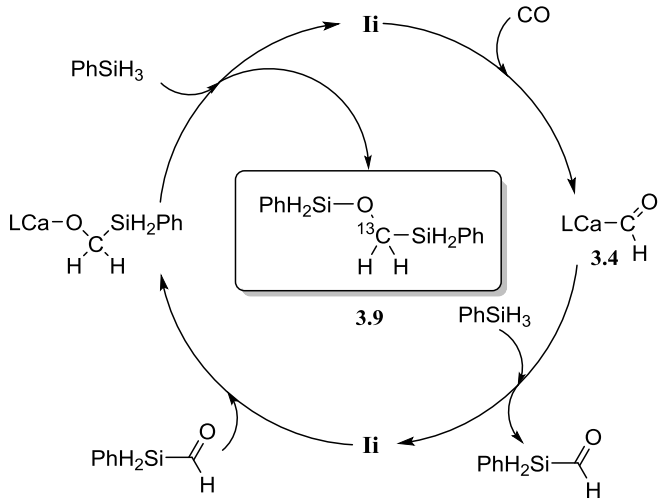

Scheme 3.12: Provisional reaction mechanism of the reduction of CO, catalysed by **Ii**.

During the course of this study, crystallisation from a typical catalytic reaction evidenced the solid state structure of a *β*–diketiminato calcium methoxysilane species, **3.10**, Figure 3.13. While it is evident from the solid state structure of **3.10** that $PhSiH_3$ has also redistributed to a Ph_2SiH– unit, it provides further support for the proposed catalytic pathway in Scheme 3.12. Compound **3.10**, is dimeric with *β*–diketiminate ligands capping the two calcium centres, Ca1 and Ca1^{i}. The bridging oxygens, O1 and O1^{i}, between Ca1 and Ca1^{i} complete a distorted tetrahedral geometry for the calcium centres. Repeated attempts to devise a rational synthesis of **3.10** were unsuccessful and no spectroscopic data is available.

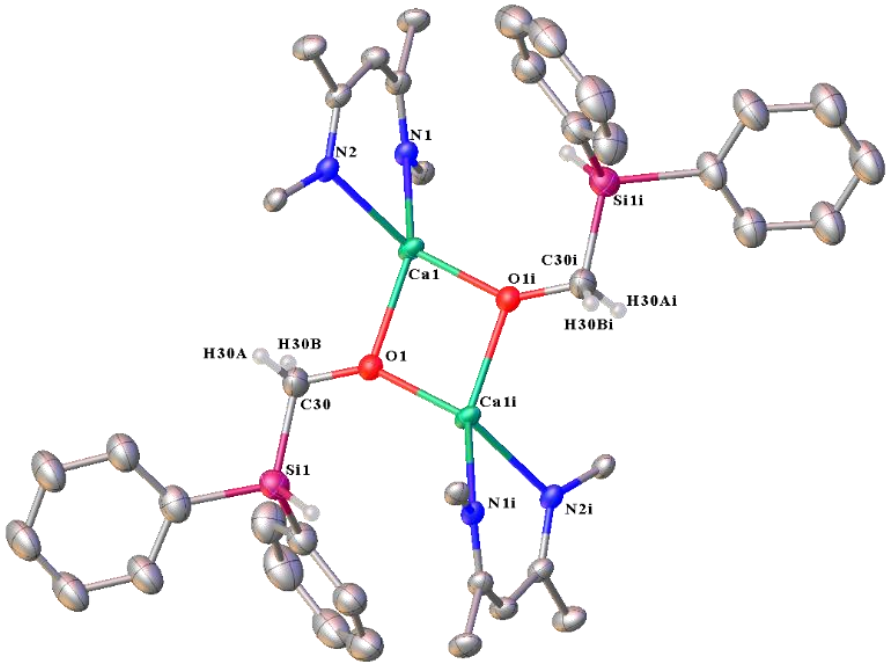

Figure 3.13: ORTEP representation of compound **3.10** (30% probability ellipsoids). Hydrogen atoms except those attached to C36 and C37 and di-iso–propylphenyl groups except the *ipso*-C atoms are removed for clarity. Selected bond lengths (Å) and angles (°): Ca1–O1 2.2057(15), Ca1–O1^{i} 2.2507, O1–C30 1.409(3), C30–Si1 1.820(10). O1–Ca1–O1^{i} 79.90(6), Ca1–O1–Ca1^{i} 101.0(6), O1–C30–Si1 112.25(16).

This divergence in chemistries of **Ih** and **Ii** toward the reduction of CO emphasizes the variations in alkaline earth metal characteristics on descending the group. In order to gain a deeper understanding of the reaction pathways of these alkaline earth hydrides, DFT computational analysis was employed in collaboration with Professor Laurent Maron.

3. 6 Computational Studies of Alkaline Earth Mediated CO Reduction

The calculation of the first insertion of CO into the Mg–H bond to give the catalytic intermediate related to **3.3** is analogous to that computed for enediolate formation, Figure 3.14.

This formyl–hydrido alkaline earth complex, **3.3**, is intercepted by phenylsilane *via*, **T1**, (14.4 kcal mol^{-1}). Exothermic σ–bond metathesis of the Si–H/Mg–CO bonds yields a magnesium silylmethoxide, **3.11**, (–41.5 kcal mol^{-1}, Figure 3.14) analogous to **3.10**. A subsequent σ–bond metathesis Si–H/Mg–H *via* a barrier of 20.1 kcal mol^{-1} (**T2**) produces a magnesium methoxysilicate species, with a significant hydrogen interaction between both Mg and Si, **3.12**. Dissociation of the methoxysilane **3.9**, from the magnesium centre regenerates Mg–H. Reinsertion of **3.9** into the Mg–H bond proceeds *via* a rate determining transition state (33.9 kcal mol^{-1}, **T3**) Figure 3.14, although methylphenylsilane extrusion is highly exothermic, –60.7 kcal mol^{-1}, generating the magnesium siloxide **3.12**, which undergoes a final Si–H/Mg–O σ–bond metathesis to regenerate **Ih** and a siloxide. Due to time constraints the DFT calculations for the calcium system have not been computed in time for comparison in this thesis.

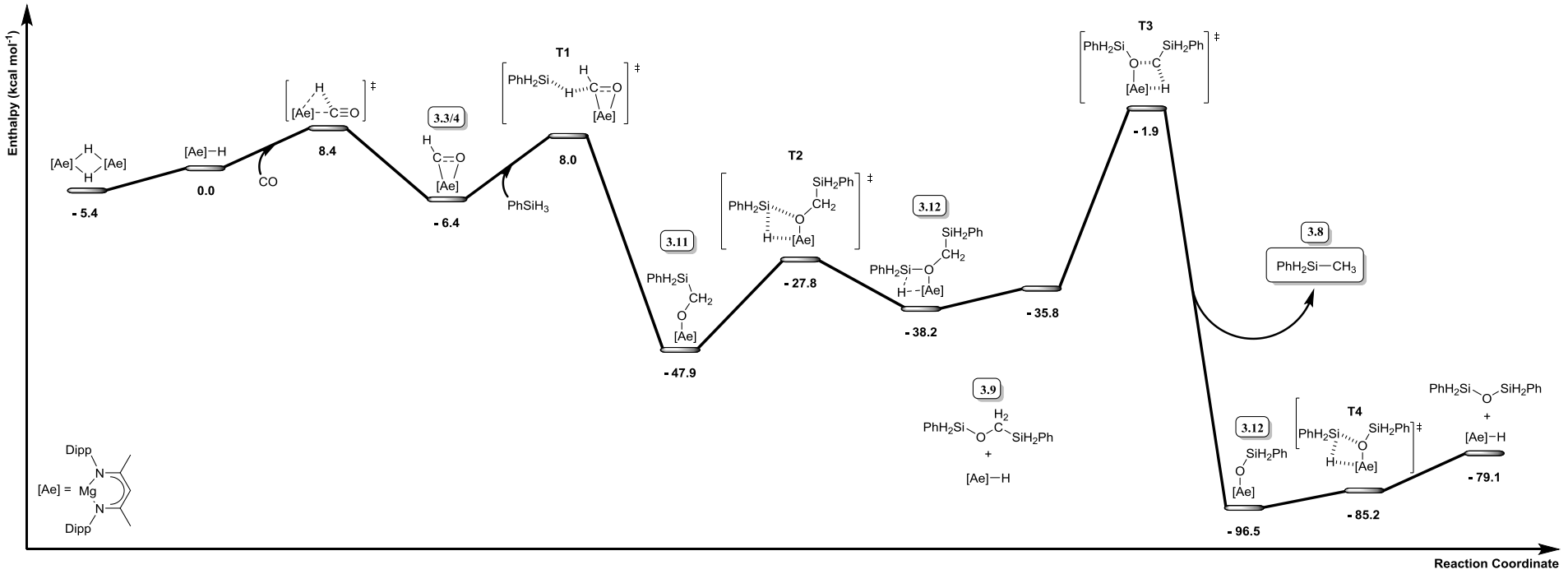

Figure 3.14: DFT calculations of the mechanism for the **Ih** catalysed reduction of CO to the methylphenylsilane **3.8**.

In conclusion, it has been shown that the application of the magnesium **Ih**, and calcium **Ii**, hydride complexes allow the facile homologation of CO to the *cis*–endiolate species **3.1** and **3.2** respectively. These hydrides also provide a means for selective homogeneous catalytic reduction of CO under very mild conditions to either a methoxysilane product, in the case of calcium, or deoxygenative reduction to a methyl silane product with magnesium. The next Chapter extends this carbonylation chemistry beyond reactions with Ae–H bonds.

3.7 References

1. a) A. A. Adesina, *Applied Catalysis A: General*, 1996, **138**, 345–367; b) H. Schulz, *Applied Catalysis A: General*, 1999, **186**, 3–12; c) P. M. Maitlis, *Journal of Organometallic Chemistry*, 2004, **689**, 4366–4374; d) P. M. Maitlis and V. Zanotti, *Chemical Communications*, 2009, 1619–1634; e) B. H. Davis and M. L. Occelli, *Advances in Fischer–Tropsch synthesis, catalysts, and catalysis*, CRC Press, 2009.
2. N. M. West, A. J. M. Miller, J. A. Labinger and J. E. Bercaw, *Coordination Chemistry Reviews*, 2011, **255**, 881–898.
3. a) J. M. Manriquez, D. R. McAlister, R. D. Sanner and J. E. Bercaw, *Journal of the American Chemical Society*, 1976, **98**, 6733–6735; b) J. M. Manriquez, D. R. McAlister, R. D. Sanner and J. E. Bercaw, *Journal of the American Chemical Society*, 1978, **100**, 2716–2724; c) P. J. Fagan, K. G. Moloy and T. J. Marks, *Journal of the American Chemical Society*, 1981, **103**, 6959–6962; d) W. J. Evans, J. W. Grate and R. J. Doedens, *Journal of the American Chemical Society*, 1985, **107**, 1671–1679; e) C. C. Cummins, G. D. Van Duyne, C. P. Schaller and P. T. Wolczanski, *Organometallics*, 1991, **10**, 164–170; f) E. L. Werkema, L. Maron, O. Eisenstein and R. A. Andersen, *Journal of the American Chemical Society*, 2007, **129**, 2529–2541.
4. S. J. Bonyhady, C. Jones, S. Nembenna, A. Stasch, A. J. Edwards and G. J. McIntyre, *Chemistry – A European Journal*, 2010, **16**, 938–955.
5. J. Spielmann and S. Harder, *Chemistry – A European Journal*, 2007, **13**, 8928–8938.
6. D. C. Sonnenberger, E. A. Mintz and T. J. Marks, *Journal of the American Chemical Society*, 1984, **106**, 3484–3491.
7. R. Lalrempuia, C. E. Kefalidis, S. J. Bonyhady, B. Schwarze, L. Maron, A. Stasch and C. Jones, *Journal of the American Chemical Society*, 2015, **137**, 8944–8947.

Chapter Four

Carbonylation of Alkaline Earth Nitrogen bonds

4.1 Introduction

There is a single literature precedent for the insertion of CO into a N–H bond, reported by Bergman and co–workers in 2003.[1] In this case, reaction of the iron complex $(dmpe)_2Fe(H)(NH_2)$, **XXVIII**, under one atmosphere of CO resulted in the formation of an iron formamidate complex $(dmpe)_2Fe(H)(NHCHO)$, **XXIX**. It is rationalised to form by the initial dissociation of one arm of a 1,2–bis(dimethylphosphino)ethane (dmpe) ligand from the iron centre and concurrent coordination of CO. Subsequent migratory insertion of CO into the Fe–N bond yields a carbenic carboxamide intermediate *trans*–$(dmpe)Fe(H)(C(O)NH_2)$, **XXX**, which undergoes a "rearrangement" to produce **XXIX**, Scheme 4.1. This final rearrangement is a 1,2 hydrogen shift from the nitrogen to the carbenic carbon and is thus, reminiscent of the reactivity described previously in Chapter Three of this thesis. The work described in this current Chapter seeks to extend this activity to the carbonylation of alkaline earth amide complexes. Accessing this CO insertion chemistry would enable the direct synthesis of formamidate derivatives that could undergo hydrodeoxygenation chemistry, as described in Chapter Two of this thesis, providing a novel route to value added chemicals which directly utilize CO as a C_1 carbon source.

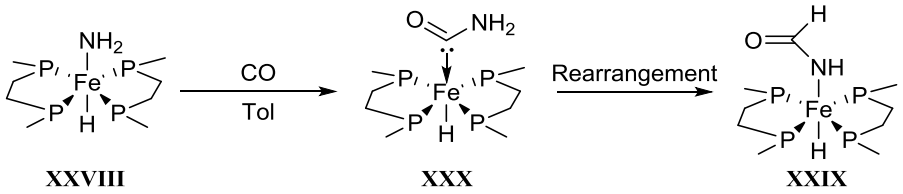

XXVIII **XXX** **XXIX**

Scheme 4.1: Bergman's postulated pathway to the formation of *trans*–$(dmpe)Fe(H)(NHCHO)$, **XXIX**.

4.2 Carbonylation of LAe–NH_2

In an attempt to synthesise a *β*–diketiminato magnesium amide, a solution of magnesium complex **Ih**, in THF was added to an equimolar solution of ammonia in 1,4–dioxane. This procedure, however, provided an insoluble white powder. All other attempts to synthesise the *β*–diketiminato magnesium amide by other means were similarly unsuccessful and resulted in isolation of an insoluble white powder that provided no meaningful spectroscopic data. Under the same conditions **Ii**, however, reacted readily with an equimolar

solution of ammonia in dioxane to yield the *β*–diketiminato calcium amide complex **4.1**, Scheme 4.2.

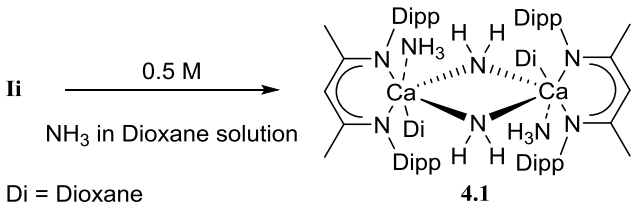

Scheme 4.2: Addition of **Ii** to a solution 0.5 M solution of ammonia in dioxane yields calcium compound **4.1**.

Storage of the reaction solution at –35°C overnight resulted in crystallisation of large colourless needles suitable for an X–ray diffraction analysis. The solid state structure of **4.1** (Figure 4.1) is dimeric, with terminal *β*–diketiminate ligands and symmetrically bridging NH_2^- ligands. One additional NH_3 and one dioxane ligand coordinate to Ca1 and Ca1^i respectively to complete a distorted octahedral arrangement. The structure of compound **4.1** is reminiscent of the THF–coordinated calcium amide reported by Harder and co–workers[2] obviating further comment. Exposure of **4.1** to a dynamic vacuum at room temperature removed the coordinated NH_3 ligand, although, even at elevated temperatures (*ca.* ~80°C) the dioxane remained coordinated and did not yield the solvent free complex.

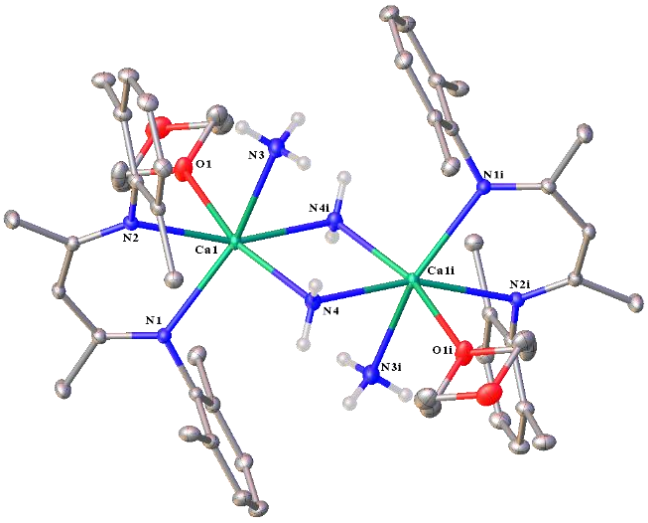

Figure 4.1: ORTEP representation of compound **4.1** with thermal ellipsoids at 30% level of probability. Isopropyl methyl groups and hydrogen atoms except H(N4/N4^i) and H(N3/N3^i) have been removed for clarity. Selected bond lengths (Å) and bond angles (°): Ca1–O1 2.5247(12), Ca1–N1 2.5030(12), Ca–N2 2.5264(12), Ca1–N3 2.5551(14), Ca1–N4 2.4431(12), O1–Ca1–N2 84.15(4), O1–Ca1–N3 94.27(5), N1–Ca1–O1 92.06(4), N4–Ca1–O1 84.15(4), N1–Ca1–N2 75.69(4), N1–Ca1–N3 157.30(4),

N2–Ca1–N3 83.30(4), N4^{i}–Ca1–N1 97.84(4), N4–Ca1–N1 119.81(4), N4^{i}–Ca1–N2 111.66(4), N4–Ca1–N2 160.89(4), N4^{i}–Ca1–N3 81.87(5), N4–Ca1–N3 82.56(5), N4^{i}–Ca1–N4 78.92(5), Ca1–N4–Ca1^{i} 101.08(5).

In order to assess the activity of the Ca–NH_2 bond toward CO insertion, **4.1** was exposed to one atmosphere of ^{13}CO at room temperature. This was postulated to provide conversion to the *β*–diketiminato calcium formamidate, **4.2**, Scheme 4.3.

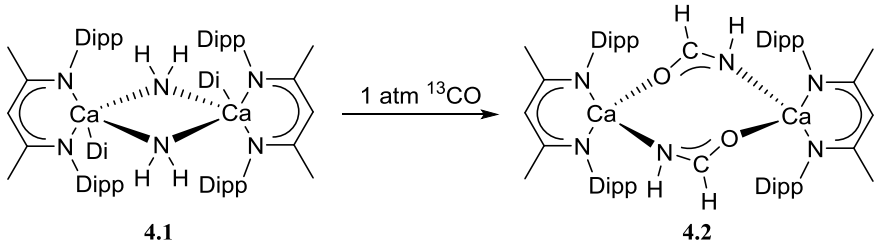

4.1 **4.2**

Scheme 4.3: Exposure of compound **4.1** to one atmosphere of ^{13}CO provides calcium formamidate complex **4.2**.

Interrogation of the resultant NMR spectra revealed complete consumption of the calcium starting material. The presence of a new singlet resonance at δ 174.3 ppm in the $^{13}C\{^{1}H\}$ NMR spectrum indicated that no carbon coupling or enediolate formation had occurred as earlier observed with **Ih** and **Ii**. In the ^{1}H–^{13}C gated spectrum this resonance was observed to split into a doublet of doublets, ($^{1}J_{CH}$ = 183.1, $^{2}J_{CH}$ = 2.9 Hz, Figure 4.2, (a)) consistent with the formation of a new ^{13}C–H bond, adjacent to a further single proton with a *β*–disposition with respect to the carbon. A subsequent HSQC experiment identified the corresponding doublet of doublets at δ 6.58 ppm ($^{1}J_{HC}$ = 183.1, $^{3}J_{HH}$ = 6.1 Hz, Figure 4.2, (b)) in the ^{1}H NMR spectrum. This experiment also comprised a highly shielded broad singlet at δ –2.04 ppm with a 1H integral and no corresponding carbon signal. This signal was thus, tentatively assigned as arising from the N–H proton. These data suggested that CO had inserted into the Ca–NH_2 bond and subsequently undergone a single 1,2–hydrogen shift to yield the formamidate complex **4.2**.

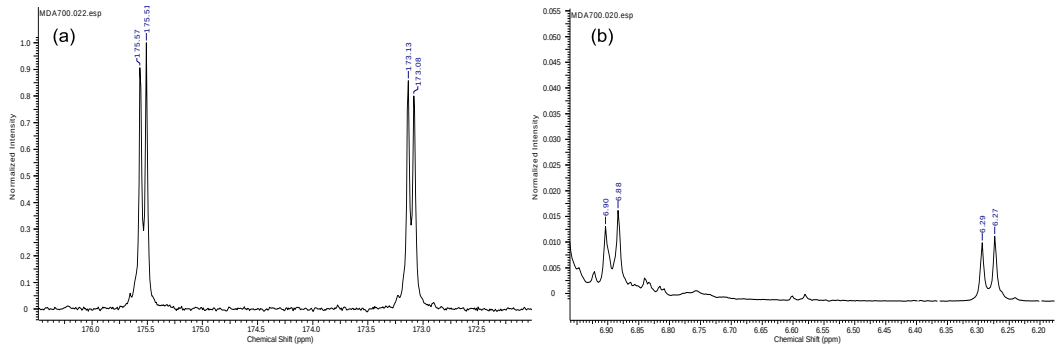

Figure 4.2: (a) (Left) ^{1}H –^{13}C (75.5 MHz) gated spectrum of compound **4.2**, ($^{1}J_{CH}$ = 183.1, $^{2}J_{CH}$ = 2.9 Hz) and (b) (Right) the corresponding doublet of doublets at δ 6.58 ppm ($^{1}J_{HC}$ = 183.1, $^{3}J_{HH}$ = 6.1 Hz) in the ^{1}H NMR (300 MHz) spectrum.

A saturated THF/hexane solution of **4.2** that was allowed to slowly evaporate for three days at room temperature afforded crystalline colourless blocks suitable for a single crystal X–ray diffraction experiment. The solid state structure of **4.2** confirmed the formation of a dimeric *β*–diketiminato calcium formamidate. The bridging formamidate ligands bond unsymmetrically, Figure 4.3. One formamidate unit (O1–C30–N3, Figure 4.3) is bound symmetrically η^3–from O1, C30 and N3 to both Ca1 and Ca2. The second formamidate is approximately orthogonal to the first and is only bound κ^1 to Ca1 through the oxygen O2, while it is bound κ^2 to Ca2 through both the oxygen, O2, and nitrogen, N4, atoms. Both calcium centres, Ca1 and Ca2, display a distorted octahedral geometry, with the final coordination site on Ca1 filled by a THF ligand, Figure 4.3.

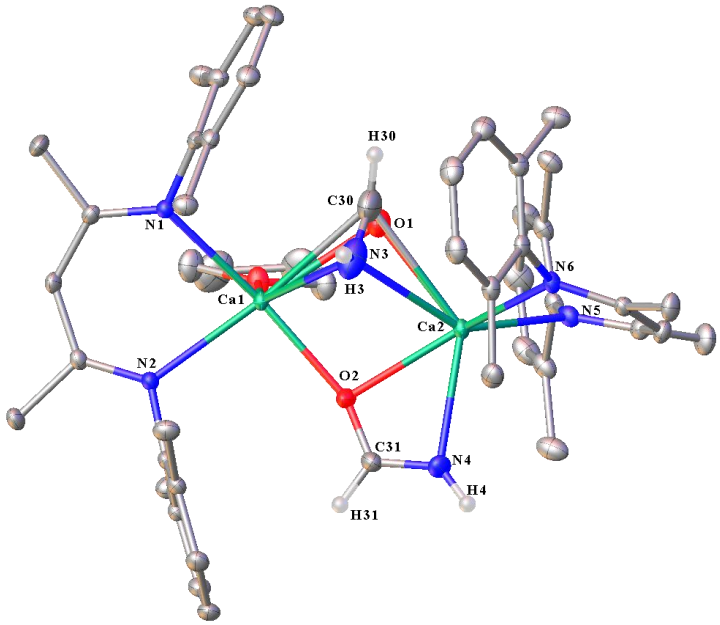

Figure 4.3: ORTEP representation of compound **4.2** with thermal ellipsoids at 30%. Isopropyl groups and hydrogen atoms except H59 and H64 have been removed for clarity. Selected bond lengths (Å) and bond angles (°): Ca1–O1 2.476(2), Ca1–O2 2.2602(16), Ca1–O3 2.3538(15), Ca1–N1 2.4053(16), Ca1–N2 2.4061(16), Ca1–N3 2.575(3), Ca2–O1 2.443(2), Ca2–O2 2.4473(15), Ca2–N3 2.616(3), Ca2–N4 2.4468(19), Ca2–N5 2.3649(16), Ca2–N6 2.3600(16), O1–C30 1.191(5), O2–C31 1.284(3), N3–C30 1.302(5), N4–C31 1.270(3), O1–Ca1–N3 50.18(10), O2–Ca1–O1 81.99(6), O2–Ca1–O3 94.57(7), O2–Ca1–N1 166.73(7), O2–Ca1–N2 95.80(6), O2–Ca1–N3 80.60(8), O3–Ca1–N3 80.60(8), O3–Ca1–O1 83.82(8), O3–Ca1–N1 98.13(6), O3–Ca1–N2 99.65(6), O3–Ca1–N3 134.00(9), N1–Ca1–O1 103.15, N1–Ca1–N2 78.32(5), N1–Ca1–N3 93.23(7), N2–Ca1–O1 176.05(7), N2–Ca1–N3 126.32(9), O1–Ca2–O2 79.00(6), O1–Ca2–N3 49.99(10), O1–Ca2–N4 132.59(7), O2–Ca2–N3 76.47(8), N4–Ca2–O2 53.84(6), N4–Ca2–N3 107.28(9), N5–Ca2–O1 103.66(8), N5–Ca2–O2 123.06(7), N5–Ca2–N3 146.75(9), N5–Ca2–N4 105.89(7), N6–Ca2–O1 108.91(7), N6–Ca2–O2 154.60(7), N6–Ca2–N3 90.14 (7), N6–Ca2–N4 112.31(6), N6–Ca2–N5 79.48(6).

The solution structure of **4.2** does not allow for differentiation between the two formamidate moieties by ^{1}H and $^{13}C\{^{1}H\}$ NMR spectroscopy even at reduced temperatures down to the lower limit of –93°C. Facile exchange between the two bonding modes, thus, occurs faster than the NMR time scale.

Although repetition of the reaction with an excess of CO led to the formation of compound **4.2**, as identified by NMR spectroscopy, it was envisaged that onward reaction could lead to a further CO insertion into the second Ae–NH bond Scheme 4.4. Despite extended exposure and the application of elevated temperatures, no evidence for a second CO insertion could be observed.

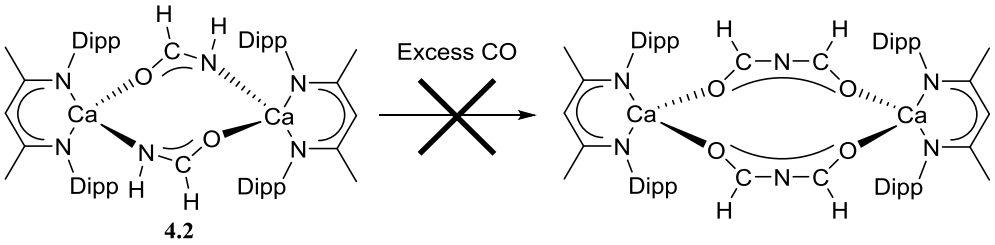

Scheme 4.4: Extended exposure of compound **4.2** to CO gave no further insertion.

4.3 Carbonylation of LAe–NHR (R = Alkyl or Aryl)

Having extended the insertion chemistry of CO into the Ca–NH_2 moiety to yield the parent formamidate, the reactivity was further generalised to a range of *β*–diketiminato magnesium and calcium aryl and alkyl amides, ([(HC{(Me)CN(2,6–$^{i}Pr_2C_6H_3$)}$_2$MNHR)] M = Mg or Ca and R = aryl or alkyl).[3] Preliminary *in situ* reactions between the magnesium and calcium hydrides, **Ih**, and **Ii**, and a stoichiometric equivalent of *n*–butyl amine were performed in d_8–toluene, degassed and exposed to one atmosphere of ^{13}CO at room temperature, Scheme 4.5.

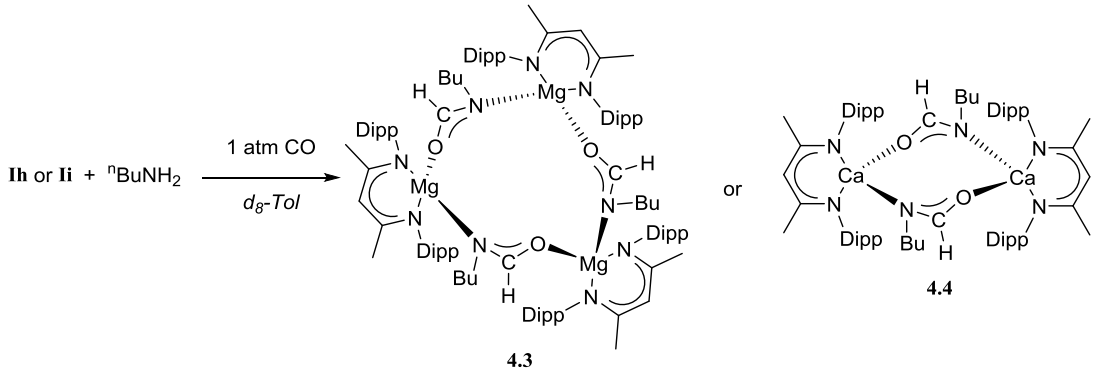

Scheme 4.5: *In situ* generated *β*–diketiminato magnesium and calcium *n*–butyl amide complexes exposed to ^{13}CO.

Both ^{1}H and ^{13}C{^{1}H} NMR data for the reaction with the magnesium species, recorded immediately after addition of ^{13}CO, indicated no reaction had occurred. The reaction was, thus, left at room temperature for 12 hours, to provide *ca.* 30% conversion to **4.3**, thought to be the alkyl formamidate which was identified through the appearance of two new highly deshielded doublet signals at δ 7.87 ppm and 6.88 ppm ($^{1}J_{CH}$ = 177.4 Hz and $^{1}J_{CH}$ = 182.9 Hz) in a two to one ratio in the ^{1}H NMR spectrum. Elevation of the reaction temperature to 60°C for 12 hours provided complete conversion to **4.3**, as identified by the emergence of two singlet resonances at δ 171.9 ppm and δ 165.0 ppm in the ^{13}C{H^{1}} NMR spectrum. The signal at δ 171.9 ppm was observed to split into a sharp doublet of triplets ($^{1}J_{CH}$ = 177.4, $^{3}J_{CH}$ = 9.9

Hz) while the signal at δ 165.0 ppm split into a broad doublet ($^1J_{CH}$ = 182.9 Hz) in the ^1H–^{13}C gated spectrum, indicating CO insertion had occurred with a 1,2–hydrogen shift from the nitrogen to the carbon to provide an alkyl formamidate product in two different environments, **4.3**. In contrast, the analogous reaction with calcium occurred with complete consumption of the amide complex by ^1H NMR spectroscopy and conversion to a new compound, **4.4**, at the first point of analysis immediately after CO addition. Examination of the $^{13}C\{^1H\}$ NMR spectrum revealed a new singlet resonance at δ 168.8 ppm, that in the ^1H–^{13}C gated spectrum split into a doublet of triplets ($^1J_{CH}$ = 180.5, $^3J_{CH}$ = 8.1 Hz), showing the clear formation of a new C–H bond. A corresponding doublet at δ 8.06 ppm ($^1J_{HC}$ = 180.5 Hz) with a relative integral of 1H was clearly evident in the ^1H NMR spectrum, confirming the formation of a *N*–*n*–butyl formamidate.

Crystallisation of the magnesium complex **4.3**, direct from the reaction solution at 60°C and storage of the calcium reaction solution at –35°C yielded large colourless block crystals suitable for X–ray diffraction experiments. The solid state structure of **4.3**, revealed an unusual trimeric magnesium structure (Figure 4.4).[4] Three *N*–*n*–butyl formamidate moieties and three magnesium centres make up a near planar, twelve membered macrocycle, Figure 4.4 (a). Each formamidate moiety bonds in a κ^1– fashion from the oxygen to one magnesium centre and κ^1– from its respective nitrogen to a second magnesium centre to make up one third of the trimer. Each magnesium is also bound to a bidentate *β*–diketiminate ligand, which is perpendicular to the twelve–membered macrocycle, completing a distorted tetrahedral arrangement, Figure 4.4 (b). The solid state structure of **4.3**, in the horizontal view (Figure 4.4, (a)) displays the hydrogens of the formamidate moieties in two different environments, H59 and H64 are above the plain of the heterocycle, whilst H98 is below the plain. The different formamidate environments evidenced in the solution structure of **4.3** are tentatively assigned to these spatially inequivalent hydrogen atoms. Variable temperature experiments provided no simplification of these spectra at either reduced or elevated temperatures, indicating that the formamidate methine resonances continue to be conformationally differentiated on the NMR timescale.

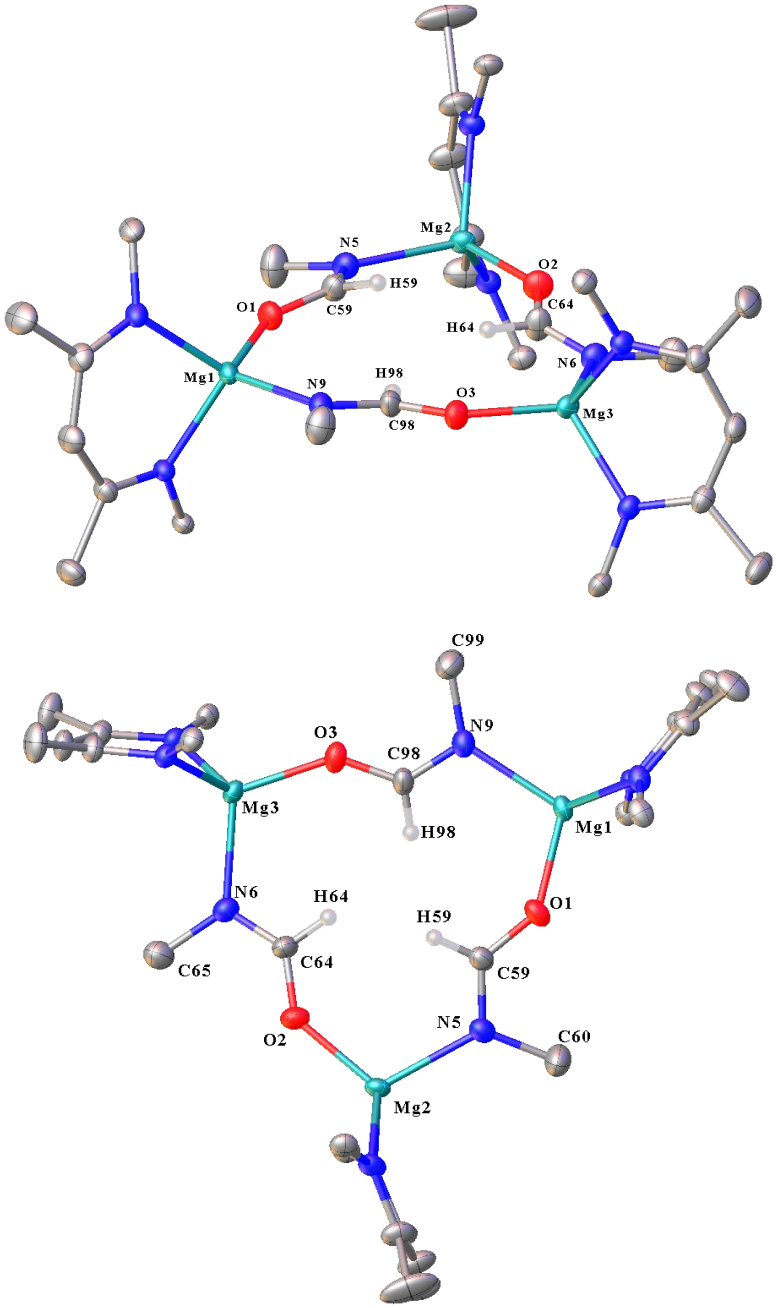

Figure 4.4: ORTEP representation of compound **4.3** with thermal ellipsoids at 30%. (a) Top: Horizontal view. (b) Bottom: aerial perspective. Di-iso-propylphenyl groups except for the *ipso* carbons and hydrogen atoms except on C59, C64 and C98 have been removed for clarity. Selected bond lengths (Å) and bond angles (°): Mg1–O1 1.9088(18), Mg1–N1 2.0339(18), Mg1–N2 2.0436(17), Mg1–N9 2.099(2), Mg2–O2 1.9272(18), Mg2–N3 2.0389(19), Mg2–N4 2.0493(19), Mg2–N5 2.110(2), O1–C59 1.281(3), O2–C64 1.266(3), N5–C59 1.291(3), N6–C64 1.277(3). O1–Mg1–N1 111.23(8), O1–Mg1–N2 114.53(8), O1–Mg1–N2 95.13(7), N1–Mg1–N9 116.33(8), N2–Mg1–N9 109.82(8), O2–Mg2–N3 108.69(8), O2–Mg2–N4 118.01(8), O2–Mg2–N5 111.50(8), N3–Mg2–N4 95.08(8), N3–Mg–N5 113.875(8), N4–Mg2–N5 108.95(8), O1–C59–N5 126.7(2), O2–C64–N6 130.1(2), O3–C98–N9 126.8(2).

The X–ray diffraction analysis of **4.4**, Figure 4.5, revealed a contrasting dimeric complex. The bidentate *β*–diketiminate ligands cap the calcium centres in a manner reminiscent of **4.2**, with symmetrically bridging *n*–butyl formamidate ligands, which adopt a coplanar orientation with respect to each other. Compound **4.4** displays a marked difference in formamidate bonding when compared to the magnesium complex **4.3**. The formamidate ligand (O1–C59–N5) binds κ^2– to Ca1 through O1 and N5, with the final contact μ_2– to Ca2 through O1. The second formamidate ligand (O2–C64–N6) displays identical bonding modes but is κ^2– to Ca2 through O2 and N6, then μ_2– to Ca1 through O2 to complete a distorted trigonal bipyramidal arrangement. This increase in denticity between **4.3** and **4.4** is attributed to the increase in ionic radius from magnesium (0.78 Å) to calcium (1.06 Å).

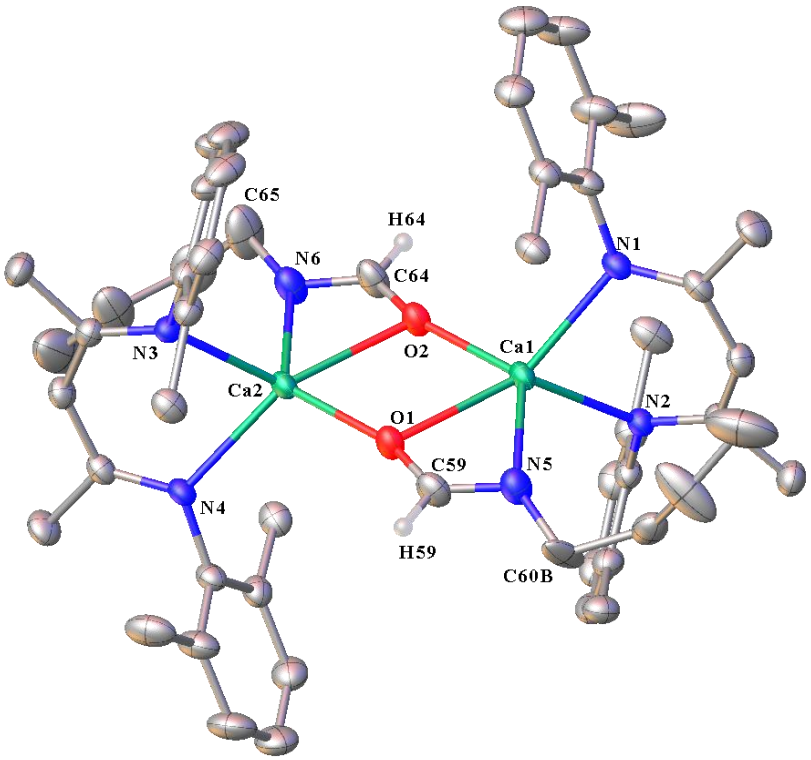

Figure 4.5: ORTEP representation of compound *β*–diketiminato calcium butyl formamidate, **4.4**, with thermal ellipsoids at 30%. Isopropyl methyl groups and hydrogen atoms except hydrogens on C59 and C64 have been removed for clarity. Selected bond lengths (Å) and bond angles (°): Ca1–O1 2.4470(17), Ca1–O2 2.2387(19, Ca1–N1 2.3284(19), Ca1–N2 2.3333(19), Ca1–N5 2.466(2), Ca1–C59 2.811(3), Ca2–O1 2.2351(19), Ca2–O2 2.4501(17), Ca2–N3 2.3295(19), Ca2–N4 2.3235(18), Ca2–N6 2.450(2), Ca2–C64 2.802(3), N5–C59 1.275(4), N6–C64 1.272(4), O1–C59 1.297(3), O2–C64 1.290(3). O1–Ca1–N5 54.41(7), O2–Ca1–N1 108.42(7), O2–Ca1–N2 112.74(7), N1–Ca1–N2 82.84(7), O2–Ca1–N5 130.33(7), O1–Ca2–N3 114.56(7), O1–Ca2–N4 108.62(7), N6–Ca2–O2 54.39(7), N4–Ca2–N3 81.05(7), N5–C59–O1 121.7(2), N6–C64–O2 121.9(3).

Encouraged by these results, the reaction scope was extended to the range of *in situ* generated alkyl and aryl amides summarised in Table 4.1.

Table 4.1: Exposure of *in situ* generated alkaline earth amide compounds to one atmosphere of CO yields the alkaline earth alkyl formamidate. All reactions reached > 99% conversion as determined by NMR spectroscopy.

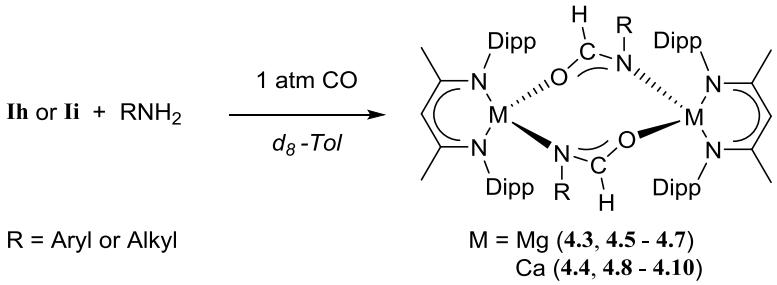

Entry	Ar/R	Time (h)	Temp. (°C)	NMR Conv. (%)
4.5	^{i}Pr	48	60	99
4.6	$CH_2CH_2C_6H_5$	72	100	99
4.7	Dipp	72	60	99
4.8	^{t}Bu	<1	25	99
4.9	$CH_2CH_2C_6H_5$	<1	25	99
4.10	Dipp	12	60	71

Exposure of the *in situ* generated *β*–diketiminato magnesium and calcium amide complexes to CO led to the facile formation of the corresponding alkyl formamidate complexes. Increasing substituent steric demands provided significantly longer reaction times in the case of magnesium complexes, (Table 4.1, entries **4.5** – **4.7**), however, no such restrictions were observed for the calcium complexes, aside from the most sterically encumbered derivative derived from reaction with 2,6–di–isopropylphenyl aniline (Table 4.1, entries **4.8** – **4.10**). Compounds **4.5 – 4.10** were all crystallographically defined.

The *β*–diketiminato magnesium *N*–*iso*–propyl formamidate, **4.5**, diverges from the previously described trimeric, **4.3**, and more closely resembles the calcium *N*–*n*–butyl formamidate, **4.4**. The solid state structure demonstrates **4.5** to be dimeric (Figure 4.6), with

capping *β*–diketiminate ligands. The perpendicular, symmetrically bridging *N*–^{i}Pr formamidate ligands, (O1–C30–N3 and O1^{i}–C30^{i}–N3^{i}), are bound in a μ_2–fashion through O1 and O1^{i} to both Mg1 and Mg1^{i} and κ^2– from N3/O1 and N3^{i}/O1^{i} to Mg1 and Mg^{i} respectively. These bonding modes complete a distorted trigonal bipyramidal geometry for both magnesium centres.

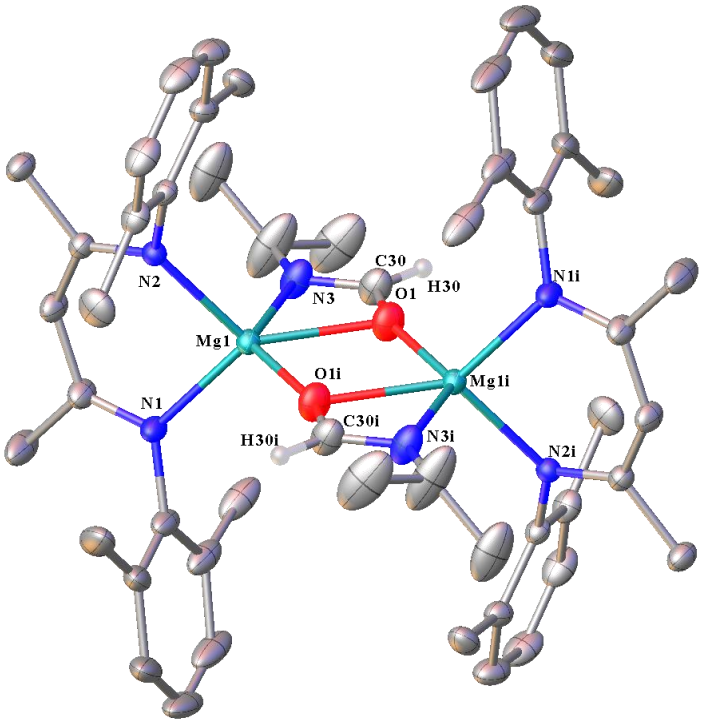

Figure 4.6: ORTEP representation of compound **4.5** with thermal ellipsoids at 30%. Isopropyl methyl groups and hydrogen atoms except H30/30^{i} have been removed for clarity. Selected bond lengths (Å) and bond angles (°): Mg1–N2 2.0810(15), Mg1–N1 2.0751(17), Mg1–O1^{i} 1.9901(17), Mg1–O1 2.1789(18), Mg1–N3 2.240(2), N3–C30 1.259(3), O1–C30 1.299(3). N2–Mg1–O1 129.64(7), N2–Mg1–N3 103.45(7), N1–Mg1–N2 92.61(6), N1–Mg1–O1 135.13(7), N1–Mg1–N3 102.24(8), O1–Mg1–N3 58.69(7), N3–C30–O1 115.8(2).

The solid state structure of the *β*–diketiminato magnesium *N*–2–phenyl ethyl formamidate, **4.6**, also retains a dimeric structure, Figure 4.7. Chelating *β*–diketiminate ligands cap the magnesium centres analogously to **4.5**, however, the bridging formamidate moieties are no longer symmetrical. O1–C30–N3 binds μ_2– through O1 to both Mg1 and Mg2 and κ^2– from the N3 and O1 atoms to Mg1. O2–C39–N4, in contrast, only binds κ^1– from O2 and N3 to Mg1 and Mg2 respectively. These bonding modes yield unsymmetrical magnesium centres. Mg1 has a distorted trigonal bipyramidal geometry similar to **4.5**, while Mg2 retains a distorted tetrahedral arrangement comparable to those of **4.3**.

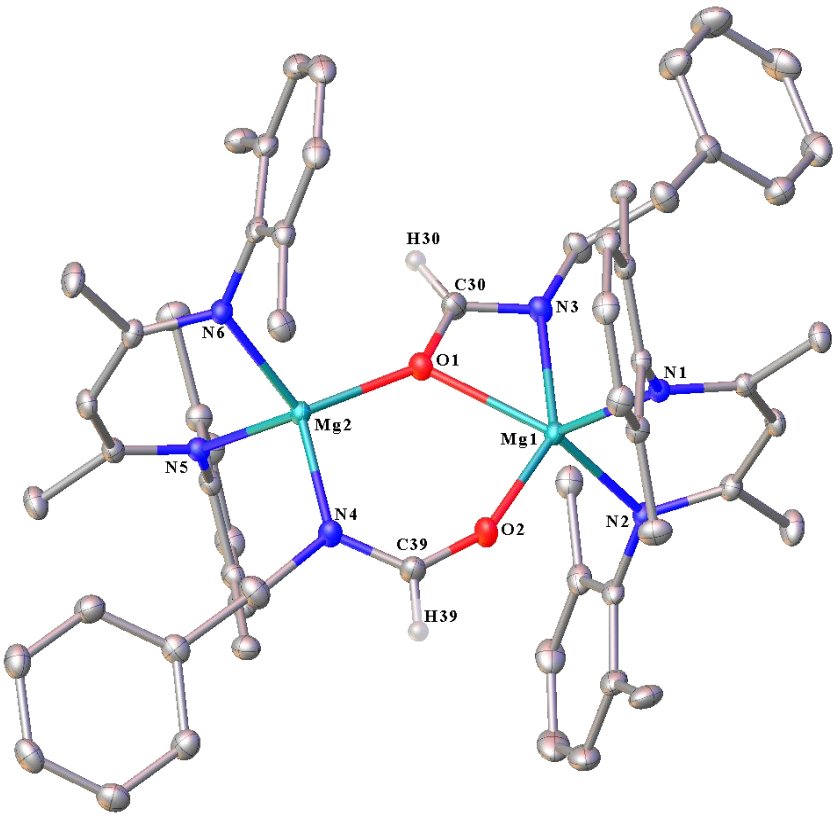

Figure 4.7: ORTEP representation of compound **4.6** with thermal ellipsoids at 30%. Isopropyl methyl groups and hydrogen atoms except hydrogens attached to C30 and C39 have been removed for clarity. Selected bond lengths (Å) and bond angles (°): Mg1–O1 2.1727(14), Mg1–O2 1.9612(14), Mg1–N1 2.0711(15), Mg1–N2 2.0700(15), Mg1–N3 2.2698(16), Mg2–O1 1.9409(13), Mg2–N4 2.0760(16), Mg2–N5 2.0604(15), Mg1–N6 2.0476(15), O1–C30 1.310(2), O2–C39 1.255(2), N3–C30 1.267(2), N4–C39 1.297(2). O1–Mg1–N3 59.51(5), O2–Mg1–O1 86.23(5), O2–Mg1–N1 106.65(6), O2–Mg1–N2 99.87(6), O2–Mg1–N2 144.22(6), N2–Mg1–N1 92.65, O1–Mg2–N4 104.15(6), O1–Mg2–N5 122.66(6), O1–Mg2–N6 112.30(6), N5–Mg2–N4 106.15(6), N6–Mg2–N4 118.40(6), N3–C30–O1 117.78(16), O2–C39–N4 126.59(18).

The adjustment in bonding mode between **4.5** and **4.6**, is most likely imposed by the increased steric demands of the *N*–2–phenyl ethyl function. It was also possible to discriminate between the individual bonding modes of the two *N*–2–phenyl ethyl formamidate ligands of **4.6** by NMR spectroscopy. One formamidate displayed a heavily deshielded signal at δ 173.0 ppm, ($^{1}J_{CH}$ = 176.1, $^{3}J_{CH}$ = 9.5 Hz, Figure 4.8 (a)) in the ^{1}H–^{13}C gated NMR spectrum, with a corresponding resonance at δ 7.84 ppm, (1H, d, $^{1}J_{HC}$ = 176.1 Hz, Figure 4.8 (b)), in the ^{1}H NMR spectrum. The second formamidate ligand displayed equivalent signals in both the ^{1}H–^{13}C gated, (168.0 ppm ($^{1}J_{CH}$ = 180.5, $^{3}J_{CH}$ = 8.6 Hz, Figure 4.8 (a)), and ^{1}H NMR spectra, (7.81 (1H, d, $^{1}J_{HC}$ = 180.5 Hz, Figure 4.8 (b)).

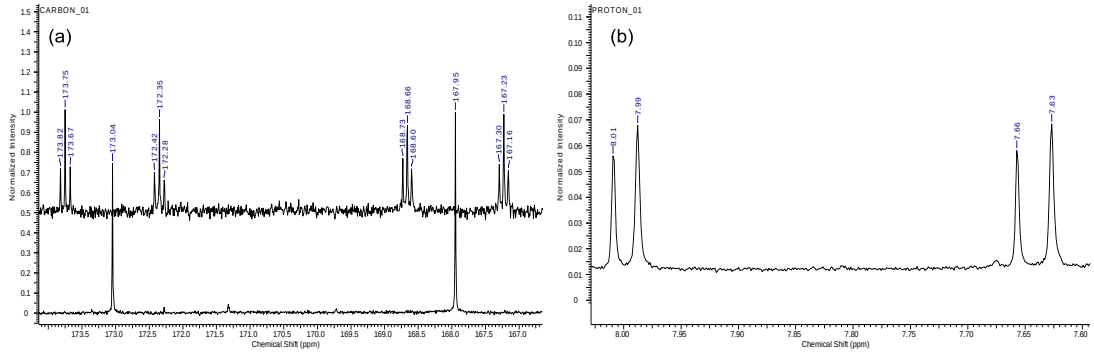

Figure 4.8: (a) (Left) Stacked $^{13}C\{^{1}H\}$ and $^{1}H–^{13}C$ gated spectrum (125.75 MHz) of compound **4.6**, the former displaying two singlet resonances and the latter displaying two doublets of triplets, δ 173.0 ppm ($^{1}J_{CH}$ = 176.1, $^{3}J_{CH}$ = 9.5 Hz) and δ 168.0 ppm ($^{1}J_{CH}$ = 180.5, $^{3}J_{CH}$ = 8.6 Hz). (b) (Right) the corresponding two doublets at δ 7.84 (1H, d, $^{1}J_{HC}$ = 176.1 Hz), and δ 7.81 (1H, d, $^{1}J_{HC}$ = 180.5 Hz), in the ^{1}H NMR spectra (500 MHz).

The solid state structure of **4.7**, the isotopologue of **2.1**, is illustrated in Figure 4.9, the increased steric demands enforced by the *N*–Dipp moiety yielding a monomeric complex. The *β*–diketiminate ligand provides two contacts to the magnesium centre, with the remaining two comprising the O1–C30–N3 formamidate unit, which is bound κ^2– from O2 and N3 to Mg1 to complete a distorted tetrahedral arrangement. This structure demonstrates that the reduction of an isocyanate with an alkaline earth hydride provides an identical formamidate product (Chapter 2) to that generated by insertion of CO into an Ae–N bond. While this seems a trivial observation, a point of note is the expense and limited range of commercially available isocyanates, in comparison to the availability of a plethora of inexpensive amines.

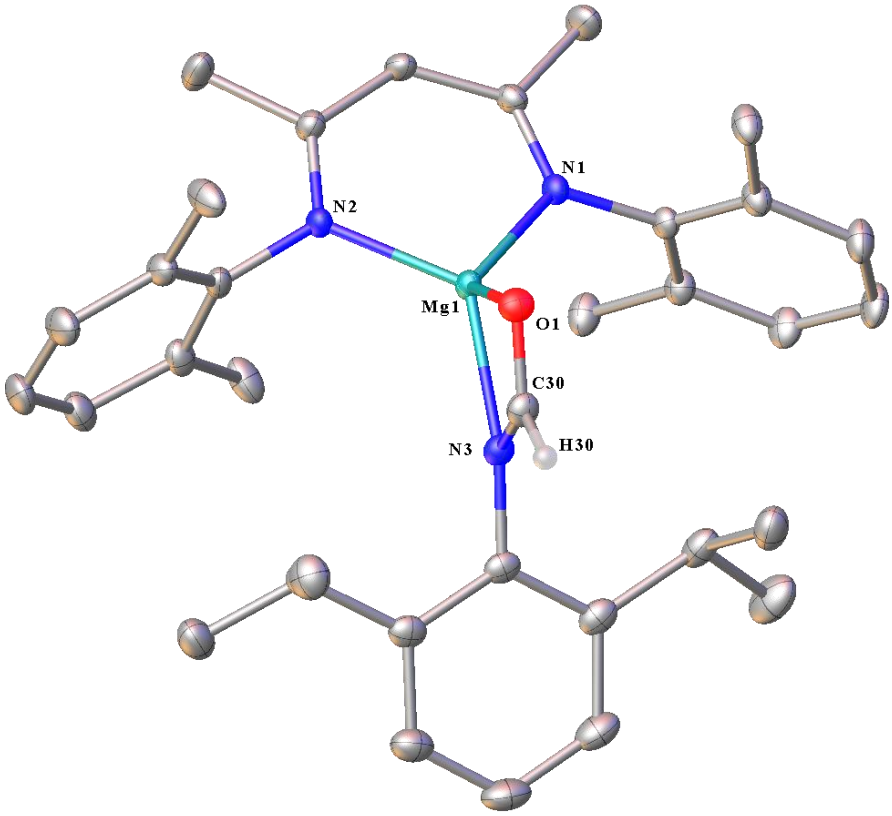

Figure 4.9: ORTEP representation of compound **4.7** with thermal ellipsoids at 30%. Isopropyl groups and hydrogen atoms except H30 been removed for clarity. Selected bond lengths (Å) and bond angles (°): Mg1–O1 2.0118(10), Mg1–N1 2.0179(11), Mg1–N2 2.0156(11), Mg1–N3 2.0983(11), O1–Mg1–N1 121.64, O1–Mg1–N2 122.69, O1–Mg1–N3 65.86(4), N1–Mg1–N3 128.04(4), N1–Mg1–N2 95.09(4), N2–Mg1–N3 125.20(5).

This series of magnesium formamidate complexes, possesses incrementally larger R substituents across the progression from **4.3** to **4.5** – **4.7**. This results in a consequent decrease in nucleicity from trimer to dimer and finally monomer, highlighting the influence of changes in steric demand on their solid state structures. In unadorned contrast to these observations, the solid state structures of the calcium complxes **4.8** and **4.9**, (Figure 4.10, (a) and (b)), exhibit an isostructural composition to that of **4.4**, rendering further comment unnecessary.

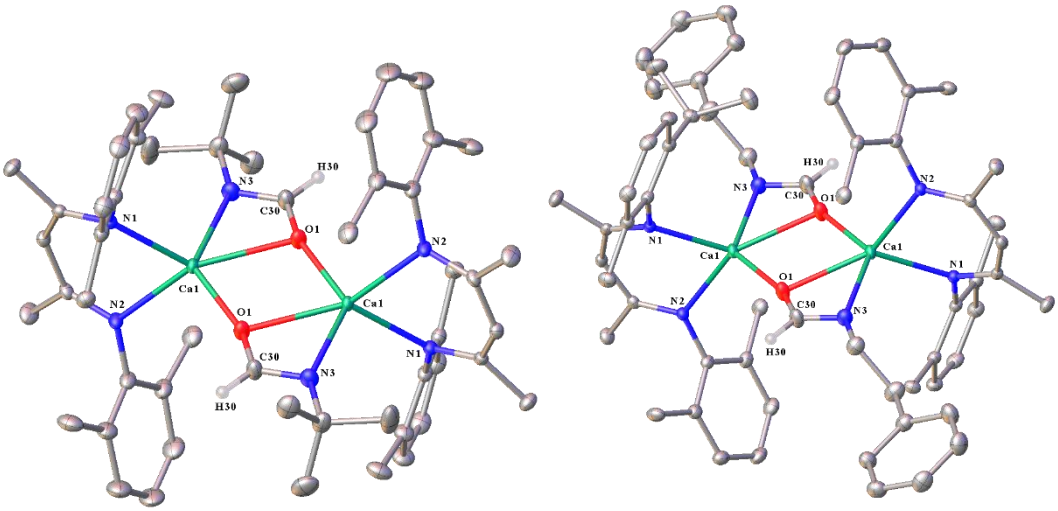

Figure 4.10: ORTEP representations of compounds **4.8** (left) and **4.9** (right) with thermal ellipsoids at 30%. Isopropyl methyl groups and hydrogen atoms except H30/H30^{i} have been removed for clarity. Selected bond lengths (Å) and bond angles (°): **4.8**: Ca1–O1 2.2549(12), Ca1–O1^{i} 2.4211(13), Ca1–N1 2.3392(13), Ca1–N2 2.3263(14), Ca1–N3 2.4472(15), N3–C30 1.288(3), O1–C30^{i} 1.303(2). O1–Ca1–O1^{i} 76.26(5), O1–Ca10–N1 110.49(5), O1–Ca1–N2 107.18(5), O1^{i}–Ca–N3 55.20(5), O1–Ca1–N3 131.21(5), N2–Ca1–N1 81.99(5), N1–Ca1–N3 107.33(5), N2–Ca1–N3 107.59(5), N3–C30–O1^{i} 121.08(17). **4.9**: Ca1–O1^{i} 2.2528(14), Ca1–O1 2.4198(13), Ca1–N1 2.3293(14), Ca1–N2 2.3339(14), Ca1–N3 2.4834(16), N3–C30 1.274(3), O1–C30 1.293(2). O1–Ca1–O1^{i} 76.01(5), O1–Ca–N3 54.67(5), N1–Ca1–O1 138.11(5), N1–Ca1–N2 83.50(5), N1–Ca1–N3 108.70(5), N2–Ca1–N3 102.59(5), N3–C30–O1 121.56(18).

Synthesis of the more sterically congested calcium formamidate, **4.10**, required heating (60°C) to evidence any CO insertion into the Ca–N(H)Dipp bond (Table 4.1). Solvent was removed *in vacuo* from **4.10**, while dissolution in hexane and storage at –35°C overnight gave colourless blocks suitable for an X–ray diffraction analysis. The solid state structure of **4.10**, Figure 4.11, did not display the anticipated monomeric *β*–diketiminato calcium *N*–Dipp formamidate, analogous to the magnesium complex **4.7**. As previously discussed in Chapter One, the heavier alkaline earth congeners have a higher propensity for Schlenk type redistribution, forming the homoleptic species in favour of the heteroleptic complexes, Scheme 4.6.[5]

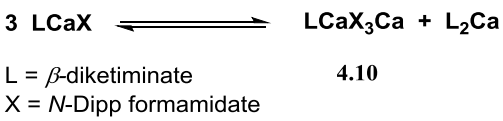

Scheme 4.6: The Schlenk–like redistribution to which alkaline earth M^{2+} complexes are prone.

Heating increases the tendency for this redistribution and explains the bimetallic solid state structure of **4.10**, Figure 4.11. While a solitary *β*–diketiminate ligand is bound in a bidentate fashion to Ca1, three *N*–Dipp formamidate ligands bridge in a μ_2–fashion from their oxygen centres (O1, O2 and O3) between Ca1 and Ca2. The final Ca1 contact from a coordinated THF, completes a distorted octahedral geometry. The coordination sphere of the second calcium centre, Ca2, comprises three *N*–Dipp formamidate ligands bound κ^2– from both oxygen and nitrogen atoms. A second terminal THF comprises the final contact to Ca2 to complete a distorted pentagonal bipyramidal geometry.

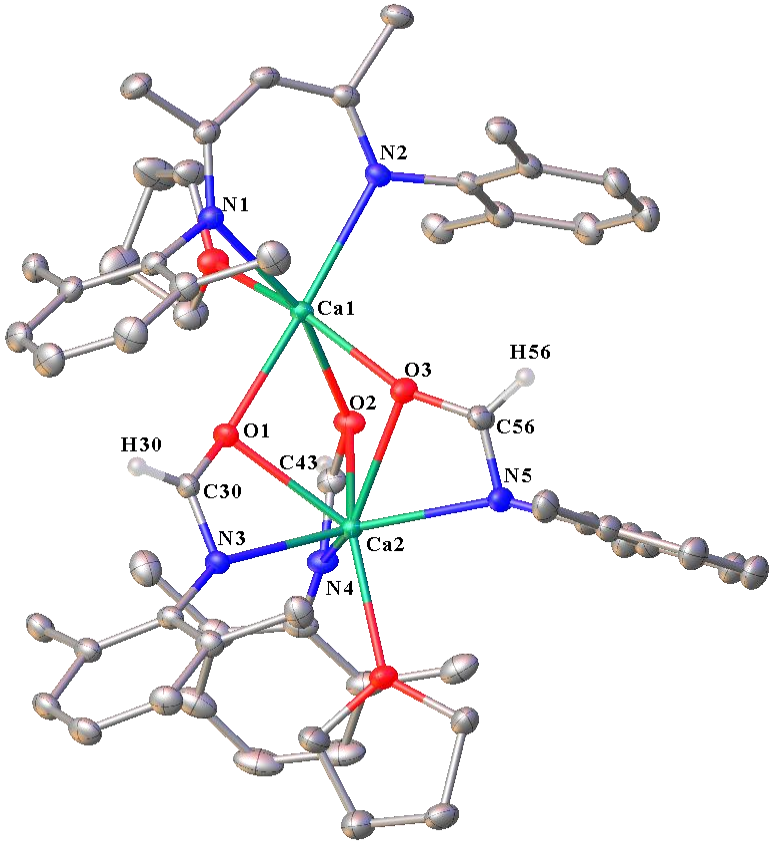

Figure 4.11: ORTEP representation of compound **4.10** with thermal ellipsoids at 30%. Isopropyl methyl groups and hydrogen atoms except those attached to C30, C43 and C56, have been removed for clarity. Selected bond lengths (Å) and bond angles (°): Ca1–O1 2.3338(13), Ca1–O2 2.3809(14) Ca1–O3 2.3330(14), Ca2–O1 2.4183(14), Ca2–O2 2.4953(14), Ca2–O3 2.4212(14), Ca1–N1 2.4300(16), Ca1–N2 2.4188(15), Ca2–N3 2.5113(16), Ca2–N4 2.4995(17), Ca2–N5 2.5572(17), O1–C30 1.288(2), O2–C43 1.278(2), O3–C56 1.284(2), N3–C30 1.291(2), N4–C43 1.294(3), N5–C56 1.298(3). O1–Ca1–O2 75.01(5), O1–Ca1–O4 101.22(5), O1–Ca1–N1 92.49(5), O1–Ca1–N2 165.92(5), O2–Ca1–N1 162.71(5), O2–Ca1–N2 116.84(5), O3–Ca1–N1 114.04(5), O3–Ca1–N2 98.69(5), O1–C30–N3 120.97(18), O2–C43–N4 122.01(18), O3–C56–N5 121.91(18), O1–Ca2–O2 71.48(5), O1–Ca2–O3 73.15(5), O1–Ca2–N3 54.14(5), O2–Ca2–N4 53.54(5),O3–Ca2–N5 53.84(5).

4.4 Mechanistic Considerations

Based on these experimental observations and building on those explored in Chapter Three, it is proposed that the carbonylation reaction pathway proceeds as shown in Scheme 4.7. Insertion of CO into the Ae–N(H)R (R = Alkyl or Aryl) bond initially yields a carbenic carboxamide complex, **4.11**, which then rapidly undergoes a 1,2–hydrogen shift to quench the reactive intermediate and provide the final *β*–diketiminato alkaline earth formamidate product.

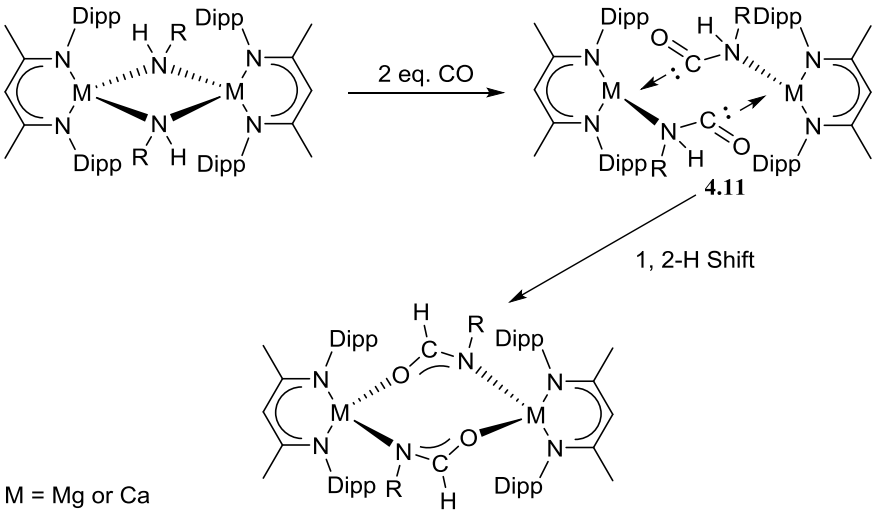

Scheme 4.7: Proposed reaction pathway for CO insertion into an alkaline earth primary amide.

Although the proposed intermediate, **4.11**, (Scheme 4.7) could neither be isolated nor identified by NMR spectroscopy, a related reaction between **Ih** and *N*–methylaniline under one atmosphere of ^{13}CO provided a snapshot of the proposed mechanistic pathway, Scheme 4.8.

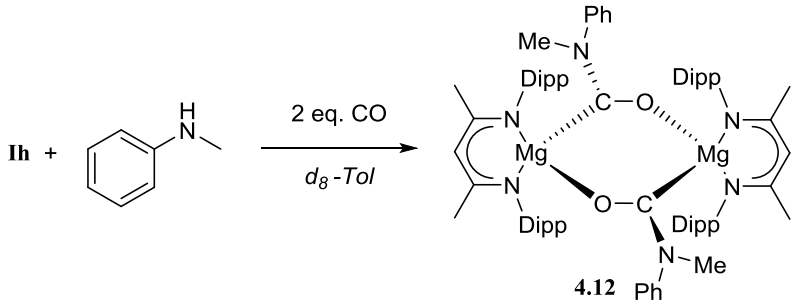

Scheme 4.8: CO insertion into a metal nitrogen bond with no *β* protons available for a 1,2–hydrogen shift.

^{1}H NMR spectroscopic analysis of **4.12** demonstrated limited change from the initially formed anilide. The ^{13}C{^{1}H} NMR spectrum was also similar to that of the starting material, except for a single new highly deshielded resonance at δ 230.0 ppm, Figure 4.12.

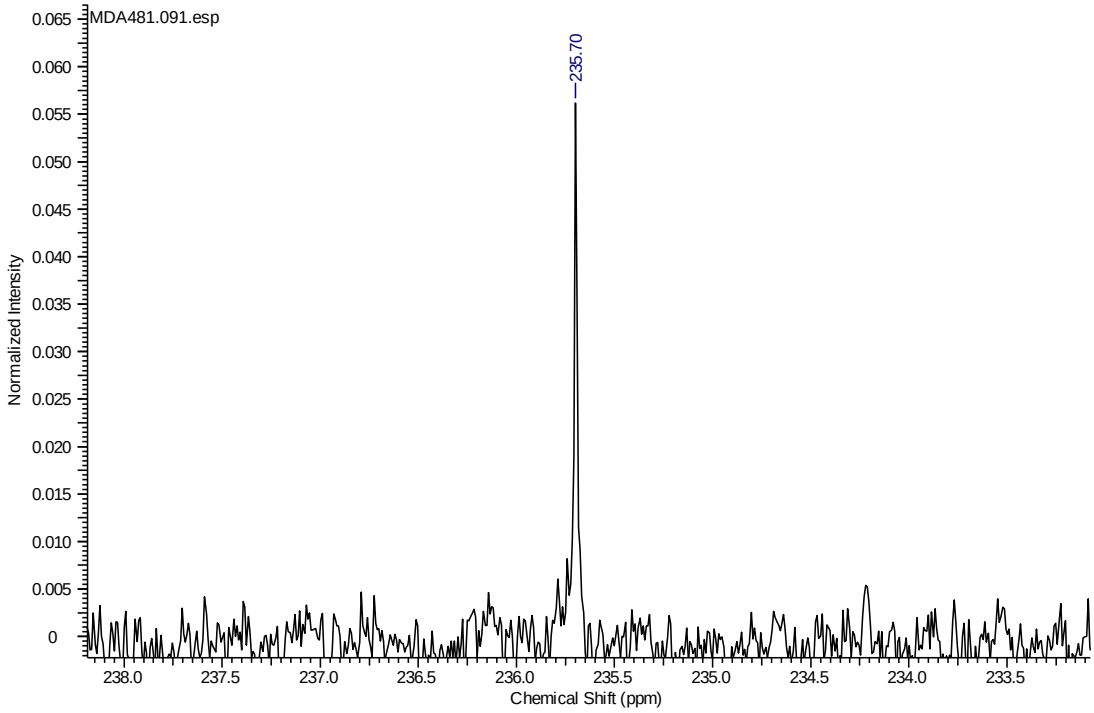

Figure 4.12: Highly deshielded singlet resonance in the ^{13}C{^{1}H} NMR spectrum (125.75 MHz) of the carbenic carbon of **4.12**.

Crystallisation of **4.12** from the reaction solution provided crystals suitable for an X–ray diffraction analysis, Figure 4.13. The solid state structure of **4.12** is a symmetrical dimer. The *β*–diketiminate ligands cap each Mg1/Mg1^{i} respectively, with two bridging carbonylated *N*–methylanilide ligands. The carbonyl (O1–C30) bond length of 1.252(2) Å suggests double bond character, an observation supported by the near planar angles subtended at C30. The Mg1–C30 bond length (2.2051(19) Å) is in the range (2.194 – 2.279 Å) of values reported for Mg–NHC bond lengths (Figure 4.14).[6] It is however, significantly shorter than the related [(Me$_3$Si)$_2$N]$_2$Mg–IPr, **XXI**, Mg–C bond length of 2.276(2)Å.[7] This shortening is ascribed to greater electrostatic component of the bonding of the acyl carbon as a component of a formally uninegative carboxamide ligand.

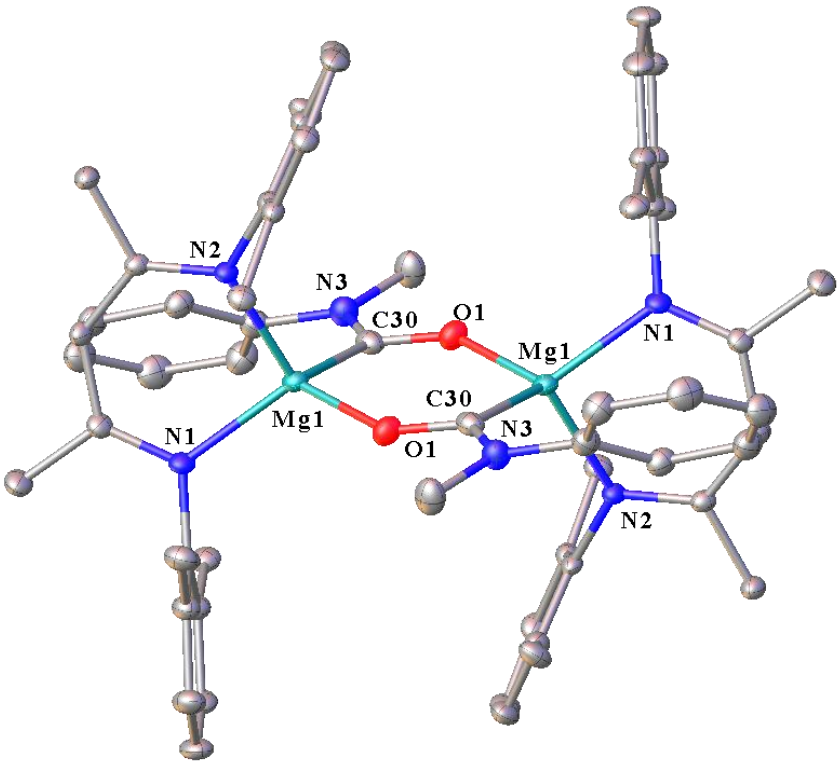

Figure 4.13: ORTEP representation of compound **4.12** with thermal ellipsoids at 30%. Isopropyl methyl groups and hydrogen atoms have been removed for clarity. Selected bond lengths (Å) and bond angles (°): Mg1–N1 2.0580(15, Mg1–N2 2.0774(14), Mg1–O1 1.9239(14), Mg1–C30 2.2051(19), O1–C30^{i} 1.252(2), N3–C30 1.382(3), N3–C32 1.425(2), N3–C31 1.464(3). N2–Mg1–C30 112.09(6), O1–Mg1–N2 113.23(6), O1–Mg1–N1 111.00(6), O1–Mg–C30 104.00(7), N1–Mg1–N2 93.79(6), N1–Mg1C30 122.91(7), C30^{i}–O1–Mg1 140.15(13), C30–N3–C32 122.13(16), C30–N3–C31 120.88(16), C32–N3–C31 116.85(16), O1^{i}–C30–Mg1 111.15(13), O1^{i}–C30–N3 114.15(16), N3–C30–Mg1 133.81(13).

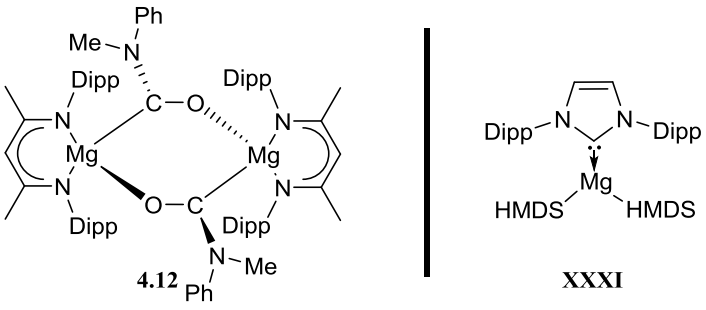

Figure 4.14: Comparison between magnesium carbene complexes **4.12** and **XXXI**.

Although a handful of isolated carbenic C(O)R (R = N, C) adducts are known, these were all synthesised by the reduction of a CO bound to transition metal.[8] To the best of our knowledge, **4.12**, represents the first isolated main group carbenic C(O)R (R = N(Me)Ph)

adduct and the first species of its type to be synthesised from sequestered CO. The isolation of **4.12**, implicates the proposed intermediate **4.11** (Scheme 4.7) in the reaction pathway for the formation of the alkaline earth formamidate complexes.

4.5 Computational Studies of the Carbonylation of Ae–N bonds

In collaboration with Professor L. Maron, DFT calculations were performed on the carbonylation of Ae–N(H)Ph bonds. Initial calculations demonstrated that the *in situ* generation of the *β*–diketiminato calcium anilide, (Figure 4.15) is mildly exothermic, (ΔH = –4.9 kcal mol^{-1}). The initial rupture of the dimeric alkaline earth amide by the coordination and formal insertion of CO into the Ca–N bond, requires the assembly of a transition state (**T1**) of some 20.6 kcal mol^{-1}, Figure 4.15. CO reduction is computed to be sequential rather than simultaneous and the carbenic intermediate **4.13**, undergoes the second CO insertion *via* a sequence of effectively isoenergetic reaction steps to provide the experimentally postulated species, **4.11** (Figure 4.15). Although **4.11** then rearranges *via* the relatively high energy **T3** and **T4** (21.2 and 22.1 kcal mol^{-1}), the overall formation of the formamidate **4.14** is highly exothermic (ΔH = –67.7 kcal mol^{-1}) with respect to the starting materials. Although the comparable calculations have not yet been performed, the longer reaction times necessary for conversion to the magnesium formamidates (**4.3**, **4.5** – **4.7**) infer that the comparable barrier heights will be higher for the magnesium system.

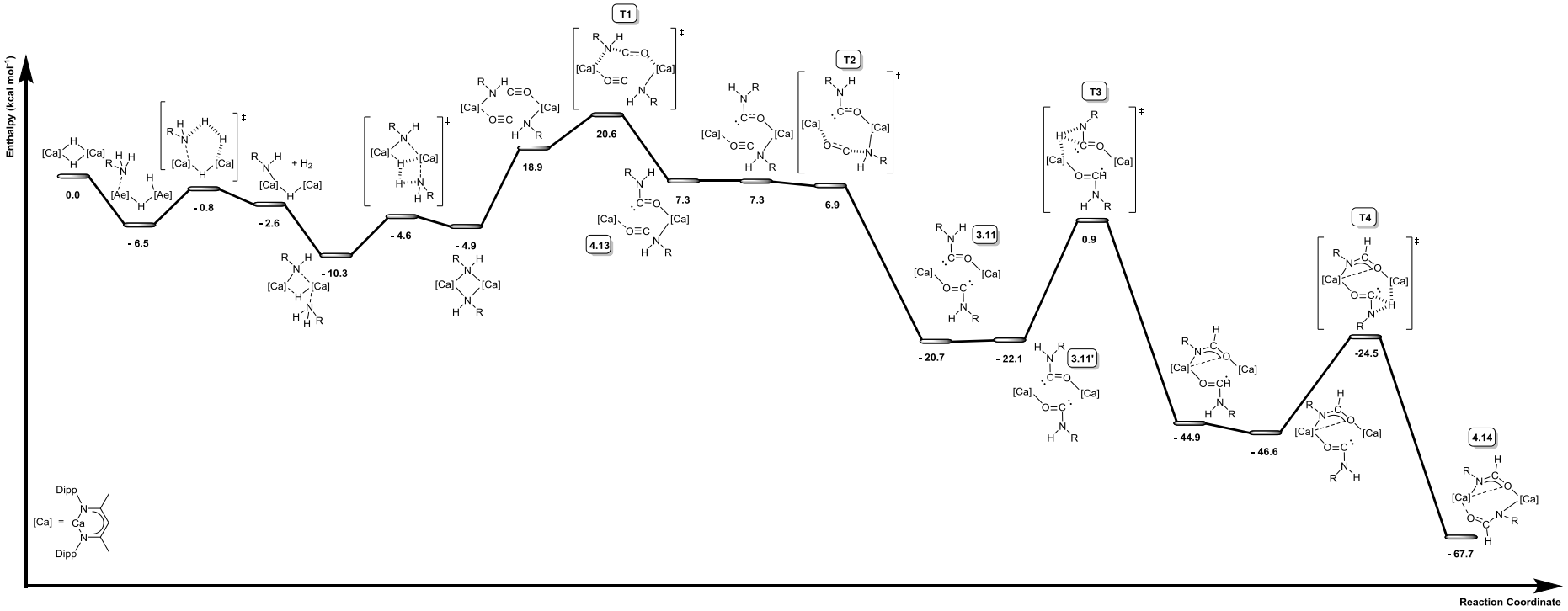

Figure 4.15: DFT calculations of the initial protolytic reaction between aniline and **Ii**, and subsequent carbonylation mechanism to provide **4.16**.

Having successfully extended this CO insertion chemistry to the carbonylation of Ca–NR_2 (R = H, alkyl or aryl) bonds, further work was directed towards the development of transformations that could be applied to compounds **4.2 – 4.10** to provide novel reaction pathways to value added chemicals. The previously discussed (*vide supra*) hydrodeoxygenation of isocyanates with HBpin catalysed by **Ib**, provided a facile route to borylated *N*–methyl amines. Magnesium formamidates (**2.1**) where identified as key intermediates during the catalysis. It was, thus, envisaged that addition of HBpin to **4.2** – **4.10** would similarly generate *N*–methyl amines in which CO acts as the C_1 carbon source.

4.6 Calcium Formamidate Hydrodeoxygenation

It was postulated that the addition of six equivalents of HBpin to complex **4.2**, prepared from ^{13}CO, would deoxygenate the formamidate to yield the bis(borylated) *N*–methyl amine, **4.15** and a calcium boryloxide, **4.16**, (Scheme 4.9) analogous to the magnesium boryloxide, **2.3**, previously discussed in Chapter Two.

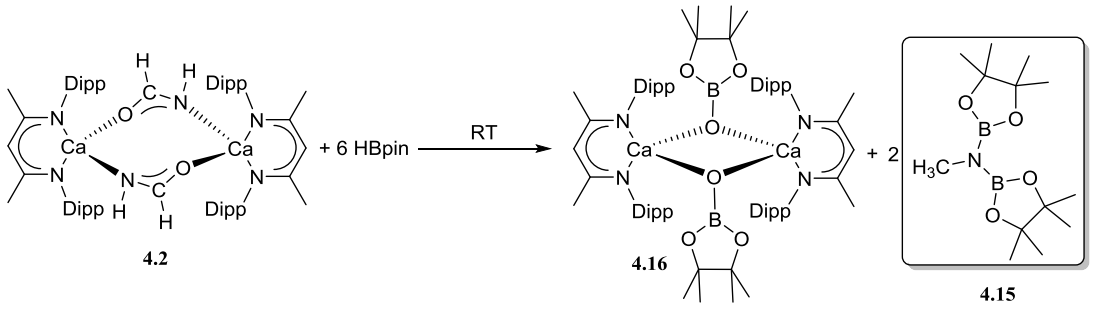

Scheme 4.9: Stoichiometric reduction of complex **4.2** with three equivalents of HBpin to yield a calcium boryloxide, **4.16** and the bis(boryl) *N*–methyl product, **4.15**.

Immediate interrogation of the reaction by NMR spectroscopy after the addition of HBpin evidenced formation of the bis(borylated) *N*–methyl amine derivative through the appearance of a major resonance at δ 30.9 ppm in the $^{13}C\{^1H\}$ NMR spectrum. This signal was observed to split into a quartet ($^1J_{CH}$ = 136.4 Hz, Figure 4.16, (a)) in the corresponding ^1H–^{13}C gated spectrum. Further evidence for the formation of the borylated *N*–methyl amine product was established by the ^1H NMR spectrum which displayed a doublet ($^1J_{HC}$ = 136.4 Hz, Figure 4.16, (b)) at δ 2.05 ppm, which was shown to be correlated with the resonance at δ 30.9 ppm in the $^{13}C\{^1H\}$ NMR spectrum by a HSQC experiment. Finally the ^{11}B NMR spectrum evidenced complete consumption of HBpin and comprised a major singlet resonance at δ 26.0 ppm, congruent with analogous data reported for the borylated amines described in Chapter Two, and confirming the formation of the bis(borylated) *N*–methyl amine.

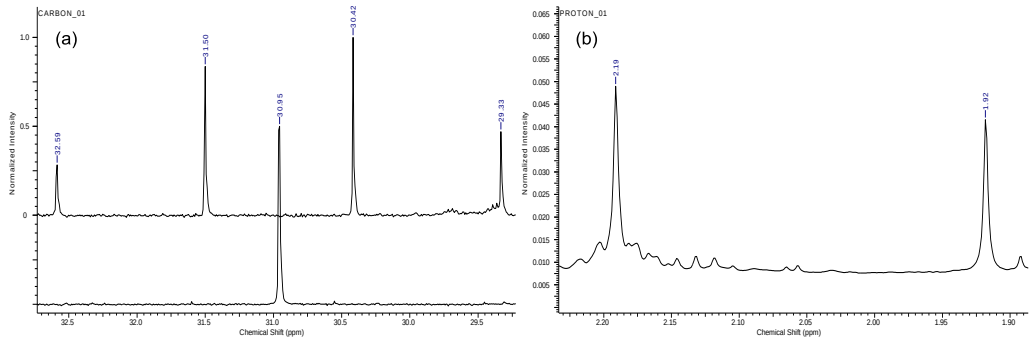

Figure 4.16: a) (Left) Stacked $^{13}C\{^{1}H\}$ (125.75 MHz) and $^{1}H–^{13}C$ gated NMR spectra, the former displaying a singlet resonance and the later displaying a quartet, δ 30.9 ppm ($^{1}J_{CH}$ = 136.4 Hz) (b) (Right) the corresponding ^{1}H NMR spectrum (500 MHz) displaying the new methyl resonance of compound **4.15** at δ 2.05 ppm, ($^{1}J_{HC}$ = 136.4 Hz).

Stimulated by this outcome, analogous reactions were carried out on all the aforementioned isolated formamidate complexes **4.3** – **4.10**. These results are summarised in Table 4.2.

Table 4.2: Addition of four equivalents of HBpin to compounds **4.3** – **4.10** respectively, provides the magnesium or calcium boryloxide, **2.3** or **4.16**, and the respective *N*–methyl amine.

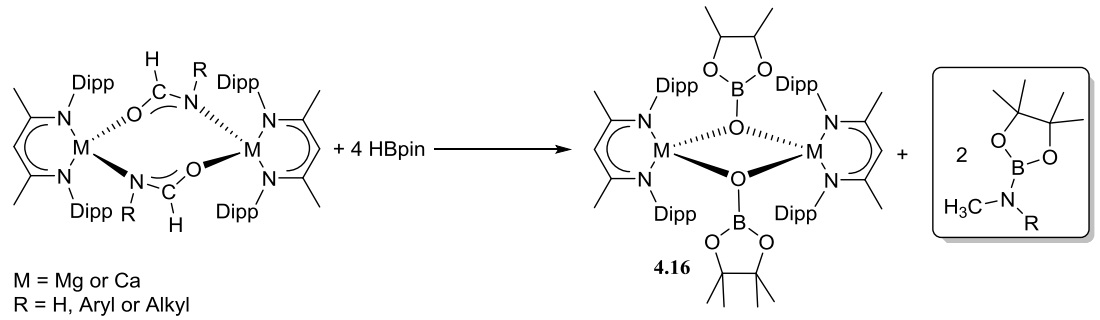

Entry	Ar/R	Time (h)	Temp. (°C)	NMR Conv. (%)
4.3	^{n}Bu	24	60	99
4.5	^{i}Pr	48	60	99
4.6	$CH_2CH_2C_6H_5$	24	80	87
4.7	Dipp	72	60	99
4.4	^{n}Bu	2	25	87
4.8	^{t}Bu	<1	25	99
4.9	$CH_2CH_2C_6H_5$	<1	25	90
4.10	Dipp	12	60	99

There is a marked difference in reactivity between the magnesium and calcium formamidates. Compounds **4.3** and **4.5** – **4.7** require elevated temperatures and extended reaction times to provide high (*ca.* ~ 90%) conversions to the *N*–methyl amine products. In contrast, the calcium complexes **4.4** and **4.8** – **4.10** were observed to undergo facile reduction at ambient temperature. To further explore the origin of these observations, a series of stoichiometric reactions were undertaken with the calcium compounds **4.4** and **4.8** – **4.10**. Addition of one equivalent of HBpin to **4.4** and **4.8** – **4.9** led to complete consumption of the borane to provide a distribution of starting material, **4.16** and the respective *N*–^{13}C methyl amine. Conversely, the activity of compound **4.10** ((a), Scheme 4.10) towards hydrodeoxygenation was retarded in comparison to **4.4** and **4.8** – **4.9**. Addition of one

equivalent of HBpin to **4.10** in d_8–toluene at room temperature provided ^{1}H and ^{11}B NMR spectra reminiscent of those provided by the previously discussed magnesium borate species **2.2**, ((b), Scheme 4.10) in Chapter Two, with only limited production of the borylated *N*–Dipp borylamine after five minutes at room temperature.

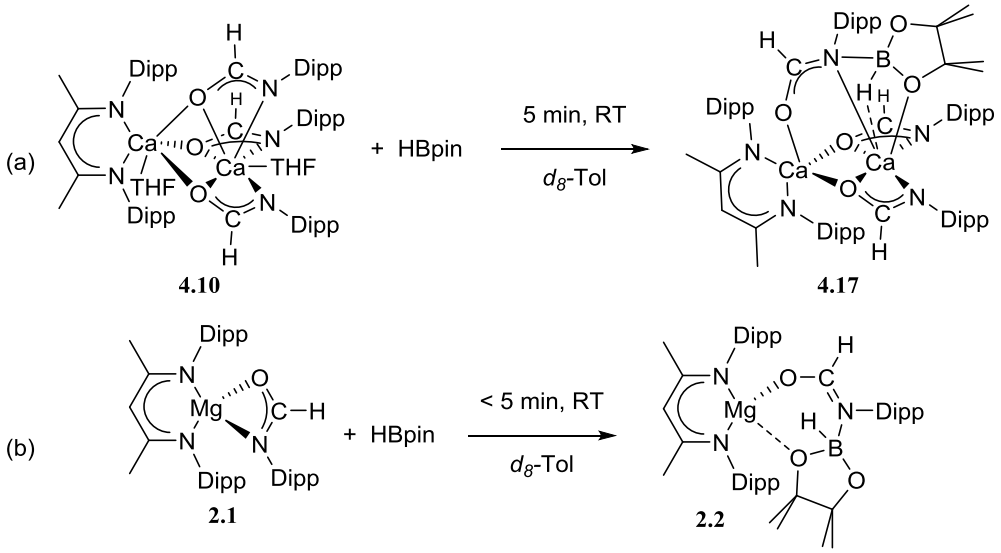

Scheme 4.10: (a) Addition of HBpin at room temperature to **4.10** yields the bimetallic calcium borohydride species, **4.17**.(b) Addition of HBpin at room temperature to **2.1** yields magnesium borohydride species, **2.2**, in an effectively quantitative yield.

One equivalent of HBpin was added to a vial containing an equimolar solution of **4.10** in hexane and stirred for 5 minutes before being stored at –35°C overnight. Crystallisation from the reaction solution provided colourless plates of **4.17** suitable for an X–ray diffraction experiment, Figure 4.17. The solid state structure of **4.17** is comparable to **4.10** in comprising a solitary *β*–diketiminate ligand which is terminally bound in a bidentate fashion to Ca1. Three *N*–Dipp formamidate ligands bind via μ_2–bridging interactions through their oxygen atoms (O1, O2 and O3) to Ca1, completing a trigonal bipyramidal geometry for Ca1. The second calcium centre (Ca2), however, now has two *N*–Dipp formamidate ligands bound κ^2– from both the oxygen (O2 and O3) and the nitrogen (N4 and N5) atoms of each formamidate ligand. The final two contacts to Ca2 are provided by a coordinated oxygen, O4, from the pinacolbo fragment which has formally inserted into the Ca–N bond of the N3–containing formamidate ligand. The inserted HBpin function has displaced the κ^2– binding of the formamidate moiety previously seen in **4.10**, which now only binds κ^1– from the nitrogen to Ca2 and thus achieves a distorted octahedral geometry. Unlike **4.10**, there are no coordinated THF ligands to either of the calcium centres in **4.17**. This is likely to be due to the increased steric congestion imposed by the insertion of the HBpin fragment which forces the Dipp moieties closer to the

calcium centres. The boron–bound hydride was readily located and freely refined, clearly demonstrating a Ca–H interaction in the solid state, Figure 4.17. The boron–bound hydride of the magnesium formamidinatoborate, **2.2**, was also located and freely refined, however, in this instance the molecule demonstrated no Mg–H interaction in the solid state. This divergence in solid state structure is attributed to the increase in ionic radius from magnesium (0.78 Å) to calcium (1.06 Å).

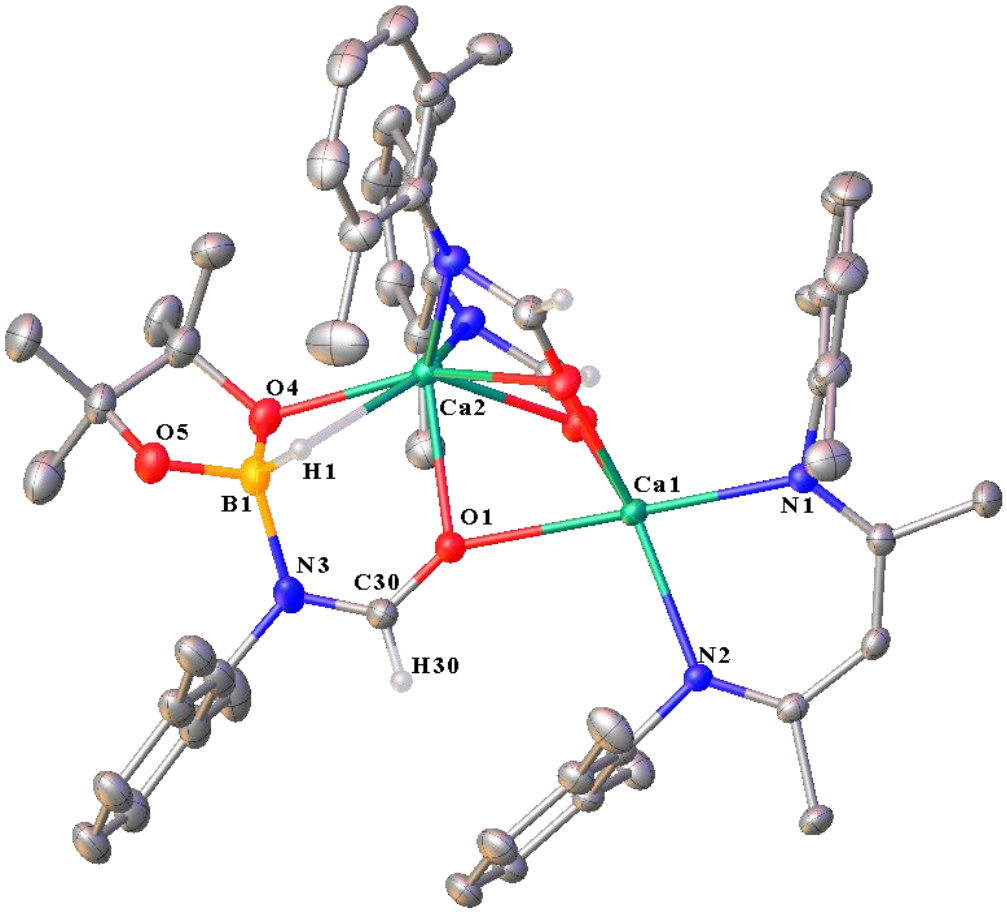

Figure 4.17: ORTEP representation of compound **4.17** with thermal ellipsoids at 30%. Isopropyl methyl groups and hydrogen atoms except hydrogens attached to C30, C43, C56 and B1, have been removed for clarity. Selected bond lengths (Å) and bond angles (°): Ca1–O1 2.503(2), Ca1–O2 2.228(2), Ca1–O3 2.224(2), Ca1–N1 2.389(2), Ca1–N2 2.353(2), Ca2–O1 2.376(2), Ca2–O2 2.412(2), Ca2–O3 2.503(2), Ca2–O4 2.293(3), Ca2–N4 2.487(2), Ca2–N5 2.455(2), O1–C30 1.268(4), O2–C43 1.281(3), O3–C56 1.286(3), B1–N3 1.685(6), N3–C30 1.267(4), N4–C43 1.295(4), N5–C56 1.292(4). O1–Ca1–O2 75.72(7), N1–Ca1–O1 167.01(8), N2–Ca1–O1 100.72(7), N3–C30–O1 123.9(3), N4–C43–O2 121.0(3), N5–C56–O3 121.3(3), C30–N3–B1 116.2(3), O4–B1–N3 105.5(3), O5–B1–O5 106.3(4), B1–O4–Ca2 92.4(2).

Encouraged by this result, a second equivalent of HBpin was added to **4.17** in an attempt to generate the bis–borylated hemiaminal, **2.4**, (Chapter 2, Dipp(pinB)NCH_2OBpin). Although it was postulated that this reaction would also generate the calcium hydride, **Ii**, along with a homoleptic calcium *N*–Dipp formamidate (Scheme 4.11), all attempts to evidence any such reactivity were unsuccessful.

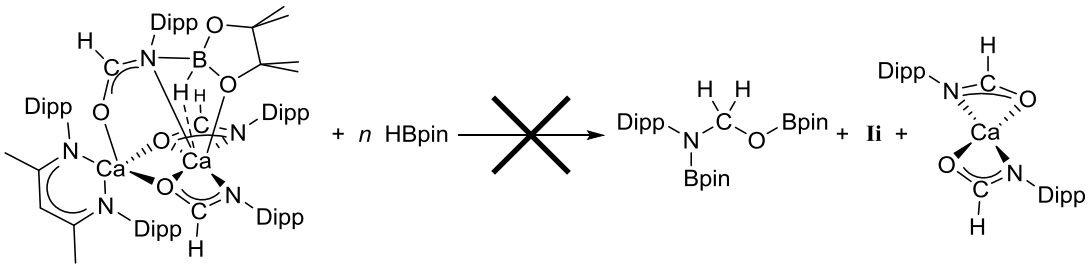

4.17 **2.4** **4.18**

Scheme 4.11: Addition of varying quantities of HBpin to **4.17** did not yield the bis–borylated hemiaminal, **2.4**, or regenerate the calcium hydride and produce a homoleptic calcium formamidate complex such as **4.18**.

On the basis of both the experimental and computational results a catalytic cycle for the hydrodeoxygenation of formamidates generated from amine carbonylation with **Ih** or **Ii**, can be envisaged. A protonolysis reaction between either **Ih** or **Ii** and an amine (RNH_2, R = Alkyl, Aryl or H) generates dihydrogen and a *β*–diketiminato alkaline earth amide, **4.19**, ***Cycle 1***, Scheme 4.12. Subsequent CO insertion into the Ae–N(H)R bond produces a short lived carbenic intermediate that rapidly undergoes a 1,2–hydrogen shift to create an alkaline earth formamidate, **4.20**. Initial interaction of **4.20** with HBpin yields an alkaline earth borate species similar to the aforementioned **2.2** and **4.15**, while ensuing reduction is then predicated on a sequence of C–O/Ae–H and Ae–O/B–H (Ae = Mg or Ca) metathesis steps reminiscent of the reactivity summarised in Chapter Two, Scheme 4.12.

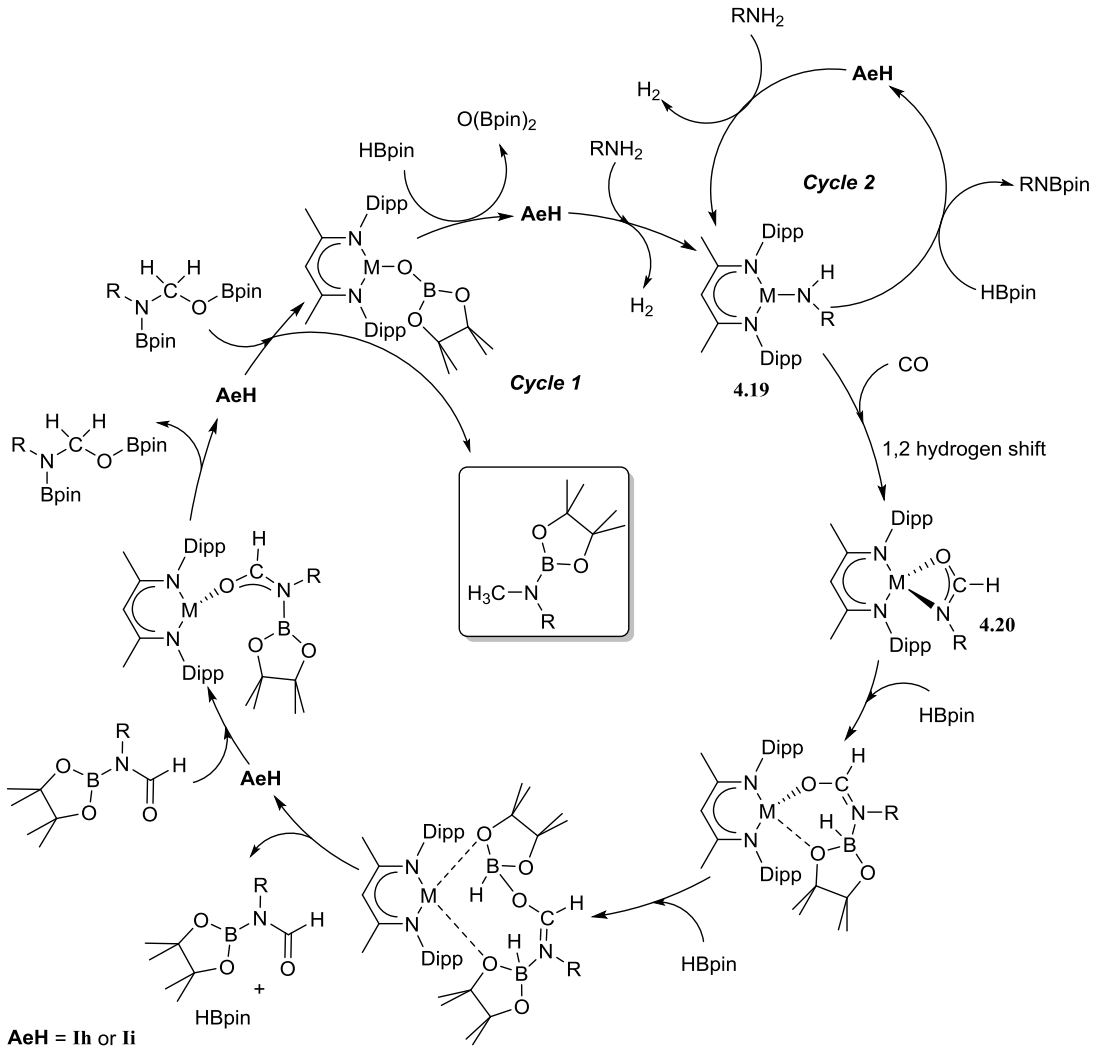

Scheme 4.12: Proposed catalytic cycle for the hydrodeoxygenation of CO sequestered formamidates by **Ih** or **Ii**.

Although the stoichiometric reactions carried out in both this Chapter and Chapter Two, coupled with the computational results confirm the viability of the aforementioned catalytic cycle (***Cycle 1***, Scheme 4.12), this could not be experimentally observed. Rather, these reactions resulted in the facile dehydrocoupling reaction between the amines and HBpin substrates catalysed by **Ih** and **Ii** (***Cycle 2***, Scheme 4.12) in a manner analogous to that previously discussed in Chapter One, (Section 1.5.1) by Hill and co–workers.[9] While the catalytic conditions employed presented this undesired result, research by Hill and co–workers is continuing to identify the conditions, particularly through the application of higher CO pressures, required to access such chemistries.

In summary, this chapter has demonstrated the facile insertion of CO into Ae–NHR bonds (Ae = Mg, Ca; R = Aryl, Alkyl and H) at pressures not exceeding one atmosphere. A

subsequent 1,2–hydrogen shift generates *β*–diketiminato alkaline earth (Mg or Ca) formamidates. These complexes are formed *via* carbenic intermediates, an inference which is strongly supported by the isolation of a *N*–methylaniline–derived magnesium carboxamide complex. DFT calculations support the experimentally observed results and demonstrate that the energy barrier presented by a 1,2–methyl shift is significantly less kinetically accessible than the corresponding 1,2–hydrogen shift. All compounds were subjected to stoichiometric hydrodeoxygenation conditions with HBpin as a reductant, revealing the ability of the heavier calcium congeners to undergo facile reduction at room temperature compared to the elevated temperatures (*ca.* ~60°C) required for the magnesium species. These stoichiometric reactions proceeded *via* a reduction pathway analogous to those deduced for the magnesium formamidates generated from isocyanates and **Ih** which were described in Chapter Two. Although this reactivity holds the potential to be incorporated into a catalytic regime, dehydrocoupling between the amine and HBpin substrates proved more facile generating borylated amines rather than the desired borylated methyl amine product under the applied reaction conditions and only one atmosphere of CO.

4.7 References

1. a) D. J. Fox and R. G. Bergman, *Journal of the American Chemical Society*, 2003, **125**, 8984–8985; b) D. J. Fox and R. G. Bergman, *Organometallics*, 2004, **23**, 1656–1670.
2. C. Ruspic and S. Harder, *Inorganic Chemistry*, 2007, **46**, 10426–10433.
3. A. G. M. Barrett, M. R. Crimmin, M. S. Hill, P. B. Hitchcock, S. L. Lomas, M. F. Mahon, P. A. Procopiou and K. Suntharalingam, *Organometallics*, 2008, **27**, 6300–6306.
4. a) M. Arrowsmith, M. S. Hill, A. L. Johnson, G. Kociok–Köhn and M. F. Mahon, *Angewandte Chemie International Edition*, 2015, **54**, 7882–7885; b) M. Ma, A. Stasch and C. Jones, *Chemistry – A European Journal*, 2012, **18**, 10669–10676.
5. M. Arrowsmith, M. S. Hill and G. Kociok–Köhn, *Organometallics*, 2011, **30**, 1291–1294.
6. a) A. J. Arduengo Iii, H. V. R. Dias, F. Davidson and R. L. Harlow, *Journal of Organometallic Chemistry*, 1993, **462**, 13–18; b) A. J. Arduengo, F. Davidson, R. Krafczyk, W. J. Marshall and M. Tamm, *Organometallics*, 1998, **17**, 3375–3382; c) H. Schumann, J. Gottfriedsen, M. Glanz, S. Dechert and J. Demtschuk, *Journal of Organometallic Chemistry*, 2001, **617–618**, 588–600.
7. M. Arrowsmith, M. S. Hill, D. J. MacDougall and M. F. Mahon, *Angewandte Chemie International Edition*, 2009, **48**, 4013–4016.
8. a) K. J. Ahmed and M. H. Chisholm, *Organometallics*, 1986, **5**, 185–189; b) M. Galakhov, A. Martin, M. Mena, F. Palacios, C. Yelamos and P. R. Raithby, *Organometallics*, 1995, **14**, 131–136; c) M. A. St. Clair, B. D. Santarsiero and J. E. Bercaw, *Organometallics*, 1989, **8**, 17–22; d) M. Aresta, P. Giannoccaro, I. Tommasi, A. Dibenedetto, A. M. Manotti Lanfredi and F. Ugozzoli, *Organometallics*, 2000, **19**, 3879–3889.
9. D. J. Liptrot, M. S. Hill, M. F. Mahon, A. S. S. Wilson, *Angewandte Chemie International Edition*, 2015, **45**, 13362–13365.

Conclusions and Future Work

In conclusion, *Chapter Two* has described a mild protocol for the catalytic transformation of the isocyanate function to a methyl amine, using a *β*–diketiminato magnesium *n*–butyl pre–catalyst. The activation of the heterocumulene occurs through a magnesium–centred hydroboration, demonstrated by the isolation and characterisation of the magnesium formamidato and magnesium boryloxide species, and ultimately the complete cleavage of the C=O bond. This reaction is further explored through a DFT study which complements the experimental findings. Moving forward, continuation of this study to include deuterated pinacolborane could provide hydrodeoxygenation to provide the $D_3CN(R)Bpin$ moiety that has possible applications in medicinal chemistry. This hydrodeoxygenation protocol could be extended and applied more generally to include carbonyl moieties of aldehydes, ketones, amides, (Scheme 4.13).

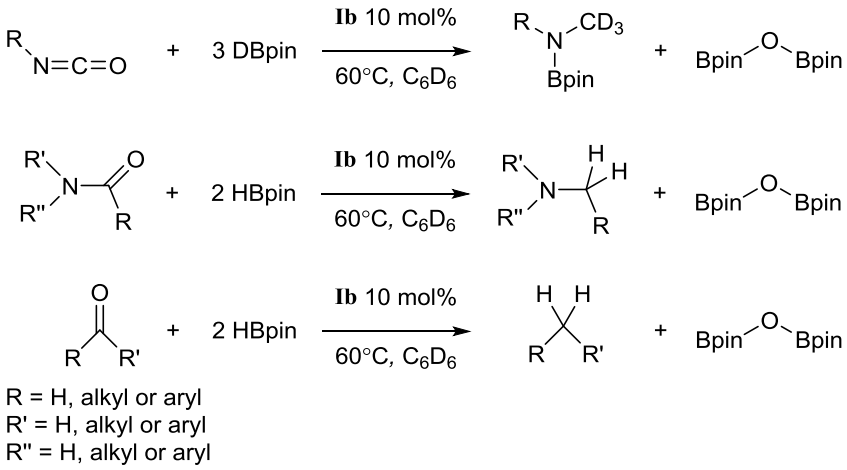

Scheme 4.13: Extension of the hydrodeoxygenation protocol with **Ib**, to amides, aldehydes and ketones.

This study also acts as a model system for the alkaline earth mediated hydroboration of the isoelectronic heterocumulene, carbon dioxide. Insights gained in this study may help explain the necessity of a $B(C_6F_5)_3$ co–catalyst for the current alkaline earth carbon dioxide reduction system.

Chapter Three demonstrates that the application of magnesium and calcium hydride complexes allows the facile homologation of CO to *cis*–enediolate species. These hydrides also provide a means for selective homogeneous catalytic reduction of CO under very mild conditions (one atmosphere of CO, 60°C) to either a methoxysilane product in the case of

calcium or deoxygenative reduction to a methyl silane product with magnesium. DFT calculations again support the experimental findings and provide further support for the postulated mechanistic pathways to the formation of the alkaline earth *cis*–enediolate species. While it has not been reported in this study, the *β*–diketiminato magnesium *n*–butyl complex (**Ib**) has been demonstrated to react with CO. An in–depth study to elucidate the mechanism of this reaction and the final products is needed. This study could be extended to the heavier congener, the newly synthesised *β*–diketiminato calcium *n*–ethyl complex.

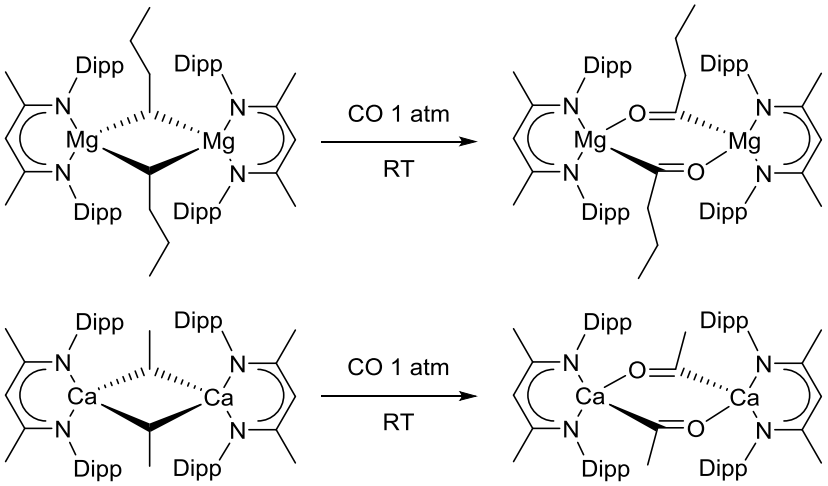

Scheme 4.14: Proposed reaction of *β*–diketiminato magnesium *n*–butyl and *β*–diketiminato calcium *n*–ethyl complex with CO.

All of the CO chemistry that has been carried out in this thesis has been performed at one atmosphere of CO. Repetition of the reported chemistry at increased pressures (>1 atm. of CO) could provide decreased reaction times, in the case of catalysis with **Ih** and **Ii**, and potentially access to higher carbon containing compounds. Furthermore, the synthesis of the *β*–diketiminato calcium *n*–ethyl complex, is performed directly between **Ii** and ethene. This provides the potential to extend this chemistry to the hydroformylation of non–activated alkenes. This, for example, could be dependent on a sequence of reaction steps involving Ca–H/C=C and Ca–C/CO insertions, followed by Ca–O/E–H (E = Si or B) σ–bond metathesis reaction using $PhSiH_3$ or HBpin as a hydride source to provide a formylated alkane.

Chapter Four has built on the experimental observations of both Chapters One and Two. The insertion of CO has been extended beyond Ae–H bonds, into Ae–NHR bonds (Ae = Mg, Ca; R = Aryl, Alkyl and H) at pressures not exceeding one atmosphere. A subsequent 1,2–hydrogen shift analogous to that observed in Chapter Three, generates *β*–diketiminato alkaline earth formamidates. These complexes are formed *via* carbenic intermediates, an inference which is strongly supported by the isolation of a *N*–methylaniline–derived

magnesium carboxamide complex. DFT calculations support the experimentally observed results. The hydrodeoxygenation reaction investigated in Chapter Two is extended to stoichiometric hydrodeoxygenation conditions with HBpin as a reductant, revealing the ability of the heavier calcium congeners to undergo facile reduction at room temperature compared to the elevated temperatures (*ca.* ~60°C) required for the magnesium species. These stoichiometric reactions proceeded *via* a reduction pathway analogous to those deduced for the magnesium formamidates generated from isocyanates. Although this reactivity holds the potential to be incorporated into a catalytic regime, dehydrocoupling between the amine and HBpin substrates proved more facile generating borylated amines rather than the desired borylated methyl amine product under the applied reaction conditions and only one atmosphere of CO.

Continuation of this study to explore the ability of different atoms' ability to undergo a 1,2 shift could be important to understand the more general applications of this reactivity, ((a) Scheme 4.**15**). This CO insertion chemistry into the Ae–N bond could then be extended to a range of new Ae–E bonds, (E = P, Si, B), (b) Scheme 4.**15**.

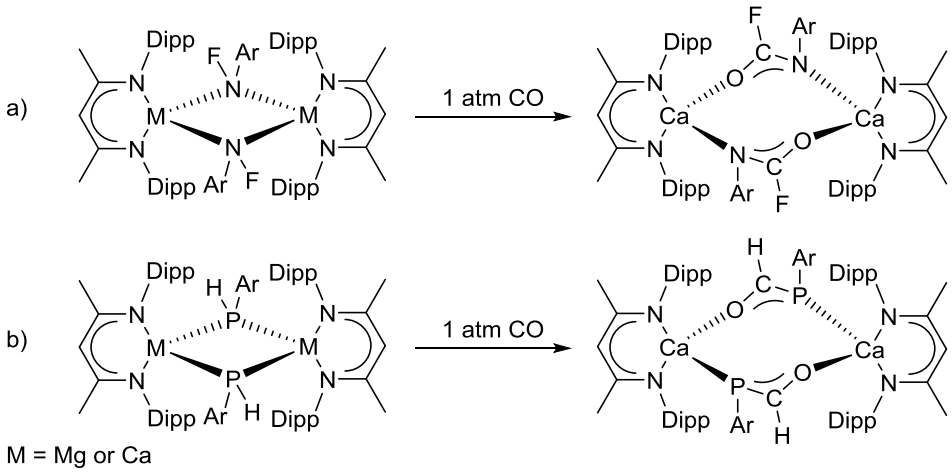

Scheme 4.15**:** a) Proposed 1,2– fluorine shift to provide a fluorinated alkaline earth formamidate. b) Proposed CO insertion into a Ae–P bond followed by a 12,–hydrogen shift to provide the analogous phosphorus-centred anion.

Chapter Five

Experimental Data

5.1 General Experimental Procedures

All reactions dealing with air– and moisture–sensitive compounds were carried out under an argon atmosphere using standard Schlenk line and glovebox techniques in an MBraun Labmaster glovebox at O_2, H_2O < 0.1 ppm. NMR experiments using air–sensitive compounds were conducted in J. Young's tap NMR tubes prepared and sealed in a glovebox under argon. All NMR data were acquired on a Bruker 300 Ultrashield™ for ^1H (300 MHz) and $^{13}C\{^1H\}$ (75.48 MHz) spectra at room temperature or a Bruker 400 Ultrashield™ for ^1H (400 MHz) and $^{13}C\{^1H\}$ (125.76 MHz) spectra. $^1H/^{13}C$ NMR spectra were referenced using residual solvent resonances. Elemental analyses of all moisture– and air–sensitive compounds were performed by Stephen Boyer of London Metropolitan Enterprises. Solvents for air– and moisture–sensitive reactions were provided by an Innovative Technology Solvent Purification System. C_6D_6 and toluene–d_8 were purchased from Fluorochem and dried over molten potassium prior to vacuum transfer into a sealed ampoule and storage in the glovebox under argon. CO was purchased from BOC. Di–*n*–butylmagnesium (1.0 M solution in n–heptane), pinacolborane (HBpin), Phenylsilane ($PhSiH_3$) and ^{13}CO were purchased from Sigma–Aldrich Ltd. Organic isocyanates and organic amines were purchased from the same supplier and dried over P_2O_5 before either distillation or vacuum transfer. **Ib**, **Ih** and **Ii** were synthesized by literature procedures.[1]

5.2 Chapter Two Experimental Data

5.2.1 Synthetic Procedures

Synthesis of [(HC{(Me)CN(2,6–^{i}PrC$_6$H$_3$)}$_2$MgOC(H)N(2,6–^{i}PrC$_6$H$_3$)], 2.1

Addition of 2,6–di–isopropylphenyl isocyanate (0.067 mmol), to a J Young's NMR tube containing a solution of $[HC\{(Me)CN(2,6\text{–}^iPr_2C_6H_3)\}_2MgH]_2$, generated by addition of HBpin (0.067 mmol) to a solution of compound **Ib** (0.067 mmol), in d_8–toluene resulted in the immediate formation of compound **2.1**. Volatiles were removed *in vacuo* and the compound was redissolved in hexane. Storage at −35°C overnight yielded compound **2.1** as colourless needles suitable for single crystal X–ray characterisation (76%). ^1H NMR (d_8–tol, 300 MHz): δ 7.92 (1H, s, NC(*H*)O), 7.06 (6H, br. s, Ar–*H*), 6.90 (3H, s, Ar–*H*), 4.96 (1H, s, C–*H*), 3.44 (2H, br. m, C*H*$(CH_3)_2$), 3.17 (2H, br. m, C*H*$(CH_3)_2$), 1.98 (2H, m, $^3J_{HH}$ = 6.78 Hz, C*H*$(CH_3)_2$), 1.66 (6H, s, NC(C*H*$_3$)CH), 1.33 (6H, br. m, CH(C*H*$_3$)$_2$), 1.11 (12H, d, $^3J_{HH}$ = 6.78

Hz, CH(CH_3)$_2$), 0.96 (6H, br. m, CH(CH_3)$_2$), 0.80 (6H, d, $^3J_{HH}$ = 6.78 Hz, CH(CH_3)$_2$). ^{13}C{^{1}H} NMR (d$_8$–tol, 125.76 MHz): δ 175.0 (N*C*(H)O),169.7 (N*C*(CH$_3$)CH), 143.9, 143.5, 140.3, 125.95, 125.40, 124.3, 122.9 (*C*–Ar), 95.1 (NC(CH$_3$)*C*H), 28.1, 27.8 (N*C*H(CH$_3$)$_2$), 24.7, 23.8 (CH(*C*H$_3$)$_2$). Despite multiple attempts, a meaningful microanalysis could not be obtained for this compound.

Synthesis of [(HC{(Me)CN(2,6–^{i}PrC$_6$H$_3$)}$_2$MgOC(H)N(2,6–^{i}PrC$_6$H$_3$)(HBpin)], 2.2

Addition of 4,4,5,5,–tetramethyl–1,3,2–dioxaborolane (0.067 mmol), to a J Young's NMR tube containing a solution of compound **2.1** (0.067 mmol) in toluene resulted in the immediate formation of compound **2.2**. Solvent was removed *in vacuo* and the solid was redissolved in hexane. Storage at −35°C overnight provided compound **2.2** as colourless crystalline blocks suitable for single crystal X–ray diffraction analysis (70%). ^{1}H NMR (d$_8$–tol, 280K, 400 MHz): δ 7.69 (1H, s, NC(*H*)O), 7.14 (6H, br. m, Ar–*H*), 7.03 – 6.98 (3H, br. s, Ar–*H*), 4.92 (1H, s, C–*H*), 3.40 (3H, m, $^3J_{HH}$ = 6.82 Hz, C*H*(CH$_3$)$_2$), 3.28 (1H, m, $^3J_{HH}$ = 6.06 Hz, C*H*(CH$_3$)$_2$), 3.15 (2H, spt, $^3J_{HH}$ = 6.82 Hz, C*H*(CH$_3$)$_2$), 1.74 (6H, s, NC(C*H*$_3$)CH), 1.37 (10H, br. m, CH(C*H*$_3$)$_2$), 1.26 (10H, br. m, CH(C*H*$_3$)$_2$), 1.20 (6H, br. m, CH(C*H*$_3$)$_2$), 1.11 (10H, br. m, CH(C*H*$_3$)$_2$), 0.79 (6H, s, OC(C*H*$_3$)$_2$), 0.58 (3H, s, OC(C*H*$_3$)$_2$), 0.47 (3H, s, OC(C*H*$_3$)$_2$). ^{11}B NMR (d$_8$–tol, 125.76 MHz): δ 4.3 (H*B*Pin). Anal. Calcd. for C$_{48}$H$_{73}$MgBN$_3$O$_3$: C, 74.37; H, 9.49; N, 5.42%; Found: C, 74.36; H, 9.13; N, 5.32%.

Synthesis of [(HC{(Me)CN(2,6–^{i}PrC$_6$H$_3$)}$_2$MgOBpin)], 2.3

Addition of 2,6–diisopropylphenyl isocyanate (0.067 mmol), to a J Young's tube containing a solution of compound **Ib** (0.067 mmol) and 4,4,5,5,–tetramethyl–1,3,2–dioxaborolane (0.201 mmol), in toluene. The reaction was heated at 60°C for 24 hours and compound **2.3** crystallized from the reaction solution as colourless blocks suitable for single crystal X–ray diffraction analysis (85%). Once crystallized, compound **2.3** displayed only sparing solubility in arene solvents necessitating analysis by NMR spectroscopy in d$_8$–THF. ^{1}H NMR (d$_8$–THF, 300 MHz): δ 7.14 – 7.03 (4H, m, Ar–*H*), 6.91 (1H, d, $^3J_{HH}$ = 3.01 Hz, Ar–*H*), 6.89 (1H, d, $^3J_{HH}$ = 3.01 Hz, Ar–*H*), 4.79 (1H, s, C–*H*), 3.58 (THF), 3.30 (2H, m., $^3J_{HH}$ = 6.78 Hz, C*H*(CH$_3$)$_2$), 3.04 (2H, m., $^3J_{HH}$ = 6.78 Hz, C*H*(CH$_3$)$_2$), 1.73 (THF), 1.37 (6H, s, NC(C*H*$_3$)CH), 1.23 (6H, d, $^3J_{HH}$ = 6.78 Hz, CH(C*H*$_3$)$_2$), 1.18 (6H, s, C(C*H*$_3$)$_2$), 1.11 (6H, d, $^3J_{HH}$ = 6.78 Hz, CH(C*H*$_3$)$_2$), 0.98 (6H, d, $^3J_{HH}$ = 6.78 Hz, CH(C*H*$_3$)$_2$), 0.97 (6H, d, $^3J_{HH}$ = 6.78 Hz, CH(C*H*$_3$)$_2$), 0.07 (6H, s, C(C*H*$_3$)$_2$), 0.05 (6H, s, C(C*H*$_3$)$_2$). ^{13}C{^{1}H} NMR (d$_8$–THF, 125.76 MHz): δ 169.7 (N*C*(CH$_3$)CH), 148.4, 144.5, 143.3, 125.9, 124.7, 124.0 (*C*–Ar), 97.4 (NC(CH$_3$)*C*H), 82.4 (O*C*(CH$_3$)$_2$), 29.5, 28.6 (N*C*H(CH$_3$)$_2$), 27.1, 26.9 ((OC(*C*H$_3$)$_2$), 24.4,

23.4(CH(CH$_3$)$_2$). ^{11}B NMR (d$_8$–THF, 125.76 MHz): δ 21.6 OBPin. Anal. Calcd. for $C_{70}H_{106}B_2Mg_2N_4O_6$: C, 71.87; H, 9.13; N, 4.79%; Found: C, 71.92; H, 8.93; N, 4.56%.

5.2.2 Catalytic Hydroboration of Isocyanates General Procedure:

10 mg (0.02 mmol, i.e. 10 mol%) of **Ib** was dissolved in 0.5 ml of C_6D_6. 90.0 μL (0.62 mmol) of pinacolborane was then added followed by either 0.2 or 0.4 mmol of the relevant isocyanate. This mixture was then transferred to a sealed Young's tap NMR tube and the reaction was either allowed to react at room temperature or was heated in an oil bath at 60 °C for the reaction times shown in Table 2.1. These reactions were regularly monitored by ^{1}H and ^{11}B NMR spectroscopy until maximum conversion was observed. On exposure to ambient atmosphere or on deliberate addition of a drop of aqueous dilute HCl the *N*–borylated amines were observed to hydrolyse rapidly to liberate the protonated parent methyl amines.

Synthesis of N,O–{B(OCMe$_2$)$_2$}$_2$–(methoxy)–2,6–diisopropyl–phenylamine, 2.4.

Synthesis performed using 42.8 μL of 2,6–diisopropylphenyl isocyanate. ^{1}H NMR (400 MHz, C_6D_6, 300 K) δ_H (ppm): 7.14 (1H, t, J_{HH} = 4 Hz, p–H), 7.10 (2H, d, J_{HH} = 4 Hz, m–H), 5.35 (2H, s, NCH_2O), 3.55 (2H, sept, J_{HH} = 8 Hz, CH(CH$_3$)$_2$), 1.39 (6H, d, J_{HH} = 8 Hz, CH(CH$_3$)$_2$), 1.29 (6H, d, J_{HH} = 8 Hz, CH(CH$_3$)$_2$), 0.99 (O–B(OC(CH$_3$)$_2$)$_2$), 0.92 (N–B(OC(CH$_3$)$_2$)$_2$). ^{13}C{^{1}H} NMR (125.8 MHz, C_6D_6, 300 K) δ_C (ppm): 155.3 (ipso–C), 148.2 (o–C), 137.2 (p–C), 123.6 (m–C), 83.3 (O–B(OC(CH$_3$)$_2$)$_2$), 82.6 (N–B(OC(CH$_3$)$_2$)$_2$), 77.9 (NCH_2O), 28.9 (CH(CH$_3$)$_2$), 25.3 (CH(CH$_3$)$_2$), 25.0 (O–B(OC(CH$_3$)$_2$)$_2$), 24.9 (N–B(OC(CH$_3$)$_2$)$_2$). ^{11}B NMR (96.3 MHz, C_6D_6, 300K) δ_B (ppm): 28.3 (br. s, NB), 24.8 (br. s. OB).

Synthesis of N,O–{B(OCMe$_2$)$_2$}$_2$–(methoxy)–2,4,6–trimethylphenylamine, 2.5.

32.2 mg of 2,4,6–trimethylphenyl isocyanate. Compound **2.5** was isolated by crystallization from the reaction solvent at room temperature (65%). ^{1}H NMR (d$_8$–tol, 300 MHz): δ 6.75 (2H, s, Ar–H), 5.29 (2H, s, CH_2), 2.37 (6H, s, Ar–o–CH_3), 2.10 (3H, s, Ar–para–CH$_3$), 0.91 (12H, s, OC(CH_3)$_2$). ^{13}C{^{1}H} NMR (d$_8$–tol, 125.76 MHz): δ 139.7, 137.1, 135.6, 129.7 (C–Ar), 83.0, 82.5 (OC(CH$_3$)$_2$), 76.9 (NCH$_2$O), 24.9 (Ar–CH$_3$), 24.7 ((OC(CH$_3$)$_2$), 19.3 (Ar–CH$_3$). ^{11}B NMR (d$_8$–tol, 125.76 MHz): δ 27.2 (NBPin), 25.3 (OBPin). Anal. Calcd. for $C_{22}H_{41}B_2NO_7$: C, 58.31; H, 9.12; N, 3.36%; Found: C, 58.58; H, 8.89; N, 3.30%.

Synthesis of [N–(2,6–^{i}PrC$_6$H$_3$)(Bpin)CH(O)], 2.6.

Addition of 2,6–diisopropylphenyl isocyanate (2.0 mmol), to a J Young's tube containing a solution of compound **Ib** (0.02 mmol) and 4,4,5,5,–tetramethyl–1,3,2–dioxaborolane (2.0 mmol), in 0.5 ml of toluene. The reaction was left at room temperature 5 minutes and compound **2.6** crystallised from the reaction solution as colourless needles

suitable for single crystal X–ray diffraction analysis (85%). ^{1}H NMR (d_8–tol, 300 MHz): δ 9.13 (1H, s, O*H*C), 7.14 – 7.05 (3H, m, Ar–*H*), 2.98 (2H, spt, $^{3}J_{HH}$ = 6.85 Hz, C*H*$(CH_3)_2$), 1.21, 1.19 (6H, d, $^{3}J_{HH}$ = 6.85 Hz, CH(C*H*$_3)_2$), 0.96 (12H, s, Bpin). ^{13}C{^{1}H} NMR (d_8–tol, 125.76 MHz): δ 164.8 (OHC), 146.2, 128.8, 124.0 (*C*–Ar), 84.5 (O*C*$(CH_3)_2$),) 29.6 (*C*H$(CH_3)_2$), 24.7 (OC(*C*H$_3)_2$), 24.6, 24.4 (CH(*C*H$_3)_2$). ^{11}B NMR (d_8–tol, 125.76 MHz): δ 25.6 (O*B*Pin). Anal. Calcd. for $C_{19}H_{30}BNO_3$: C, 68.89; H, 9.13; N, 4.23%; Found: C, 68.71; H, 9.05; N, 4.22%.

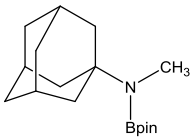

Hydroboration of 1–adamantyl isocyanate; N,N–methyl–{B(OCMe$_2)_2$}–adamantylamine: 35 mg of adamantyl isocyanate. ^{1}H NMR (500 MHz, C_6D_6, 300 K) δ_H (ppm): 2.73 (3H, s, NCH_3), 1.99 – 1.58 (ca. 15H, m, Ad–H), 1.10 (12H, s, OC$(CH_3)_2$). ^{13}C{^{1}H} NMR (125.8 MHz, C_6D_6, 300 K) δ_C (ppm): 83.5 (OC$(CH_3)_2$), 42.6 (NCH_3), 37.4 (Ad–C), 30.8 (Ad–C), 25.3 (OC$(CH_3)_2$), 25.1 (Ad–C). ^{11}B NMR (160.4 MHz, C_6D_6, 300K) δ_B (ppm): 27.5 (br. s, NB).

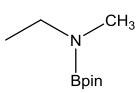

Hydroboration of ethyl isocyanate; N,N–methyl–{B(OCMe$_2)_2$}–ethylamine: 15.8 µL of ethyl isocyanate. ^{1}H NMR (500 MHz, C_6D_6, 300 K) δ_H (ppm): 3.00 (2H, q, J_{HH} = 5 Hz, NCH_2), 2.62 (3H, s, NCH_3), 1.11 (12H, s, OC$(CH_3)_2$), 0.98 (3H, t, J_{HH} = 5 Hz, NCH_2CH_3). ^{13}C{^{1}H} NMR (125.8 MHz, C_6D_6, 300 K) δ_C (ppm): 82.3 (OC$(CH_3)_2$), 43.7 (NCH_2), 33.4 (NCH_3), 25.0 (OC$(CH_3)_2$), 15.0 (NCH_2CH_3). ^{11}B NMR (160.4 MHz, C_6D_6, 300K) δ_B (ppm): 27.2 (br. s, NB).

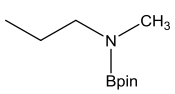

Hydroboration of propyl isocyanate; N,N–methyl–{B(OCMe$_2)_2$}–propylamine: 18.7 µL of propyl isocyanate. ^{1}H NMR (500 MHz, C_6D_6, 300 K) δ_H (ppm): 2.93 (2H, t, J_{HH} = 5 Hz, NCH_2), 2.60 (3H, s, NCH_3), 1.40 (2H, q, J_{HH} = 5 Hz, NCH_2CH_2), 1.11 (12H, s, OC$(CH_3)_2$), 0.81 (3H, t, J_{HH} = 5 Hz, CH_2CH_3). ^{13}C{^{1}H} NMR (125.8 MHz, C_6D_6, 300 K) δ_C (ppm): 83.5 (OC$(CH_3)_2$), 50.9 (NCH_2), 33.7 (NCH_3), 25.3 (OC$(CH_3)_2$), 22.0 (NCH_2CH_2), 11.5 (CH_2CH_3). ^{11}B NMR (160.4 MHz, C_6D_6, 300K) δ_B (ppm): 27.4 (br. s, NB).

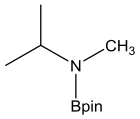

Hydroboration of iso–propyl isocyanate; N,N–methyl–{B(OCMe$_2)_2$}–iso–propylamine: 19.7 µL of *iso*–propyl isocyanate. ^{1}H NMR (500 MHz, C_6D_6, 300 K) δ_H (ppm): 3.79 (1H, sept, J_{HH} = 5 Hz, CH$(CH_3)_2$), 2.56 (3H, s, NCH_3), 1.11 (12H, s, OC$(CH_3)_2$), 1.03 (6H, d, J_{HH} = 10 Hz, CH$(CH_3)_2$). ^{13}C{^{1}H} NMR (125.8 MHz, C_6D_6, 300 K) δ_C (ppm): 83.2 (OC$(CH_3)_2$), 46.8 (NCH_3), 27.5 (NCH$(CH_3)_2$), 25.2 (OC$(CH_3)_2$), 21.4 (CH$(CH_3)_2$). ^{11}B NMR (160.4 MHz, C_6D_6, 300K) δ_B (ppm): 27.2 (br. s, NB).

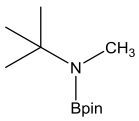

Hydroboration of tert–butyl isocyanate; N,N–methyl–{B(OCMe$_2$)$_2$}–tert–butylamine: 22.8 µL of *tert*–butyl isocyanate. ^{1}H NMR (500 MHz, C_6D_6, 300 K) δ_H (ppm): 2.69 (3H, s, NCH_3), 1.28 (9H, s, $C(CH_3)_3$), 1.09 (12H, s, $OC(CH_3)_2$). $^{13}C\{^1H\}$ NMR (125.8 MHz, C_6D_6, 300 K) δ_C (ppm): 83.5 ($OC(CH_3)_2$), 52. ($C(CH_3)_3$), 30.2 ($C(CH_3)_3$), 25.1 ($OC(CH_3)_2$). ^{11}B NMR (160.4 MHz, C_6D_6, 300K) δ_B (ppm): 24.3 (br. s, NB).

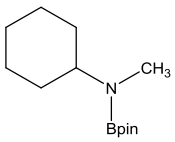

Hydroboration of cyclohexyl isocyanate; N,N–methyl–{B(OCMe$_2$)$_2$}–cyclohexylamine: 25.5 µL of cyclohexyl isocyanate. ^{1}H NMR (500 MHz, C_6D_6, 300 K) δ_H (ppm): 3.29 (1H, m, NCH), 2.63 (3H, s, NCH_3), 1.62 (4H, m, $NCH(CH_2)_2$), 1.45 (4H, m, $NCH(CH_2)_2(CH_2)_2$), 1.12 (12H, s, $OC(CH_3)_2$), 0.88 (2H, m, $(CH_2)_2CH_2$). $^{13}C\{^1H\}$ NMR (125.8 MHz, C_6D_6, 300 K) δ_C (ppm): 83.5 ($OC(CH_3)_2$), 55.7 (NCH), 32.3 (NCH_3), 29.1 ($NCH(CH_2)_2$), 26.8 ($NCH(CH_2)_2(CH_2)_2$), 25.9 ($OC(CH_3)_2$), 14.7 ($(CH_2)_2CH_2$). ^{11}B NMR (160.4 MHz, C_6D_6, 300K) δ_B (ppm): 27.4 (br. s, NB).

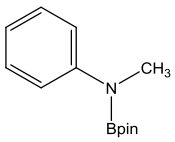

Hydroboration of phenyl isocyanate; N,N–methyl–{B(OCMe$_2$)$_2$}–phenylamine: 21.7 µL of phenyl isocyanate. ^{1}H NMR (500 MHz, C_6D_6, 300 K) δ_H (ppm): 7.45 (2H, m, o–H), 7.21 (1H, m, p–H), 6.87 (2H, m, m–H), 3.01 (3H, s, NCH_3), 1.08 (12H, s, $OC(CH_3)_2$). $^{13}C\{^1H\}$ NMR (125.8 MHz, C_6D_6, 300 K) δ_C (ppm): 164.2 (ipso–C), 148.3 (o–C), 129.2 (p–C), 121.4 (m–C), 83.5 ($OC(CH_3)_2$), 34.7 (NCH_3), 25.3 ($OC(CH_3)_2$). ^{11}B NMR (160.4 MHz, C_6D_6, 300K) δ_B (ppm): 27.7 (br. s, NB).

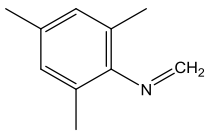

Formation of N–2,4,6–trimethylphenyl imine: A sample of compound **2.5** in C_6D_6 was heated for 12 hours at 60 °C, providing ca. 50% conversion to $MesN{=}CH_2$. ^{1}H NMR (500 MHz, C_6D_6, 300 K) δ_H (ppm): 7.24 (1H, d, J_{HH} = 12 Hz, NCH_2), 6.82 (1H, d, J_{HH} = 12 Hz, NCH_2), 6.76 (2H, s, *m–H*), 2.25 (6H, s, *o*–CH_3), 2.09 (3H, s, *p*–CH_3). $^{13}C\{^1H\}$ NMR (75.5 MHz, C_6D_6, 300 K) δ_C (ppm): 138.2 (*ipso–C*), 135.2 (*o–C*), 133.4 (*p–C*), 129.4 (NCH_2), 124.7 (*m–C*), 23.4 (*o–C*H_3), 18.6 (*p–C*H_3).

5.2.3 Single Crystal X–ray Diffraction analysis:

Single Crystal X–ray diffraction data for compound **2.6** were collected on a Nonius Kappa CCD with a low temperature device at 150 K, utilizing Mo–Kα radiation monochromated with graphite (λ = 0.71070 Å) while those for **2.5** were attained on an Agilent Xcalibur machine. Processing utilized the Nonius software,[3] with structure solution and refinement using Olex2,[4] suite of programmes throughout and visualised utilizing ORTEP 3.[5] For compounds **2.1** – **2.4** and **2.7** data were collected on a SuperNova, Dual Cu at zero, EosS2 diffractometer. The crystal was kept at 150(2) K during data collection. Using Olex2,[4] the

structures were solved via SHELXS[6] and refined with the ShelXL refinement package using Least Squares minimisation. The asymmetric unit of compound **2.2** incorporated one molecule of the magnesium complex and one molecule of toluene. C25 and C26 were modelled as being disordered over 2 sites in a 65:35 ratio. Distances from the arising fractional occupancy carbon atoms were refined subject to being similar and ADP restraints were included for C26A. H1, attached to B1, was readily located and refined freely. Disorder also prevailed in the solvent region such that the toluene entity has been modelled as being distributed over 3 overlaid sites. In a 50:25:25 ratio. The associated phenyl rings were treated as rigid hexagons and planarity, distance and ADP restraints were employed on merit to achieve the optimal chemically sensible refinement. The asymmetric unit of compound **2.3** incorporated half of a dimer molecule and a half of a molecule of toluene. Both moieties lie proximate to crystallographic inversion centres. All atoms in the Bpin ligand, with the exception of the B1, were seen to be disordered over 2 proximate locations in a 55:45 ratio. Distance and ADP restraints were employed in this region to assist convergence. It was very evident that the solvent equates to half of one molecule of toluene per asymmetric unit, and allowance for this has been made in the formula as presented herein. However, proximity to an inversion centre plus disorder did not facilitate a ready treatment with a model and, hence, the PLATON SQUEEZE algorithm was employed in this instance. The carbon atoms in both Bpin anions of compound **2.4** exhibited 65:35 disorder, which was successfully modelled, subject to distance restraints being applied to chemically similar bonds involving fractional occupancy carbons. Compound **2.5** contained 2 molecules per asymmetric unit.

Table 5.1: Single Crystal X–ray Data Parameters for compounds **2.1** – **2.6**.

Compound	**2.1**	**2.2**	**2.3**	**2.4**	**2.5**	**2.6**
Empirical formula	$C_{42}H_{59}MgN_3O$	$C_{55}H_{80}BMgN_3O_3$	$C_{38.5}H_{57}BMgN_2O_3$	$C_{25}H_{43}B_2NO_5$	$C_{22}H_{37}B_2NO_5$	$C_{25}H_{43}B_2NO_5$
Formula weight	646.23	866.34	630.98	459.22	417.14	459.22
Temperature/K	150.01(10)	150.01(10)	150.00(10)	150.01(10)	150(2)	150.00(10)
Crystal system	monoclinic	monoclinic	monoclinic	orthorhombic	monoclinic	trigonal
Space group	$P2_1/n$	$P2_1/c$	$P2_1/n$	$P2_12_12_1$	$P2_1/n$	$P3_1$
a/Å	11.59209(14)	9.17488(14)	13.48093(17)	10.0273(4)	11.5490(2)	9.7577(2)
b/Å	26.2784(3)	19.0562(3)	14.64625(15)	12.4499(7)	33.1610(6)	9.7577(2)
c/Å	12.80407(16)	30.0078(6)	18.8268(2)	21.5324(9)	13.3198(2)	17.8748(4)
α/°	90	90	90	90	90	90
β/°	91.4753(11)	93.2810(17)	94.1686(12)	90	105.633(1)	90
γ/°	90	90	90	90	90	120
Volume/Å^3	3899.10(8)	5237.92(16)	3707.42(8)	2688.1(2)	4912.46(15)	1473.89(7)
Z	4	4	4	4	8	3
ρ_{calc} g/cm^3	1.101	1.099	1.130	1.135	1.128	1.552
μ/mm^{-1}	0.641	0.617	0.691	0.076	0.077	0.825
F(000)	1408.0	1888.0	1372.0	1000.0	1808.0	750.0
Crystal size/mm^3	0.133×0.091×0.076	0.178×0.046×0.046	0.235×0.119×0.053	0.505×0.133×0.116	0.5×0.4×0.3	0.393×0.129×0.087
2Θ range for data collection/°	6.728 to 139.614	5.496 to 139.68	7.656 to 139.576	6.552 to 54.964	7.346 to 54.798	10.468 to 147.178
Reflections collected	23319	31806	22162	22144	59286	11789
Independent reflections	7278 [R_{int}= 0.0259]	9773 [R_{int} = 0.0362]	6916 [R_{int}= 0.0297]	6057 [R_{int} = 0.0521]	10990[R_{int}= 0.0910]	3061 [R_{int}= 0.0334]
Data/restraints/parameters	7278/0/438	9773/98/703	6916/79/469	6057/154/426	10990/0/564	3061/1/225
Goodness–of–fit on F^2	1.017	1.017	1.024	1.049	1.011	1.049
Final R indexes [I>=2σ (I)]	R_1 = 0.0367, wR_2 = 0.0894	R_1 = 0.0472, wR_2 = 0.1163	R_1 = 0.0482, wR_2 = 0.1230	R_1 = 0.0529, wR_2 = 0.0897	R_1= 0.0498, wR_2= 0.1237	R_1 = 0.0413, wR_2 = 0.1037
Final R indexes [all data]	R_1 = 0.0473, wR_2 = 0.0952	R_1 = 0.0623, wR_2 = 0.1262	R_1 = 0.0607, wR_2 = 0.1306	R_1 = 0.0879, wR_2 = 0.1010	R_1= 0.0775, wR_2= 0.1390	R_1 = 0.0433, wR_2 = 0.1053
Largest diff. peak/hole / e Å^{-3}	0.26/–0.24	0.56/–0.48	0.44/–0.35	0.17/–0.15	0.33/–0.23	0.29/–0.16

5.2.4 Computational details

Geometry optimizations were performed using Gaussian09 suite of programs[7] using the Becke's 3–parameter hybrid functional,[8] combined with the non–local correlation functional provided by Perdew/Wang.[9] The 6–311+G(d) all–electron basis set was used for the magnesium and calcium atoms and the 6–31G(d,p) for the remaining atoms.[10] All stationary points have been identified for minimum (Nimag=0) or transition states (Nimag=1). Intrinsic Reaction Paths (IRPs)[11] were traced from the various transition structures to obtain the connected intermediates.

Cartesian coordinates of all optimized structures are available in the electronic supplementary.

5.3 Chapter Three Experimental Data

5.3.1 Synthetic Procedures

Synthesis of [(HC{(Me)CN(2,6–^{i}PrC$_6$H$_3$)}$_2$Mg)$_2$(OHC=CHO)], 3.1

A solution of compound **Ih** (70 mg, 0.15 mmol) in 0.5 ml toluene was freeze–thaw degassed and exposed to ~1 atm. of CO. The reaction flask was resealed and left at room temperature for two hours before the solution was interrogated by NMR spectroscopic analysis, which revealed stoichiometric conversion to compound **3.1**. The solvent was then removed *in vacuo* and the resultant pale yellow solid was redissolved in *n*–pentane. Storage of this solution at –30ºC for two days afforded crystals of compound **3.1** suitable for single crystal X–ray diffraction analysis. NMR Yield: 100% (Isolated Yield: 86%, 60 mg). ^{1}H NMR (d$_8$–Tol): δ 7.05 – 7.02 (6H, m, Ar–*H*), 5.53 (1H, s, O(*H*C=C*H*)O), 4.79 (1H, s, C–*H*), 3.14 (4H, m., $^{3}J_{HH}$ = 6.85 Hz, C*H*(CH$_3$)$_2$), 1.56 (6H, s, NC(C*H*$_3$)CH), 1.17 (12H d, $^{3}J_{HH}$ = 6.85 Hz, CH(C*H*$_3$)$_2$), 1.02 (12H d, $^{3}J_{HH}$ = 6.85 Hz, CH(C*H*$_3$)$_2$). ^{13}C{^{1}H} NMR (d$_8$–Tol, 125.76 MHz): δ 170.0 (N*C*(CH$_3$)CH), 144.6 (*ipso*–Ar), 142.5 (*o*–Ar), 131.9 (O(H*C*=*C*H)O), 125.8 (*p*–Ar), 123.8 (*m*–Ar), 95.5 (NC(CH$_3$)*C*H), 28.6 (N*C*H(CH$_3$)$_2$), 24.7, 24.2(CH(*C*H$_3$)$_2$). Anal. Calcd. for C$_{60}$H$_{84}$Mg$_2$N$_4$O$_2$.2H$_2$O: C, 73.74; H, 9.05; N, 5.72%. Found: C, 73.88; H, 9.14; N, 7.71%. The sample was highly hydroscopic and sequestered two water molecules on exposure to atmosphere.

Synthesis of [(HC{(Me)CN(2,6–^{i}PrC$_6$H$_3$)}$_2$Ca)$_2$(OHC=CHO)], 3.2

A solution of compound **Ii** (50 mg, 0.09 mmol) in 0.5 ml toluene was freeze–thaw degassed and exposed to ~1 atm. of CO. The reaction flask was resealed and left at room temperature for 1 hour before the solution was interrogated by NMR spectroscopic analysis,

which revealed stoichiometric conversion to compound **3.2**. Storage of this solution at RT for two days afforded crystals of compound **3.2** suitable for single crystal X–ray diffraction analysis. NMR Yield: 100% (Isolated Yield: 92%, 64 mg). ^{1}H NMR (d_8–Tol): δ 7.06 – 6.97 (6H, m, Ar–*H*), 5.00 (1H, s, O(*H*C=C*H*)O), 4.65 (1H, s, C–*H*), 3.38 (THF), 3.08 (4H, m., $^{3}J_{HH}$ = 6.40 Hz, C*H*(CH_3)$_2$), 1.63 (6H, s, NC(C*H*$_3$)CH), 1.40 (THF), 1.19 (12H d, $^{3}J_{HH}$ = 6.40 Hz, CH(C*H*$_3$)$_2$). ^{13}C{^{1}H} NMR (d_8–Tol, 125.76 MHz): δ 165.3 (N*C*(CH_3)CH), 148.0 (*ipso*–Ar), 142.3 (*o*–Ar), 131.9 (O(H*C*=*C*H)O), 124.1 (*p*–Ar), 123.5 (*m*–Ar), 93.6 (NC(CH_3)*C*H), 69.1 (THF), 28.7, 26.0 (N*C*H(CH_3)$_2$), 25.4 (THF), 25.1, 24.9 (CH(*C*H$_3$)$_2$). Anal. Calcd. for $C_{68}H_{100}Ca_2N_4O_4$: C, 73.07; H, 9.02; N, 5.01%. Found: C, 74.23; H, 9.10; N, 4.89%.

Synthesis of [(HC{(ᵗBu)CN(2,6–^{i}PrC$_6$H$_3$)}$_2$Mg)$_2$(OHC=CHO)], 3.7

A solution of compound **XXVII** (70 mg, 0.15 mmol) in 0.5 ml toluene was freeze–thaw degassed and exposed to ~1 atm. of CO. The reaction flask was resealed and left at room temperature for two hours before the solution was interrogated by NMR spectroscopic analysis, which revealed stoichiometric conversion to compound **3.7**. The solvent was then removed *in vacuo* and the resultant pale yellow solid was redissolved in *n*–pentane. Storage of this solution at −30ºC for two days afforded crystals of compound **3.7** suitable for single crystal X–ray diffraction analysis. NMR Yield: 100% (Isolated Yield: 72%, 50 mg). ^{1}H NMR (d_8–Tol): δ 7.05 – 7.02 (6H, br. m, Ar–*H*), 5.39 (1H, s, C–*H*), 5.16 (1H, s, O(*H*C=C*H*)O), 3.63, 3.34, 3.23, 2.87 (4H, br. m., C*H*(CH_3)$_2$), 1.31 (24H, br. m, CH(C*H*$_3$)$_2$), 1.16 (18H, br. m, NC(C(C*H*$_3$)$_3$)CH). ^{13}C{^{1}H} NMR (d_8–Tol, 125.76 MHz): δ 171.6, 169.0 (N*C*(CH_3)CH), 148.1, 142.9, (*C*–Ar), 130.8 (O(H*C*=*C*H)O), 124.2, 123.9, 123.4 (*C*–Ar), 97.2 (NC(C(CH_3)$_3$)*C*H), 44.8 (NC(*C*(CH_3)$_3$)CH), 33.7 (NC(C(*C*H$_3$)$_3$)CH), 28.8 (br. s, *C*H(CH_3)$_2$), 24.9 (br. s, CH(*C*H$_3$)$_2$). Anal. Calcd. for $C_{72}H_{108}Mg_2N_4O_2$: Accurate elemental analysis could not be recorded.

5.3.2 Catalytic reduction of CO (representative procedure)

In a glovebox, to a vial containing compound **Ih** or **Ii**, (0.02 mmol, 10 mg), was added toluene–d_8 (0.5 mL) followed by $PhSiH_3$ (0.2 mmol, 27.8µl). The resultant solution was transferred to a NMR tube equipped with a J. Young's tap which was sealed and removed from the glovebox. The solution was then freeze pumped thaw degassed to remove argon, exposed to 1 atmosphere of CO, resealed and warmed to 60ºC. NMR analysis was performed at regular intervals and conversions were analysed by ratios of starting material to product, with products identified by comparison to literature values.

5.3.2 Single Crystal X–ray Diffraction analysis:

Single Crystal X–ray diffraction data for compound **3.1–3.4** were collected on a SuperNova, Dual Cu at zero, EosS2 diffractometer. The crystal was kept at 150(2) K during data collection. Using Olex2,[4] the structures were solved via SHELXS[6] and refined with the ShelXL refinement package using Least Squares minimisation. The asymmetric unit of **3.2** comprises one molecule of the calcium dimer, and one molecule of hexane. The latter is disordered over 2 proximate sites in a 55:45 ratio. C–C distances were restrained to being similar in the disordered solvent region and isotropic ADP restraints were included for some of the partial occupancy carbons therein, to assist convergence. The asymmetric unit of **3.7** comprises 2 molecules. The structural model includes 75:25 disorder modelling for C59, C60, C128 and C129 with (respectively) C58A, C60A, C1A and C1B. Some distance and ADP restraints were included in the disordered region, to assist convergence. The asymmetric unit of **3.10** contains half of one molecule, the remainder being generated *via* an inversion centre proximate to the alkaline earth contender. H1 was located but ultimately included at a calculated position 1.3 Å from Si1. The phenyl ring based on C37 was refined subject to being disordered over 2 proximate sites in a 55:45 ratio. The minor ring component was treated as a rigid hexagon and the ADPs of all fractional occupancy carbons were restrained, to assist convergence. A solvent mask (Olex–2) was included to treat a region of disordered guest solvent in the lattice. An allowance for half of a molecule of hexane per asymmetric unit has been made in the formula as presented here.

Table 5.2: Single Crystal X–ray Data Parameters for compounds **3.1**, **3.2**, **3.7** and **3.10**.

Compound	**3.1**	**3.2**	**3.7**	**3.10**
Empirical formula	$C_{60}H_{84}Mg_2N_4O_2$	$C_{74}H_{114}Ca_2N_4O_4$	$C_{72}H_{108}Mg_2N_4O_2$	$C_{45}H_{61}CaN_2OSi$
Formula weight	941.93	1203.85	1110.24	714.12
Temperature/K	150(2)	149.99(10)	292.06(10)	150.01(10)
Crystal system	monoclinic	monoclinic	monoclinic	monoclinic
Space group	$P2_1/n$	I2/a	$P2_1/c$	$P2_1/n$
a/Å	13.3888(2)	22.1065(3)	15.31492(11)	13.7508(2)
b/Å	29.4751(4)	12.64458(13)	22.59972(18)	15.0080(2)
c/Å	14.56423(18)	53.0432(8)	39.3251(4)	21.5613(3)
α/°	90	90	90	90
β/°	93.8392(12)	101.9948(14)	95.2592(8)	90
γ/°	90	90	90	90
Volume/Å^3	5734.67(13)	14503.3(3)	13553.64(19)	4449.65(11)
Z	4	8	8	4
ρ_{calc} g/cm^3	1.091	1.103	1.088	1.066
μ/mm^{-1}	0.695	1.723	0.653	1.708
F(000)	2048.0	5264.0	4864.0	1548.0
Crystal size/mm^3	0.1531×0.1115×0.0816	0.2050×0.1185×0.0478	0.192×0.167×0.156	0.306 × 0.175 × 0.063
2Θ range for data collection/°	8.546 to 139.702	8.178 to 143.898	5.796 to 139.666	7.176 to 147.068
Reflections collected	22315	54447	87144	63736
Independent reflections	10569 [R_{int} = 0.0423]	14051 [R_{int} = 0.0359]	25355 [R_{int} = 0.0222]	8938 [R_{int} = 0.0420, R_{sigma} = 0.0214]
Data/restraints/parameters	10569/0/635	14051/93/835	25355/36/1537	8938/186/464
Goodness–of–fit on F^2	1.018	1.038	1.024	1.067
Final R indexes [I>=2σ (I)]	R_1 = 0.0482, wR_2 = 0.1136	R_1 = 0.0562, wR_2 = 0.1427	R_1 = 0.0394, wR_2 = 0.0985	R_1 = 0.0572, wR_2 = 0.1734
Final R indexes [all data]	R_1 = 0.0691, wR_2 = 0.1249	R_1 = 0.0679, wR_2 = 0.1495	R_1 = 0.0454, wR_2 = 0.1020	R_1 = 0.0641, wR_2 = 0.1804
Largest diff. peak/hole / e Å^{-3}	0.42/–0.28	0.48/–0.43	0.51/–0.33	0.86/–0.85

5.4 Chapter Four Experimental Data

5.4.1 Synthetic Procedures

Synthesis of [HC{(Me)CN(2,6–^{i}PrC$_6$H$_3$)}$_2$CaNH$_2$(Dioxane)]$_2$, 4.1

To a stirred solution of **Ii** (500 mg, 0.94 mmol) in toluene was added 0.5 M solution of ammonia in dioxane (1.88 ml) and allowed to stir overnight. The solvent was then removed *in vacuo* to yield an off white powder (81%, 430 mg). A saturated toluene solution of **4.1** stored at –35°C overnight yielded large colourless needles suitable for an X–ray diffraction experiment. ^{1}H NMR (d$_8$–Tol, 300 MHz): δ 7.00 (6H, s, Ar–*H*), 4.72 (1H, s, C–*H*), 3.35 (Dioxane), 3.15 (4H, m., $^{3}J_{HH}$ = 6.78 Hz, C*H*(CH$_3$)$_2$), 1.63 (6H, s, NC(C*H*$_3$)CH), 1.13 (12H d, $^{3}J_{HH}$ = 6.78 Hz, CH(C*H*$_3$)$_2$), 1.03 (12H d, $^{3}J_{HH}$ = 6.78 Hz, CH(C*H*$_3$)$_2$) –1.54 (2H, br. s, NH$_2$). ^{13}C{^{1}H} NMR (d$_8$–Tol, 125.76 MHz): δ 165.3 (N*C*(CH$_3$)CH), 147.8, 142.2, 124.6, 124.2 (*C*–Ar), 94.3 (NC(CH$_3$)*C*H), 67.5 (dioxane) 28.6 (*C*H(CH$_3$)$_2$), 25.3, 24.7 (CH(*C*H$_3$)$_2$). Anal. Calcd. for C$_{68}$H$_{106}$Ca$_2$N$_6$O$_4$: C, 72.58; H, 9.41; N, 7.69% Found: C, 72.45; H, 9.85; N, 7.40%

Synthesis of [(HC{(Me)CN(2,6–^{i}PrC$_6$H$_3$)}$_2$Ca(OC(H)NH)]$_2$, 4.2

A solution of compound **4.1** (70 mg, 0.15 mmol) in 0.5 ml toluene was freeze–thaw degassed and exposed to 1 atmosphere of CO. The reaction flask was resealed and left at room temperature for two hours before the solution was interrogated by NMR spectroscopic analysis, which revealed stoichiometric conversion to compound **4.2**. The solvent was then removed *in vacuo* and the resultant pale yellow solid was re–dissolved in *n*–hexane. Storage of this solution at −30ºC for two days afforded crystals of compound **4.2** suitable for single crystal X–ray diffraction analysis. NMR Yield: 80% (Isolated Yield: 69%, 48 mg). ^{1}H NMR (d$_8$–Tol, 500 MHz): δ 7.01 (6H, 3, Ar–*H*), 6.61 (1H, dd, $^{1}J_{HC}$ = 183.1, $^{3}J_{HH}$ = 6.1 Hz, ^{13}C*H*) 4.65 (1H, s, C–*H*), 3.44 (THF), 3.15 (4H, bsept., $^{3}J_{HH}$ = 6.65 Hz, C*H*(CH$_3$)$_2$), 1.63 (6H, s, NC(C*H*$_3$)CH), 1.43 (THF), 1.19 (12H bd, CH(C*H*$_3$)$_2$), 1.02 (12H bd, CH(C*H*$_3$)$_2$) –1.93 (1H, br. s, NH$_2$). ^{13}C{^{1}H} NMR (d$_8$–Tol, 125.76 MHz): 174.3 N*C*(H)O, 165.1 (N*C*(CH$_3$)CH), 148.2, 143.1, 142.3, 142.0, 120.2, 124.3, 124.0 (*C*–Ar), 94.0 (NC(CH$_3$)*C*H), 68.8, 67.53 (Dioxane), 29.0, 28.46 (*C*H(CH$_3$)$_2$), 26.0, 25.6, 25.0, 24.8, 23.8 (CH(*C*H$_3$)$_2$). Anal. Calcd. for C$_{60}$H$_{86}$Ca$_2$N$_6$O$_2$: C, 71.81; H, 8.64; N, 8.37%. Found: C, 73.88; H, 9.14; N, 7.71%.

General procedure for the synthesis of [HC{(Me)CN(2,6–^{i}PrC$_6$H$_3$)}$_2$M(OC(H)NR)]$_2$. (M = Mg or Ca. R = aryl or alkyl)

A solution of compound **Ih** or **Ii** (30 mg, 0.067 or 0.056 mmol) in 0.5 ml toluene with two equivalents of a secondary amine were mixed in a J. Young tube and left for one hour. The solution was then interrogated by NMR to ensure complete conversion to the corresponding amide. The solution was then freeze–thaw degassed and exposed to ~1 atm. of CO and the reaction followed by NMR till complete conversion the formamidate product.

Synthesis of [HC{(Me)CN(2,6–^{i}PrC$_6$H$_3$)}$_2$Mg(OCH=NBu)]$_3$, 4.3

Reaction reached full conversion within 24 hours at 60ºC temperature, direct Cooling of this solution to RT afforded crystals of compound **4.3** suitable for single crystal X–ray diffraction analysis. NMR Yield: 99% (Isolated Yield: 94%, 28 mg). ^{1}H NMR (d$_8$–Tol, 300 MHz): δ 7.87, (0.25H, d, $^{1}J_{CH}$ = 177.4 Hz, NC(*H*)O), (0.75H, d, $^{1}J_{CH}$ = 182.9 Hz, NC(*H*)O), 7.35 (1H, d, $^{1}J_{CH}$ = 177.4 Hz, NC(*H*)O), 7.15 – 7.02 (5H, br. m, Ar–*H*), 6.98 (1H, br. m, Ar–*H*), 4.82, 4.70 (1H, s, C–*H*), 3.38 (1H, br. sept., C*H*(CH$_3$)$_2$), 3.10 (3H, br. sept., C*H*(CH$_3$)$_2$), 1.60 (6H, s, NC(C*H*$_3$)CH), 1.52 (3H, br. m, CH(C*H*$_3$)$_2$), 1.24–1.13 (21H, br. m, CH(C*H*$_3$)$_2$), 1.02 (3H, t, $^{3}J_{HH}$ = 7.16 Hz, CH$_2$C*H*$_3$), CH$_2$C*H*$_3$). 0.87 (2H, br. m, CH$_2$C*H*$_3$), 0.42–0.28 (4H, br. m, NC*H*$_2$C*H*$_2$). ^{13}C{^{1}H} NMR (d$_8$–tol, 125.76 MHz): δ 171.9, 1.65.0 (N*C*(H)O), due to the poor solubility of **4.3**, no other meaning full ^{13}C{^{1}H} NMR data could be attained. Anal. Calcd. for C$_{102}$H$_{153}$Mg$_3$N$_9$O$_3$: C, 75.33; H, 9.48; N, 7.75%. Found: C, 74.36; H, 9.12; N, 5.31%.

Synthesis of [HC{(Me)CN(2,6–^{i}PrC$_6$H$_3$)}$_2$Ca(OCH=NBu)]$_2$, 4.4

Reaction reached full conversion within an hour at room temperature. Storage of this solution at RT for two days afforded crystals of compound **4.4** suitable for single crystal X–ray diffraction analysis. NMR Yield: 99% (Isolated Yield: 76%, 23 mg). ^{1}H NMR (d$_8$–THF, 300 MHz): δ 7.09 (6H, br. m, Ar–*H*), 5.92 (1H, d, $^{1}J_{HC}$ = 179.48 Hz, NC(*H*)O), 4.91 (1H, s, C–*H*), 3.15 (4H, sept., $^{3}J_{HH}$ = 6.92 Hz C*H*(CH$_3$)$_2$), 1.69 (6H, s, NC(C*H*$_3$)CH), 1.55 (3H, br. m, CH(C*H*$_3$)$_2$), 1.20 (12H, d, $^{3}J_{HH}$ = 7.16 Hz, CH(C*H*$_3$)$_2$), 1.20 (12H, d, $^{3}J_{HH}$ = 7.16 Hz, CH(C*H*$_3$)$_2$), 0.85 (2H, NC*H*$_2$CH$_2$), CH$_2$C*H*$_3$).^{13}C{^{1}H} NMR (d$_8$–THF, 125.76 MHz): δ 170.9 (N*C*(H)O), due to the poor solubility of **4.3**, no other meaning full ^{13}C{^{1}H} NMR data could be attained. Anal. Calcd. For C$_{76}$H$_{118}$Ca$_2$N$_6$O$_4$: C, 72.45; H, 9.44; N, 6.67%. Found: C, 70.68; H, 9.06; N, 7.35%.

Synthesis of [(HC{(Me)CN(2,6–^{i}PrC$_6$H$_3$)}$_2$MgOC(H)N^{i}Pr)]$_2$, 4.5

Reaction reached full conversion within 48h at 60°C using ^{12}CO. Storage of this solution at RT for two days afforded crystals of compound **4.4** suitable for single crystal X–ray diffraction analysis. NMR Yield: 99% (Isolated Yield: 68%, 20 mg). ^{1}H NMR (d$_8$–Tol, 300 MHz): δ 7.94 (1H, s, NC(*H*)O), 7.07 (6H, br. m, Ar–*H*), 4.73 (1H, s, C–*H*), 3.56 (2H, sept., $^{3}J_{HH}$ = 6.82 Hz C*H*(CH$_3$)$_2$), 3.35 (1H, sept., $^{3}J_{HH}$ = 6.78 Hz C*H*(CH$_3$)$_2$), 3.04 (2H, sept., $^{3}J_{HH}$ = 6.82 Hz C*H*(CH$_3$)$_2$), 1.48 (6H, s, NC(C*H*$_3$)CH), 1.16 (12H, d, $^{3}J_{HH}$ = 6.82 Hz, CH(C*H*$_3$)$_2$), 1.13 (12H, d, $^{3}J_{HH}$ = 6.82 Hz, CH(C*H*$_3$)$_2$), 0.23 (2H, d., $^{3}J_{HH}$ = 6.78 Hz C*H*(CH$_3$)$_2$). ^{13}C{^{1}H} NMR (d$_8$–tol, 125.76 MHz): δ 177.8 (N*C*(H)O), 168.8 (N*C*(CH$_3$)CH), 147.2, 143.4, 142.6, 124.5, 123.9, 123.7, 115.4 (*C*–Ar), 95.7 (NC(CH$_3$)*C*H), 48.6 (N*C*(CH$_3$)$_2$H), 32.5, 28.9, 25.4, 25.2 (*C*H(CH$_3$)$_2$), 24.9, 24.3, 23.5, 14.8 (CH(*C*H$_3$)$_2$). Anal. Calcd. for C$_{66}$H$_{98}$Mg$_2$N$_6$O$_2$: C, 75.06; H, 9.35; N, 7.96%. Found: C, 75.21; H, 9.71; N, 7.58%.

Synthesis of [(HC{(Me)CN(2,6–^{i}PrC$_6$H$_3$)}$_2$MgOC(H)NCH$_2$CH$_2$C$_6$H$_5$)]$_2$, 4.6

The reaction flask was resealed and left at 100°C for 72h, inspection of the reaction flask after 12h revealed the formation of X–ray quality crystals. **4.6**, is extremely insoluble and NMR characterisation was carried out in a saturated THF solution. NMR Yield: 99% (Isolated Yield: 52%, 15 mg). ^{1}H NMR (d$_8$–THF, 300 MHz): δ 7.84 (1H, d, $^{1}J_{HC}$ = 176.07 Hz NC(*H*)O), 7.81 (1H, d, $^{1}J_{HC}$ = 180.48 Hz NC(*H*)O), 7.24 – 7.21 (5H, br. m, Ar–*H*), 7.07 – 7.04 (12H, br. m, Ar–*H*), 6.98 – 6.95 (3H, br. m, Ar–*H*), 6.91 – 6.88 (4H, br. m, Ar–*H*) 4.92, 4.86 (1H, s, C–*H*), 3.24, 3.15 (4H, sept, $^{3}J_{HH}$ = 6.85 Hz, C*H*(CH$_3$)$_2$), 2.80, 2.66, (2H, bt, $^{3}J_{HH}$ = 7.34 Hz, NC*H*$_2$CH$_2$), 2.49, 1.92 (2H, bt, $^{3}J_{HH}$ = 7.34 Hz, NCH$_2$C*H*$_2$), 1.81, 1.65 (6H, s, NC(C*H*$_3$)CH), 1.26 (6H, d, $^{3}J_{HH}$ = 6.85 Hz, CH(C*H*$_3$)$_2$), 1.22 – 1.19 (24H, br. m, CH(C*H*$_3$)$_2$), 1.07 (6H, d, $^{3}J_{HH}$ = 6.85 Hz, CH(C*H*$_3$)$_2$), 1.02 (6H, d, $^{3}J_{HH}$ = 6.85 Hz, CH(C*H*$_3$)$_2$), 0.17 (6H, d, $^{3}J_{HH}$ = 6.85 Hz, CH(C*H*$_3$)$_2$). ^{13}C{^{1}H} NMR (d$_8$–tol, 125.76 MHz): δ 174.2 (N*C*(H)O), 172.52 (N*C*(CH$_3$)CH), 169.1 (N*C*(H)O), 143.2, 129.6, 129.4, 127.0, 126.2, 125.7, 124.7, 124.2, 113.9, 123.7 (*C*–Ar), 95.2 (NC(CH$_3$)*C*H), 29.2, 29.1 (N*C*H$_2$CH$_2$), 28.9, 28.8, (NCH$_2$*C*H$_2$), 24.9 (*C*H(CH$_3$)$_2$), 24.6, 24.2 (CH(*C*H$_3$)$_2$), 24.1 (*C*H(CH$_3$)$_2$), 23.6, 23.4 (CH(*C*H$_3$)$_2$). Anal. Calcd. for C$_{76}$H$_{102}$Mg$_2$N$_6$O$_2$: Accurate elemental analysis could not be recorded.

Synthesis of [(HC{(Me)CN(2,6–^{i}PrC$_6$H$_3$)}$_2$MgOC(H)N(2,6–^{i}PrC$_6$H$_3$)]$_2$, 4.7/2.1

The reaction flask was resealed and left at room temperature for one hour before the solution was interrogated by NMR spectroscopic analysis, which revealed stoichiometric conversion to compound **4.7/2.1**. All spectroscopic data was concordant with the aforementioned **2.1**

Synthesis of [HC{(Me)CN(2,6–^{i}PrC$_6$H$_3$)}$_2$Ca(OCH=N^{t}Bu)]$_2$, 4.8

The reaction flask was resealed and left at room temperature for one hour before the solution was interrogated by NMR spectroscopic analysis, which revealed stoichiometric conversion to compound **4.8**. NMR Yield: 99% (Isolated Yield: 91%, 27 mg). ^{1}H NMR (d$_8$–Tol, 500 MHz): δ 8.06 (1H, d, $^{1}J_{CH}$ = 179.34 Hz, NC(*H*)O), 7.13 – 7.04 (10H, m, Ar–*H*), 4.72 (1H, s, C–*H*), 3.39, 3.03 (1H, sept., $^{3}J_{HH}$ = 6.78 Hz, C*H*(CH$_3$)$_2$), 2.95 (2H, sept., $^{3}J_{HH}$ = 6.78 Hz, C*H*(CH$_3$)$_2$), 1.58, 1.55 (3H, s, NC(C*H*$_3$)CH), 1.30 (3H d, $^{3}J_{HH}$ = 6.78 Hz, CH(C*H*$_3$)$_2$), 1.21, 1.19 (18H br. d, CH(C*H*$_3$)$_2$), 1.13 (9H, s, C(C*H*$_3$)$_3$), 0.42 (3H d, $^{3}J_{HH}$ = 6.78 Hz, CH(C*H*$_3$)$_2$). ^{13}C{^{1}H} NMR (d$_8$–Tol, 125.76 MHz): δ 167.3 O*C*(H)N, 165.7 (N*C*(CH$_3$)CH), 136.7, 129.6, 128.6, 125.8, 124.6, 124.4, 123.9, 123.7 (*C*–Ar), 93.2 (NC(CH$_3$)*C*H), 53.4 (N*C*(CH$_3$)$_3$), 32.4, 32.1, 32.0, 29.0 (N*C*H(CH$_3$)$_2$), 28.8 (CH(*C*H$_3$)$_2$), 27.7, 25.9, 25.1, 24.9, 24.7, 24.4 (NC(*C*H$_3$)CH), 24.1 (NC(*C*H$_3$)$_3$), 23.8 (NC(*C*H$_3$)CH), 23.5 (CH(*C*H$_3$)$_2$). Anal. Calcd. for C$_{76}$H$_{118}$Ca$_2$N$_6$O$_4$: C, 72.45; H, 9.44; N, 6.67%. Found: C, 71.93; H, 8.94; N, 4.55%.

Synthesis of [HC{(Me)CN(2,6–^{i}PrC$_6$H$_3$)}$_2$Ca(OCH=NCH$_2$CH$_2$C$_6$H$_5$)]$_2$, 4.9

The reaction flask was resealed and left at room temperature for one hour before the solution was interrogated by NMR spectroscopic analysis, which revealed stoichiometric conversion to compound **4.9**. NMR Yield: 99% (Isolated Yield: 84%, 25 mg). ^{1}H NMR (d$_8$–Tol, 500 MHz): δ 7.45 (1H, d, $^{1}J_{CH}$ = 180.09 Hz, NC(*H*)O), 7.13 – 7.05 (10H, m, Ar–*H*), 4.74 (1H, s, C–*H*), 3.16 (3H, br. m., C*H*(CH$_3$)$_2$), 2.95 (1H, sept., $^{3}J_{HH}$ = 6.76 Hz, C*H*(CH$_3$)$_2$), 2.85 (qt., $^{3}J_{HH}$/$^{3}J_{CH}$ = 7.16 Hz, CH$_2$C*H*$_2$N), 1.63 (5H, s, NC(C*H*$_3$)CH), 1.55 (1H, s, NC(C*H*$_3$)CH), 1.21, 1.20 (12H d, $^{3}J_{HH}$ = 6.76 Hz, CH(C*H*$_3$)$_2$), 0.91 (3H, t., $^{3}J_{HH}$ = 7.16 Hz, C*H*$_2$CH$_3$). ^{13}C{^{1}H} NMR (d$_8$–Tol, 125.76 MHz): δ 168.8 O*C*(H)N, 165.9 (N*C*(CH$_3$)CH), 146.5, 142.1, 136.7, 124.7, 124.2, 123.7 (*C*–Ar), 93.7 (NC(CH$_3$)*C*H), 50.2 (NCH$_2$*C*H$_2$Ar), 35.0 (N*C*H$_2$CH$_2$Ar), 29.0, 28.7 (N*C*H(CH$_3$)$_2$), 25.5, 24.8, 24.6, 24.1, 23.5 (CH(*C*H$_3$)$_2$). Anal. Calcd. for C$_{84}$H$_{118}$Ca$_2$N$_6$O$_4$: Accurate elemental analysis could not be recorded.

Synthesis of [HC{(Me)CN(2,6–^{i}PrC$_6$H$_3$)}$_2$Ca(OCH=NDipp)]$_2$, 4.10

The reaction flask was resealed and left at room temperature for one hour before the solution was interrogated by NMR spectroscopic analysis, which revealed stoichiometric conversion to compound **4.10**. NMR Yield: 71% (Isolated Yield: 56%, 17 mg).) ^{1}H NMR (d$_8$–Tol, 500 MHz): δ 7.41 (1H, d, $^{1}J_{CH}$ = 183.41 Hz, NC(*H*)O), 7.17 – 6.77 (9H, m, Ar–*H*), 4.95 (1H, s, C–*H*), 3.54 THF, 3.44 (1H, sept., $^{3}J_{HH}$ = 6.85 Hz, C*H*(CH$_3$)$_2$), 3.11 (1H, sept., $^{3}J_{HH}$ = 6.85 Hz, C*H*(CH$_3$)$_2$), 2.98 (1H, sept., $^{3}J_{HH}$ = 6.85 Hz, C*H*(CH$_3$)$_2$), 2.58 (1H, sept., $^{3}J_{HH}$ = 6.85 Hz, C*H*(CH$_3$)$_2$), 1.83, 1.71, 1.57 (2H, s, NC(C*H*$_3$)CH), 1.51 (3H d, $^{3}J_{HH}$ = 6.85 Hz, CH(C*H*$_3$)$_2$),

1.73 (4H d, $^{3}J_{HH}$ = 6.85 Hz, CH(CH_3)$_2$), 1.28 (3H d, $^{3}J_{HH}$ = 6.85 Hz, CH(CH_3)$_2$), 1.23 (7H d, $^{3}J_{HH}$ = 6.85 Hz, CH(CH_3)$_2$), 1.19 (11H d, $^{3}J_{HH}$ = 6.85 Hz, CH(CH_3)$_2$), 1.00, 0.97 (2H d, $^{3}J_{HH}$ = 6.85 Hz, CH(CH_3)$_2$), 0.47, 0.43 (2H d, $^{3}J_{HH}$ = 6.85 Hz, CH(CH_3)$_2$). ^{13}C{^{1}H} NMR (d$_8$–Tol, 125.76 MHz): δ 174.2 (N*C*(CH$_3$)CH), 171.2 O*C*(H)N, 151.1, 149.3, 145.7, 144.5, 143.6, 142.5, 142.1, 141.9, 141.4, 140.8, 124.7, 124.4, 124.3, 124.1, 123.6, 123.2 (*C*–Ar), 94.9 (NC(CH$_3$)*C*H), 68.8 THF, 32.4, 28.7, 28.4, 28.1, 27.8, 27.1, 26.2, 26.1 (N*C*H(CH$_3$)$_2$), 25.9, 25.6 (CH(*C*H$_3$)$_2$), 25.4 THF, 24.9, 24.70, 24.06, 23.5, 22.9 (CH(*C*H$_3$)$_2$). Anal. Calcd. for $C_{76}H_{111}Ca_2N_5O_5$: Accurate elemental analysis could not be recorded.

Synthesis of [HC{(Me)CN(2,6–^{i}PrC$_6$H$_3$)}$_2$MgOHCN(Me)C$_6$H$_5$)]$_2$, 4.12

One atm. Of ^{13}CO was added to a J Young's tube containing a degassed solution of compound Ih (0.067 mmol) and *N*–methyl aniline (0.067 mmol) in toluene. The reaction was left at room temperature and probed by NMR spectroscopy after initiation of the reaction. Incipient crystallisation directly from the J Young's tube afforded 4.12 as X–ray quality crystals. NMR yield 68% (Isolated Yield: 8 mg). ^{1}H NMR (d$_8$–Tol): δ 7.21–7.18 (3H, m, Ar–*H*), 7.14–7.13 (2H, m, Ar–*H*), 7.00–6.94 (2H, t, $^{3}J_{HH}$ = 7.16 Hz Ar–*H*), 6.60–6.55 (1H, t, $^{3}J_{HH}$ = 7.16 Hz Ar–*H*), 5.95–5.92 (2H, d, $^{3}J_{HH}$ = 7.16 Hz Ar–*H*), 4.99 (1H, s, C–*H*), 3.15 (4H, spt., $^{3}J_{HH}$ = 6.78 Hz, C*H*(CH$_3$)$_2$), 2.18 (3H, s, NCH_3) 1.69 (6H, s, NC(CH_3)CH), 1.20, 1.75 (24H d, $^{3}J_{HH}$ = 6.78 Hz, CH(CH_3)$_2$). ^{13}C{^{1}H} NMR (d$_8$–Tol, 125.76 MHz): δ 235.7 (O*C*N(CH$_3$)Ph).

Synthesis of [H$_3$^{13}CN(Bpin)$_2$], 4.15

Addition of 4,4,5,5,–tetramethyl–1,3,2–dioxaborolane (0.402 mmol) to a J Young's tube containing a solution of compound **4.2** (0.067 mmol) in toluene. The reaction was left at room temperature and probed by NMR spectroscopy after initiation of the reaction. ^{1}H NMR (d$_8$–THF, 500 MHz): δ 2.98 (3H, d, $^{1}J_{HC}$ = 136.5 Hz N^{13}CH_3), 2.18, 2.08, (12H, s, OC(CH$_3$)$_2$). ^{13}C{^{1}H} NMR (d$_8$–THF, 125.76 MHz): δ 79.0 (O*C*(CH$_3$)$_2$), 34.4 (N*C*H$_3$), 28.7 (OC(*C*H$_3$)$_2$). ^{11}B NMR (d$_8$–THF, 125.76 MHz): δ 27.3.

Synthesis of [(HC{(Me)CN(2,6–^{i}PrC$_6$H$_3$)}$_2$CaOBpin)], 4.16

Addition of 4,4,5,5,–tetramethyl–1,3,2–dioxaborolane (0.402 mmol) to a J Young's tube containing a solution of compound **4.2** (0.067 mmol) in toluene. The reaction was left at room temperature and probed by NMR spectroscopy after initiation of the reaction ^{1}H NMR (d$_8$–Tol, 500 MHz): δ 7.19 – 7.05 (6H, m, Ar–*H*), 4.84 (1H, s, C–*H*), 3.31 (4H, sept., $^{3}J_{HH}$ = 6.85 Hz, C*H*(CH$_3$)$_2$), 2.09 (6H, s, NC(CH_3)CH), 1.62 (12H, d, $^{3}J_{HH}$ = 6.85 Hz, CH(CH_3)$_2$), 1.57 (12H, d, $^{3}J_{HH}$ = 6.85 Hz, C(CH_3)$_2$). ^{13}C{^{1}H} NMR (d$_8$–Tol, 125.76 MHz): δ 169.2 (N*C*(CH$_3$)CH), 146.8, 144.4, 142.0, 130.5, 129.7, 127.3, 126.4, 125.1 (*C*–Ar), 95.6

(NC(CH_3)*C*H), 83.3 (O*C*(CH_3)$_2$), 29.4 ((OC(*C*H_3)$_2$), 26.5, 26.4, 26.3, 26.28 (N*C*H(CH_3)$_2$), 26.0, 25.8, 25.7, 25.0 (CH(*C*H_3)$_2$). ^{11}B NMR (d_8–Tol, 125.76 MHz): δ 23.6 O*B*Pin.

Synthesis of [HC{(Me)CN(2,6–^{i}PrC$_6$H$_3$)}$_2$Ca(OCH=NDipp)$_3$(HBpin)Ca], 4.17

Addition of 4,4,5,5,–tetramethyl–1,3,2–dioxaborolane (0.023 mmol) to a J Young's tube containing a solution of compound **4.10** (0.023 mmol, 30 mg) in toluene. The reaction was left at room temperature and probed by NMR spectroscopy after initiation of the reaction. NMR Yield: 71% (Isolated Yield: 9 mg). (^{1}H NMR (d_8–Tol, 500 MHz): δ 7.13 – 7.03 (8H, m, Ar–*H*, OC(*H*)N), 6.94 – 6.89 (4H, m, Ar–*H*), 6.74 – 6.71 (1H, m, Ar–*H*), 4.94 (1H, s, C–*H*), 3.39–3.29 (3H, b sept., C*H*(CH_3)$_2$), 3.24–3.17 (3H, b sept., C*H*(CH_3)$_2$), 3.16–3.12 (1H, b sept., C*H*(CH_3)$_2$), 3.01–2.93 (2H, b sept., C*H*(CH_3)$_2$), 2.60–2.56 (3H, sept., $^3J_{HH}$ = 6.85 Hz, C*H*(CH_3)$_2$), 1.82 (2H, s, NC(C*H*$_3$)CH), 1.75 (1H, s, NC(C*H*$_3$)CH), 1.65 (1H, s, NC(C*H*$_3$)CH), 1.56 (2H, s, NC(C*H*$_3$)CH), 1.36 (6H, d, $^3J_{HH}$ = 6.85 Hz, CH(C*H*$_3$)$_2$), 1.30–1.13 (40H, multiple overlaid d, C(C*H*$_3$)$_2$), 0.99–0.95 (12H, b d, C(C*H*$_3$)$_2$), 0.45, 0.41 (3H, d, $^3J_{HH}$ = 6.85 Hz, CH(C*H*$_3$)$_2$). ^{13}C{^{1}H} NMR (d_8–Tol, 125.76 MHz): δ 170.2, 168.8 (O*C*(H)N), 166.6 (N*C*(CH_3)CH), 151.1, 145.9, 143.6, 142.3, 141.9, 141.4, 140.8, 125.5, 124.4, 124.3, 124.2, 123.7, 123.2 (*C*–Ar), 94.9 (NC(CH_3)*C*H), 77.9 (O*C*(CH_3)$_2$), 32.4, 28.7, 28.0, 27.7, 27.1, 26.2, (N*C*H(CH_3)$_2$), 26.0 (O*C*(CH_3)$_2$), 25.6, 25.2, 24.8, 24.7, 24.0, 23.4, 22.9 (CH(*C*H_3)$_2$). ^{11}B NMR (d_8–Tol, 125.76 MHz): δ 2.9 H*B*pin. Anal. Calcd. for $C_{82}H_{124}BCa_2N_5O_7$: Accurate elemental analysis could not be recorded.

5.4.2 Magnesium and Calcium Formamidate Hydrodeoxygenation

A solution of compound **Ih** or **Ii** (30 mg, 0.067 or 0.056 mmol) in 0.5 ml toluene with two equivalents of a secondary amine were mixed in a J. Young tube. The solution was then interrogated by NMR spectroscopy to ensure complete conversion to the corresponding amide. The solution was then freeze–thaw degassed and exposed to ~1 atm. of CO and the reaction followed by NMR spectroscopy until complete conversion to the formamidate product. Two equivalents of pinacolborane (0.134 or 0.112 mmol) were then added and the reaction was monitored by ^{1}H, ^{13}C{^{1}H} and ^{1}H–^{13}C gated NMR spectroscopy. Conversion to the methyl amine product from the reactions of **4.5**, **4.7**, **4.8** and **4.10** and pinacolborane were identified in comparison to the previously reported NMR data listed in Chapter Two.[2] Compounds **4.3**, **4.4**, **4.6** and **4.9** were identified by the characteristic doublet resonance in the ^{1}H NMR spectra centred *ca.*2 – 3 ppm and the corresponding splitting patterns in the ^{1}H–^{13}C gated NMR spectra: **4.3** and **4.6**: ^{1}H NMR (d_8–Tol, 500 MHz): 2.61 (3H, d, $^1J_{HC}$ = 134.47 Hz, (NC*H*$_3$)). ^{1}H–^{13}C NMR (d_8–Tol, 125.76 MHz): 33.7 (qt, $^1J_{CH}$ = 134.47 Hz, $^3J_{CH}$ = 4.77 Hz, (CH_2N*C*H$_3$)).

4.4 and **4.9**: ^{1}H NMR (d_8–Tol, 500 MHz): 2.75 (3H, d, $^{1}J_{HC}$ = 134.01 Hz, (NC*H*$_3$)). ^{1}H–^{13}C NMR (d_8–Tol, 125.76 MHz): 33.9 (qt, $^{1}J_{CH}$ = 134.01 Hz, $^{3}J_{CH}$ = 5.72 Hz, (CH_2NCH_3)).

5.4.3 Single Crystal X–ray Diffraction analysis:

Single Crystal X–ray diffraction data for compound **4.1** – **4.6**, **4.8** – **4.10**, **4.12** and **4.17** were collected on a SuperNova, Dual Cu at zero, EosS2 diffractometer. The crystal was kept at 150(2) K during data collection. Using Olex2,[4] the structures were solved via SHELXS[6] and refined with the ShelXL refinement package using Least Squares minimisation. The asymmetric unit of **4.1** comprises half of a dimer molecule. The remainder can be generated via a crystallographic inversion centre. The asymmetric unit of **4.2** in this structure contains 2 molecules of the calcium based dimer and 2 molecules of toluene. Disorder in a 65:35 ratio was modelled for C16, C17, C62, C63, C92 C93, C126 and C127. ADP and distance restraints were included for C–C bonds involving fractional occupancy carbons, to assist convergence.

The asymmetric unit of **4.3** is constituted by 2 molecules of the magnesium based trimer, 2 molecules of ordered toluene and 2.5 molecules of disordered toluene. The latter was treated via PLATON SQUEEZE, in preference to modelling significant disorder and smearing of the electron density. There was some disorder prevalent in the main structure also. In particular, C62, C63, C185, C186, C187, C217, C218, C219 were disordered over 2 sites in a 50:50 ratio, while C54, C55, C164 and C265 were similarly disordered in a 55:45 ratio. ADP and C–C distance restraints were included, on merit, for fractional occupancy carbons and their associated metrics, to assist convergence. The asymmetric unit of **4.4** in this structure contains one dimer and two crystallographically independent dimer halves. The latter are proximate to inversion centres which serve to generate the remaining dimer portion in each case. Disorder prevailed in some of the pendant moieties in this structure. In particular, fractional occupancy atom pairs C102/C12A, C135/C13A, C127/C1D and C128/C1E represent one whole carbon each, split between 2 sites in respective rations of 70:30, 70:30, 60:40 and 60:40. C60A–C63A are also disordered with C60B–C63B in a 70:30 quotient while C66A–C68A exhibit a 60:40 split with C66B–C68B. Some N–C and C–C distances were restrained to being similar in disordered regions, and ADP restraints were added, on merit, to assist convergence. In compound **4.5**, the asymmetric unit comprises half of a dimer molecule and half of one molecule of solvent (toluene). The remainder of the former is generated via a crystallographic inversions centre. The solvent moiety also lies close to an inversion centre, but a combination of disorder (particularly relating to the methyl group) plus smearing of the electron density in

the associated phenyl ring precluded derivation of a sensible disorder model without an overwhelming number of restraints. Thus, the solvent was ultimately treated with PLATON SQUEEZE, and due allowance made for same in the empirical formula presented herein. The asymmetric unit comprises one half of a dimer located proximate to a crystallographic inversion centre which serves to generate the remainder of the molecule. The asymmetric unit of **4.8** comprises one half of a dimer located proximate to a crystallographic inversion centre which serves to generate the remainder of the molecule. Asymmetric unit of **4.9** consists of half of one dimer molecule. The remainder is generated via a crystallographic inversion centre. The asymmetric unit of **4.10** contains 1 molecule of the calcium based dimer in this structure, one ordered half of a hexane molecule (close to a crystallographic inversion centre with generates the remainder), and another hexane half in which the electron density was quite smeared. This latter moiety was treated via PLATON SQUEEZE. C70 in the main feature is disordered over 2 sites in a 75:25 ratio. C–C distances involving these 2 fractional occupancy carbon atoms were restrained in the final least squares, to abet convergence. The asymmetric unit of **4.12** comprises half of a dimer molecule and half of a molecule of benzene. Both moieties are located proximate to crystallographic inversion centres which serve to generate the remainder. In this structure, **4.17**, the asymmetric unit comprise one molecule of the dimer, 1 molecule of hexane with full occupancy and an additional hexane fragment with an overall occupancy of 80%. The Bpin in the main feature was seen to be disordered over 2 sites in a 65:35 ratio. Chemically equivalent bond distances involving the disordered components were restrained to being similar in order to assist convergence. The boron bound fractional hydrogens were included at calculated positions but with freely refined U_{iso} values. C85 and C86 in the 80% occupancy solvent moiety were disordered in a 50:50 ratio. The electron density in the region of this guest was a somewhat smeared and, as a consequence, some C–C and ADP restraints were included in order to achieve a chemically sensible refinement.

Table 5.3: Single Crystal X–ray Data Parameters for compounds **4.1** – **4.6**.

Compound	**4.1**	**4.2**	**4.3**	**4.4**	**4.5**	**4.6**
Empirical formula	$C_{33}H_{54}CaN_4O_2$	$C_{142}H_{203}Ca_4N_{12}O_6$	$C_{117.75}H_{171}Mg_3N_9O_3$	$C_{136}H_{204}Ca_4N_{12}O_4$	$C_{69.5}H_{102}Mg_2N_6O_2$	$C_{76}H_{102}Mg_2N_6O_2$
Formula weight	578.88	2334.47	1833.56	2231.42	1102.18	1180.25
Temperature/K	150.00(10)	150.00(10)	150.01(10)	273.24(10)	150.00(10)	150.00(10)
Crystal system	monoclinic	triclinic	triclinic	triclinic	monoclinic	orthorhombic
Space group	$P2_1/n$	P–1	P–1	P–1	$P2_1/n$	$P2_12_12_1$
a/Å	12.52130(10)	12.3167(2)	16.9200(3)	15.6880(5)	12.9593(2)	13.40560(10)
b/Å	14.27210(10)	22.2227(4)	26.0844(5)	20.7648(6)	14.3504(2)	22.4368(2)
c/Å	18.8389(2)	25.1147(4)	28.3888(4)	22.7564(6)	18.5552(3)	22.9956(2)
α/°	90	90.035(1)	67.212(2)	74.394(2)	90	90
β/°	95.3870(10)	98.119(1)	89.8810(10)	72.719(3)	95.8960(10)	90
γ/°	90	90.410(1)	82.1420(10)	77.315(3)	90	90
Volume/Å^3	3351.74(5)	6805.1(2)	11425.1(4)	6738.4(4)	3432.48(9)	6916.59(10)
Z	4	2	4	2	2	4
ρ_{calc} g/cm^3	1.147	1.139	1.066	1.100	1.066	1.133
μ/mm^{-1}	1.862	1.822	0.630	1.806	0.651	0.680
F(000)	1264.0	2534.0	4002.0	2432.0	1202.0	2560.0
Crystal size/mm^3	0.191×0.145×0.118	0.237 × 0.198 × 0.175	0.284 × 0.219 × 0.129	0.1694×0.0987× 0.0891	0.251 × 0.137 × 0.089	0.260 × 0.110 × 0.107
2Θ range for data collection/°	7.784 to 146.826	7.11 to 146.862	5.922 to 147.12	5.97 to 144.044	7.804 to 146.934	5.504 to 147.058
Reflections collected	25873	54860	91161	56557	25278	58616
Independent reflections	6685 [R_{int} = 0.0313]	26890 [R_{int} = 0.0285]	44927 [R_{int} = 0.0281]	25833 [R_{int} = 0.0294]	6842 [R_{int} = 0.0341]	13812 [R_{int} = 0.0276]
Data/restraints/parameters	6685/0/372	26890/95/1594	44927/140/2417	25833/83/1553	6842/0/355	13812/0/795
Goodness–of–fit on F^2	1.044	1.032	1.017	1.036	1.085	1.030
Final R indexes [I>=2σ (I)]	R_1 = 0.0387, wR_2 = 0.0989	R_1 = 0.0516, wR_2 = 0.1389	R_1 = 0.0731, wR_2 = 0.2066	R_1 = 0.0542, wR_2 = 0.1398	R_1 = 0.0602, wR_2 = 0.1592	R_1 = 0.0293, wR_2 = 0.0753
Final R indexes [all data]	R_1 = 0.0429, wR_2 = 0.1018	R_1 = 0.0629, wR_2 = 0.1476	R_1 = 0.0871, wR_2 = 0.2214	R_1 = 0.0824, wR_2 = 0.1555	R_1 = 0.0724, wR_2 = 0.1679	R_1 = 0.0308, wR_2 = 0.0763
Largest diff. peak/hole / e Å^{-3}	0.40/–0.45	0.81/–0.63	1.34/–0.64	0.66/–0.45	0.69/–0.67	0.19/–0.17

Table 5.4: Single Crystal X–ray Data Parameters for compounds **4.8** – **4.12** and **4.15**.

Compound	**4.8**	**4.9**	**4.10**	**4.12**	**4.17**
Empirical formula	$C_{34}H_{51}N_3OCa$	$C_{76}H_{102}Ca_2N_6O_2$	$C_{82}H_{129}Ca_2N_5O_5$	$C_{40}H_{52}MgN_3O$	$C_{84.8}H_{133.2}BCa_2N_5O_5$
Formula weight	557.85	1211.79	1345.05	615.15	1393.73
Temperature/K	150.01(10)	150.00(10)	150.00(10)	150.00(10)	150.00(10)
Crystal system	monoclinic	monoclinic	triclinic	monoclinic	triclinic
Space group	C2/c	$P2_1/n$	P–1	$P2_1/n$	P–1
a/Å	21.9505(4)	13.2289(2)	12.3369(3)	13.88039(16)	15.3517(7)
b/Å	14.60243(19)	19.8454(3)	14.1438(3)	11.90132(12)	15.5044(6)
c/Å	22.8491(4)	14.1282(2)	24.9534(6)	21.6100(2)	19.1840(6)
α/°	90	90	100.966(2)	90	85.931(3)
β/°	113.987(2)	108.7856(17)	91.498(2)	100.0066(11)	76.247(3)
γ/°	90	90	110.918(2)	90	72.926(4)
Volume/Å^3	6691.3(2)	3511.53(10)	3971.84(17)	3515.56(7)	4239.8(3)
Z	10	2	2	4	2
ρ_{calc} g/cm^3	1.384	1.146	1.125	1.162	1.092
μ/mm^{-1}	2.274	1.774	1.634	0.690	1.544
F(000)	3040.0	1312.0	1472.0	1332.0	1524.0
Crystal size/mm^3	0.18 ×0.158×0.083	0.21 ×0.14 × .103	0.161×0.07 ×0.05	0.461×0.365×0.248	0.187×0.126×0.051
2Θ range for data collection/°	7.488 to 139.584	7.966 to 139.608	6.848 to 147.038	7.052 to 139.514	5.964 to 146.968
Reflections collected	21184	11731	31950	22341	33340
Independent reflections	6258 [R_{int} = 0.0213]	6467 [R_{int} = 0.0260]	15669 [R_{int} = 0.0317]	6584 [R_{int} = 0.0253]	16638 [R_{int} = 0.0439]
Data/restraints/parameters	6258/0/364	6467/0/398	15669/7/852	6584/0/417	16638/130/1028
Goodness–of–fit on F^2	1.027	1.021	1.012	1.040	1.041
Final R indexes [I>=2σ (I)]	R_1 = 0.0435, wR_2 = 0.1145	R_1 = 0.0427, wR_2 = 0.1114	R_1 = 0.0460, wR_2 = 0.1146	R_1 = 0.0510, wR_2 = 0.1369	R_1 = 0.0675, wR_2 = 0.1795
Final R indexes [all data]	R_1 = 0.0454, wR_2 = 0.1161	R_1 = 0.0501, wR_2 = 0.1171	R_1 = 0.0637, wR_2 = 0.1258	R_1 = 0.0557, wR_2 = 0.1411	R_1 = 0.0932, wR_2 = 0.1999
Largest diff. peak/hole / e Å^{-3}	0.74/–0.27	0.74/–0.44	0.50/–0.46	0.77/–0.41	1.03/–0.59

All NMR spectra are available in the electronic supplementary

5.5 References

1 a) S. J. Bonyhady, C. Jones, S. Nembenna, A. Stasch, A. J. Edwards and G. J. McIntyre, *Chemistry – A European Journal*, 2010, **16**, 938–955. b)) S. Harder, J. Spielmann, J. Intemann and H. Bandmann, *Angewandte Chemie*, 2011, **123**, 4242–4246.

2 a) M. D. Anker, Y. Yang, J. Fang, M. F. Mahon, L. Maron, C. Weetman and M. S. Hill. *Chemical Science*, 2017, 10.1039/C7SC00117G.